

## Autogenous shrinkage of early age cement paste and mortar

Lu, Tianshi

**DOI**

[10.4233/uuid:e06bd615-7fc4-481b-a334-37627f142e3d](https://doi.org/10.4233/uuid:e06bd615-7fc4-481b-a334-37627f142e3d)

**Publication date**

2019

**Document Version**

Final published version

**Citation (APA)**

Lu, T. (2019). *Autogenous shrinkage of early age cement paste and mortar*. [Dissertation (TU Delft), Delft University of Technology]. <https://doi.org/10.4233/uuid:e06bd615-7fc4-481b-a334-37627f142e3d>

**Important note**

To cite this publication, please use the final published version (if applicable).  
Please check the document version above.

**Copyright**

Other than for strictly personal use, it is not permitted to download, forward or distribute the text or part of it, without the consent of the author(s) and/or copyright holder(s), unless the work is under an open content license such as Creative Commons.

**Takedown policy**

Please contact us and provide details if you believe this document breaches copyrights.  
We will remove access to the work immediately and investigate your claim.

# **Autogenous shrinkage of early age cement paste and mortar**

## **Proefschrift**

ter verkrijging van de graad van doctor  
aan de Technische Universiteit Delft,  
op gezag van de Rector Magnificus prof.dr.ir. T.H.J.J. van der Hagen;  
voorzitter van het College voor Promoties,  
in het openbaar te verdedigen op  
dinsdag 7 mei, 2019 om 15:00 uur

door

Tianshi LU

Master of Engineering, Hohai University, P.R. China  
geboren te Cangzhou, P.R. China

Dit proefschrift is goedgekeurd door de promotor.

Samenstelling Promotiecommissie:

Rector Magnificus, Prof.dr.ir. K. van Breugel	voorzitter Technische Universiteit Delft, promotor
--	---

Onafhankelijke leden:

Prof.dr. K. Kovler	Technion – Israel Institute of Technology, Israël
Prof.dr. V. Baroghel-Bouny	University of Paris-Est Marne-la-Vallée, Frankrijk
Dr. H. Hedlund	Luleå University of Technology, Zweden
Prof.dr.ir. K. Jansen	Technische Universiteit Delft
Prof.dr.ir. E. Schlangen	Technische Universiteit Delft
Dr. G. Ye	Technische Universiteit Delft

Keywords: autogenous shrinkage, capillary tension, creep, silica fume, fly ash, blast furnace slag, cement paste, cement mortar, concrete.

Printed: Ipskamp Printing

Cover design: Tianshi Lu & Yu Chen

Copyright © 2019 by Tianshi Lu

ISBN: 978-94-6384-040-8

All rights reserved. No part of the material protected by this copyright notice may be reproduced or utilized in any form or by any means, electronic or mechanical, including photocopying, recording or by any information storage and retrieval system, without written permission from the author.

Printed in the Netherlands

*So we beat on, boats against the current, borne back ceaselessly into the past.*

*-F. Scott Fitzgerald(1896-1940)*

# Propositions

Accompanying the PhD Thesis  
Autogenous shrinkage of early age cement paste and mortar

Tianshi Lu

1. Autogenous shrinkage is closely related to the internal relative humidity of cement paste. The most effective way to mitigate the autogenous shrinkage is decreasing the drop of internal relative humidity of cement paste (this thesis).
2. Cement paste performs visco-elastic. Autogenous shrinkage of cement paste caused by the change of internal relative humidity should be divided into two part, i.e. an elastic part and a creep part. For accurate prediction of the autogenous shrinkage of cement paste creep cannot be ignored (this thesis).
3. A PhD study is like a training camp. Academic veterans instruct recruits to become a qualified soldier.
4. For a PhD candidate results are important, but the process of getting these results is even more important.
5. Data is the word of science and logic is the grammar of it.
6. The most valuable thing of a good book is not the knowledge it contains, but the thinking it arouse.
7. Language is not only the way how people express their thoughts, but also the way how people's thoughts were formed.
8. The essence of forgiving others is relieving ourselves from bad feeling.
9. Rules themselves will not make things running smoothly, rule-conscious people is the key of a well-ordered world.
10. Nothing in life is to be feared, it is only to be understood. Now is the time to understand more, so that we may fear less. (Marie Curie)

*These propositions are regarded as opposable and defendable, and have been approved as such by the promoter Prof. dr. ir. Klaas van Breugel*



# Acknowledgements

The research work reported in this thesis was sponsored by China Scholarship Council (CSC) and Delft University of Technology (TU Delft). This research was carried out in Microlab, Section of Materials and Environment at the Faculty of Civil Engineering and Geosciences, TU Delft. CSC and TU Delft are gratefully acknowledged. The realization of this thesis would not have been possible without the support and help provided by many people, to whom I would like to express my sincere gratitude.

I would like to express my deepest appreciation to my promotor Prof. dr. ir. Klaas van Breugel, who gave me the opportunity to work and study at the section of Materials and Environment in TU Delft. I deeply respect his knowledge, experience, insights and enthusiasm in research. His tireless efforts and constructive comments on this dissertation are highly appreciated. My thesis would not be accomplished without his guidance.

I also would like to deliver my special thanks to Dr. Guang Ye. Dr. Guang Ye has shown his concern for me and always been supportive in every aspect. I thank him for his encouragement and suggestions.

The committee members, Prof. dr. Konstantin Kovler, Prof. dr. Véronique Baroghel-Bouny, Prof. dr. Hans Hedlund, Prof. dr. ir. Kaspar Jansen and Prof. dr. ir. Erik Schlangen, are very appreciated for their greatest insights, which is very helpful for improving the quality of my thesis. I would like to thank them for spending their time on reviewing my thesis, giving comments and attending my PhD defence.

I would like to thank Mr. Cees Timmers and Ms. Franca Post, from the Center for International Cooperation and Appropriate Technology (CICAT) of TU Delft, for their support during my stay in the Netherlands.

I warmly acknowledge all the colleagues and former colleagues of Microlab. I owe gratitude to Gerrit Nagtegaal, Maiko van Leeuwen, Ton Blom, John van den berg and Arjan Thijssen for their help with my experimental work. Many thanks to secretaries, Claire de Bruin, Jacqueline van Unen, Claudia Baltussen, Nynke Verhulst, Iris Batterham and Melanie Holtzapffel for their kind help with the daily administration affairs. I also want to thank Dr. Henk Jonks, Dr. Dessi Koleva, Dr. Branko Savija, Dr. Oguzhan Copuroglu, Agus Susanto, Stefan Chaves Figueiredo, Claudia Romero Rodriguez, Albina Kostiuchenko, Damian Palin and Renée Mors for their smile and encouragement. I would like to give my thanks to my former and current office mates, Dr. Haoliang Huang, Richard Aquino, Dr. Hooman Hoornahad, Hao Huang, Dr. Hua Dong, Dr. Farhad Pargar, Dr. Natakli Carr, Dr. Kai Zhang, Dr. Marija Nedelkovic, Gabriel and Luca. They always provided the nice atmosphere in the office. I am very grateful to my Chinese colleagues, Dr. Zhiwei Qian, Dr. Jie Zhao, Dr. Quantao Liu, Dr. Mingzhong Zhang, Dr. Qi Zhang, Dr. Yuwei Ma, Dr. Jie Hu, Dr. Ying Wang, Dr. Zhuqing Yu (Dr. Ning Li), Dr. Zhengxian Yang, Dr. Yong Zhang, Bei Wu, Dr. Peng Gao, Dr. Chunping Gu, Dr. Xiaowei Ouyang, Jiayi Chen (Dr. Wenqin Shi), Xuliang Hou (Dr. Ying Yang), Dr. Xu Ma, Zhipei Chen, Dr. Leyang Lu, Yibing Zuo, Hongzhi Zhang, Zhenming Li, Wenjuan LYU, Shizhe Zhang, Shi Xu, Yu Chen, Yidong Gan, Yading Xu, Boyu Chen, Ze Chang, Xuhui Liang, Yun Chen etc. for all great time that we have shared.

I would like to thank all the friends that I met in the Netherlands. Their friendship is a great treasure I gained during the PhD period. I owe my thanks to Jing Xiao, Dr. Jiawen Song, Dr. Peng Yao, Dr. Min Su, Dr. Mingxin Zhang, Dr. Lixia Niu, Xialu Wang, Qiushi

Wu, Dr. Hongkai Gao, Tao Lu, Dr. Wenqing Liao, Yinglin Cao, Dr. Xiaoyu Zhang, Kelly Tseng and Qian Li. I would like to express my sincere gratitude to my former and current roommates, Dr. Zhou Zhou(Shan Shen & Xiao You), Dr. Yanqing Hou, Dr. Haixing Fang, Dejian Peng, Guanqu Yu, Xiao Guo & Guotai Li. We shared a lot of fun, happiness and good time together.

Last but not least, I would like to express my gratitude to my family, parents, grandparents, for their love, support and sacrifice. I love you forever.

Tianshi Lu  
Delft,2019



# Table of Contents

---

Table of Contents.....	i
List of Figures.....	v
List of Tables.....	xi
List of Symbols.....	xiii
List of Abbreviation.....	xvii
 Chapter 1.....	 1
<b>Introduction</b>	
1.1 Background of this research.....	1
1.2 Objective of this research.....	2
1.3 Research strategy of this study.....	3
1.4 Scope of the research.....	3
1.5 Outline of the thesis.....	4
 Chapter 2.....	 7
<b>Early-Age deformation of cement paste and concrete - A Literature Survey</b>	
2.1 Introduction.....	7
2.2 Hydration and formation of microstructure.....	7
2.2.1 Hydration process.....	8
2.2.2 Microstructure and porosity.....	8
2.2.3 State of water.....	9
2.3 Early-Age deformation of cement paste and concrete.....	9
2.3.1 Early-age expansion.....	10
2.3.2 Early-age shrinkage.....	11
2.3.3 Chemical shrinkage.....	11
2.3.4 Autogenous shrinkage.....	12
2.4 Factors affecting autogenous deformation of cementitious material.....	12
2.4.1 Effect of water-cement ratio.....	12
2.4.2 Effect of cement type, fineness and composition.....	13
2.4.3 Effect of supplementary materials on autogenous shrinkage.....	14
2.4.3.1 Blast furnace slag.....	14
2.4.3.2 Fly ash.....	15
2.4.3.3 Silica fume.....	16
2.4.4 Effect of temperature.....	16
2.4.5 Effect of sand and aggregate on autogenous shrinkage.....	16
2.5 Mechanisms and numerical models of autogenous shrinkage.....	17
2.5.1 Surface tension of solid particles.....	17
2.5.2 Disjoining pressure.....	18
2.5.3 Capillary tension.....	19
2.5.4 Discussion.....	20

2.6	Analytical expressions for autogenous shrinkage - phenomenological approach....	21
2.6.1	Freisleben-Hansen and Pedersen model.....	21
2.6.2	The CEB FIP MC 90.....	22
2.6.3	Unified shrinkage model of Ya Wei.....	22
2.6.4	Tazawa and Miyazawa Model.....	22
2.6.5	Engineering expressions/formulae – Discussion.....	23
2.7	Concluding remarks.....	23
Chapter 3.....		25
<b>Mechanism and numerical simulation of autogenous shrinkage</b>		
3.1	Introduction.....	25
3.2	Mechanisms for autogenous shrinkage.....	25
3.2.1	Microstructure of concrete.....	25
3.2.2	Disjoining pressure.....	27
3.2.2.1	Disjoining pressure - The Van der Waals term.....	27
3.2.2.2	Disjoining pressure - Electrostatic term.....	29
3.2.2.3	Disjoining pressure - Structural term.....	30
3.2.2.4	Calculation of disjoining pressure.....	31
3.2.3	Capillary tension.....	32
3.2.3.1	Calculation of capillary tension.....	33
3.2.3.2	Calculation of the Kelvin radius.....	33
3.2.3.3	Relationship between internal relative humidity and dissolved ions....	34
3.2.3.4	Effect of ion concentration on relative humidity and capillary tension - example.....	34
3.2.4	Discussion.....	37
3.3	Deformation of hardening cement paste under changing internal load - autogenous shrinkage of cement paste.....	37
3.3.1	Elastic deformation $\varepsilon_{el}$ .....	38
3.3.2	Effective stress $\sigma_e$ .....	38
3.3.2.1	Theoretical basis of effective stress.....	38
3.3.2.2	Degree of saturation $S_w$ .....	40
3.3.2.3	Elastic deformation of cement paste under internal load-example...41	
3.3.3	Time-dependent deformation $\varepsilon_{cr}(t, \tau)$ .....	43
3.3.3.1	Theoretical basis of Activation energy concept.....	43
3.3.3.2	Creep of the hardening cement paste under changing load.....	44
3.3.4	Calculation of autogenous shrinkage of early-age cement paste.....	46
3.3.4.1	Proposed simulation model of autogenous shrinkage of early-age cement paste.....	46
3.3.4.2	Example.....	47
3.4	Concluding remarks.....	48
Chapter 4.....		49
<b>Experimental study of early-age properties and autogenous shrinkage of ordinary Portland cement paste and cement paste with supplementary materials</b>		
4.1	Introduction.....	49
4.2	Materials.....	49
4.3	Experimental methods and equipment.....	51
4.3.1	Final setting time.....	51
4.3.2	Non-evaporable water content.....	51

4.3.3	Chemical shrinkage.....	52
4.3.4	Internal relative humidity.....	52
4.3.5	Compressive strength.....	53
4.3.6	Autogenous deformation.....	53
4.4	Results and discussion.....	54
4.4.1	Final setting time.....	54
4.4.2	Non-evaporable water content.....	55
4.4.3	Chemical shrinkage.....	57
4.4.4	Internal relative humidity.....	58
4.4.5	Compressive strength.....	60
4.4.6	Autogenous deformation as function of time.....	61
4.4.7	Autogenous deformation as function of relative humidity.....	64
4.5	Concluding Remarks.....	65
Chapter 5.....		69
<b>Numerical simulation of autogenous shrinkage of ordinary Portland cement paste and cement paste with supplementary materials</b>		
5.1	Introduction.....	69
5.2	Mixture compositions of cement pastes used for verifying the numerical model....	70
5.3	Determination of material parameters used for numerical simulation of autogenous shrinkage.....	70
5.3.1	Calculation of the degree of saturation.....	70
5.3.2	Capillary tension.....	72
5.3.3	Elastic modulus.....	76
5.4	Autogenous deformation—Elastic plus time-dependent part.....	78
5.4.1	Portland cement pastes with w/b ratio 0.3 and 0.4.....	79
5.4.2	Portland cement pastes with 10% silica fume and w/b ratio 0.3 and 0.4.....	80
5.4.3	Portland cement pastes with 30% fly ash and w/b ratio 0.3 and 0.4.....	81
5.4.4	Blast furnace slag cement pastes with w/b ratio 0.3 and 0.4.....	84
5.4.5	Discussion.....	85
5.5	Conclusions.....	88
Chapter 6.....		91
<b>Restraining effect of sand on shrinking cement mortar and concrete</b>		
6.1	Introduction.....	91
6.2	Background.....	91
6.3	Simulation models of autogenous shrinkage of cement mortar.....	92
6.3.1	General introduction of composite models.....	92
6.3.2	Theoretical basis of Pickett's model.....	94
6.3.2.1	One particle restraint.....	94
6.3.2.2	Multi particles restraint.....	97
6.3.2.3	Autogenous shrinkage of cementitious material as a function of aggregate content.....	97
6.3.3	Evaluation of microcracking of cement mortar.....	98
6.3.3.1	Calculation of tangential tensile stress.....	99
6.3.3.2	Estimation of tensile strength of mortars.....	100
6.3.3.3	Evaluation of microcracking of cement mortar.....	101
6.3.4	Extended Pickett's model considering the effect of creep of cement paste on autogenous shrinkage of cement mortar.....	102

6.3.4.1	One particle restraint.....	102
6.3.4.2	Multi particles restraint.....	104
6.3.4.3	Autogenous shrinkage of cementitious material as a function of aggregate content.....	104
6.4	Experimental program of autogenous shrinkage of cement mortar.....	105
6.4.1	Materials.....	105
6.4.2	Experimental methods and equipment.....	106
6.5	Experimental results.....	106
6.5.1	Final setting time.....	106
6.5.2	Autogenous deformation.....	108
6.6	Simulation results of autogenous deformation and discussion.....	110
6.6.1	Calculation procedure.....	110
6.6.2	Portland cement mortars (sand-solid phase (cement and sand) weight ratio = 0.1 and 0.3, water-binder ratio = 0.3 and 0.4).....	111
6.6.3	Silica fume cement mortars (silica fume addition = 10%, sand-solid phase (cement and sand) weight ratio = 0.1 and 0.3, water-binder ratio = 0.3 and 0.4).....	113
6.6.4	Fly ash cement mortars (fly ash addition = 30%, sand-solid phase (cement and sand) weight ratio = 0.1 and 0.3, water-binder ratio = 0.3 and 0.4).....	115
6.6.4.1	Fly ash cement mortars with water-binder ratio 0.3.....	115
6.6.4.2	Fly ash cement mortars with water-binder ratio 0.4.....	117
6.6.4.3	Effect of change of ion concentration on the calculated autogenous shrinkage of fly ash mortars.....	118
6.6.5	BFS cement mortars (sand-solid phase (cement and sand) weight ratio = 0.1 and 0.3, water-binder ratio = 0.3 and 0.4).....	119
6.6.6	Effect of change of ion concentration on the calculated autogenous shrinkage of Portland and BFS cement mortars.....	121
6.7	Prediction of autogenous shrinkage of concrete at 28 days.....	122
6.7.1	Mixture design.....	122
6.7.2	Portland concrete (Zhang et al. 2003).....	123
6.7.2.1	Testing method (used by Zhang et al. 2003).....	123
6.7.2.2	Numerical simulation of autogenous shrinkage.....	124
6.7.3	Blast furnace slag concrete (Mors 2011).....	126
6.7.3.1	Testing method (used by Mors, 2011).....	126
6.7.3.2	Numerical simulation of autogenous shrinkage.....	127
6.7.4	Evaluation of prediction of autogenous shrinkage of concrete.....	128
6.8	Discussion and Conclusion.....	129
Chapter 7	.....	131
<b>Retrospection, Conclusions and Prospects</b>		
7.1	Retrospection.....	131
7.2	Conclusions.....	132
7.3	Contribution of this study to autogenous shrinkage of cementitious material.....	133
7.4	Prospects.....	134
Summary	.....	135
Samenvatting	.....	137
Appendix	.....	139
References	.....	141

# List of Figures

---

1.1	Diagram of shrinkage types (after Holt 2001).....	2
1.2	Scheme of this thesis.....	5
2.1	Schematic view of state of Self-desiccation of a cement paste (van Breugel 1991, Lura 2003).....	7
2.2	Rate of heat evolution during the hydration of Portland cement (after Mindess et al. 1981).....	8
2.3	Thickness of adsorption layer as a function of relative humidity (Hagymassy 1969).....	9
2.4	Measured autogenous deformations at 20°C of two types of concrete (CEM I 52.5N, w/c: 0.45; CEM III/A 42.5 LA, w/c: 0.45) (Darquennes et al. 2011).....	10
2.5	Typical results of autogenous deformation and chemical shrinkage test (Jensen et al. 2001b).....	11
2.6	Measured autogenous deformations of ordinary Portland cement pastes at three water cement ratios (cement paste was cast in rig and deformation was measured by LVDT) (Wei 2008).....	13
2.7	Autogenous shrinkage of different mineral compositions of Portland cement (Jensen 2000).....	13
2.8	Autogenous deformation of different concretes containing 0%, 30% and 50% blast furnace slag(w/b =0.42 and aggregate weight ratio =0.8) (Lee et al. 2006).....	14
2.9	Autogenous deformation of different cement mortars containing 0%, 40% and 60% fly ash (w/b =0.42 and aggregate weight ratio =0.8) (Bentz et al. 2013).....	15
2.10	Autogenous deformation of different cement pastes containing 0%, 5% and 10% silica fume (Zhang et al. 2003).....	16
2.11	Surfaces of hindered adsorption and distribution of disjoining pressure.....	18
2.12	Measured and calculated autogenous deformation of Portland cement paste as a function of internal relative humidity (w/b=0.37) (Lura 2003).....	20
2.13	Long term autogenous shrinkage of cement paste (w/b=0.37) (Lange 2016).....	21
3.1	Schematic representation of the multi-scale microstructure of concrete: (a) concrete; (b) schematic microstructure of cement paste; (c) schematic microstructure of C-S-H gel (Wittmann 1976).....	26
3.2	Example of differential pore size distribution of Portland cement pastes with water-binder ratio 0.3 measured by MIP at seven days (after Zeng et al. 2012).....	26
3.3	Schematic microstructure of C-S-H gel (b), geometry of two surfaces $s$ and $s'$ across water $w$ (a) and geometry of two surfaces $s$ and $s'$ with adsorbed layers $w$ and $w'$ across air $a$ (c).....	28
3.4	Van der Waals term vs. pore size (Equation 3.2).....	28
3.5	Schematic microstructure of C-S-H gel (a) and two positive charged surfaces separated a distance $D$ in water (b) (after Jacob 2011).....	29

3.6	Electrostatic term vs. pore size (Equation 3.3).....	30
3.7	Schematic representation of mechanism of structural term of disjoining pressure (after Churaev 1985).....	31
3.8	Structural term vs. pore size (Equation 3.7).....	31
3.9	Scheme of disjoining pressure calculation.....	32
3.10	Disjoining pressure vs. pore size.....	32
3.11	Schematic microstructure of hardening cement paste (a) and Simplified cylindrical capillary pore system (b).....	33
3.12	Measured $RH$ and calculated $RH_K$ of Portland cement paste with w/b ratio of 0.4.....	35
3.13	Calculated Kelvin radius of Portland cement paste with w/b ratio of 0.4...35	
3.14	Calculated capillary tension in the pore fluid for Portland cement paste with water-binder ratio of 0.4.....	36
3.15	Simulated Degree of hydration (with HYMOSTRUC) vs. age of Portland cement paste with water-binder ratios of 0.4.....	36
3.16	Schematic representation of deformation of the cement paste under constant external load.....	37
3.17	Schematic representation of the internal pressure $p^s$ and resulted compressive pressure $p^{s'}$ in the adsorbed water.....	39
3.18	Degree of saturation of BFS cement paste with water-binder ratio of 0.3 calculated from measurements.....	40
3.19	Measured non-evaporable water content and chemical shrinkage as a function of time of BFS cement paste with water-binder ratio of 0.3.....	41
3.20	Measured relative humidity, calculated capillary tension and effective stress of blast furnace slag cement paste (CEM III 42.5N) with water-binder ratio 0.3.....	42
3.21	Calculated elastic modulus and degree of saturation of blast furnace slag cement paste (CEM III 42.5N) with water-binder ratio 0.3.....	42
3.22	Calculated elastic deformation of blast furnace slag cement paste (CEM III 42.5N) with water-binder ratio 0.3 under capillary tension (Equation 3.21).....	43
3.23	Schematic representation of autogenous shrinkage of hardening cement paste.....	45
3.24	Scheme of simulation model of autogenous shrinkage.....	47
3.25	Calculated autogenous shrinkage of blast furnace slag cement paste (CEM III 42.5N) with water-cement ratio of 0.3.....	48
4.1	Particle size distribution of materials powders used in this thesis.....	50
4.2	Equipment for chemical shrinkage measurement.....	52
4.3	Apparatus for internal relative humidity measurement.....	53
4.4	Setup for the autogenous shrinkage measurement.....	54
4.5	Final setting time of cement pastes with different supplementary materials. Code: See Table 4.3.....	54
4.6	Non-evaporable water content as a function of age for different kinds of cement paste with water binder ratio of 0.3.....	56
4.7	Non-evaporable water content as a function of age for different kinds of cement paste with water binder ratio of 0.4.....	56
4.8	Chemical shrinkage as a function of age.....	57
4.9	Internal relative humidity vs. age for different kinds of cement paste with water binder ratio of 0.3.....	58

4.10	Internal relative humidity vs. age for different kinds of cement paste with water binder ratio of 0.4.....	58
4.11	Internal relative humidity vs. age for different kinds of cement paste with water binder ratio of 0.3 and 0.4.....	59
4.12	Compressive strength vs. age for different kinds of cement paste with water binder ratio of 0.3.....	60
4.13	Compressive strength vs. age for different kinds of cement paste with water binder ratio of 0.4.....	60
4.14	Autogenous deformation vs. age for different kinds of cement paste with water binder ratio of 0.3 (Starting time: final setting time).....	61
4.15	Autogenous deformation vs. age for different kinds of cement paste with water binder ratio of 0.4 (Starting time: final setting time).....	62
4.16	Autogenous deformation vs. age for different kinds of cement paste with water binder ratio of 0.3 (Starting time: after early age swelling).....	62
4.17	Autogenous deformation vs. age for different kinds of cement paste with water binder ratio of 0.4 (Starting time: after early age swelling).....	63
4.18	Autogenous deformation vs. internal relative humidity for different kinds of cement paste with water binder ratio of 0.3.....	64
4.19	Autogenous deformation vs. internal relative humidity for different kinds of cement paste with water binder ratio of 0.3.....	65
5.1	Scheme of autogenous shrinkage calculation.....	70
5.2	Calculated degree of saturation as a function of age for different cement pastes with water binder ratio of 0.3 (calculated with Equation 5.1).....	71
5.3	Calculated degree of saturation as a function of age for different cement pastes with water binder ratio of 0.4 (calculated with Equation 5.1).....	72
5.4	Measured internal relative humidity vs. age for different cement pastes (Section 4.4.4).....	73
5.5	Calculated radius of the largest water-filled pore of different cement pastes with water binder ratio of 0.3 (calculated with Equation 5.3).....	73
5.6	Calculated radius of the largest water-filled pore of different cement pastes with water binder ratio of 0.4 (calculated with Equation 5.3).....	74
5.7	Calculated capillary tension in the pore fluid for different cement pastes with water binder ratio of 0.3 as a function of age (calculated with Equation 5.2).....	74
5.8	Calculated capillary tension in the pore fluid for different cement pastes with water binder ratio of 0.4 as a function of age (calculated with Equation 5.2).....	75
5.9	Calculated capillary pressure (tension) using Kelvin's equation and calculated water saturation, both as function of relative humidity (w/c:0.3) (after Lebental et al. 2012).....	75
5.10	Calculated elastic modulus vs. age for different kinds of cement paste with water binder ratio of 0.3 and 0.4 (calculated by Equation 5.4).....	77
5.11	Measured elastic modulus (after Tian et al. 2013) and calculated elastic modulus vs. degree of hydration for Portland cement paste with water binder ratio of 0.3 and 0.4.....	78
5.12	Schematic representation of autogenous shrinkage of hardening cement paste.....	79
5.13	Measured and calculated autogenous deformation of Portland cement paste with water binder ratio 0.3 (Note: Vertical scales are different).....	79

5.14	Measured and calculated autogenous deformation of Portland cement paste with water binder ratio 0.4 (Note: Vertical scales are different).....	80
5.15	Measured and calculated autogenous deformation of silica fume cement paste (10% silica fume by weight of cement) with water binder ratio 0.3 (Note: Vertical scales are different).....	80
5.16	Measured and calculated autogenous deformation of silica fume cement paste (10% silica fume by weight of cement) with water binder ratio 0.4 (Note: Vertical scales are different).....	81
5.17	Measured and calculated autogenous deformation of fly ash cement paste (30% fly ash by weight of cement) with water binder ratio 0.3 (Note: Vertical scales are different).....	82
5.18	Measured and calculated autogenous deformation of fly ash cement paste (30% fly ash by weight of cement) with water binder ratio 0.4 (Note: Vertical scales are different).....	82
5.19	Measured and calculated autogenous deformation of fly ash cement paste (taking change of ion concentration into account) with water-binder ratio 0.3 and 0.4.....	83
5.20	Measured and calculated autogenous deformation of blast furnace slag cement paste with water binder ratio 0.3 (Note: Vertical scales are different).....	84
5.21	Measured and calculated autogenous deformation of blast furnace slag cement paste with water binder ratio 0.4 (Note: Vertical scales are different).....	84
5.22	Schematic representation of autogenous shrinkage of hardening cement paste.....	85
5.23	Comparison between the measured and calculated $\varepsilon_{0.3}/\varepsilon_{0.4}$ of different cement pastes.....	87
5.24	Measured and calculated autogenous deformation of blast furnace slag cement paste with water binder ratio of 0.3.....	87
5.25	Measured and calculated autogenous deformation of Portland cement paste with water-binder ratio 0.3 and 0.4.....	88
6.1	Measured autogenous shrinkage of ordinary Portland cement paste and concrete with different aggregate contents by volume (Wei 2008).....	92
6.2	Schematic representation of mechanism for (a) restraining effect of aggregate particle on shrinking cement paste (after Hansen et al. 1965) and (b) relationship between stress $\sigma_t$ and radius $r$ .....	94
6.3	Schematic representation of restraining effect of an aggregate particle on the volume shrinkage of the outer shell of cement paste (after Hansen et al. 1965).....	95
6.4	Schematic representation of restraining inner aggregate particle (after Pickett 1956).....	96
6.5	Empirical relationship between factor $\beta$ and ratio $E_p/E_s$ .....	96
6.6	Calculated autogenous deformation of BFS cement paste and mortar (sand-solid phase (cement and sand) weight ratio is 0.1, 0.3, 0.5 and 0.7) with Pickett's model (Equation 6.16) with water-binder ratio of 0.3.....	98
6.7	Schematic representation of the microcracking generated on the interface of the shrinkage cement paste and inert particle (after Wei 2008).....	98
6.8	Calculated tangential tensile stress (Equation 6.17) in different BFS cement mortars and schematic representation of the tangential tensile stress.....	100



6.9	Measured compressive strength and calculated tensile strength of BFS cement paste (Equation 6.18) with water-binder ratio of 0.3 (Note: Vertical scales are different).....	100
6.10	Calculated tangential tension (Equation 6.17) at the surface between the sand and cement paste in BFS cement mortars and tensile strength (Equation 6.18) of BFS cement mortars (sand-solid phase weight ratio is 0.1, 0.3 ,0.5 and 0.7, water-binder ratio is 0.3).....	101
6.11	Schematic representation of change of radius of the outer shell $\delta_r$ .....	102
6.12	Relationships between the ratio $E_p/E_s$ and the factors $\beta$ and $\beta_\phi$ (Equation 6.12 and Equation 6.26).....	104
6.13	Calculated autogenous deformation of BFS cement paste and mortar (sand-solid phase (cement and sand) weight ratio is 0.1, 0.3, 0.5 and 0.7) with Pickett model (Equation 6.16) and the extended Pickett model (Equation 6.27) with water-binder ratio of 0.3.....	105
6.14	Final setting time of Portland cement pastes and mortars. Specimen code: See Table 6.1.....	107
6.15	Final setting time of cement pastes and mortars with silica fume. Specimen code: See Table 6.1.....	107
6.16	Final setting time of cement pastes and mortars with fly ash. Specimen code: See Table 6.1.....	107
6.17	Final setting time of BFS cement pastes and mortars. Specimen code: See Table 6.1.....	108
6.18	Autogenous deformation as a function of age for Portland cement pastes and mortars (The starting time of the measurement is the final setting time)...	108
6.19	Autogenous deformation as a function of age for silica fume cement pastes and mortars (The starting time of the measurement is the final setting time).....	109
6.20	Autogenous deformation as a function of age for fly ash cement pastes and mortars (The starting time of the measurement is the final setting time).....	109
6.21	Autogenous deformation as a function of age for BFS cement pastes and mortars (The starting time of the measurement is the final setting time).....	110
6.22	Measured and calculated autogenous deformation of Portland cement mortar (10% sand) with water binder ratio of 0.3.....	111
6.23	Measured and calculated autogenous deformation of Portland cement mortar (30% sand) with water binder ratio of 0.3.....	111
6.24	Measured and calculated autogenous deformation of Portland cement mortar (10% sand) with water binder ratio of 0.4.....	112
6.25	Measured and calculated autogenous deformation of Portland cement mortar (30% sand) with water binder ratio of 0.4.....	112
6.26	Measured and calculated autogenous deformation of silica fume cement mortar (10% sand) with water binder ratio of 0.3.....	113
6.27	Measured and calculated autogenous deformation of silica fume cement mortar (30% sand) with water binder ratio of 0.3.....	114
6.28	Measured and calculated autogenous deformation of silica fume cement mortar (10% sand) with water binder ratio of 0.4.....	114
6.29	Measured and calculated autogenous deformation of silica fume cement mortar (30% sand) with water binder ratio of 0.4.....	115
6.30	Measured and calculated autogenous deformation of fly ash cement mortar (10% sand) with water binder ratio of 0.3.....	116

6.31	Measured and calculated autogenous deformation of fly ash cement mortar (30% sand) with water binder ratio of 0.3.....	116
6.32	Measured and calculated autogenous deformation of fly ash cement mortar (10% sand) with water binder ratio of 0.4.....	117
6.33	Measured and calculated autogenous deformation of fly ash cement mortar (30% sand) with water binder ratio of 0.4.....	117
6.34	Measured and calculated autogenous deformation of fly ash cement mortar (taking change of ion concentration into account) with water-binder ratio of 0.3.....	118
6.35	Measured and calculated autogenous deformation of fly ash cement mortar (taking change of ion concentration into account) with water-binder ratio of 0.4.....	118
6.36	Measured and calculated autogenous deformation of BFS cement mortar (10% sand) with water binder ratio of 0.3.....	119
6.37	Measured and calculated autogenous deformation of BFS cement mortar (30% sand) with water binder ratio of 0.3.....	120
6.38	Measured and calculated autogenous deformation of BFS cement mortar (10% sand) with water binder ratio of 0.4.....	120
6.39	Measured and calculated autogenous deformation of BFS cement mortar (30% sand) with water binder ratio of 0.4.....	121
6.40	Measured and calculated autogenous deformation of Portland cement mortar (with and without taking the change of ion concentration into account) with water-binder ratio of 0.4.....	121
6.41	Measured and calculated autogenous deformation of BFS cement mortar (with and without taking the change of ion concentration into account) with water-binder ratio of 0.4.....	122
6.42	Measured autogenous deformation of OPC concrete (Zhang et al. 2003) and calculated autogenous deformation of concrete with the extended Pickett's model (water-binder ratio: 0.3, volume fraction of aggregate: 71%).....	123
6.43	Measured and calculated relative humidity (black cross: measured relative humidity; blue line: calculated relative humidity) and capillary tension of OPC concrete (water-binder ratio: 0.3).....	124
6.44	Calculated degree of saturation and elastic modulus (with HYMOSTRUC) of OPC concrete (water-binder ratio: 0.3).....	125
6.45	Measured autogenous deformation of BFS concrete (w/b:0.44) (Mors 2011) and calculated autogenous deformation of BFS concrete with the extended Pickett model.....	126
6.46	Measured autogenous deformation of BFS concrete (w/b:0.5) (Mors 2011) and calculated autogenous deformation of BFS concrete with the extended Pickett model.....	126
6.47	Estimated relative humidity and capillary tension of BFS concrete with water-binder ratio 0.44 and 0.5 (Estimation based on the simulation results of Portland concrete (CEM I 42.5N) with same water-binder ratio using HYMOSTRUC).....	127
6.48	Estimated degree of saturation and elastic modulus of BFS concrete with water-binder ratio 0.44 and 0.5 (Estimation based on the simulation results of Portland concrete (CEM I 42.5N) with same water-binder ratio using HYMOSTRUC).....	128

# List of Tables

---

3.1	Ion concentration in the pore solution of a two days old Portland cement paste (Lura 2003).....	30
4.1	Mineral composition of Portland cement (% by weight).....	50
4.2	Chemical composition of materials (% by weight).....	50
4.3	Mixture composition of Portland cement paste and blended cement paste (% by weight).....	51
4.4	Mixture composition of Portland cement and blended cement (% by weight).....	57
5.1	Practical values of correction factor $k_2$ for pastes made with different binders.....	76
5.2	Measured autogenous shrinkages $\varepsilon_{0.3}$ and $\varepsilon_{0.4}$ after maximum swelling of Portland cement pastes and cement pastes with supplementary materials with water-binder ratio 0.3 and 0.4 (measurements continued up to seven days).....	86
5.3	Calculated autogenous shrinkages $\varepsilon_{0.3}$ and $\varepsilon_{0.4}$ after maximum swelling of Portland cement pastes and cement pastes with supplementary materials with water-binder ratio 0.3 and 0.4 (calculations continued up to seven days).....	86
6.1	Mixture composition of different cement pastes and mortars (% by weight).....	106
6.2	Mixture composition of different concrete (% by weight).....	123



# List of Symbols

---

## Roman lower case letters

$a$	Radius of inner sand particle	[m]
$b$	Radius of outer shell	[m]
$f_c$	Compressive strength	[MPa]
$f_{c,p}$	Compressive strength of cement paste	[MPa]
$f_{cm,28}$	Mean compressive strength of concrete at age of 28 days	[MPa]
$h$	Relative vapour pressure	[-]
$k_1$	Correction factor with respect to the type of aggregate	[-]
$k_2$	Correction factor with respect to the type of mineral admixture	[-]
$l$	Length of the sample	[m]
$m$	Change rate of activation energy	[KJ/mol]
$p$	Pressure exerted by the shrinking outer shell	[MPa]
$p^s$	Pressure exerted by the pore water	[MPa]
$p^{s'}$	Generated compressive pressure in the adsorbed water	[MPa]
$q$	Cross-section of the sample	[m <sup>2</sup> ]
$r$	Radial coordinate	[m]
$r_k$	Kelvin radius	[m]
$t$	Time	[days]
$x$	Deformation	[m]
$x_{H_2O}$	Mole fraction of the water in the pore solution	[mol/mol]

## Roman capital letters

$A$	Hamaker constant	[J]
$C_s$	Compressibility coefficient of the solid particle	[m <sup>2</sup> /N]
$D$	Distance of the two opposing surfaces	[m]
$E$	Elastic modulus	[MPa]
$E_p$	Elastic modulus of the outer shell (cement paste)	[MPa]
$E_s$	Elastic modulus of the sand particle	[MPa]
$F$	Load	[N]
$G_A$	Shear modulus of the aggregates	[MPa]
$G_p$	Shear modulus of the paste	[MPa]
$I$	Unit tensor of second order	[-]
$K_P$	Bulk modulus of the cement paste	[MPa]
$K_S$	Bulk modulus of the solid material	[MPa]
$K$	Parameter related to liquid molecular	[N/m <sup>2</sup> ]
$L$	Parameter related to correlation length	[m]
$M_a$	Amount of adsorbed water	[mol]
$N$	Number of initial cement per unit volume	[-]
$Q$	Experimental activation energy	[KJ/mol]
$R$	Universal gas constant	[J/(mol·K)]

$R_p$	Parameter of proportionality	[N/m]
$RH$	Relative humidity	[-]
$RH_K$	Relative humidity related to air-water menisci	[-]
$RH_S$	The effect of dissolved ions on relative humidity	[-]
$S_{cs}$	Chemical shrinkage ratio	[-]
$S_w$	Degree of saturation	[-]
$T$	Temperature	[K]
$V$	Volume of outer sphere	[m <sup>3</sup> ]
$V_a$	Volume of the adsorbent	[m <sup>3</sup> ]
$V_c$	Volume of cement in the sample before mixing	[m <sup>3</sup> ]
$V_{cs}$	Volume of chemical shrinkage	[m <sup>3</sup> /m <sup>3</sup> ]
$V_{ew}$	Evaporable water content	[m <sup>3</sup> /m <sup>3</sup> ]
$V_{hc}$	Volume of hydrated cement in the sample	[m <sup>3</sup> ]
$V_{hp}$	Volume of hydration products in the sample	[m <sup>3</sup> ]
$V_{hw}$	Volume of water in the sample that has reacted with cement	[m <sup>3</sup> ]
$V_{iw}$	Initial water content	[m <sup>3</sup> /m <sup>3</sup> ]
$V_m$	Molar volume of pore solution	[m <sup>3</sup> /mol]
$V_{new}$	Non-evaporable water content	[m <sup>3</sup> /m <sup>3</sup> ]
$V_p$	Pore volume of the paste	[m <sup>3</sup> /m <sup>3</sup> ]
$V_s$	Volume of the inner sand particle	[m <sup>3</sup> ]
$V_{sw}$	Specific volume of the adsorbed water	[m <sup>3</sup> /g]
$V_w$	Volume of water in the sample before mixing	[m <sup>3</sup> ]
$W$	Work done during the creep	[J]
$W_{el}$	Elastic component of work done during the creep	[J]
$W_f$	Frictional component of work done during the creep	[J]
$W_m$	Molecular weight of adsorbed water	[g/mol]
$Z$	Interaction constant	[J/m]

### Greek letters

$\alpha$	Degree of hydration	[-]
$\alpha_{au}$	Coefficient related to the notional autogenous shrinkage	[-]
$\beta$	Factor in Pickett's model	[-]
$\beta_{au}$	Factor describes the relationship between shrinkage and time	[-]
$\beta_\emptyset$	Factor in extended Pickett's model	[-]
$\gamma$	Surface tension of the liquid	[N/m]
$\delta_r$	Change of radius of the outer shell	[m]
$\delta_{r,cr}$	Time-dependent part of the change of radius of the outer shell	[m]
$\delta_{r,el}$	Elastic part of the change of radius of the outer shell	[m]
$\varepsilon$	Total deformation	[m/m]
$\varepsilon_{au}$	Autogenous shrinkage	[m/m]
$\varepsilon_{au,\infty}$	Ultimate autogenous shrinkage at a given w/c ratio	[m/m]
$\varepsilon_{cr}$	Time-dependent deformation	[m/m]
$\varepsilon_{el}$	Elastic deformation	[m/m]
$\varepsilon_{nau}$	Notional autogenous shrinkage coefficient	[m/m]
$\varepsilon_p$	Strain in the radial direction caused by the pressure	[m/m]

$\varepsilon_{sh,a}$	Shrinkage of the aggregates	[m/m]
$\varepsilon_{sh,c}$	Shrinkage of concrete	[m/m]
$\varepsilon_{sh,m}$	Shrinkage of mortar	[m/m]
$\varepsilon_{sh,p}$	Shrinkage of paste	[m/m]
$\eta$	Structurally dependent parameter	[m <sup>2</sup> /N]
$\kappa$	Biot coefficient	[-]
$\kappa_D$	Debye length	[m]
$\lambda$	Curve-fit parameter	[-]
$\vartheta$	Poisson's ratio	[-]
$\vartheta_p$	Poisson's ratio of the outer shell (cement paste)	[-]
$\vartheta_s$	Poisson's ratio of sand particle	[-]
$\Pi$	Disjoining pressure	[MPa]
$\Pi_e$	Electrostatic term	[MPa]
$\Pi_s$	Structural term	[MPa]
$\Pi_v$	Van der Waals term	[MPa]
$\rho$	Unit weight of the cement paste or concrete	[N/m <sup>3</sup> ]
$\sigma$	Applied stress	[MPa]
$\sigma_{cap}$	Capillary tension	[MPa]
$\sigma_e$	Effective stress	[MPa]
$\sigma_r$	Normal stress in the radial direction	[MPa]
$\sigma_t$	Normal stress perpendicular to the radius	[MPa]
$\tau$	Time at loading	[days]
$\tau_p$	Time parameter	[days]
$\Phi_A$	Volume ratio of sand/aggregate	[-]
$\varphi$	Fitting coefficient	[-]
$\omega$	Structurally dependent parameter	[-]





# List of abbreviations

---

Al <sub>2</sub> O <sub>3</sub>	alumina oxide
BFS	blast furnace slag
C <sub>3</sub> A	tricalcium aluminate
C <sub>4</sub> AF	ferrite
CaCO <sub>3</sub>	calcium carbonate
CH	Calcium hydroxide
C <sub>3</sub> S	tricalcium silicate
C <sub>2</sub> S	dicalcium silicate
CSH	calcium silicate hydrate
LDPE	low-density polyethylene plastic
LVDT	linear variable differential transducers
OPC	ordinary Portland cement
PFA	pulverised fuel ash
PSD	particle size distribution
RH	relative humidity
rpm	round per minute
SF	silica fume
SiO <sub>2</sub>	silica dioxide
w/b	water to binder ratio
w/c	water to cement ratio



# Chapter 1

## Introduction

### 1.1 Background of this research

Portland cement was invented in the early 19th century. Since then, it has gained universal popularity and is widely used in many different fields, e.g. civil engineering. The primary application of Portland cement is concrete, that consists of Portland cement paste and aggregate (sand and gravel). It is a strong and durable building material used for most of the infrastructures such as buildings, roads, bridges, towers, dams and underground structures.

Designers of concrete structures have traditionally focused on the strength characteristics of the material. In recent decades the durability of infrastructures has become a more and more important issue. Many structures are in serious need of repair, retrofitting or replacement after a certain period of time. It would be a real step forward if concrete structures can serve for a long period without repair and with only minimum maintenance. Therefore, the durability of concrete is now considered as important as the structural safety.

There are many factors affecting the durability of cementitious materials. Among these factors, cracking is a serious problem. Cracks may promote degradation of the concrete due to chemical and microbiological processes, sulfate attack, corrosion of reinforcing steel and alkali-silica reaction. Shrinkage is one of the major causes of cracking in concrete structures. Early-age cracking of concrete occurs due to restrained deformations. Restraint can be external, e.g. caused by adjoining structures, or internal, caused by the reinforcement (Sule 2003) or non-shrinking aggregates (Dela 2000). External restraint may cause through-cracking, while internal restraint will probably result in surface or internal microcracking.

Volume changes of concrete are caused by several factors, e.g. loss of moisture to the environment and carbonation (Figure 1.1). The paste phase undergoes internal drying of the pore system due to consumption of moisture from the pore system for hydration, known as self-desiccation. Unlike external drying that occurs from the outside of the specimen inwardly, self-desiccation occurs more or less uniformly throughout the cross section of concrete and results in autogenous shrinkage. This autogenous shrinkage causes cracking if there are external (adjoining structures) or internal (reinforcement or non-shrinking aggregates) restraints.

Although the phenomenon of autogenous shrinkage has been recognized for several decades already (Paillere et al. 1989, Tazawa et al. 1995), the mechanism behind it is not fully understood yet and no consensus has yet been reached in the scientific community on standard test methods (JCI 1999). A number of influencing factors have been investigated to get a better understanding of autogenous shrinkage. The influencing factors include the chemical compositions and physical properties of the cement, water-binder ratio, presence of supplementary cementitious materials and temperature.

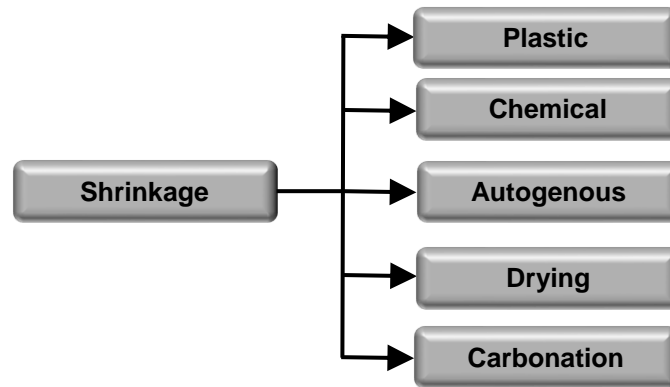


*Figure 1.1 Diagram of shrinkage types (after Holt 2001)*

Given the increasing utilization of high-performance concrete, containing supplementary cementitious materials and produced with a low water-cement ratio, quantifying autogenous shrinkage of cementitious systems becomes more and more important for controlling premature cracking in concrete structures. In the past few decades, internal self-desiccation has been considered as the major cause of early-age autogenous deformation. A few simulation models were built based on this theory (Powers 1965, Koenders 1997, Bentz et al. 1998, Lura 2003, Wei et al. 2011). In those simulation models, cementitious systems were considered elastic materials, and autogenous shrinkage was modelled as a function of the internal relative humidity. However, simulations often show discrepancies between the measured and calculated autogenous deformations. At later ages these discrepancies become more pronounced (Lura 2003). A few researchers believed that these discrepancies are caused by the time-dependent behavior of the material, i.e. creep (Hua et al. 1995, Person 1999, Lura 2003, Gawin et al. 2007).

In this study creep is assumed to play an important role in autogenous shrinkage of hydrating cement paste indeed and should not be neglected. Many mechanisms of creep and creep-promoting factors have been proposed in the past few decades (Neville et al. 1983, Gilbert 1988), e.g. viscous flow and microcracking. Although no single theory proposed so far describes the creep phenomena comprehensively, the mechanisms proposed in the past have one thing in common: they are all related predominantly to the microstructure and water content of the cement paste and to changes thereof (Lokhorst et al. 1997).

Simulation of autogenous shrinkage of cement *paste* is the first step to predict the autogenous shrinkage of *mortar* and *concrete*. Shrinkage of the cement paste in hardening mortar or concrete is restrained by the stiff, non-shrinking sand and aggregate particles. Measured shrinkage of mortar or concrete is, in fact, the result of the shrinking cement paste and the interaction between the inert inclusions and cement paste. Taking the restraining effect of rigid aggregate particles into consideration, autogenous deformation of mortar or concrete mixtures could be predicted from the autogenous shrinkage of the cement paste.

## 1.2 Objective of this research

The main aim of this research is to get a better understanding of the mechanism of self-desiccation shrinkage, the role that time-dependent behavior of cement paste plays on

autogenous shrinkage and the influence of supplementary materials on autogenous shrinkage.

The objectives of this research are listed as follows:

1. To investigate the role of creep plays on autogenous shrinkage of Portland cement pastes and Portland cement pastes blended with different supplementary materials.
2. To investigate the effect of rigid inclusions (sand and aggregate) on the time-dependent behaviour of heterogeneous mixtures, i.e. mortar and concrete.

### 1.3 Research strategy of this study

The strategy to achieve the objectives of this research is described below:

Autogenous shrinkage of cement pastes and Portland cement pastes blended with different supplementary materials will be studied experimentally and numerically. Hardening cementitious material is considered as a system that is internal loaded by capillary stress. This load is supposed to generate elastic deformation followed by time-dependent deformation. The elastic deformation and the time-dependent deformation together determine the magnitude of autogenous shrinkage. Due to the different early-age properties, e.g. internal relative humidity, ion concentration and elastic modulus, the autogenous shrinkage of different cement pastes are different. The influence of these early-age properties on the autogenous shrinkage will be studied by simulation. In the simulation the elastic and time-dependent part of autogenous shrinkage are calculated separately. The time-dependent part of autogenous shrinkage is simulated with formulas based on the activation energy theory. The simulated autogenous shrinkage of different cement pastes will be compared with experimental results to evaluate the simulation.

Autogenous shrinkage of cement mortar<sup>1)</sup> with fine sand (0.125~0.25 mm) will be studied experimentally and numerically. The restraining effect of rigid sand on the shrinking mortar will be simulated by a numerical model. This numerical model also takes the time-dependent behaviour of heterogeneous mixtures, i.e. mortar, into account. The simulated autogenous shrinkages of different cement mortars will be compared with the experimental results to evaluate the proposed numerical model. This model will be also used to simulate the autogenous shrinkage of concrete with larger aggregate particles and higher aggregate volume ratio.

### 1.4 Scope of the research

In this thesis, autogenous shrinkage of hydrating cementitious systems is studied with following restrictions:

1. Only mixtures made with ordinary Portland cement (CEM I 42.5N), silica fume, fly ash and blast furnace slag cement (CEM III 42.5N) were studied.
2. Mixtures with water-binder ratios of 0.3 and 0.4 were considered.

---

1) Fine sand <0.25 mm has also been denoted as fillers. In this thesis, cement paste with fillers is defined as mortar (see also in standard ASTM C144-17 (ASTM 2004)).

3. Only cement paste and mortar with fine sand (0.125~0.25 mm) were experimentally studied.
4. In the mortar mixtures quartz micro-sized sand with the size of 0.125~0.25 mm was added at an amount of 10% and 30% by weight.
5. The autogenous shrinkage of cement paste and mortar were studied at a constant temperature of 20°C. The effect of temperature on autogenous shrinkage was not taken into consideration.
6. Study of autogenous shrinkage focuses on the period from final setting up to 28 days.

## 1.5 Outline of the thesis

This thesis consists of seven chapters. The structure is shown in Figure 1.2.

- General introduction and literature survey (chapter 1 and chapter 2)
- Study of autogenous shrinkage of cement paste, which includes the presentation of the simulation model (chapter 3), experimental research (chapter 4) and evaluation (chapter 5)
- Numerical and experimental study of autogenous shrinkage of cement mortar and concrete (chapter 6)
- Discussion and conclusions (chapter 7)

Chapter 1 gives a general introduction including the background, objective, scope and outline of this research.

Chapter 2 provides a literature review on early-age macroscopic expansion, chemical shrinkage, microstructure and porosity, internal driving forces of autogenous shrinkage, properties and influences on autogenous shrinkage of supplementary materials and existing analytical expressions and formulae of autogenous shrinkage.

In Chapter 3 a simulation model for autogenous deformation that includes an elastic part and a time-dependent part is proposed. Self-desiccation of hydrating cement paste is considered as the main cause of the occurrence of autogenous shrinkage.

In Chapter 4 the experimental work conducted in this research and the results of autogenous shrinkage tests are presented in detail. It covers the determination of final setting time, non-evaporable water content, chemical shrinkage, internal relative humidity, compressive strength and autogenous shrinkage. Information on materials and mixture design is provided.

In Chapter 5 measurements of early-age properties of cement pastes, presented in Chapter 4, are used as input for the proposed simulation model of autogenous shrinkage. The calculated autogenous shrinkage of different cement pastes is compared with the experimental result.

In Chapter 6 autogenous shrinkage of hardening mortar and concrete is calculated based on the autogenous shrinkage of the cement paste. An existing numerical model, developed by Pickett for drying shrinkage of concrete, was extended to take the effect of creep into consideration. The simulation is validated by experimental results.

In Chapter 7 general conclusions and recommendations for further work are presented.

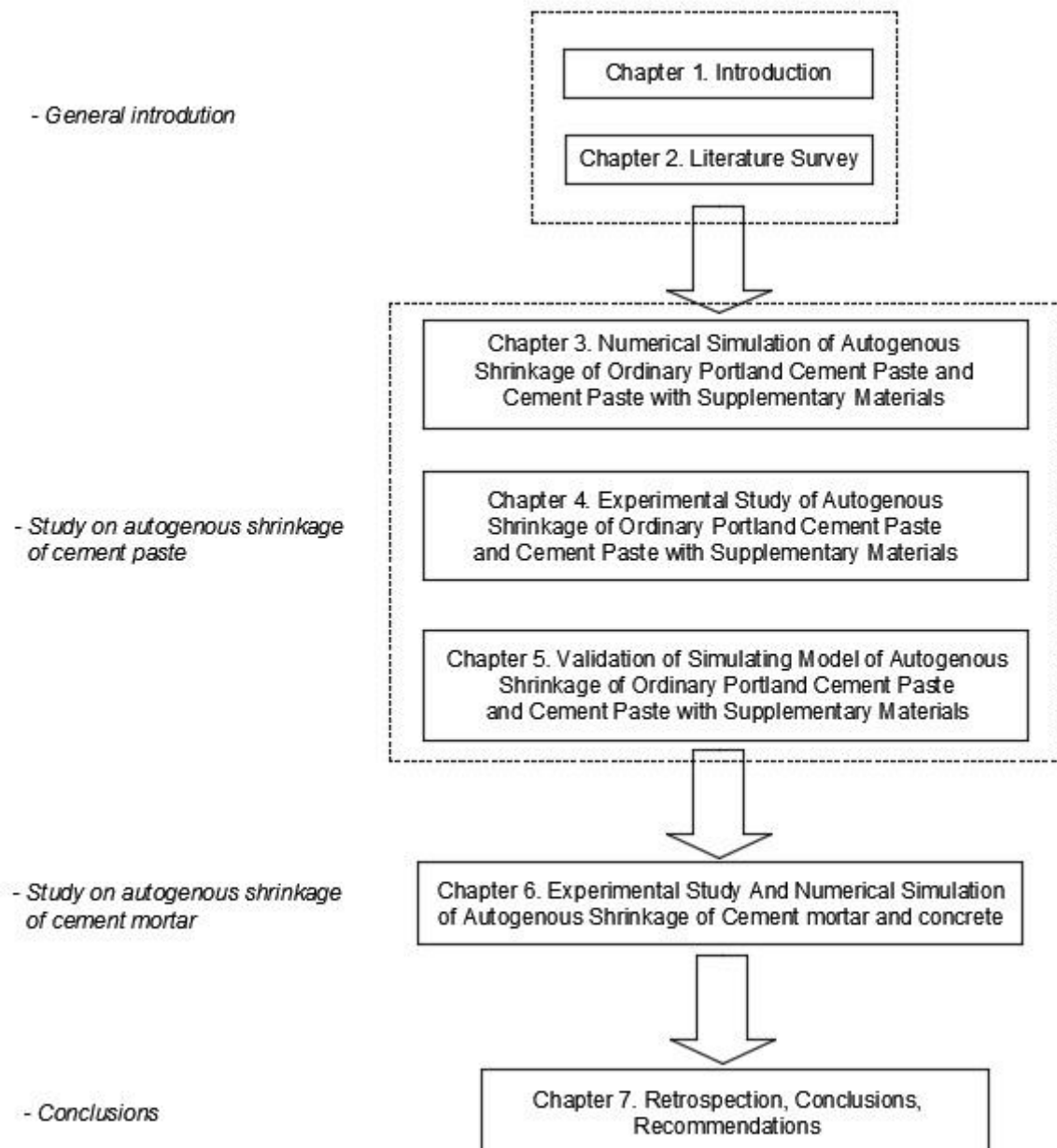


Figure 1.2 Scheme of this thesis





# Chapter 2

## Early-Age deformation of cement paste and concrete - A Literature Survey

### 2.1 Introduction

In this chapter, a brief overview of the most important aspects of early-age deformations of cement-based materials will be given. First, hydration, microstructure formation and self-desiccation of Portland cement paste are briefly discussed. Second, the phenomenon ‘early-age deformation’ is described. Early-age deformations observed on macroscale are often the result of two competing processes, i.e. early-age expansion and shrinkage. These two processes are reviewed separately in this chapter. Third, proposed mechanisms for autogenous shrinkage are briefly discussed. Numerical models based on these proposed mechanisms are also presented. Fourth, the existing analytical expressions and formulae of autogenous shrinkage used in engineering practice are reviewed. Finally, concluding remarks are made.

### 2.2 Hydration and formation of microstructure

The reaction of Portland cement with water is called hydration. During the hydration process a number of complex chemical reactions take place and a solid skeleton is formed. The absolute volume of hydration products is less than the total volume of unhydrated

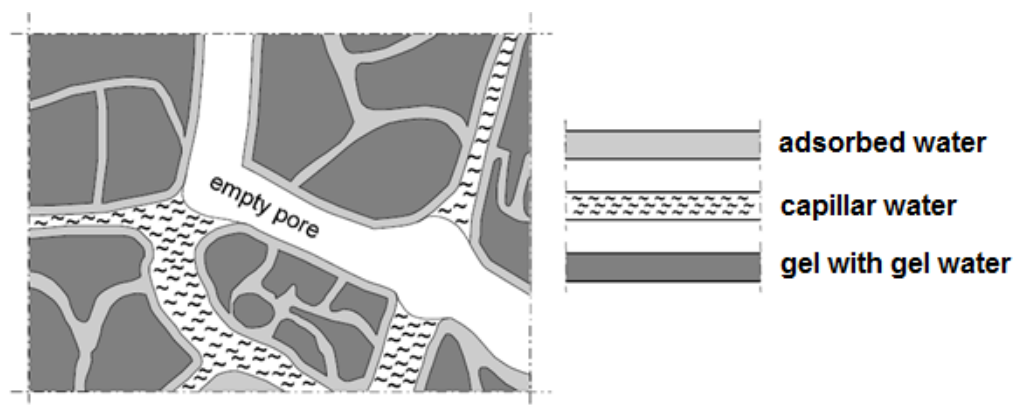


*Figure 2.1 Schematic view of state of self-desiccation of a cement paste (van Breugel 1991, Lura 2003)*

cement and water before hydration. This phenomenon is called chemical shrinkage. Due to chemical shrinkage, empty pores are created in the paste and air-water menisci are formed as illustrated in Figure 2.1. This process is called self-desiccation. The early-age volume change of cement paste and concrete is related to self-desiccation and is called autogenous shrinkage.

### 2.2.1 Hydration process

The hydration process of cement is a transformation of a system from a high energy state to a lower one, which develops with liberation of heat (Mindess et al. 1981). Measuring the heat of hydration provides information about the chemical reactions of the cement during hydration. Based on a typical heat evolution curve (Figure 2.2), hydration of Portland cement can be divided into four stages: pre-induction period, dormant stage, acceleration stage and post-acceleration stage (Mindess et al. 1981). During hydration cement particles become interconnected and a solid skeleton is formed. The water-cement system evolves from a colloidal suspension in water to a partially saturated porous solid. Along with the formation of a microstructure the state of water and the external volume change.

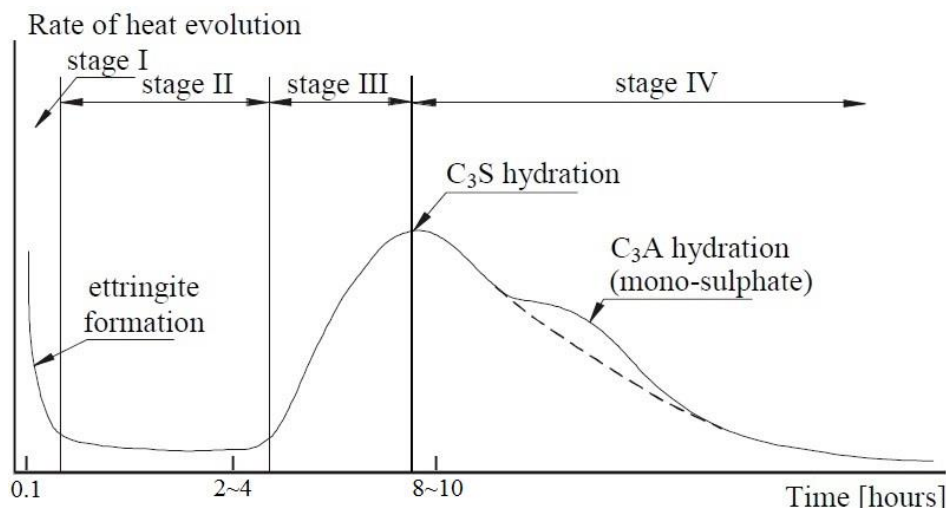


Figure 2.2 Rate of heat evolution during the hydration of Portland cement (after Mindess et al. 1981)

### 2.2.2 Microstructure and porosity

Hardening cement paste is a porous system in which the formation of the pore structure depends on the hydration process and the water-cement ratio. Supplementary materials also have an influence on the microstructure and porosity. For example, slag cement pastes have a finer pore structure than Portland cement pastes (Berodier 2015). Several researchers have proposed classifications of pore size (Powers et al. 1959, Mindess et al. 1981, Jennings 2004). Generally adopted classes are: gel pores, capillary pores and air voids. The finest pores, ranging from approximately 0.5 nm to 10 nm, are called gel pores. They constitute the internal porosity of the C-S-H gel phase. The larger pores, ranging from 10 nm to 10

$\mu\text{m}$ , are the residual unfilled spaces between cement grains and are defined as capillary pores. Pores bigger than  $100 \mu\text{m}$  are denoted as air voids.

### 2.2.3 State of water

In a hydrating water-cement system water is present in roughly three different forms, i.e. chemically bound water, physically bound water and capillary water. Chemically bound water is considered part of the C-S-H gel. For completely hydrated cement, an amount of water of about 22-23% of the weight of the anhydrous cement is chemically bound (Powers et al. 1948). The amount of physically bound or adsorbed water depends on the relative humidity in the pore system. The thickness of the adsorbed water layers ranges from 1 monomolecular water layer (about  $2.76 \text{ \AA}$ ) at 20% RH to about 6 monomolecular layers at 100% RH (Hagymassy et al. 1969, Setzer 1977, Badmann et al. 1981), as shown in Figure 2.3. Capillary water is the total water volume minus the adsorbed water. The amount of capillary water strongly depends on the relative humidity in the pore system.

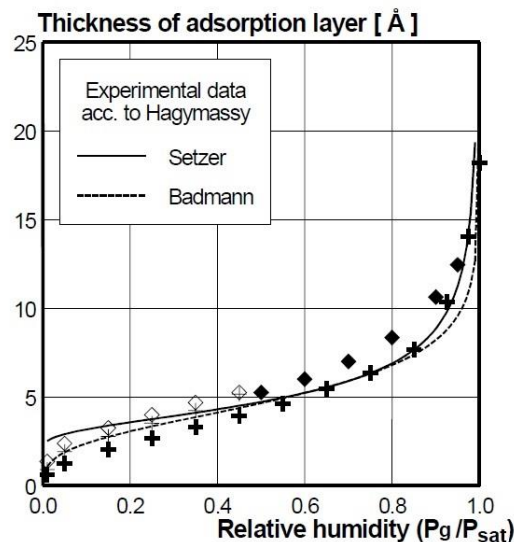


Figure 2.3 Thickness of adsorption layer of water as a function of relative humidity (Hagymassy 1969)

## 2.3 Early-Age deformation of cement paste and concrete

Early-age deformations of concrete receive increasing attention because of their effect on durability of concrete structures. As shown in Figure 2.4 early-age deformations can be expansion or shrinkage. In fact, the external volume changes observed on the macro-scale are the result of expansion and shrinkage processes, which develop simultaneously.

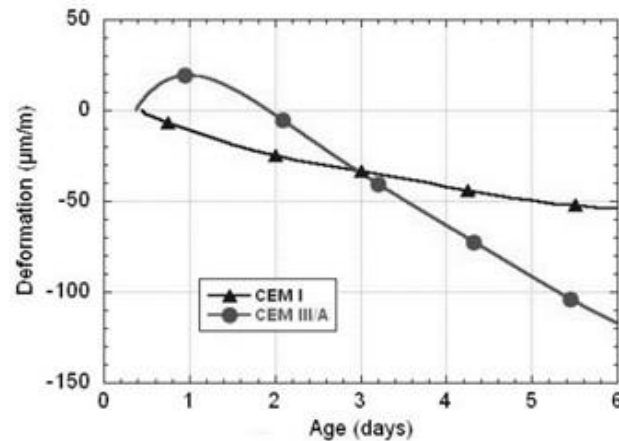


Figure 2.4 Measured autogenous deformations at 20 °C of two types of concrete (CEM I 52.5N, w/c: 0.45; CEM III/A 42.5 LA, w/c: 0.45) (Darquennes et al. 2011)

### 2.3.1 Early-age expansion

If a cement paste hydrates in saturated conditions, the reaction can go along with an external expansion, as observed already by Le Chatelier (1900). According to Neville (1995), swelling of 1000-2000  $\mu$ strain has been measured for cement pastes cured under water. In those mixtures the pore system of high water-cement ratio cement paste is supposed to remain saturated throughout hydration (Neville 1995). The effect of expansion on autogenous deformation is very important in the early stage of hydration, when the stiffness of cement paste is still very low. The expansive mechanisms act simultaneously and cause shrinkage. Several mechanisms have been proposed in the past few decades to explain this expansion, viz.:

- 1) Crystal pressure
- 2) Structure change
- 3) Shape of hydration products and the formation of ettringite

Sub 1: Crystal pressure generated by crystallization of salts in capillary pores is an important factor of the decay of rock, stone and concrete in urban areas (Erhard et al. 1972). In capillary pores filled with supersaturated solution a crystal will grow and may come into contact with a pore wall and will then stop growing, or repel the object while generating stresses. Crystal pressure may also explain the early-age expansion of cement paste. The most common solutes in the pore solution of hardening cement paste are calcium hydroxide and ettringite. According to Scherer (2002) and Steiger (2005) crystal pressure generated on the pore walls depends on the crystal size. Different formulae have been proposed to quantify crystal pressure of different crystal sizes (Scherer 2002).

Sub 2: During hydration, the macroscopic cement particles convert into a number of hydrated particles which are much smaller than the unhydrated particles (Budnikov et al. 1966). These smaller reaction products together will occupy a larger volume than the original unhydrated particle, generating an internal pressure that produces macroscopic swelling.

Sub 3: Hydration products are found with many shapes, e.g. needles, rods, tree-shaped particles (van Breugel 1991). Due to the shape of hydration products they form a spatial network and have a total surface area that is much larger than that of reactants. The repulsive forces between the solid particles will act on a growing area and will produce an expansion (Wittmann 1992). The formation of ettringite is also considered a principal cause of early-age expansion (Tezuka et al. 1986). For a discussion of mechanisms causing early-age expansion, see also Garcia (2001).

### 2.3.2 Early-age shrinkage

In recent decades the durability of infrastructures has become a more and more important issue. In this context, also early-age shrinkage has gained increasing attention. These shrinkage strains are often attributed to early-age plastic shrinkage. The primary cause of early-age plastic shrinkage is the rapid evaporation of water from the surface of the concrete. The most common solution to reduce this type of early-age volume changes is to avoid evaporation of water at the surface of the concrete by proper curing of the concrete for the first few hours after placement (Holt 2000).

Beside early-age plastic shrinkage, there are other types of shrinkage that occur at early ages without moisture exchange with the environment, e.g. chemical shrinkage and autogenous shrinkage, as shown in Figure 2.5.

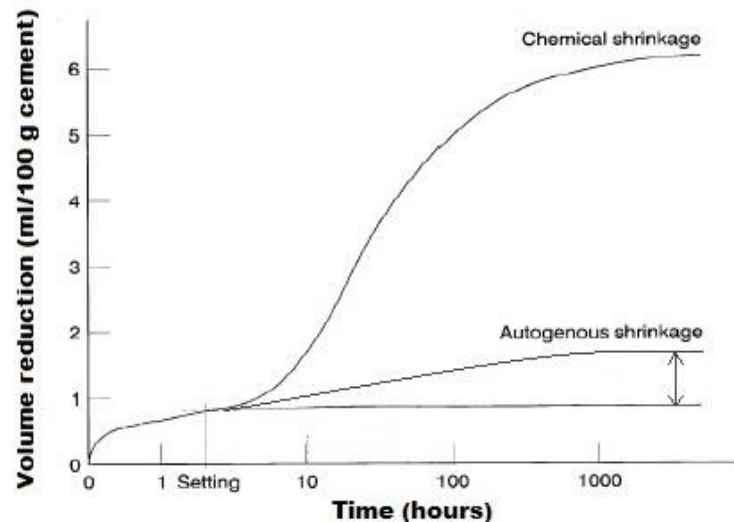


Figure 2.5 Typical results of autogenous deformation and chemical shrinkage tests (Jensen et al. 2001b)

### 2.3.3 Chemical shrinkage

Chemical shrinkage is the phenomenon that the absolute volume of hydration products is less than the total volume of unhydrated cement and water before hydration (Tazawa 1998). Chemical shrinkage amounts typically to 6-7 ml/100 g of reacted cement (Powers et al. 1948). Chemical shrinkage is described by the following equation (Tazawa 1998):

$$S_{cs} = \frac{(V_{hc} + V_{hw}) - V_{hp}}{V_c + V_w} \quad (2.1)$$

where  $S_{cs}$  [-] is chemical shrinkage ratio;  $V_c$  [m<sup>3</sup>] the volume of cement in the sample before mixing;  $V_{hc}$  [m<sup>3</sup>] the volume of hydrated cement in the sample;  $V_w$  [m<sup>3</sup>] the volume of water in the sample before mixing;  $V_{hw}$  [m<sup>3</sup>] the volume of water in the sample that has reacted with cement;  $V_{hp}$  [m<sup>3</sup>] the volume of hydration products in the sample.

The absolute value of chemical shrinkage of cement paste is hardly affected by the water-cement ratio (Gangé et al. 1999). The water-cement ratio and cement fineness will only affect the rate of the chemical shrinkage, while it does not influence the magnitude of chemical shrinkage. The final magnitude of chemical shrinkage, when the degree of hydration approaches 100%, is only influenced by the chemical composition of the cement. For a cement paste hydrating under sealed condition most of the chemical shrinkage that occurs after final setting will result in internal empty pores.

### 2.3.4 Autogenous shrinkage

Autogenous shrinkage has been known from the beginning of the 20th century (Neville et al. 1928, Lynam 1934). For a long time autogenous shrinkage has always been considered negligible compared to drying shrinkage (Tazawa 1991). In recent years, much attention is given to autogenous shrinkage due to the increasing use of concretes with low water-binder ratios. Autogenous shrinkage does not include volume change due to loss or ingress of any liquid substance, temperature variation, application of an external force and restraint (Tazawa 1998). The drop of relative humidity related to the internal empty pores is considered the major cause of autogenous shrinkage.

## 2.4 Factors affecting autogenous deformation of cementitious material

For cementitious material with different water-binder ratios and supplementary materials, the evolution of autogenous deformation can differ a lot. For the practice, autogenous shrinkage is relevant since it can cause cracking. In order to mitigate autogenous shrinkage and reduce the risk of cracking, a better understanding of the mechanism of autogenous shrinkage is needed. Factors which affect autogenous shrinkage are:

- Water-cement ratio
- Cement type, fineness and composition
- Supplementary materials
- Temperature
- Sand and aggregate

In the following these factors will be briefly discussed.

### 2.4.1 Effect of water-cement ratio

It is well known that the autogenous shrinkage of cement paste is influenced by the water-cement ratio (Hanehara et al. 1999, Feylessoufi et al. 2001, Sato et al. 1999). Mixtures with

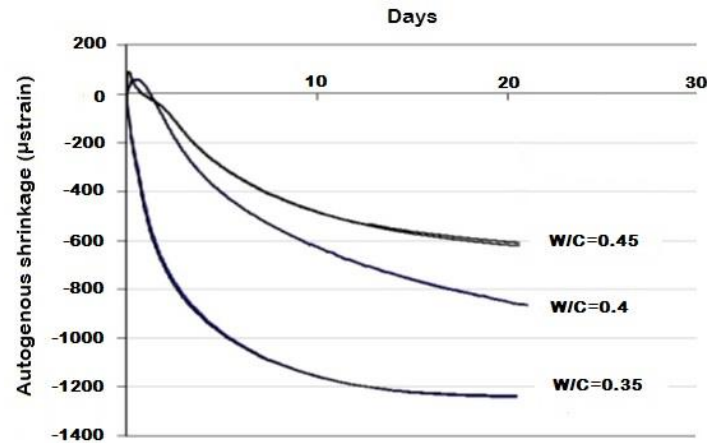


Figure 2.6 Measured autogenous deformations of ordinary Portland cement pastes at three water-cement ratios (cement paste was cast in rig and deformation was measured by LVDT) (Wei 2008)

low water-cement ratio exhibit a relatively large autogenous shrinkage, as shown in Figure 2.6. The larger autogenous shrinkage of mixtures with low water-binder ratio can be attributed to less free capillary water and lower relative humidity in cement paste with low water-binder ratio.

#### 2.4.2 Effect of cement type, fineness and composition

The type and composition of cement affect autogenous shrinkage. According to Tazawa et al. (1995) the hydration of  $C_3A$  and  $C_4AF$  plays an important role in autogenous shrinkage of cement paste. The hydration of  $C_3A$  and  $C_4AF$  result in ettringite formation and consequently expansion (Beaudoin et al. 1991, Tazawa et al. 1995). The higher the  $C_3A$  and  $C_4AF$  contents in the cement, the lower the autogenous shrinkage of cement paste will be.

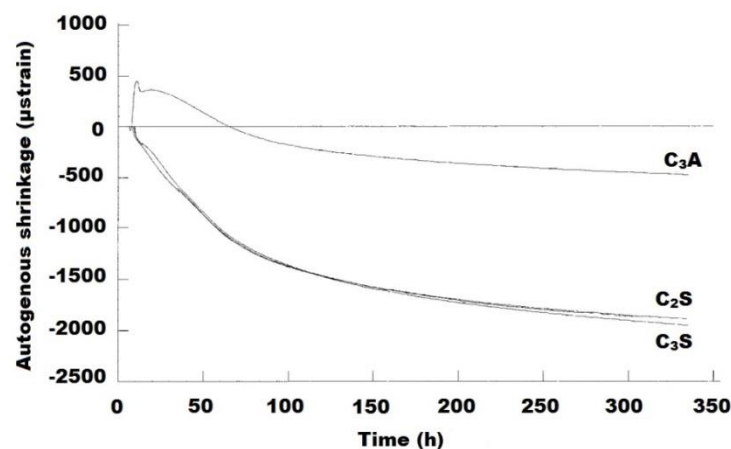


Figure 2.7 Autogenous shrinkage of different mineral compositions of Portland cement (Jensen 2000)

Park et al. (1999) reported that the autogenous shrinkage of ordinary Portland cement mixture is higher than that of high-belite Portland cement mixture with the same water-cement ratio. One of the reasons for this is that high-belite Portland cement has less  $C_3A$ . Jensen (2000) examined autogenous shrinkage of different mineral components of Portland cement, as shown in Figure 2.7. This Figure shows that the autogenous shrinkage of  $C_3A$  is much lower than that of  $C_2S$  and  $C_3S$  at the same curing age.

Besides the composition of cement also the fineness will affect autogenous shrinkage. It is shown experimentally that the cements with finer grain size cause greater autogenous shrinkage than those with coarser grains (Tazawa et al. 1995, Bentz et al. 2001, Bentz et al. 2004).

### 2.4.3 Effect of supplementary materials on autogenous shrinkage

A composite cement is a cement composed of Portland cement and one or more inorganic materials that take part in the hydration reaction and have a substantial contribution to the hydration product (Taylor 1992). Composite cements are used for various reasons. Utilizing waste materials and decreasing overall energy consumption in the process of cement production are two often mentioned reasons (Taylor 1992). Today, ground granulated blast furnace slag, pulverized-fuel ash (fly ash) and micro-silica (condensed silica fume) are the three most commonly used supplementary materials.

#### 2.4.3.1 Blast furnace slag

Blast furnace slag is formed from liquid at 1350-1550°C in the manufacture of iron (Taylor 1992). It is a mixture of lime, silica and alumina, the same oxides found in Portland cement, but not in the same proportions. Hardened blast furnace slag cement pastes have a finer pore structure and lower permeability compared to Portland cement pastes (Roy et al. 1982). The fine pore structures are the consequence of the dissolution of the calcium hydroxide crystals and the precipitation of pozzolanic C-S-H. There are indications that BFS cement

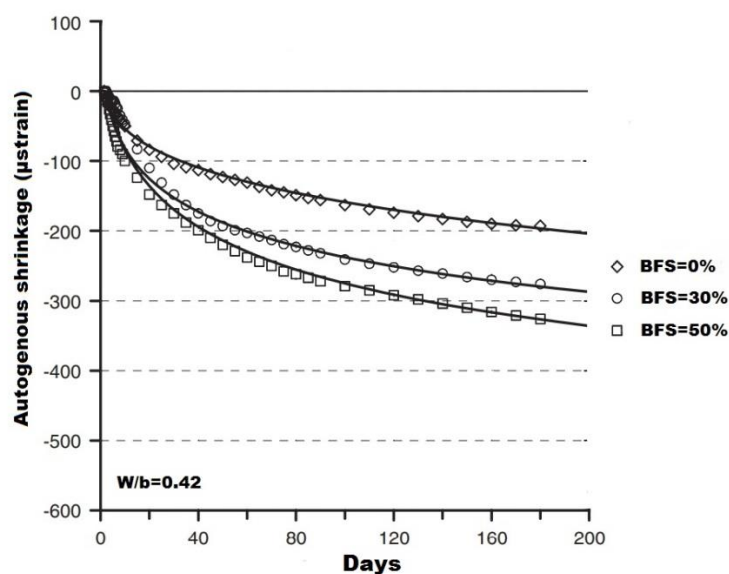


Figure 2.8 Autogenous deformation of different concretes containing 0%, 30% and 50% blast furnace slag ( $w/b=0.42$  and aggregate weight ratio = 0.8) (Lee et al. 2006)



pastes have larger autogenous shrinkage than Portland cement pastes (Figure 2.8) (Hanehara et al. 1999, Lee et al. 2006). Chan et al. (1999) showed that autogenous deformation of concrete with 40% blast furnace slag is significantly higher than that of concrete without blast furnace slag. Lee et al. (2006) attributed this phenomenon to the greater chemical shrinkage and finer pore structure of the concrete with blast furnace slag than concretes without slag.

#### 2.4.3.2 Fly ash

Fly ash, also called pulverised fuel ash (PFA), is a by-product of the combustion of coal in power plants in a temperature range of 1300 -1500°C. The fly ash particles are more or less spherical and range in diameter from less than 1  $\mu\text{m}$  to about 200  $\mu\text{m}$  (Fraay 1990). Fly ash is widely applied as a reactive mineral admixture in Portland cement concrete to improve its long-term properties and prolong the service life of concrete structures (Malhotra 1999, Malhotra et al. 2002). Fraay et al. (1989) found that after one year cement paste blended with 30% fly ash had a similar total porosity as Portland cement paste (reference sample). The cement paste blended with 30% fly ash had a finer pore structure and a smaller capillary porosity than the reference sample. In other words, the pozzolanic reaction of fly ash refines the pore structure of binary systems at later ages (Mindess et al. 1981, Fraay et al. 1989, Bijen 1996, Rilem report 38 2007).

Compared with ordinary Portland cement paste the addition of fly ash will decrease the autogenous shrinkage at early age (Tangtermsirikul 1999). Some researchers (Fang et al. 2011) considered the lower activity of fly ash compared to that of ordinary Portland cement as the reason why autogenous shrinkage of fly ash cement paste is smaller than autogenous shrinkage of ordinary Portland cement paste. Because of its low reactivity fly ash hydrates slower than cement and resulted in a slower decrease of the internal relative humidity and smaller shrinkage during the first 14 days, as shown in Figure 2.9 (Bentz et al. 2013).

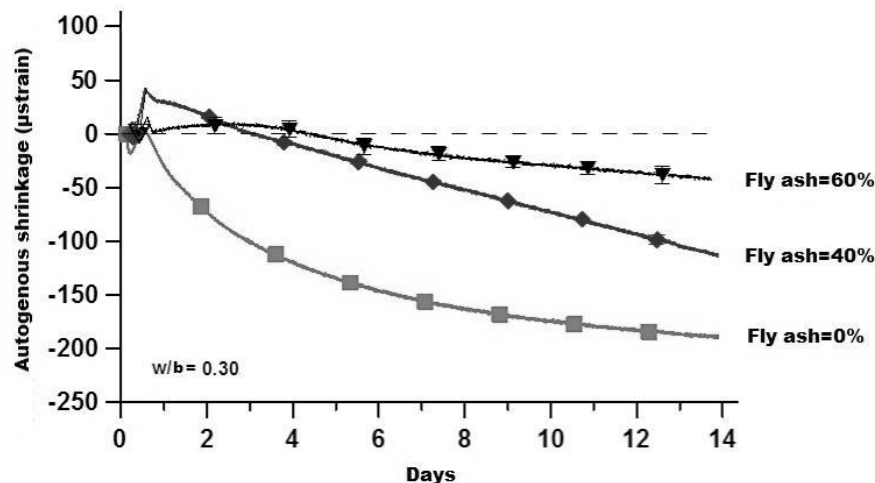


Figure 2.9 Autogenous deformation of different cement mortars containing 0%, 40% and 60% fly ash ( $w/b=0.3$  and sand weight ratio = 0.75) (Bentz et al. 2013)

### 2.4.3.3 Silica fume

Silica fume is a by-product of the production of silicon or silicon alloys. Silica fume particles are spherical, typically around 100 nm in diameter, and consist largely of glass (Taylor 1992). The main effects of silica fume on the microstructure of cement paste come from the pozzolanic reaction and the filler effect. The average silica-fume particle size (0.1  $\mu\text{m}$ ) is one order of magnitude smaller than that of cement particles. When silica fume is added to the cement paste, the total porosity of cement paste is reduced (Khan et al. 2000) and the pore structure as measured by MIP is refined (Li et al. 1996). The use of silica fume will lead to larger chemical shrinkage and autogenous shrinkage (Figure 2.10). The reaction of silica fume with calcium hydroxide results in a larger chemical shrinkage, about 22 ml/100 g compared to 6-7 ml/100 g of Portland cement (Jensen et al. 2001a). Cement pastes with silica fume show much larger autogenous shrinkage than Portland cement pastes (Jensen et al. 1996). This can be explained by the fact that the fine and well-dispersed silica fume particles accelerate cement hydration at early age (Akçay 2007).

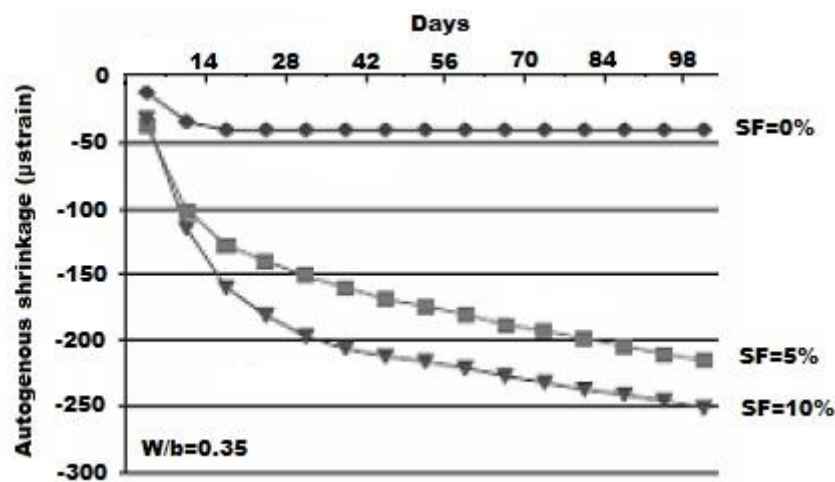


Figure 2.10 Autogenous deformation of different cement pastes containing 0%, 5% and 10% silica fume (Zhang et al. 2003)

### 2.4.4 Effect of temperature

Since the curing temperature will affect the microstructure of cement paste, the ultimate magnitude of autogenous shrinkage and the rate of autogenous shrinkage depends on the temperature. Experimental work of Bentur et al. (1979) shows that denser gel is formed at higher temperature, resulting in a coarser microstructure, i.e. a higher capillary porosity (Thomas et al. 2001). A coarser pore structure results in lower capillary tension (see Section 2.5) and self-desiccation shrinkage than that of hardening cement paste cured at lower temperature.

### 2.4.5 Effect of sand and aggregate on autogenous shrinkage

Cement mortar and concrete consists of two phases, i.e. sand/aggregate particles and the cement paste matrix. The autogenous shrinkage only takes place in the cement phase.

Autogenous shrinkage of mortar and concrete is, therefore, less than that of cement paste at the same water-cement ratio. First, because of the lower cement paste content per unit volume and, second, because of the restraining effect by aggregates (Holt 2002).

## 2.5 Mechanisms and numerical models of autogenous shrinkage

Autogenous shrinkage has been researched for decades. There is general agreement about the existence of a relationship between autogenous shrinkage and relative humidity change in the pores of the hardening cement paste. But the mechanism that causes autogenous shrinkage is still subject of debate. Three principal mechanisms of autogenous shrinkage have been proposed and a few numerical models based on these mechanisms have been developed to predict the development of autogenous shrinkage (Powers 1965, Lura 2003):

- 1) Change in the surface tension of the solid gel particles
- 2) Disjoining pressure
- 3) Tension in capillary water

### 2.5.1 Surface tension of solid particles

Surface tension results from the asymmetry of attractive forces on atoms or molecules in the vicinity of the surface of the solid (Hua et al. 1995). Surface tension of solid particles is affected by the thickness of the water layer adsorbed on solid particles. The thickness of adsorbed water is related to the internal relative humidity as shown in Figure 2.3. In general, adsorption of water causes relaxation of the surface tension of the hydration products and results in expansion. Reversely, removal of adsorbed water engenders an increase of the surface tension and the solid is compressed. Surface tension can induce compressive stresses in cement gel particles with large specific surface area of around 250 MPa (Soroka 1979) and noticeable bulk shrinkage. Only the first three layers of adsorbed water play an important role in surface tension of the solid. The effect of outer layers of adsorbed water, i.e. 4<sup>th</sup> layer and 5<sup>th</sup> etc. layer, on the surface tension of the solid is almost negligible. The linear relationship between deformation and change of the surface tension in the solid seems to hold as long as the relative humidity is below 40% (Wittmann 1977). This conclusion is also confirmed by other researchers (Powers 1965, Baron 1982, Buil 1979).

#### Numerical model - Surface tension

In hardening cement paste, the relative vapour pressure in the pore system drops due to the self-desiccation. If the relative vapour pressure changes from  $h_1$  to  $h_2$ , the change of surface tension  $\Delta\gamma$  is (Gibbs 1957):

$$\Delta\gamma = RT \int_{h_1}^{h_2} \frac{M_a}{V_a} d\ln h \quad (2.2)$$

where  $R$  [J/(mol · K)] is the universal gas constant;  $T$  [K] the temperature;  $M_a$  [mol] the amount of adsorbed water;  $V_a$  [m<sup>3</sup>] the volume of the adsorbent and  $h$  [-] the relative vapour pressure.

Based on this principle Powers (1965) derived an equation for the volume change of a solid particle:

$$\frac{\Delta V}{V} = \frac{2}{3} C_s \frac{RT}{W_m} \int_{h_1}^{h_2} \frac{M_a}{V_a} d \ln h \quad (2.3)$$

where  $C_s$  [m<sup>2</sup>/N] is compressibility coefficient of the solid particle and  $W_m$  [g/mol] the molecular weight of adsorbed water.

### 2.5.2 Disjoining pressure

The disjoining pressure is the distance-dependent pressure between two surfaces. It can be either attractive or repulsive. It is active in areas of hindered adsorption, i.e. where the distances between the solid surfaces are smaller than twice the thickness of the free adsorbed water layer, as shown in Figure 2.11.

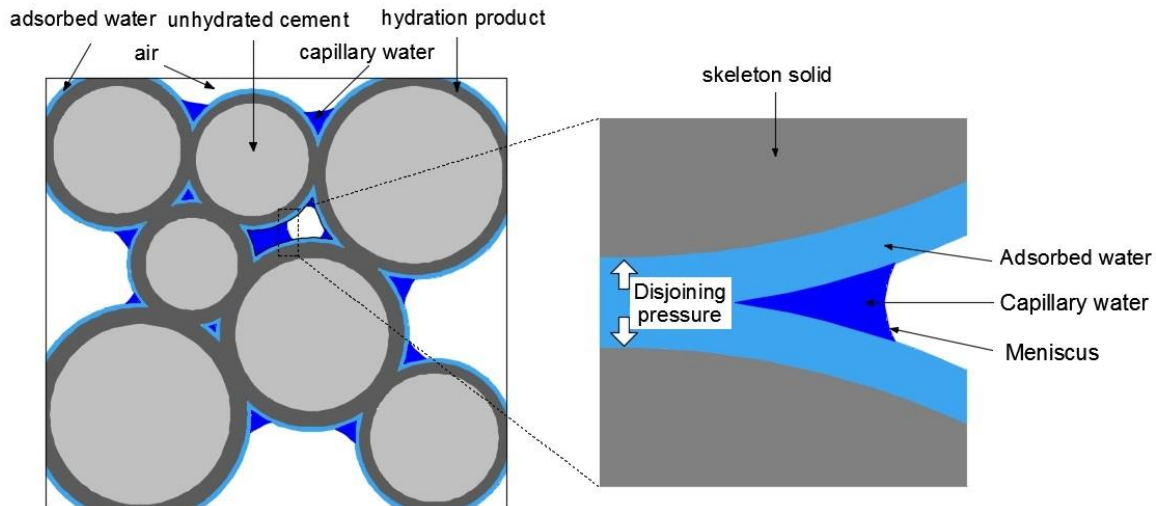


Figure 2.11 Surfaces of hindered adsorption and distribution of disjoining pressure

The disjoining pressure between the solid particles is the result of van der Waals forces, double layer repulsion and structural forces (Ferraris et al. 1987). Among these forces, van der Waals forces are always contractive, while double layer repulsion and structural forces are always repulsive. Disjoining pressure changes with the thickness of the adsorbed water layer. This thickness is determined by the relative humidity in the pore system. When the relative humidity drops the magnitude of disjoining pressure decreases, causing shrinkage of the materials. For cement-based materials, the disjoining pressure also varies with the concentration of  $Ca^{2+}$  ions in the pore fluid (Beltzung et al. 2001).

Though many researchers believe that disjoining pressure plays an important role in autogenous shrinkage, quantification of disjoining pressure is not easy. For simple geometries, it can be determined by contacting solid particles (Scovazzo et al. 2001). But for cement paste, especially for the hardening cement paste at early age, the continuously changing microstructure makes it very difficult to quantify the disjoining pressure and its associated volume changes. Moreover, at what relative humidity range disjoining pressure

is responsible for autogenous shrinkage is still a subject of debate (Hua et al. 1995, Jacob 2011). The relationship between relative humidity, ion concentration and disjoining pressure will be discussed in more detail in Chapter 3.

#### Numerical model - Disjoining pressure

A change of the relative vapour pressure in cement paste from  $h$  to  $h_0$  will cause a drop of the disjoining pressure  $\Delta\Pi$  of (Powers 1965):

$$\Delta\Pi = \frac{RT}{W_m V_{sw}} \ln h \quad (2.4)$$

where  $R$  [J/(mol · K)] is the universal gas constant;  $T$  [K] the temperature;  $W_m$  [g/mol] the molecular weight of the adsorbed water;  $h$  [-] the relative vapour pressure and  $V_{sw}$  [m<sup>3</sup>/g] the specific volume of the adsorbed water.

For the volume changes caused by disjoining pressure due to a change of the relative vapour pressure from  $h$  to  $h_0$ , Powers (1965) proposed the equation:

$$\frac{\Delta V}{V} = C_s f(M_a) \frac{RT}{W_m V_{sw}} \ln h \quad (2.5)$$

where  $C_s$  [m<sup>2</sup>/N] is the compressibility coefficient of the solid particle and  $f(M_a)$  the fraction of internal surface area over which the disjoining pressure is acting.

### **2.5.3 Capillary tension**

The capillary tension in the pore fluid is related to the water-air menisci in the partly empty pores. With the reduction in internal relative humidity, the radius of menisci between the liquid and the vapour in capillary pores decreases and the capillary tension increases. The capillary tension in the capillary pores puts the surrounding solid in compression. This compressive stress will result in a deformation of the cement paste, i.e. volume decrease. According to Soroka (Soroka 1979, Mindess et al. 1981, Bentz et al. 1998), the capillary tension mechanism for autogenous shrinkage is only effective in higher relative humidity ranges, i.e. above 45%.

#### Numerical model - Capillary tension

For the relationship between capillary tension and surface tension in the capillary water the Laplace equation applies:

$$\sigma_{cap} = -\frac{2\gamma}{r_k} \quad (2.6)$$

where  $\sigma_{cap}$  [MPa] is capillary tension;  $\gamma$  [N/m] surface tension of the liquid and  $r_k$  [m] the radius of menisci curvature.

A model that considers the cement paste as an elastic material was proposed by Bentz et al. (1998). In that model the capillary tension caused by self-desiccation was adopted as the main mechanism of autogenous shrinkage. Lura (2003) also used this model in his thesis to simulate the autogenous shrinkage of early-age cement paste. The deformation of the cement paste is calculated according to the following equation:

$$\varepsilon = \frac{S_w \sigma_{cap}}{3} \left( \frac{1}{K_p} - \frac{1}{K_s} \right) \quad (2.7)$$

where  $S_w$  [-] is the degree of saturation;  $\sigma_{cap}$  [MPa] the capillary tension that can be calculated by Equation 2.6;  $K_p$  [MPa] the bulk modulus of the whole porous body, in this case the cement paste, and  $K_s$  [MPa] the bulk modulus of the solid material.

#### 2.5.4 Discussion

The aforementioned numerical models based on proposed mechanisms have been used to predict the development of autogenous shrinkage. The reliability of these predictions, however, is not always satisfactory. Taking the capillary tension model as an example, the discrepancy between the measured and calculated autogenous deformation becomes very pronounced when the relative humidity is lower than 97%, as shown in Figure 2.12 (Lura 2003).

In the capillary tension model cement paste is considered as an elastic material and only the elastic part of autogenous shrinkage is predicted. In fact, cement paste is not ideal elastic material. When a cement paste is subjected to a sustained load, it will deform elastically and continues to deform further with time, which process is known as creep. In the early stage of hydration, when a cement paste has still an ‘open’ or ‘loose’ spatial microstructure, the framework built up by the hydration products can deform relatively easily. Powers (1965) postulated that creep will affect the autogenous shrinkage of a cement paste. Also Person (1999) and Hua et al. (1995) have pointed to the effect of creep as an important component of the deformation caused by self-desiccation. Lange (2016) found that the autogenous shrinkage of cement paste will increase further even after the internal relative humidity has reached a constant level (see Figure 2.13). Obviously, the long-term autogenous shrinkage cannot be simulated comprehensively by the capillary tension model that takes the cement paste as an elastic material. In order to predict the autogenous shrinkage more accurately, the simulation model must include two parts, i.e. elastic part and time-dependent part.

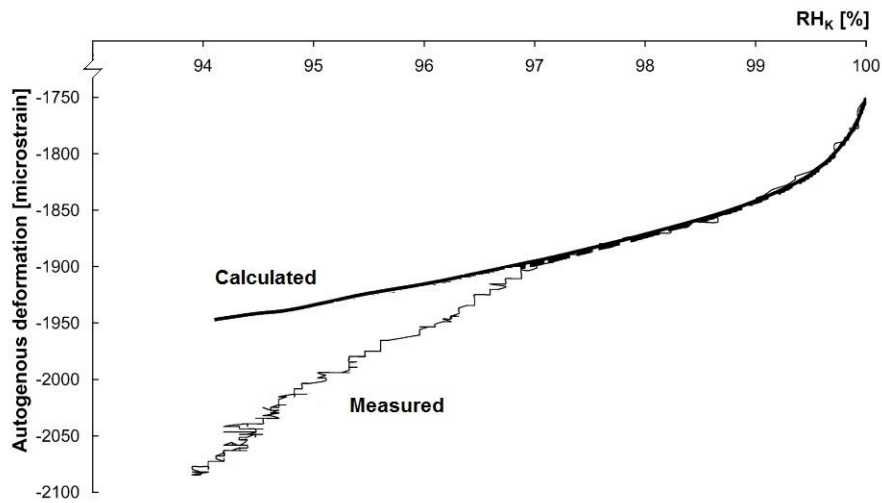


Figure 2.12 Measured and calculated autogenous deformation of Portland cement paste as a function of internal relative humidity ( $w/b=0.37$ ) (Lura 2003)

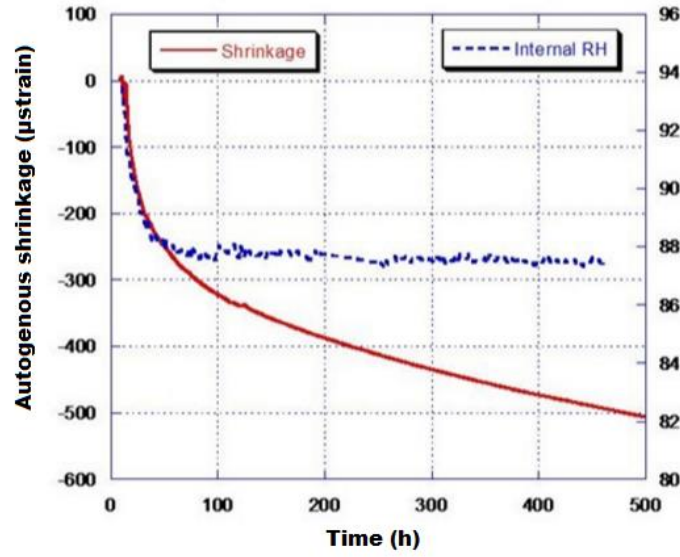


Figure 2.13 Long term autogenous shrinkage of cement paste ( $w/b=0.3$ ) (Lange 2016)

## 2.6 Analytical expressions for autogenous shrinkage - phenomenological approach

Besides the numerical models of autogenous shrinkage based on proposed mechanisms, different analytical expressions and formulae of autogenous shrinkage have been proposed for engineering practice (Naghdi 2010). Among these expressions and formulae, the empirical formulae based on experimental data, e.g. the F-H model (Hansen et al. 1977) and the Unified shrinkage model of Ya Wei (Wei et al. 2011) can be mentioned. Some are found in engineering codes, e.g. the approach in the CEB FIP MC 90 (Müller et al. 1999). Other models are based on certain specific mechanisms, such as thermodynamic models (Tazawa and Miyazawa model).

### 2.6.1 Freisleben-Hansen and Pedersen model

Freisleben-Hansen and Pedersen model, which is known as the F-H model, was proposed by Freisleben-Hansen and Pedersen (Hansen et al. 1977). This model fits a number of hydration-related processes quite well, such as the development of heat of hydration, the degree of hydration, compressive strength and elastic modulus. For autogenous shrinkage, the F-H model has been used for ordinary Portland cement paste, white cement paste and Portland cement paste blended with ground granulated blast-furnace slag. The F-H model for autogenous shrinkage can be expressed as (Note: shrinkage is positive and swelling is negative):

$$\varepsilon_{au}(t) = \varepsilon_{au,\infty} e^{-\left(\frac{\tau_p}{t}\right)^\lambda} \quad (2.8)$$

where  $\varepsilon_{au}$  is autogenous shrinkage at time  $t$ ;  $\varepsilon_{au,\infty}$  the “ultimate” value for autogenous shrinkage at a given  $w/c$  ratio;  $\tau_p$  a time parameter and  $\lambda$  a curve-fit parameter.

### 2.6.2 The CEB FIP MC 90

In order to predict autogenous shrinkage, a new approach following the CEB FIP MC 90 has been proposed by Müller et al. (1999). In this approach the total shrinkage is subdivided into autogenous shrinkage and drying shrinkage. The following factors are considered for predicting autogenous shrinkage strain: cement type, concrete age and compressive strength of concrete. According to the modified CEB-FIP Model Code 90 autogenous shrinkage can be determined as (Note: shrinkage is negative and swelling is positive):

$$\varepsilon_{au}(t) = \varepsilon_{nau}(f_{cm,28}) \cdot \beta_{au}(t) \quad (2.9)$$

where  $f_{cm,28}$  is the mean compressive strength of concrete at an age of 28 days;  $\varepsilon_{nau}(f_{cm,28})$  is the notional autogenous shrinkage coefficient and can be expressed as:

$$\varepsilon_{nau}(f_{cm,28}) = -\alpha_{au} \left( \frac{f_{cm,28}/10}{6+f_{cm,28}/10} \right)^{2.5} \cdot 10^{-6} \quad (2.10)$$

where  $\alpha_{au}$  is a coefficient which depends on the type of cement.  $\alpha_{au} = 800$  for slowly hardening cements,  $\alpha_{au} = 700$  for normal or rapidly hardening cements,  $\alpha_{au} = 600$  for rapidly hardening high-strength cements. In Equation 2.10 both the coefficient  $\alpha_{au}$  and compressive strength  $f_{cm}$  are related to the type of cement.

The factor  $\beta_{au}(t)$  in Equation 2.9 describes the relationship between the autogenous shrinkage and time and can be written as:

$$\beta_{au}(t) = 1 - \exp(-0.2 \cdot t^{0.5}) \quad (2.11)$$

### 2.6.3 Unified shrinkage model of Ya Wei

Based on experimental results, Wei et al. (2011) proposed a relationship between autogenous shrinkage development and the drop of relative humidity. The model is called Unified shrinkage model of Ya Wei and can be expressed as (Note: In Wei's model, shrinkage is positive and swelling is negative):

$$\varepsilon_{au}(t) = [6150 \cdot (1 - RH(t))] \times 10^{-6} \quad (2.12)$$

where  $RH(t)$  [-] is relative humidity in the pore system at time  $t$ .

### 2.6.4 Tazawa and Miyazawa Model

According to Tazawa et al. (1995) autogenous shrinkage of cement paste is strongly dependent on the chemical compositions of cement. It is a linear function of the shrinkage of each individual constituent, which is dependent on the degree of hydration of each component. Tazawa & Miyazawa (Tazawa et al. 1995) proposed a model that was obtained through multiple regressions of the compositions with the autogenous shrinkage measured from different types of cement at different ages. This model can be used for calculating autogenous shrinkage of Portland cement paste from its chemical compositions (Note: In Tazawa's model, shrinkage is positive and swelling is negative):



$$\begin{aligned} \varepsilon_{au}(t) = & 0.012 \cdot \alpha_{C_3S}(t) \cdot (\%C_3S) + 0.07 \cdot \alpha_{C_2S}(t) \cdot (\%C_2S) \\ & - 2.256 \cdot \alpha_{C_3A}(t) \cdot (\%C_3A) - 0.859 \cdot \alpha_{C_4AF}(t) \cdot (\%C_4AF) \end{aligned} \quad (2.13)$$

where  $\varepsilon_{au}(t)$  is autogenous shrinkage of cement paste at age  $t$ ;  $\alpha$  the degree of hydration of a cement component at age  $t$  and % the percentage of each cement component by mass.

### 2.6.5 Engineering expressions/formulae - Discussion

Analytical expressions/formulae and codes are proposed for use in engineering practice. They are based on the experimental results and used to fit the measured autogenous shrinkage. These expressions/formulae and codes do not differentiate between the elastic and time-dependent part of autogenous shrinkage. With the increase of time, the time-dependent part will play a more and more important role in autogenous shrinkage. Therefore, for long-term autogenous shrinkage, there is a discrepancy between measured and predicted results.

## 2.7 Concluding remarks

Early-age autogenous deformation is the macroscopic volume change of cementitious materials measured from the moment of final setting. In fact, it is the result of two competing processes, expansion and shrinkage. For early-age expansion, several mechanisms have been proposed, i.e. crystal pressure and the formation of ettringite. For autogenous shrinkage, a change in the surface tension of the solid gel particles, disjoining pressure and tension in capillary water are the three most proposed mechanisms. They are related to the internal relative humidity and effective in different relative humidity ranges. Simulation models based on these mechanisms consider the cement paste as an elastic material. The time-dependent part of the deformation, i.e. creep, is not considered. This simplification will lead to an underestimation of the autogenous shrinkage, particularly at later ages. Besides the mentioned numerical models for autogenous shrinkage based on the proposed mechanisms, several analytical expressions and formulae of autogenous shrinkage have been proposed by researchers in past decades for use in the engineering practice. Most of the existing analytical expressions/formulae and codes are empirical. They can only be used to simulate autogenous shrinkage of a limited number of concrete mixtures and a limited period of time.

This work aims to propose a simulation model that predicts the autogenous shrinkage more precisely. In order to achieve this aim, previously proposed mechanisms of autogenous shrinkage will be discussed in more detail, including the effect of creep. Early-age expansion will not be considered in this study.



# Chapter 3

## Mechanism and numerical simulation of autogenous shrinkage

### 3.1 Introduction

In this chapter a simulation model for autogenous deformation of early-age hardening cement paste is proposed. The mechanisms of autogenous deformation are studied first. Possible mechanisms are disjoining pressure and capillary tension. Capillary tension is considered as the driving force of the autogenous shrinkage of early-age cement paste.

A simulation model for autogenous deformation is then proposed that includes an elastic part and a time-dependent part. The time-dependent part of this model is based on the activation energy concept and extended to deal with the continuously changing physical properties of hardening cement paste. The subsequent calculation steps of the proposed simulation model are illustrated by applying the model for analysing autogenous deformation of a Portland cement paste (CEM I 42.5N) and a blast furnace slag cement paste (CEM III 42.5N). The simulations with the proposed model suggest that creep plays a substantial role in autogenous shrinkage. The accuracy of the predictions of autogenous shrinkage with the proposed simulation model will be evaluated in Chapter 5.

### 3.2 Mechanisms for autogenous shrinkage

In the past few decades many studies have been carried out on the mechanism of autogenous shrinkage. So far no consensus has been reached about the cause of autogenous shrinkage. Disjoining pressure, change in the surface tension of the solid gel particles and capillary tension are considered as the three principal mechanisms. According to Wittmann (1997) and Setzer (1996), surface tension of the solid does not play a major role when the relative humidity is higher than 50%. In early-age cement paste, the relative humidity due to self-desiccation alone does not drop below 75% (Jensen 1995). Therefore, in this thesis changes of the surface tension in solid particles will not be dealt with as a mechanism of autogenous shrinkage. Most attention will be given to disjoining pressure and capillary tension as possible cause of autogenous shrinkage.

#### 3.2.1 Microstructure of concrete

Concrete consists of cement paste matrix and aggregate as shown in Figure 3.1a. During the hydration process a number of complex chemical reactions take place in cement paste matrix, resulting in the formation of a solid skeleton. Cement paste matrix is a multi-scale porous material that comprises gel pores at the nanoscale and capillary pores at the

microscale. The finest pores, ranging from approximately 0.5 nm to 10 nm, are called gel pores. Gel pores are an intrinsic part of C-S-H gel. According to Wittmann (1976), C-S-H consists of layers of C-S-H particles and adsorbed interlayer water (Figure 3.1c). The pore space between C-S-H particles is defined as interlayer gel pores. The larger pores, ranging from 10 nm to 10  $\mu\text{m}$ , are the unfilled spaces between cement grains and are defined as capillary pores (Figure 3.1b).

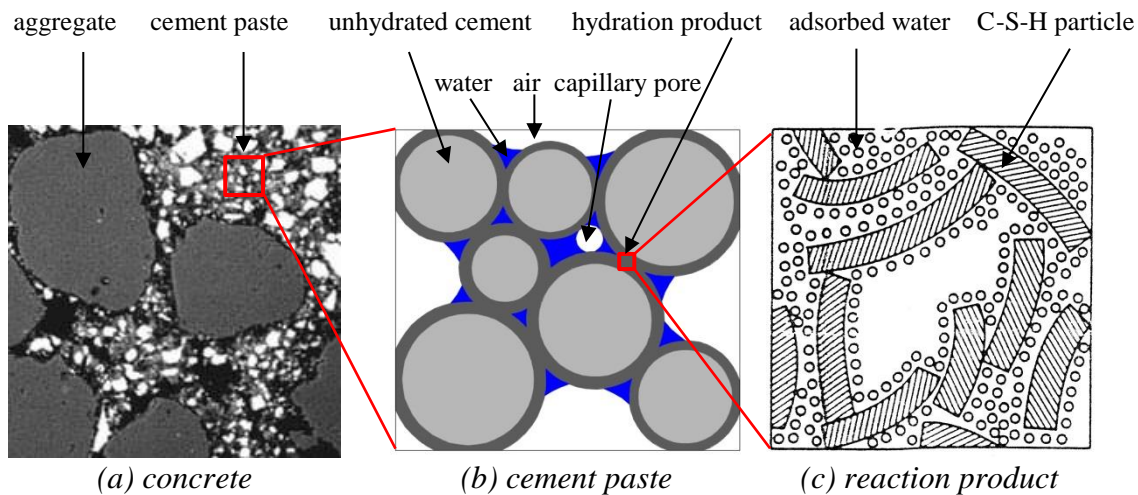


Figure 3.1 Schematic representation of the multi-scale microstructure of concrete: (a) concrete; (b) schematic microstructure of cement paste; (c) schematic microstructure of C-S-H gel (Wittmann 1976)

In Figure 3.2 an example of a measured pore size distribution of a seven days old Portland cement paste with water-binder ratio 0.3 is shown (Zeng et al. 2012). The pore

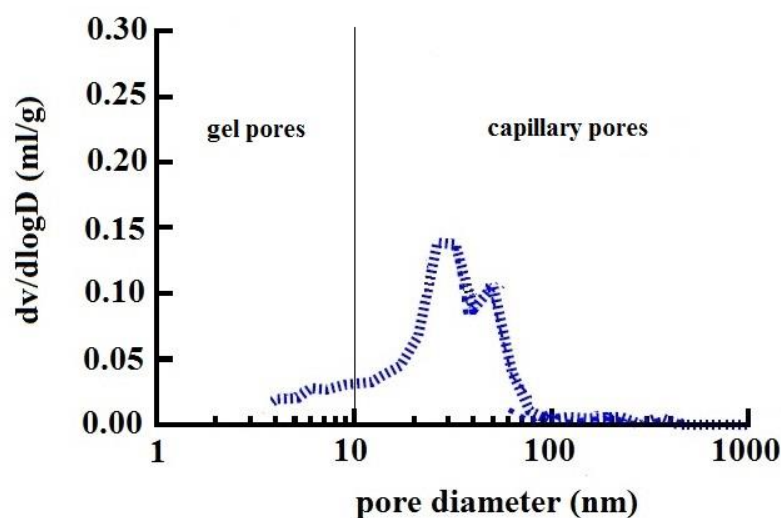


Figure 3.2 Example of differential pore size distribution of Portland cement pastes with water-binder ratio 0.3 measured by MIP at seven days (after Zeng et al. 2012)

size distribution was measured by MIP seven days after mixing. In hydrating cement paste the pore system gradually dries out and the relative humidity decreases. With the drop of relative humidity, the disjoining pressure in the gel pores and capillary tension in capillary pore increase. The disjoining pressure and capillary tension will change the shape and volume of cement paste specimen. In the following section, the disjoining pressure and capillary tension will be briefly discussed.

### 3.2.2 Disjoining pressure

Disjoining pressure in cement paste,  $\Pi(D)$  [MPa], is the interaction between two opposite surfaces across water. The pressure can be either attractive or repulsive and is distance dependent. Three different types of interacting parts constitute the disjoining pressure (Derjaguin et al. 1987): Van der Waals term (index  $v$ ), the electrostatic term (index  $e$ ) and the structural term (index  $s$ ). All three components decrease rapidly with the distance  $D$  of two opposite surfaces. Among all three types of interaction terms, the Van der Waals term is an attractive interaction. The other two components are always repulsive. The disjoining pressure can be written as:

$$\Pi(D) = \Pi_v + \Pi_e + \Pi_s \quad (3.1)$$

where  $\Pi_v$  is the Van der Waals term;  $\Pi_e$  the electrostatic term and  $\Pi_s$  the structural term.

Disjoining pressure has a significant magnitude in pores smaller than 10 nm, i.e. the gel pores. In order to study the role of disjoining pressure on the autogenous shrinkage, the calculation of the three components of disjoining pressure will be discussed in the following section.

#### 3.2.2.1 Disjoining pressure - The Van der Waals term

The Van der Waals term,  $\Pi_v$ , is the short-range *attractive* force between uncharged particles, arising from the interaction of permanent or transient electric dipole particles (Jacob 2011). It plays an important role in all phenomena involving intermolecular forces.

In a young cementitious material the pore system gradually dries out due to ongoing hydration. First the bigger pores are emptied, while the smaller pores remain filled with water. Schematically this is shown in Figure 3.3. For smaller water-filled pores (Figure 3.3a), the Van der Waals term  $\Pi_v$  per unit area between two surfaces  $s$  and  $s'$  across the water layer  $w$  can be expressed as (Jacob 2011):

$$\Pi_v = -A_{sws'}/6\pi D^3 \quad (3.2)$$

where  $D$  [m] is the distance between two opposing surfaces.  $A_{sws'}$  [J] is the Hamaker constant for surfaces  $s$  and  $s'$  interacting across the water layer  $w$ . The Hamaker constant is a material constant that determines the magnitude of the Van der Waals term between two opposite surfaces. In order to calculate the Van der Waals term in cement paste, the Hamaker constant of the C-S-H/water system is used. Note that C-S-H is not the only hydration product in cement paste. Besides C-S-H, also CH, AFm and ettringite are formed during the hydration process. The values of the Hamaker constant of CH, AFm and ettringite are different from that of C-S-H (the values of Hamaker constant of different inorganic materials vary within the range of one order of magnitude (Bergström 1997)).

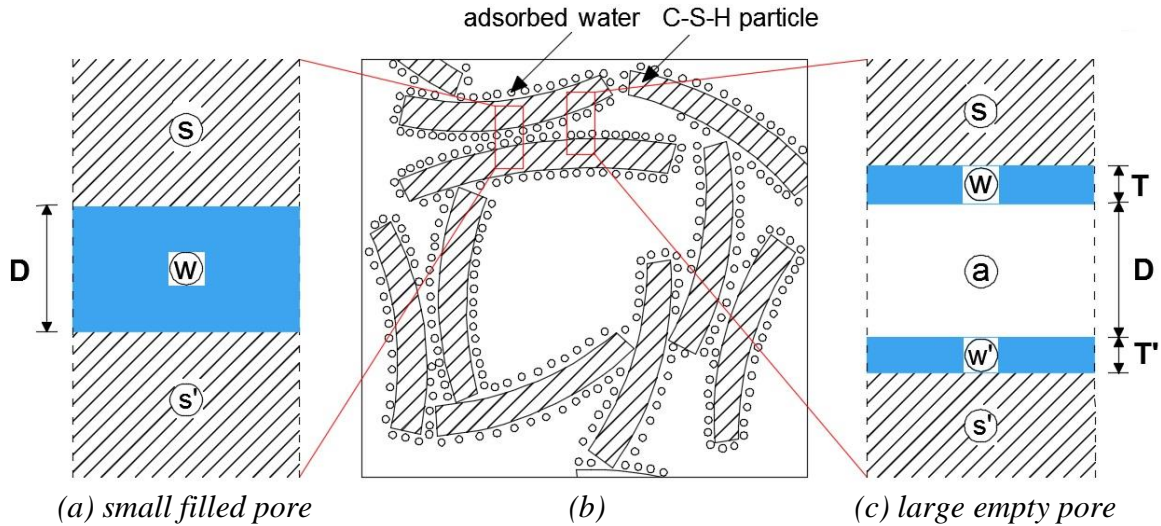


Figure 3.3 Schematic microstructure of C-S-H gel (b), geometry of two surfaces  $s$  and  $s'$  across water  $w$  (a) and geometry of two surfaces  $s$  and  $s'$  with adsorbed layers  $w$  and  $w'$  across air  $a$  (c)

Therefore, the calculation of Van der Waals term in cement paste with Hamaker constant of the C-S-H/water system is only indicative.

The Van der Waals term is dominant if the distance between surfaces is very small. These small pores are almost always water-filled. Large pores are empty, while the pore walls are covered with one or more monomolecular layers of water (Figure 3.3c). For large empty pores, the Van der Waals term  $\Pi_v$  can be calculated with another equation (For details: see Jacob's book (Jacob 2011)). In hydrating cement paste, the Van der Waals term  $\Pi_v$  in large empty pores is very small and can be neglected.

An example of the calculated Van der Waals force in water-filled pores with different pore size is shown in Figure 3.4. The calculations are carried out with Equation 3.2. In Equation 3.2 the value of the Hamaker constant of C-S-H is taken as  $10^{-20}$  J (Jonsson et al. 2004).

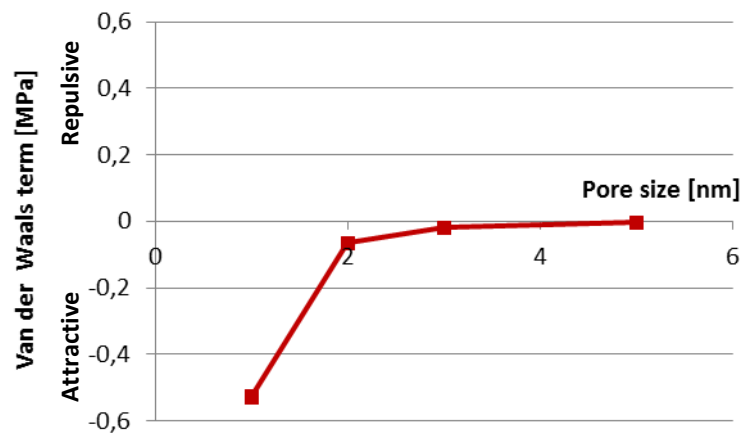


Figure 3.4 Van der Waals term vs. pore size (Equation 3.2)

Figure 3.4 shows that the Van der Waals term decreases with increasing pore size. It has a significant value in the pores smaller than 3 nm. In larger pores the Van der Waals term is close to 0 MPa.

### 3.2.2.2 Disjoining pressure - Electrostatic term

Electrostatic term,  $\Pi_e$ , is the repulsive force that exists between two opposite charged surfaces of the solid phase. The space between the opposite charged surfaces of the solid phase is filled with pore water as shown in Figure 3.5. The magnitude of the electrostatic term  $\Pi_e$  per unit area between two opposed surfaces separated by a distance  $D$  is (Jacob 2011):

$$\Pi_e = (1/2\pi\kappa_D^2)Ze^{-D/\kappa_D} \quad (3.3)$$

where  $Z$  [J/m] is an interaction constant.  $\kappa_D$  [m] is known as the Debye length. Its value depends on the properties of the pore water. For pore water containing  $NaCl$  ( $KCl$ ),  $CaCl_2$  ( $Na_2SO_4$ ,  $KSO_4$ ) and  $MgSO_4$ , Jacob gave the following formulae for calculating the Debye length  $\kappa_D$  (Jacob 2011):

$$\kappa_D = \frac{0.304}{\sqrt{[NaCl]}} \text{ nm} \quad \text{for 1:1 electrolytes (e.g. } NaCl, KCl) \quad (3.4)$$

$$\kappa_D = \frac{0.176}{\sqrt{[CaCl_2]}} \text{ nm} \quad \text{for 2:1 and 1:2 electrolytes (e.g. } CaCl_2, Na_2SO_4, KSO_4) \quad (3.5)$$

$$\kappa_D = \frac{0.152}{\sqrt{[MgSO_4]}} \text{ nm} \quad \text{for 2:2 electrolytes (e.g. } MgSO_4) \quad (3.6)$$

where  $[NaCl]$ ,  $[CaCl_2]$  and  $[MgSO_4]$  are the ion concentrations in the pore water.

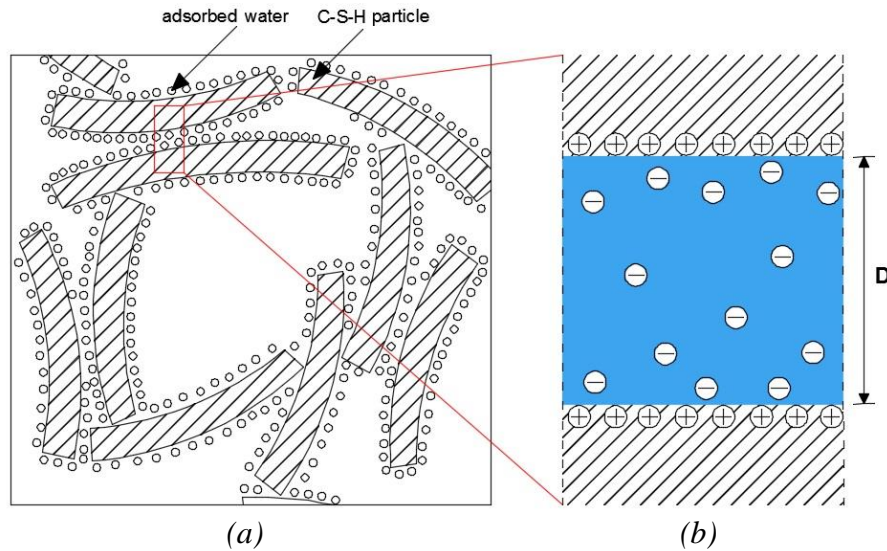


Figure 3.5 Schematic microstructure of C-S-H gel (a) and two positive charged surfaces separated a distance  $D$  in water (b) (after Jacob 2011)

An example of the calculated electrostatic term in pores with different pore size is shown in Figure 3.6. The calculation is carried out for a two days old Portland cement paste. In this thesis, the measured ion concentration of  $Na^+$ ,  $K^+$  and  $Ca^{2+}$  is shown in Table 3.1 (Lura 2003). The ion concentration of  $Ca^{2+}$  is very small compared with that of  $Na^+$  and  $K^+$  and the effect of  $Ca^{2+}$  on the electrostatic term  $\Pi_e$  can be neglected. For  $Na^+ = 1037$  mmol/l and  $K^+ = 763$  mmol/l, equation 3.4 gives a Debye length  $\kappa_D$  of 0.27 nm. According to Jacob, the interaction constant  $Z$  changes with temperature and ranges from  $5.1 \times 10^{-11}$  J/m to  $5.26 \times 10^{-11}$  J/m (Jacob 2011). In this thesis, the interaction constant  $Z$  in Equation 3.3 is taken as  $5.18 \times 10^{-11}$  J/m.

Table 3.1 Ion concentration in the pore solution of a two days old Portland cement paste (Lura 2003)

$Na^+$ [mmol/l]	$K^+$ [mmol/l]	$Ca^{2+}$ [mmol/l]
1037	763	0.316

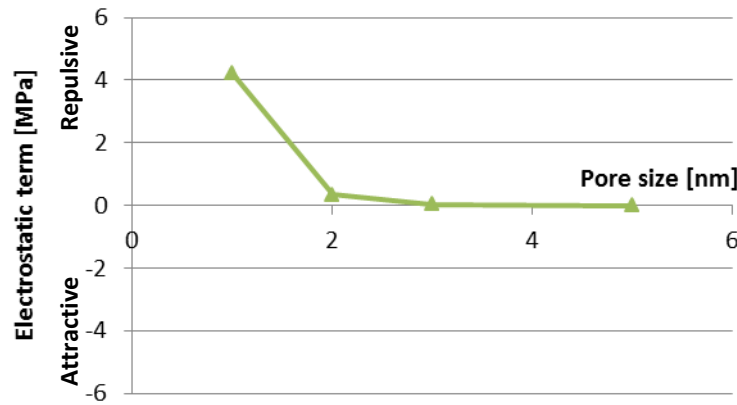


Figure 3.6 Electrostatic term vs. pore size (Equation 3.3)

Figure 3.6 shows that the electrostatic term between pore walls is repulsive. It decreases dramatically with increasing pore size. It has a substantial value in pores smaller than 3 nm.

### 3.2.2.3 Disjoining pressure - Structural term

The structural term reflects the interaction forces between neighboring particles or surfaces as a result of the overlap of boundary layers of a liquid (Churaev 1985). Schematically, this is illustrated in Figure 3.7. When the medium between the surfaces is water, the magnitude of the structural force per unit area between two flat surfaces separated by a distance  $D$  is (Churaev 1985):

$$\Pi_s = Ke^{(-\frac{D}{L})} \quad (3.7)$$

where  $K$  [N/m<sup>2</sup>] and  $L$  [m] are constant for a given system.



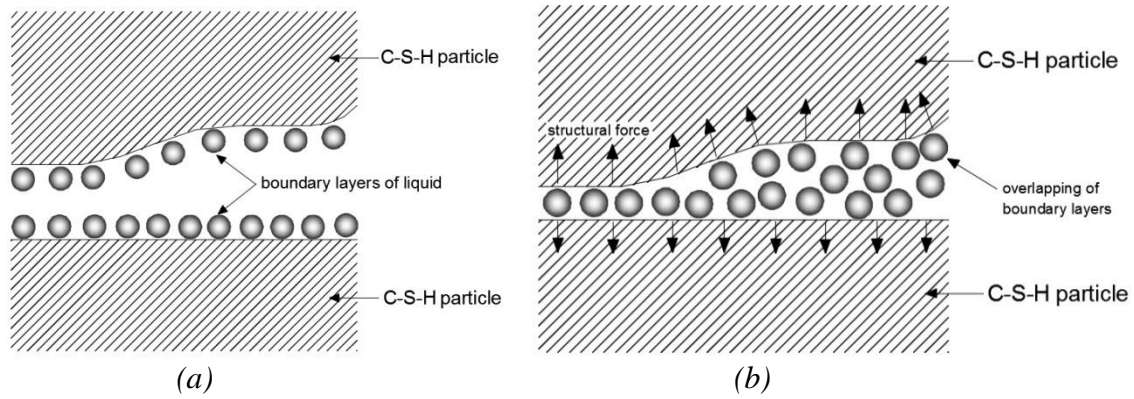


Figure 3.7 Schematic representation of mechanism of structural term of disjoining pressure (after Churaev 1985)

An example of the calculated structural term in pores with different pore size is shown in Figure 3.8. According to Churaev (1985), the parameters  $K$  and  $L$  are determined by the type of dissolved ions in the pore solution. For a two days old Portland cement paste with dissolved ions as shown in Table 3.1, the values of constant  $K$  and  $L$  in Equation 3.7 are  $10^7$  N/m<sup>2</sup> and 1 nm (Churaev 1985).

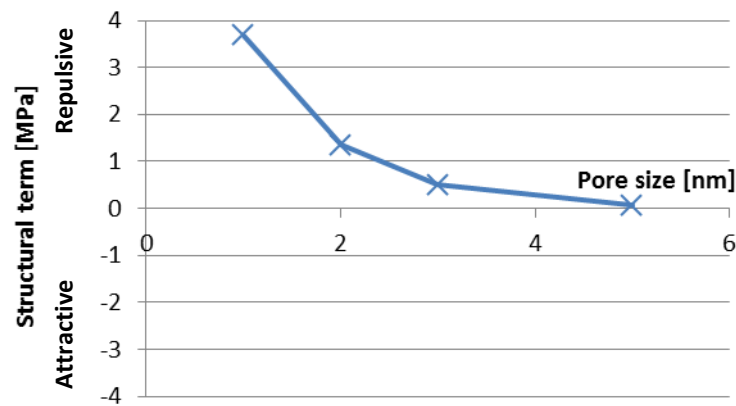


Figure 3.8 Structural term vs. pore size (Equation 3.7)

Figure 3.8 shows that the structural term between pore walls is repulsive. It decreases with increasing pore size. It has a significant value in the pores smaller than 5 nm.

#### 3.2.2.4 Calculation of disjoining pressure

If the Van der Waals term  $\Pi_v$ , the electrostatic term  $\Pi_e$  and the structural term  $\Pi_s$  are known, the resulting disjoining pressure  $\Pi$  in pores with pore sizes  $D$  in a cementitious system can be calculated with Equation 3.1. In Figure 3.9 the whole calculation procedure is shown schematically. The calculated results in previous sections are summarized in Figure 3.10.

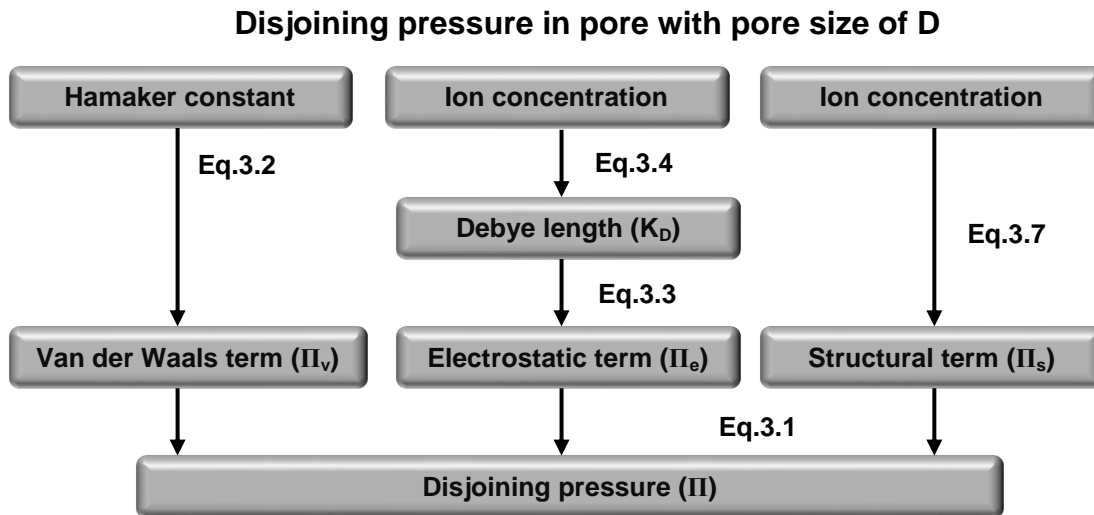


Figure 3.9 Scheme of disjoining pressure calculation

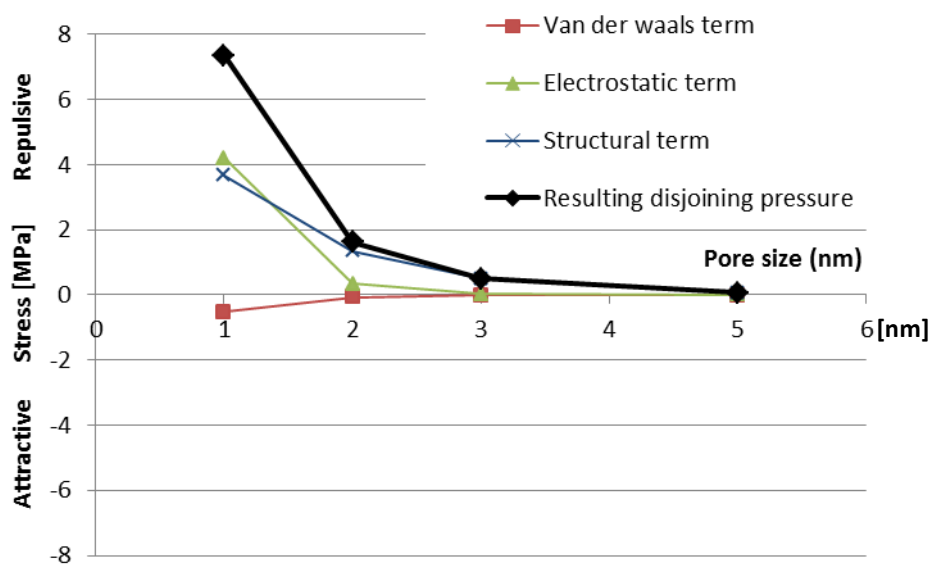


Figure 3.10 Disjoining pressure vs. pore size

Figure 3.10 shows that the calculated disjoining pressure is repulsive. This is in line with findings reported by Beltzung and Wittmann (Beltzung et al. 2005). The figure also shows that the disjoining pressure between pore walls rapidly decreases with increasing of pore size. It has a substantial value in the pores smaller than 5 nm, which are typically gel pores.

### 3.2.3 Capillary tension

The capillary tension in the pore fluid is related to the water-air menisci in the partly empty pores. With the drop of internal relative humidity, caused by self-desiccation of hydrating cement paste, the capillary tension increases. In section 2.5.3 it has been described that

capillary forces will put the solid skeleton in compression, which goes along with a decrease of the volume of the cement paste.

In the following section the relationship between capillary tension and relative humidity will be briefly discussed. For an extensive description, see Butt's paper (Butt et al. 2009)

### 3.2.3.1 Calculation of capillary tension

According to the Laplace law (Defay et al. 1966), the capillary tension  $\sigma_{cap}$  [MPa] in the pore fluid can be calculated as:

$$\sigma_{cap} = -\frac{2\gamma}{r_k} \quad (3.8)$$

where  $r_k$  [m] is the Kelvin radius and  $\gamma$  [N/m] is the surface tension of the pore solution.

### 3.2.3.2 Calculation of the Kelvin radius

In order to calculate the capillary tension with Equation 3.8, the Kelvin radius  $r_k$ , i.e. the radius of the air-water meniscus, should be known.

As a consequence of hydration, empty pores are created in the paste and air-water meniscus will form. As hydration proceeds, the internal relative humidity drops and the radius of air-water meniscus decreases. For a cylindrical pore as shown in Figure 3.11 (in this thesis the capillary pores are assumed cylindrical), the relationship between the internal

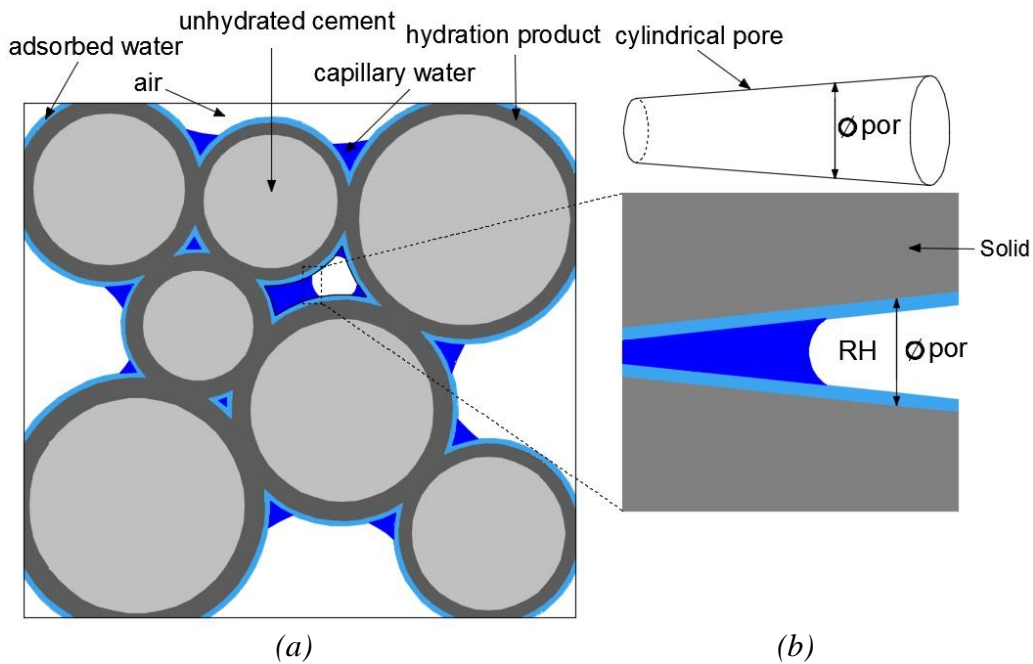


Figure 3.11 Schematic microstructure of hardening cement paste (a) and Simplified cylindrical capillary pore system (b)

relative humidity and the radius of the air-water meniscus and can be expressed as (Butt et al. 2009, Jensen 1993):

$$\frac{RH}{RH_S} = RH_K = e^{-\frac{2\gamma V_m}{r_k RT}} \quad (3.9)$$

where  $\gamma$  [N/m] is the surface tension of the pore solution;  $V_m$  [m<sup>3</sup>/mol] the molar volume of the pore solution;  $R$  [J/(mol · K)] the universal gas constant;  $T$  [K] the absolute temperature;  $RH$  the measured relative humidity;  $RH_S$  the effect of dissolved ions on relative humidity;  $RH_K$  the relative humidity related to air-water menisci.

Based Equation 3.9, the Kelvin radius can be calculated as:

$$r_k = -\frac{2\gamma V_W}{\ln RH_K RT} = -\frac{2\gamma V_W}{\ln \frac{RH}{RH_S} RT} \quad (3.10)$$

### 3.2.3.3 Relationship between internal relative humidity and dissolved ions

In order to calculate the Kelvin radius  $r_k$  with Equation 3.10, the effect of dissolved ions on relative humidity  $RH_S$  should be known.

Many researchers (Jensen et al. 1996, Bentz et al. 2001) found that the maximum values of the internal relative humidity of the cement pastes were lower than 100%. According to Raoult (in: Perrot 1998), the initial relative humidity drop can be attributed to a decrease of partial pressure of water vapour due to dissolved ions in the pore fluid. For example, for the pore solution of a two-month old cement paste with water-binder ratio 0.45, a relative humidity of 96.7% has been reported (Page et al. 1983). The 3.3% relative humidity drop is due to the dissolved alkali ions. According to Raoult's law (Jensen 1993), the effect of dissolved ions on relative humidity  $RH_S$  can be expressed as:

$$RH_S = x_{H_2O} \quad (3.11)$$

where  $x_{H_2O}$  [mol water / mol pore fluid] is the mole fraction of the water in the pore solution.

### 3.2.3.4 Effect of ion concentration on relative humidity and capillary tension - example

In order to illustrate the subsequent calculation steps of capillary tension, an example of Portland cement paste with water-cement ratio of 0.4 is given in the following section. The measured relative humidity of Portland cement paste (CEM I 42.5N) with water-cement ratio of 0.4 during the first 7 days is measured and shown in Figure 3.12<sup>1)</sup>. This figure shows that the measured maximum value of the internal relative humidity is 3% lower than 100%. As discussed in the foregoing, this is due to the dissolved ions in the pore fluid.

In order to calculate the Kelvin radius with Equation 3.10,  $RH_K$  should be known.  $RH_K$  can be calculated with Equation 3.9. The calculated evolution of  $RH_K$  is shown in Figure 3.12.

---

1) The testing method and equipment will be presented in Chapter 4.

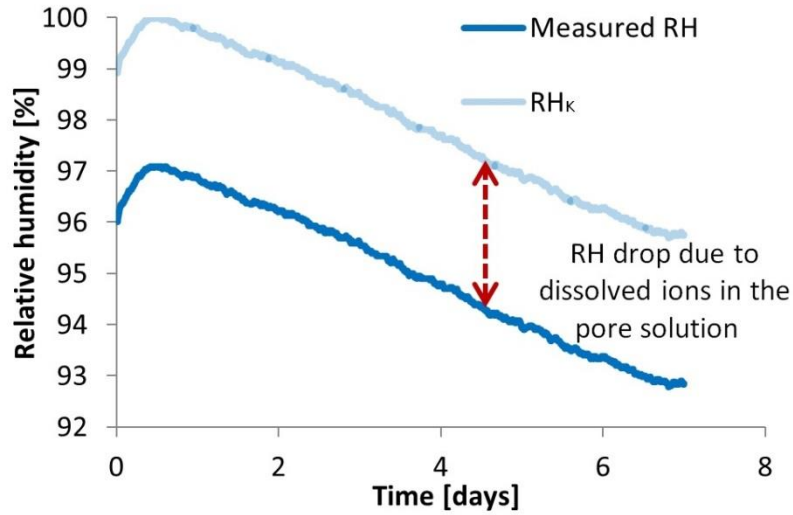


Figure 3.12 Measured RH and calculated evolution of  $RH_K$  of Portland cement paste with w/b ratio of 0.4

With the calculated  $RH_K$  the Kelvin radius  $r_k$  can be calculated with Equation 3.10. The surface tension  $\gamma$  of pore water is 0.072 N/m (Vargaftik et al. 1983). The molar volume of pore water  $V_m$  is taken as the value of molar volume of water, i.e.  $18.02 \times 10^{-6} \text{ m}^3/\text{mol}$  (Mazur 1963). The calculated Kelvin radius is shown in Figure 3.13.

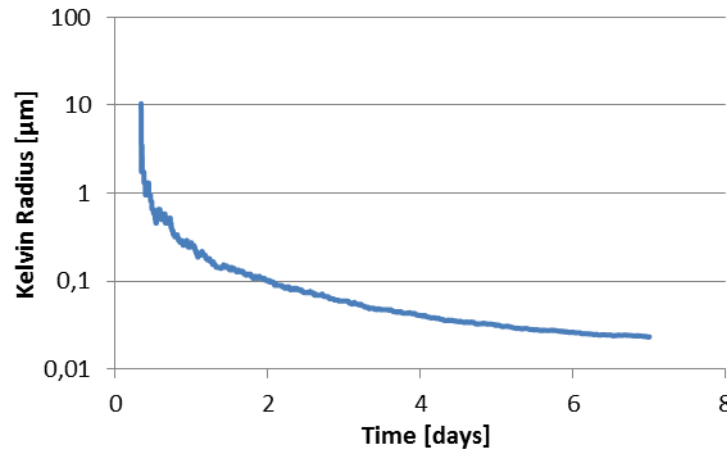


Figure 3.13 Calculated Kelvin radius of Portland cement paste with w/b ratio of 0.4

The Kelvin radius being known, the capillary tension in the pore fluid  $\sigma_{cap}$  can be calculated with the Laplace law (Equation 3.8). The calculated capillary tension is presented in Figure 3.14 as a function of both the age and the degree of hydration. Similarly calculated results of capillary tension can be found in Lebental's paper (Lebental et al. 2012)

(see also Section 5.3.2). The evolution of the degree of hydration  $\alpha$  is simulated with HYMOSTRUC<sup>2)</sup> (van Breugel 1991) and shown in Figure 3.15.

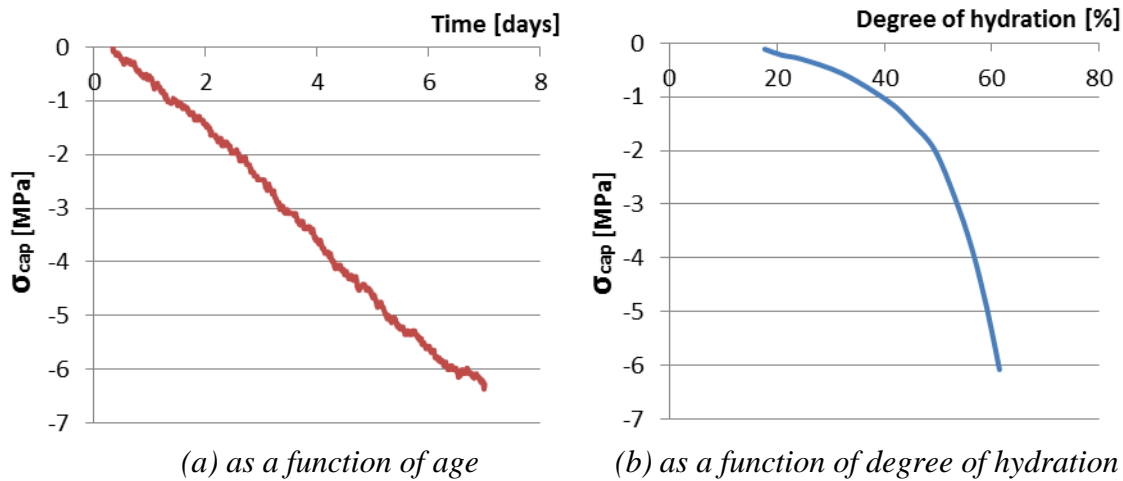


Figure 3.14 Calculated capillary tension in the pore fluid for Portland cement paste with water-binder ratio of 0.4

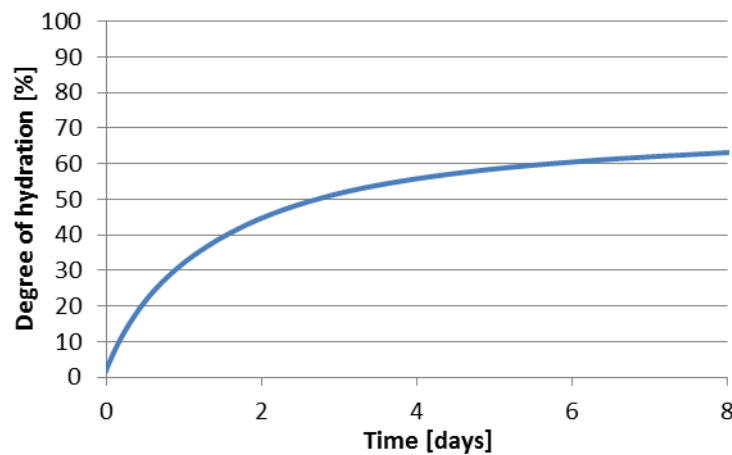


Figure 3.15 Simulated Degree of hydration (with HYMOSTRUC) vs. age of Portland cement paste with water-binder ratios of 0.4

2) HYMOSTRUC is a simulation model of reaction process and formation of the microstructure in hydrating Portland cement. In this model the degree of hydration is simulated as a function of the particle size distribution and of the chemical composition of the cement, the water/cement ratio and the reaction temperature. In this case, the particle size distribution and the chemical composition of the Portland cement are given in Figure 4.1 and Table 4.2. The water-binder ratio is 0.4 and curing temperature is 20°C.

### 3.2.4 Discussion

Disjoining pressure and capillary tension are two mechanisms, which have both been proposed for explaining autogenous deformation of early-age hydrating cement paste. Some researchers consider disjoining pressure as the dominant mechanism of autogenous shrinkage (Wittmann 2009), while others think that capillary tension is the dominant mechanism (Hua et al. 1995, Wei 2008). For the conditions considered in this chapter, the disjoining pressure is repulsion-dominated and its magnitude increases with decreasing pore size. The disjoining pressure separates the adjacent cement particles in cement paste and it has a significant magnitude in small gel pores where reaction products are densely packed (as shown in Figure 3.10). Meanwhile, the pore water in capillary pores is in tension and puts the solid skeleton of cement paste, including the water between reaction products, in compression, which results in an external volume reduction of the cement paste, i.e. autogenous shrinkage. Capillary tension increases with decreasing internal relative humidity. In cement paste the compressive forces must be in equilibrium with tensile forces. It is assumed, therefore, that capillary tension and disjoining pressure must be somehow related. If so, either disjoining pressure or capillary tension can be adopted as parameter for describing autogenous shrinkage, still leaving the question whether the first or the latter mechanism should be considered as the ‘real’ shrinkage mechanism unanswered.

### 3.3 Deformation of hardening cement paste under changing internal load - autogenous shrinkage of cement paste

Cement paste is not an ideal elastic material. The deformation of cement paste under constant external load includes two parts, an elastic and a time-dependent part, as shown in Figure 3.16. In formula form:

$$\varepsilon(t, \tau) = \varepsilon_{el}(\tau) + \varepsilon_{cr}(t, \tau) \quad (3.12)$$

where  $\varepsilon(t, \tau)$  [m/m] is the total deformation at time  $t$ ;  $\varepsilon_{el}(\tau)$  [m/m] the elastic deformation at loading time  $\tau$ ;  $\varepsilon_{cr}(t, \tau)$  [m/m] the time-dependent deformation at time  $t$ , which is called creep;  $\tau$  the time at loading.

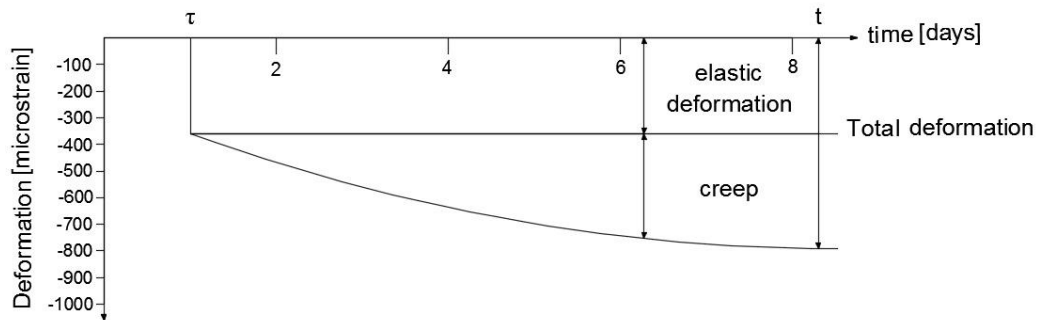


Figure 3.16 Schematic representation of deformation of the cement paste under constant external load

### 3.3.1 Elastic deformation $\varepsilon_{el}(\tau)$

For a cement paste under uni-axial load, the elastic part of the deformation,  $\varepsilon_{el}(\tau)$ , is given by Hooke's law:

$$\varepsilon_{el}(\tau) = \frac{\sigma(\tau)}{E(\tau)} \quad (3.13)$$

where  $\sigma(\tau)$  [MPa] is the applied stress at time  $\tau$ ;  $E(\tau)$  [MPa] elastic modulus of cement paste at time  $\tau$ .

For a tri-axial load condition the elastic deformation  $\varepsilon_{el}(\tau)$  in one direction can be calculated as:

$$\varepsilon_{el}(\tau) = \frac{\sigma(\tau)}{E(\tau)} (1 - 2\vartheta) = \frac{\sigma(\tau)}{3K_P(\tau)} \quad (3.14)$$

where  $\vartheta$  [-] is the Poisson ratio;  $K_P(\tau)$  [MPa] is the bulk modulus of the cement paste at time  $\tau$ .  $K_P(\tau)$  can be calculated using the following formula (Soboyejo 2002):

$$K_P(\tau) = \frac{E(\tau)}{3(1-2\vartheta)} \quad (3.15)$$

In Equation 3.13 and Equation 3.14  $\sigma(\tau)$  is considered to be a constant *external* load. For autogenous shrinkage of early-age cement paste, there is no external load, the capillary tension is the changing *internal* load. Capillary tension increases with the drop of relative humidity. In order to calculate the deformation of cement paste under a *changing internal* load, the concept of effective stress has been introduced.

### 3.3.2 Effective stress $\sigma_e$

Cement paste is a porous material of which the pores are usually partially filled with water. Even if there is no applied external load, the shape and volume of cement paste can still be changed due to the internal pressure exerted by the capillary pore water on the solid phase, e.g. capillary tension (Gawin et al. 2007). The internal pressure exerted by the pore water on the solid phase is called effective stress (called also Skempton's stress (Skempton 1961)).

#### 3.3.2.1 Theoretical basis of effective stress

According to Gray et al. (2001), the effective stress  $\sigma_e$  [MPa] may be written as:

$$\sigma_e = \kappa p^s I \quad (3.16)$$

where  $I$  [-] is the unit tensor of second order;  $p^s$  [MPa] is the internal pressure exerted by the pore water on the solid phase;  $\kappa$  [-] is the Biot coefficient. The Biot coefficient describes to which extent the internal pressure causes the deformation of porous materials (Alam et al. 2010). It can be written as:



$$\kappa = 1 - K_p/K_s \quad (3.17)$$

where  $K_s$  [MPa] is the bulk modulus of the solid material;  $K_p$  [MPa] the bulk modulus of the cement paste.

For early-age autogenous shrinkage of cement paste, only the internal pressure exerted by the pore water,  $p^s$ , acts on the solid phase (Figure 3.17). Due to the exerted internal pressure, the cement particles move toward to each other. A compressive pressure  $p^{s'}$  will be generated in the adsorbed water between cement particles to equilibrate the exerted internal pressure and the solid skeleton of the cement paste is under compression, as shown in Figure 3.17.

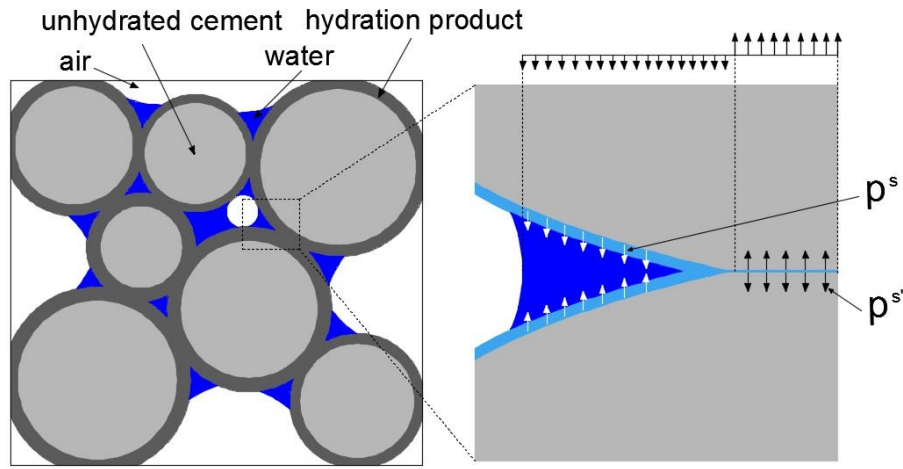


Figure 3.17 Schematic representation of the internal pressure  $p^s$  and resulted compressive pressure  $p^{s'}$  in the adsorbed water

Capillary tension is considered as the internal pressure exerted by the pore water,  $p^s$ , acts on the solid phase. According to Gawin et al. (2007), in this case, the internal pressure  $p^s$  can be written as:

$$p^s = S_w \sigma_{cap} \quad (3.18)$$

where  $S_w$  [-] is the degree of saturation and  $\sigma_{cap}$  [MPa] the capillary tension.

The effective stress  $\sigma_e$  in one direction can be written as (Bentz et al. 1998, Gawin et al. 2007):

$$\sigma_e = \kappa S_w \sigma_{cap} \quad (3.19)$$

It should be noticed that capillary tension  $\sigma_{cap}$  is multiplied by the degree of saturation  $S_w$  to calculate the effective stress in Equation 3.19. All the pores filled with water in cement paste are considered as capillary pore. But in reality, part of the pores filled with water in cement paste is gel pore (van Breugel 1991). The effective stress  $\sigma_e$  calculated by Equation 3.19 is a virtual stress (Bentz et al. 1998).

### 3.3.2.2 Degree of saturation $S_w$

In order to calculate the effective stress  $\sigma_e$ , the degree of saturation  $S_w$  should be known. The degree of saturation  $S_w$  can be calculated as the ratio between the evaporable water content in the hardening paste,  $V_{ew}$  [cm<sup>3</sup> water / cm<sup>3</sup> paste], and the pore volume of the paste,  $V_p$  [cm<sup>3</sup> pore / cm<sup>3</sup> paste] (Powers et al. 1948):

$$S_w = \frac{V_{ew}}{V_p} = \frac{V_{iw} - V_{new}}{V_{iw} - V_{new} + V_{cs}} \quad (3.20)$$

where  $V_{iw}$  [cm<sup>3</sup> water / cm<sup>3</sup> paste] is the initial water content;  $V_{new}$  [cm<sup>3</sup> non-evaporable water / cm<sup>3</sup> paste] the non-evaporable water content and  $V_{cs}$  [cm<sup>3</sup> chemical shrinkage / cm<sup>3</sup> paste] the volume of chemical shrinkage. The non-evaporable water content and the chemical shrinkage can be determined experimentally or numerically with adequate software (e.g. HYMOSTRUC).

An example of the calculated degree of saturation of BFS cement paste (CEM III 42.5N) with water-cement ratio of 0.3 is shown in Figure 3.18. For BFS cement paste (CEM III 42.5N) with water-cement ratio of 0.3, the measured values of non-evaporable water content  $V_{new}$  and volume of chemical shrinkage  $V_{cs}$  are shown in Figure 3.19<sup>3)</sup>. More detailed discussion about the calculated degree of saturation will be given in Chapter 5.

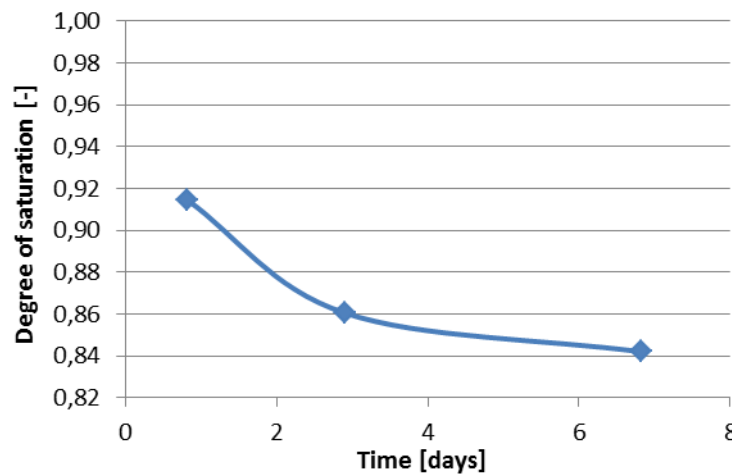


Figure 3.18 Degree of saturation of BFS cement paste with water-binder ratio of 0.3 calculated from measurements

3) The testing method and equipment will be presented in Chapter 4.

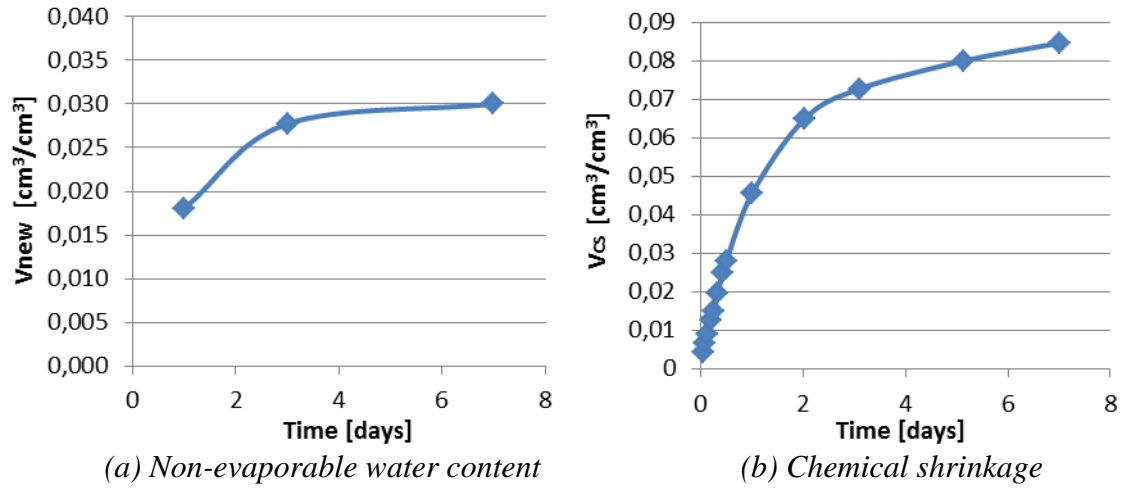


Figure 3.19 Measured non-evaporable water content and chemical shrinkage as a function of time of BFS cement paste with water-binder ratio of 0.3

### 3.3.2.3 Elastic deformation of cement paste under internal load-example

For a cement paste under internal load, i.e. capillary tension, the elastic deformation in one direction can be calculated with (Bentz et al. 1998):

$$\varepsilon_{el}(\tau) = \frac{\sigma_e(\tau)}{3K_P(\tau)} = \frac{\kappa S_w(\tau) \sigma_{cap}(\tau)}{3K_P(\tau)} = \frac{S_w(\tau) \sigma_{cap}(\tau)}{3} \left( \frac{1-2\vartheta}{E(\tau)} - \frac{1}{K_S} \right) \quad (3.21)$$

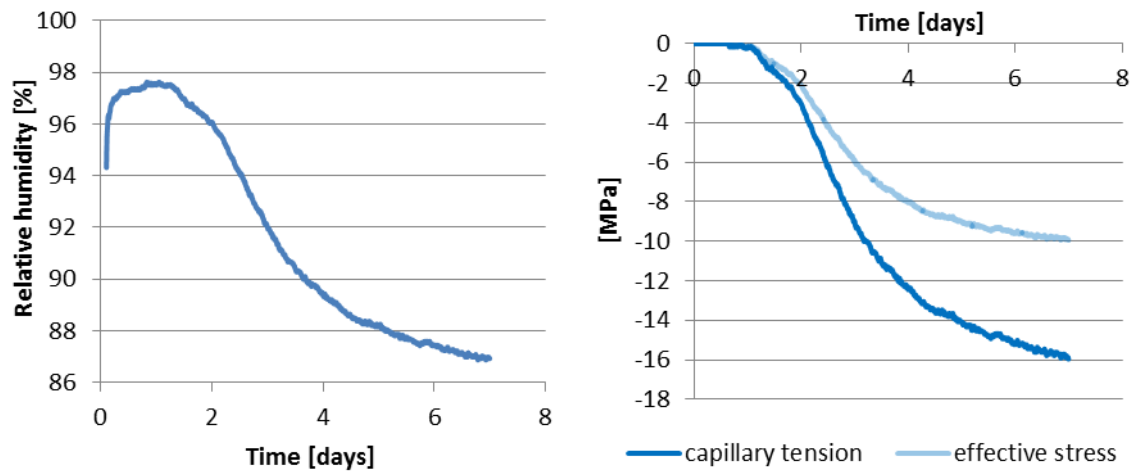
where  $\sigma_e$  is the effective stress and  $K_P$  is the bulk modulus of the cement paste.

In order to illustrate the calculation of elastic deformation of cement paste under internal load, an example of BFS cement paste (CEM III 42.5N) with water-binder ratio 0.3 is given. The capillary tension  $\sigma_{cap}$  is calculated as function of the relative humidity using Equation 3.8. The measured relative humidity<sup>4)</sup> of BFS cement paste is shown in Figure 3.20a and the calculated capillary tension and effective stress are shown in Figure 3.20b.

For calculating the elastic deformation with Equation 3.21, the physical properties of cement paste must be known. The elastic modulus is calculated from the measured compressive strength<sup>5)</sup> and shown in Figure 3.21a. The calculated degree of saturation using Equation 3.20 was given in Figure 3.21b. The bulk modulus of the solid material,  $K_S = 44$  GPa (Nielsen 1991), and the Poisson ratio,  $\vartheta = 0.2$  (Nielsen 1991), are obtained from the literature. The elastic deformation of BFS cement paste (CEM III 42.5N), calculated with Equation 3.21, is shown in Figure 3.22.

4) The testing method and equipment will be presented in Chapter 4.

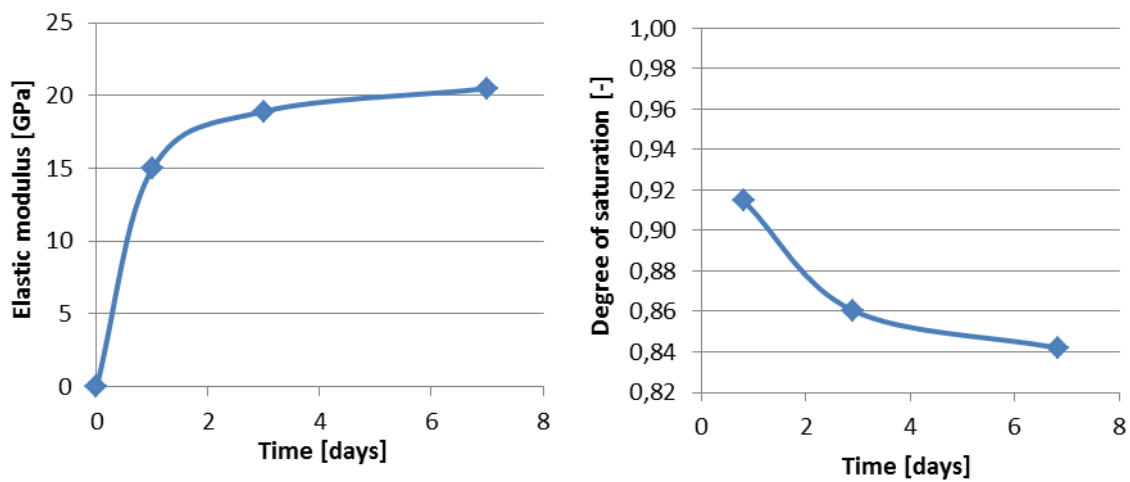
5) The measured compressive strength will be shown in chapter 4. The calculation formula of elastic modulus will be given in Chapter 5.



(a) Measured relative humidity

(b) Capillary tension and effective stress

Figure 3.20 Measured relative humidity, calculated capillary tension and effective stress of blast furnace slag cement paste (CEM III 42.5N) with water-binder ratio 0.3



(a) Calculated elastic modulus

(b) Calculated degree of saturation

Figure 3.21 Calculated elastic modulus and degree of saturation of blast furnace slag cement paste (CEM III 42.5N) with water-binder ratio 0.3

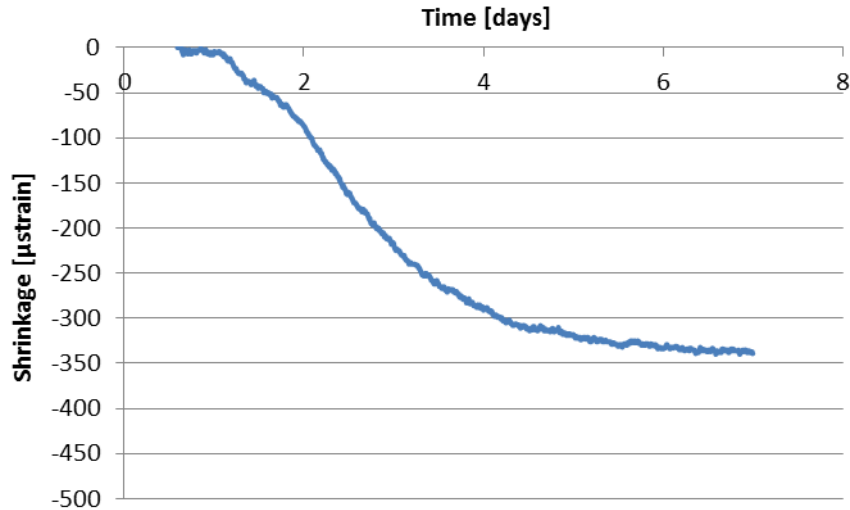


Figure 3.22 Calculated elastic deformation of blast furnace slag cement paste (CEM III 42.5N) with water-binder ratio 0.3 under capillary tension (Equation 3.21)

### 3.3.3 Time-dependent deformation $\varepsilon_{cr}(t, \tau)$

During the past few decades, many papers about creep mechanisms of hardened concrete have been published (Neville et al. 1983, Gilbert 1988). The most often mentioned mechanisms are: viscous flow, seepage, delayed elasticity and microcracking. None of these mechanisms describes the time-dependent properties comprehensively. According to Coutinho et al. (1977), several mechanisms may together determine the time-dependent properties of concrete. Different formulae and simulation models have been developed for creep of hardened concrete, e.g. double and triple power laws and solidification model. Most of these models are empirical, or semi-empirical. In this thesis, activation energy concept will be applied to calculate the time-dependent part of autogenous deformation. The activation energy equation was proposed by Svante Arrhenius in 1889 (Glasstone 1941). It has been applied to describe the temperature dependency of diffusion coefficients, creep rates and many other temperature-dependent reactions.

#### 3.3.3.1 Theoretical basis of Activation energy concept

Many researchers have used activation energy concept to calculate the creep of cementitious materials (Hirst et al. 1977, Bazant et al. 1982, Day et al. 1983). In the activation energy concept, each cement particle in mixture is fixed to its position. In order to change the position of a cement particle, a certain amount of energy is needed, which is called activation energy. During the creep process, many cement particles move. All the energy needed for changing the positions of these cement particles is called the activation energy of creep.

For a hardened cement paste under constant external load, the time-dependent strain of the cement paste specimen can be written as (For details: see Appendix):

$$\varepsilon_{cr}(t, \tau) = \frac{2\sigma(\tau)}{E(\tau)} \left(1 - \exp\left(-\frac{\omega\eta\sigma(\tau)E(\tau)}{2\sigma(\tau)\exp\left(\frac{Q(t)}{RT}\right)}t\right)\right) \quad (3.22)$$

where  $Q(t)$  [KJ/mol] is the activation energy of the cement paste;  $\omega$  [-] and  $\eta$  [m<sup>2</sup>/N] are structure dependent parameters and constant for a given material;  $\sigma(\tau)$  is the external load at time  $\tau$ ;  $E(\tau)$  [MPa] is the elastic modulus of cement paste at time  $\tau$ ;  $\tau$  is the time at loading;  $R$  [J/(mol · K)] is the universal gas constant and  $T$  [K] is the absolute temperature.

Based on the Equation 3.22, the rate of creep can be written as (Wittmann et al. 1968):

$$\dot{\varepsilon}_{cr}(t, \tau) = \omega\eta\sigma(\tau)\exp\left(-\frac{Q(t)}{RT}\right) \quad (3.23)$$

For a cement paste under internal load, the effective stress  $\sigma_e$  should be used. Inserting Equation 3.19 in Equation 3.22, the creep deformation can be calculated as:

$$\varepsilon_{cr}(t, \tau) = \frac{2\kappa S_w(\tau)\sigma_{cap}(\tau)(1-2\theta)}{E(\tau)} \left(1 - \exp\left(-\frac{\omega\eta\kappa S_w(\tau)\sigma_{cap}(\tau)E(\tau)}{2\kappa S_w(\tau)\sigma_{cap}(\tau)\exp\left(\frac{Q(t)}{RT}\right)}t\right)\right) \quad (3.24)$$

where  $S_w$  is the degree of saturation;  $\sigma_{cap}$  is the capillary tension and  $\kappa$  is the Biot coefficient as explain in section 3.3.2.

### 3.3.3.2 Creep of the hardening cement paste under changing load

For early-age autogenous shrinkage of cement paste, the internal load, e.g. capillary tension, increases with the drop of relative humidity. In the meantime, the elastic modulus increases. In order to simulate the time-dependent part of early-age autogenous shrinkage, the changing physical properties of cement paste, which are related to the changing microstructure, should be taken into consideration.

During the past few decades, several models have been proposed to simulate the early-age time-dependent deformation of hardening cement paste (van Breugel 1982, Bažant et al. 1984, Bažant et al. 1985, Tamtsia et al. 2004, Gawin et al. 2006). Lokhorst (1998) and Gawin et al. (2006) have improved solidification theory (Bažant et al. 1989) by using a flow term to deal with the effect of hydration on creep. Tamtsia et al. (2004) and Bažant et al. (1984, 1985) have improved log-double power to deal with the effect of hydration on creep. These models are based on the experimental results and only an approximation of the visco-elastic behaviour.

In the following section, an extended activation energy concept model is proposed. In this model, the effect of the changing physical properties of the hardening cement paste on creep is taken into account.

As shown in Figure 3.23, the autogenous shrinkage of early-age cement paste consists of two parts, the elastic part and the time-dependent part. The autogenous shrinkage can be expressed as:

$$\varepsilon(t_n, \tau_n) = \varepsilon_{el}(\tau_n) + \varepsilon_{cr}(t_n, \tau_n) \quad (3.25)$$

where  $\varepsilon(t_n, \tau_n)$  is the total deformation at time  $\tau_n$ ;  $\varepsilon_{el}(\tau_n)$  the elastic deformation at time  $\tau_n$ ;  $\varepsilon_{cr}(t_n, \tau_n)$  the time-dependent deformation at time  $\tau_n$ , which is called creep.

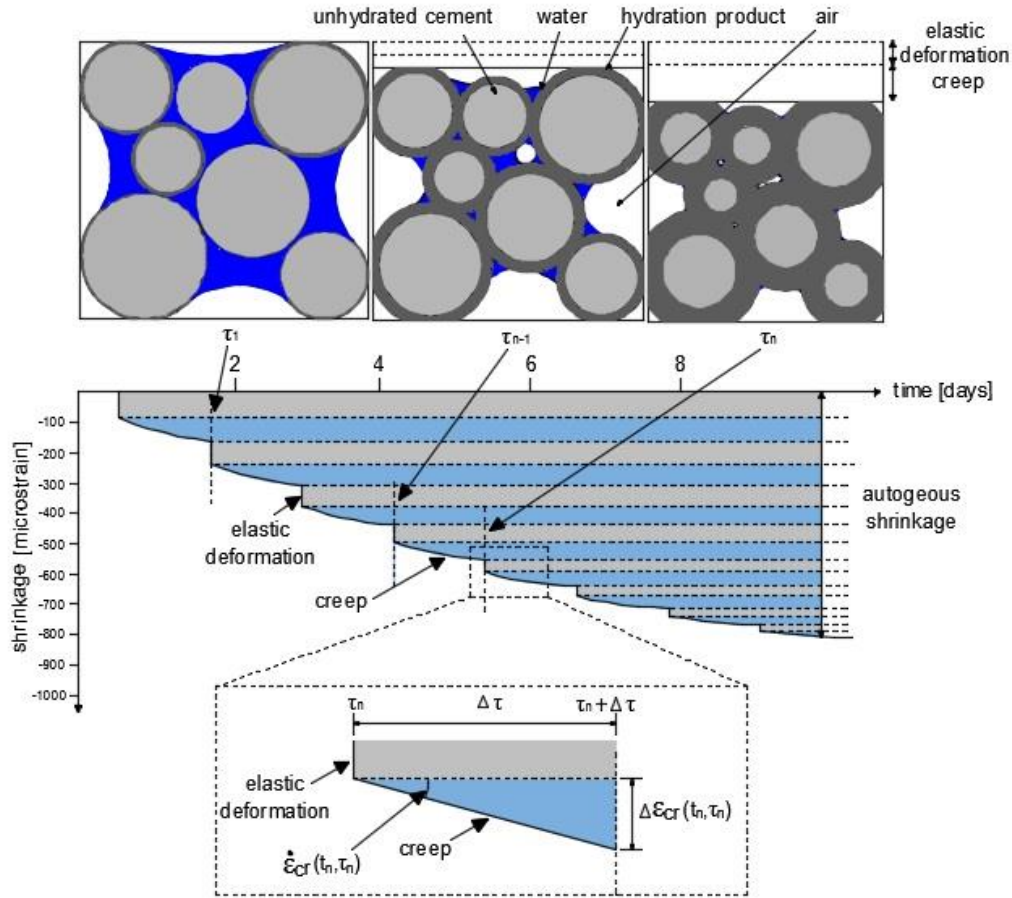


Figure 3.23 Schematic representation of autogenous shrinkage of hardening cement paste

The elastic part of autogenous shrinkage  $\varepsilon_{el}(\tau_n)$  follows Hooke's law (Equation 3.21). It is determined by the internal driving force  $\sigma(\tau_n)$  and elastic modulus of cement paste  $E(\tau_n)$  at time  $\tau_n$ .

The time-dependent part of autogenous shrinkage  $\varepsilon_{cr}(t_n, \tau_n)$  is the summation of increments of creep that formed at subsequent time intervals, e.g. from  $\tau_{n-1}$  to  $\tau_n$ . It can be expressed as:

$$\varepsilon_{cr}(t_n, \tau_n) = \sum_{k=1}^{n-1} \Delta \varepsilon_{cr}(t_k, \tau_k) \quad (3.26)$$

where  $\Delta \varepsilon_{cr}(t_k, \tau_k)$  is the increment of creep from  $\tau_k$  to  $\tau_{k+1}$ .

At time  $\tau_n$ , the internal load of autogenous shrinkage is  $\sigma(\tau_n)$ , the increasing rate of creep  $\dot{\varepsilon}_{cr}(t_n, \tau_n)$  at  $\tau_n$  (as shown in Figure 3.23) can be calculated with Equation 3.23 (Wittmann 1968):

$$\dot{\varepsilon}_{cr}(t_n, \tau_n) = \omega \eta \sigma(\tau_n) \exp\left(-\frac{Q(t_n)}{RT}\right) \quad (3.27)$$

According to Wittmann (1971), the activation energy  $Q(t_n)$  can be expressed as:

$$Q(t_n) = Q_0 + m \ln t_n \quad (3.28)$$

where  $m$  is the change rate of activation energy.

The increment of creep  $\Delta \varepsilon_{cr(t_n, \tau_n)}$  (as shown in Figure 3.23) that formed from time  $\tau_n$  to time  $\tau_n + \Delta \tau$  can be calculated as:

$$\Delta \varepsilon_{cr(t_n, \tau_n)} = \dot{\varepsilon}_{cr}(t_n, \tau_n) \Delta \tau = \omega \eta \sigma(\tau_n) \exp\left(-\frac{Q(t_n)}{RT}\right) \Delta \tau \quad (3.29)$$

The creep  $\varepsilon_{cr}(t_{n+1}, \tau_{n+1})$  at time  $\tau_n + \Delta \tau$  can be calculated as summation of increments of creep:

$$\varepsilon_{cr}(t_{n+1}, \tau_{n+1}) = \varepsilon_{cr}(t_n, \tau_n) + \Delta \varepsilon_{cr(t_n, \tau_n)} = \omega \eta \sigma(\tau_n) \exp\left(-\frac{Q(t_n)}{RT}\right) \Delta \tau + \sum_{k=1}^{n-1} \Delta \varepsilon_{cr(t_k, \tau_k)} \quad (3.30)$$

For a cement paste under internal load, i.e. capillary force, the effective stress  $\sigma_e$  should be used. Inserting Equation 3.19 in Equation 3.30, the creep deformation can be calculated as:

$$\varepsilon_{cr}(t_{n+1}, \tau_{n+1}) = \omega \eta \kappa S_w(\tau_n) \sigma_{cap}(\tau_n) \exp\left(-\frac{Q(t_n)}{RT}\right) (1 - 2\vartheta) \Delta \tau + \sum_{k=1}^{n-1} \Delta \varepsilon_{cr(t_k, \tau_k)} \quad (3.31)$$

,

### 3.3.4 Calculation of autogenous shrinkage of early-age cement paste

#### 3.3.4.1 Proposed simulation model of autogenous shrinkage of early-age cement paste

The autogenous shrinkage of hardening cement paste can be calculated as the sum of the elastic part and creep (for a cement paste under internal driving force, i.e. capillary tension, the loading time  $\tau$  is equal to the time  $t$ ):

$$\varepsilon(t, \tau) = \varepsilon_{el}(\tau) + \varepsilon_{cr}(t, \tau) = \frac{S_w(\tau) \sigma_{cap}(\tau)}{3} \left( \frac{1 - 2\vartheta}{E(\tau)} - \frac{1}{K_S} \right) + \omega \eta \kappa S_w(\tau_n) \sigma_{cap}(\tau_n) \exp\left(-\frac{Q(t_n)}{RT}\right) (1 - 2\vartheta) \Delta \tau + \sum_{k=1}^{n-1} \Delta \varepsilon_{cr(t_k, \tau_k)} \quad (3.32)$$

In Equation 3.32, the elastic and time-dependent part of the autogenous shrinkage of the cement paste are calculated according to Equation 3.21 and Equation 3.31.  $S_w$  is calculated with Equation 3.20.  $\sigma_{cap}$  is calculated with Equation 3.8. In Figure 3.24 a flow chart of the whole calculation procedure is shown.



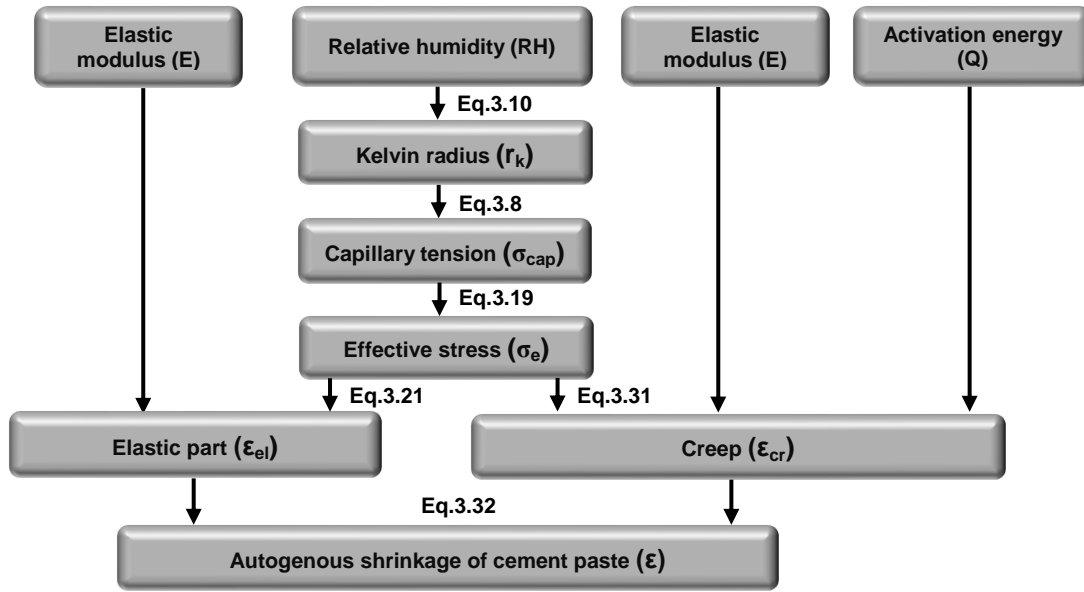


Figure 3.24 Scheme of simulation model of autogenous shrinkage

#### 3.3.4.2 Example

In order to illustrate the subsequent calculation steps of autogenous shrinkage, an example of BFS cement paste with water-cement ratio of 0.3 is given in the following. The measured relative humidity of BFS cement paste was shown in Figure 3.20a. The calculated capillary tension and effective stress were shown in Figure 3.20b. The calculated elastic modulus was shown in Figure 3.21a. The calculation of degree of saturation was shown in Figure 3.21b. More details of these inputs were given in Section 3.3.2.3. The bulk modulus of the solid material  $K_s$  is taken as 44 GPa (Nielsen 1991) and the Poisson ratio  $\nu$  is taken as 0.2 (Nielsen 1991). According to Wittmann (1967), for cement paste with water-binder ratio 0.3, the value of the parameters  $\omega$  and  $\eta$  in Equation 3.31 are 0.03 and  $4.8 \times 10^{-8} \text{ m}^2/\text{N}$ . The value of activation energy  $Q_0$  is taken as 15 kJ/mol (Wittmann 1967). For cement paste with water-binder ratio 0.3, the change rate of activation energy  $m$  is taken as 1.4 kJ/mol (Wittmann 1971).

The calculated autogenous shrinkage of blast furnace slag cement paste with water-cement ratio of 0.3 is shown in Figure 3.25. The contributions of the elastic and the time-dependent part of autogenous deformation are shown explicitly. From Figure 3.25 it can be noticed that creep plays an important role in the proposed simulation model of autogenous shrinkage. In this example, the magnitude of creep at seven days is bigger than that of the elastic deformation. Similar results were reported by other researchers (van Breugel 1980, Lura 2003, Hu 2017). Van Breugel studied the thermal stress in early-age hardening concrete. According to Van Breugel the calculated thermal stress in early-age concrete will reduce to one third by taking relaxation into consideration, which means the time-dependent part of autogenous deformation of concrete is twice as big as the elastic part. Hu and Lura also gave similar conclusion.

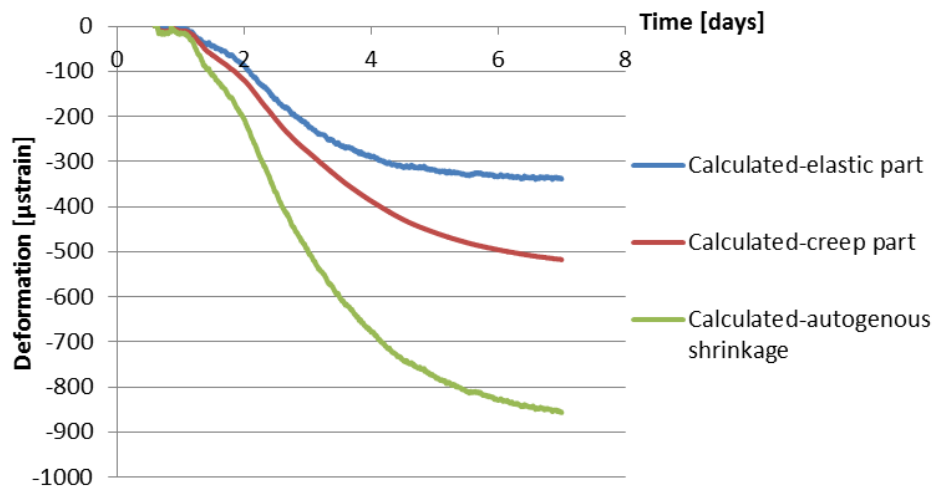


Figure 3.25 Calculated autogenous shrinkage of blast furnace slag cement paste (CEM III 42.5N) with water-cement ratio of 0.3

### 3.4 Concluding remarks

The disjoining pressure and capillary tension are two mechanisms for autogenous deformation of early-age hydrating cement paste. The disjoining pressure consists of an attractive Van der Waals term and a repulsive electrostatic term and structural term. It is repulsion-dominated and its magnitude increases with decreasing pore size. The disjoining pressure separates the adjacent cement particles in cement paste and it has a significant value in small gel pores where reaction products are densely packed. Meanwhile, the pore water in capillary pores is in tension and puts the solid skeleton of cement paste, including the water between reaction products, in compression, which results in the external volume reduction of the cement paste, i.e. autogenous shrinkage. Capillary tension increases with decreasing internal relative humidity. In cement paste the compressive forces must be in equilibrium with tensile forces. This equilibrium requirement somehow links the (compressive) disjoining pressure to the capillary tension.

A simulation model for autogenous deformation is proposed. In this model, the autogenous deformation have been split up in an elastic and a time-dependent component. The elastic component is calculated by Hooke's law. The time-dependent component of model is based on activation energy concept that can simulate the creep of hydrating cement paste under changing internal driving force. The simulation model is used to predict the autogenous shrinkage of blast furnace slag cement paste (CEM III 42.5N) with water-cement ratio of 0.3. From the simulation result it can be noticed that creep plays an important role in the proposed simulation model of autogenous shrinkage.

# Chapter 4

## Experimental study of early-age properties and autogenous shrinkage of ordinary Portland cement paste and cement paste with supplementary materials

### 4.1 Introduction

In Chapter 3 a simulation model of autogenous shrinkage has been proposed. In that model capillary tension is considered the major driving force of autogenous shrinkage. The internal driving force acts on a continuously changing microstructure. The evolution of material properties also plays an important role in the development of autogenous shrinkage. In this chapter measurements of setting time, internal relative humidity, non-evaporable water content, chemical shrinkage, compressive strength and autogenous deformation of cement paste are presented and discussed. Pure Portland cement paste and three kinds of cement paste with different supplementary material, i.e. silica fume, fly ash and blast furnace slag, were considered. Water-binder ratios of these cement pastes are 0.3 and 0.4. The objective of these experimental studies is to provide data for numerical modelling of the autogenous shrinkage (in Chapter 5). Non-evaporable water content and chemical shrinkage are measured to calculate the degree of saturation of cement paste. Internal relative humidity of cement paste is measured to calculate the capillary tension, whereas the compressive strength of cement paste is measured to calculate the elastic modulus.

### 4.2 Materials

#### *Chemical composition of binder (Type of cement and other powders)*

The materials used in this study are Portland cement (CEM I 42.5N), silica fume, fly ash, BFS cement (CEM III/B 42.5N) and de-ionized water. Portland cement (CEM I 42.5N) was produced by ENCI, The Netherlands. The mineral composition of Portland cement is presented in Table 4.1. The chemical compositions of the materials are given in Table 4.2.

*Table 4.1: Mineral composition of Portland cement (% by weight)*

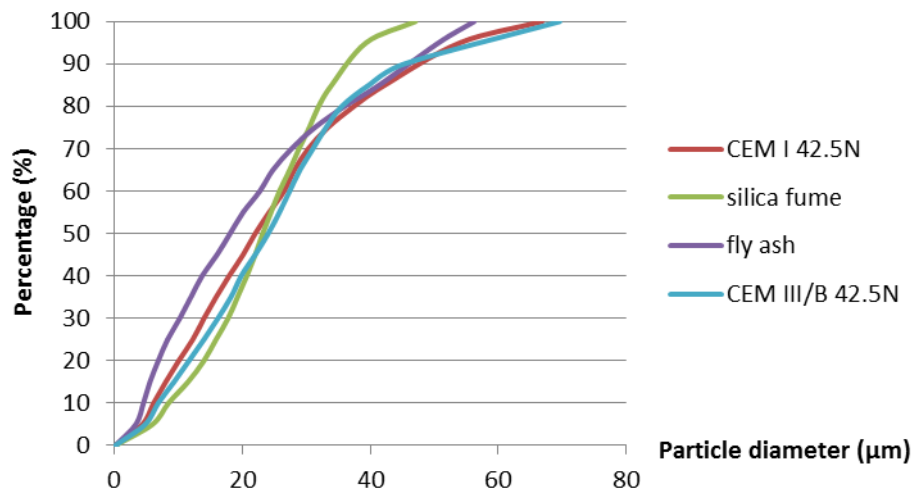
Phase	Weight(%)
C <sub>3</sub> S	67.1
C <sub>2</sub> S	5.9
C <sub>3</sub> A	7.8
C <sub>4</sub> AF	9.6
Other	9.6

*Table 4.2: Chemical composition of materials (% by weight)*

Chemical Composition	CEM I 42.5N	Silica Fume	Fly Ash	CEM III/B 42.5N
SiO <sub>2</sub>	20.36	97.2	48.4	30.61
Al <sub>2</sub> O <sub>3</sub>	4.96	0.51	31.4	10.58
CaO	64.4	0.39	7.14	45.52
Fe <sub>2</sub> O <sub>3</sub>	3.17	0.18	4.44	1.42
K <sub>2</sub> O	0.64	1.04	1.64	0.58
MgO	2.09	-	1.35	7.33
SO <sub>3</sub>	2.57	0.26	1.18	2.66
Na <sub>2</sub> O	0.14	-	0.72	0.31
Total	98.33	99.58	96.7	99.01

*Particle size distribution*

Figure 4.1 shows the particle size distribution curves of Portland cement, silica fume, fly ash and BFS cement measured by laser diffraction. The mean particle sizes,  $D_{50}$ , of Portland cement, silica fume, fly ash and BFS cement are 22  $\mu\text{m}$ , 23  $\mu\text{m}$ , 18  $\mu\text{m}$  and 24  $\mu\text{m}$ , respectively.

*Figure 4.1 Particle size distribution of materials powders used in this thesis*

The silica fume used in this thesis is commercial dry densified silica fume produced by Elkem. Silica fume is a reactive pozzolan and can be supplied in various forms, i.e. slurry form and dry densified silica fume. The dry densified form used in this thesis is said to be by far the most commonly used form (Diamond et al. 2006).

#### *Mixture design*

The experimental series considered in this study comprise eight mixtures. Portland cement pastes (CEM I 42.5N) serve as reference. The silica fume and fly ash dosages in blended mixtures are 10% and 30% by weight of the binder respectively. BFS cement (CEM III/B 42.5N) is also used, in which clinker accounts for 34% by mass. The water/binder ratios are 0.3 and 0.4. The mixture compositions are listed in Table 4.3. Cement paste is mixed in a 5 l epicyclic Hobart mixer. De-ionized water is mixed with the admixtures and added in two steps to ensure homogeneity. Total mixing time from first water addition is 3 minutes.

*Table 4.3: Mixture composition of Portland cement paste and blended cement paste (% by weight)*

Name	CEM I 42.5N (%)	CEM III/B 42.5N (%)	Silica fume (%)	Fly ash (%)	Water/Binder (w/b)
OPC 0.3	100	0	0	0	0.3
OPC 0.4	100	0	0	0	0.4
SF 0.3	90	0	10	0	0.3
SF 0.4	90	0	10	0	0.4
FA 0.3	70	0	0	30	0.3
FA 0.4	70	0	0	30	0.4
BFS 0.3	0	100	0	0	0.3
BFS 0.4	0	100	0	0	0.4

### **4.3 Experimental methods and equipment**

#### **4.3.1 Final setting time**

After final setting a solid skeleton of cement paste forms. The final setting time is taken as the beginning of the built up of the driving force of autogenous shrinkage. In this study, the final setting time was determined by the Vicat method according to standard NEN-EN 196-3:2005. An automatically recording Vicat apparatus was used.

#### **4.3.2 Non-evaporable water content**

The non-evaporable water content will be used for calculating the degree of hydration and degree of saturation of the hardening cement paste. For determining the non-evaporable water content, about 10 g of fresh cement paste was placed in a plastic vial. The height of the cement paste sample was about 5 mm. The vials were capped to ensure sealed curing conditions. The samples were stored at 20°C until the moment of testing. At the required age, samples for the determination of non-evaporable water content,  $W_n$  [g water / g cementitious material], were ground to powder and flushed with liquid nitrogen to stop

hydration, using a porous ceramic filter and vacuum. The powder was divided into two approximately equal parts and placed in two crucibles of known mass, which were left overnight in an oven at 105°C (for about 20 hours). When removed from the oven, the crucibles and samples were weighed before placing them in a furnace at 950°C for at least 4 hours. The non-evaporable water content was calculated as the average difference of the mass measurements between 105°C and 950°C for the two crucibles, corrected for the loss on ignition of the cement powder itself, which was assessed in a separate measurement.

### 4.3.3 Chemical shrinkage

About 50 g of freshly mixed cement paste was put in an Erlenmeyer flask (Figure 4.2a), with a capacity of 250 ml. The thickness of the cement paste sample was about 8 mm. After the cement paste was covered with a thin layer of distilled water, the Erlenmeyer flask was filled with paraffin oil and sealed with a rubber stopper encasing a graduated tube with a total volume of  $5 \pm 0.1$  ml. The flask was then immersed in a constant temperature water bath at 20°C (Figure 4.2b). The first measurement was performed after 30 min immersion of the samples in the water bath. Measurements were performed for 7 days. The chemical shrinkage is presented as the volume decrease of the paste per gram of cement and supplementary materials. For each measurement two specimens were tested.



(a) Glass Erlenmeyer flask with graduated tube      (b) Constant-temperature water bath

Figure 4.2 Equipment for chemical shrinkage measurement

### 4.3.4 Internal relative humidity

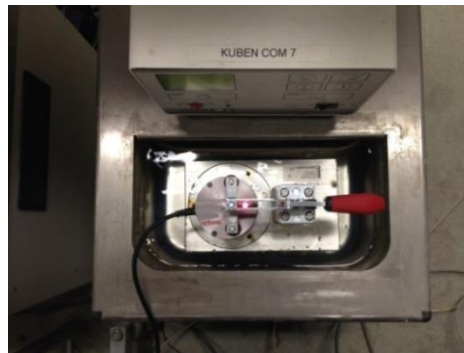
The development of the internal relative humidity cement pastes was measured by Rotronic HygroLab C1 (Figure 4.3a) equipment with two HC2-AW RH station probes with an accuracy  $\pm 0.5\%$  (Figure 4.3b). The RH probes were placed in a temperature controlled water bath at 20°C (Figure 4.3c). The RH probes were calibrated using saturated salt solutions with known constant RH in the range of 65-95%. After calibration the freshly mixed cement pastes were cast in two plastic containers and then put into the measuring chambers. The RH in the samples and the temperature were recorded every 2 minutes. The duration of the test was 7 days.



(a) Rotronic HygroLab C1



(b) HC2-AW RH station probes



(c) Top view of temperature controlled water bath

Figure 4.3 Apparatus for internal relative humidity measurement

#### 4.3.5 Compressive strength

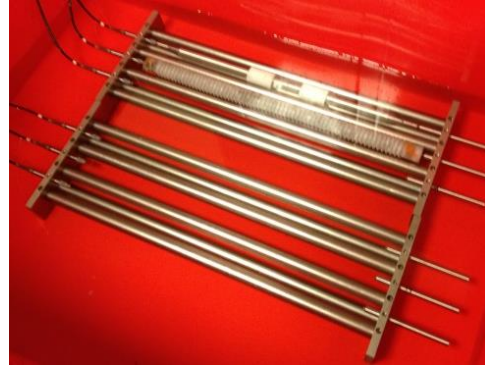
Compressive strength tests were carried out after 1, 3 and 7 days of sealed curing on cement paste cubes,  $40 \times 40 \times 40 \text{ mm}^3$ . The cubes were cured in sealed condition at  $20^\circ\text{C}$ . At least three specimens were tested for each measurement.

#### 4.3.6 Autogenous deformation

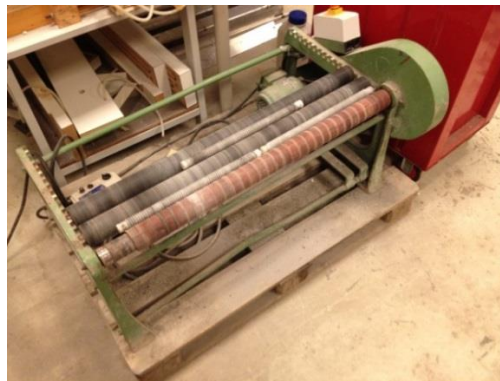
The cement paste was cast under vibration into tight plastic molds (low-density polyethylene plastic, LDPE), which were corrugated to minimize restraint on the paste (Figure 4.4a). The length of the samples was approximately 430 mm and the diameter 25 mm. Measurement of autogenous shrinkage starts after the final setting time when a solid skeleton of cement paste forms. Before that time the specimens were placed on a rotation machine at a speed of 10 rpm to avoid bleeding (Figure 4.4c). The specimens were placed in a dilatometer and immersed into a temperature controlled glycol bath at  $20 \pm 0.1^\circ\text{C}$ . A top view of the dilatometer is shown in Figure 4.4b. The dilatometer frame consisted of two steel plates joined rigidly by six solid invar rods (diameter 20 mm). Each specimen was longitudinally supported by two parallel rods attached to the steel plates. The specimens were gripped by screws at one end, while the rest could slide freely on the rods, which were lubricated by the glycol bath. The longitudinal deformation was measured at the free end by a TRANS-TEK 350-000 displacement transducer. Three samples were tested in the dilatometer simultaneously, with a measurement accuracy of  $\pm 5 \text{ }\mu\text{strain}$ . Length changes were recorded every 5 minutes.



(a) Corrugated plastic tube



(b) Dilatometer



(c) Rotation machine

Figure 4.4 Setup for the autogenous shrinkage measurement

## 4.4 Results and discussion

### 4.4.1 Final setting time

In Figure 4.5 the final setting times of cement pastes with water-binder ratio of 0.3 and 0.4, cured at 20°C, are shown. From Figure 4.5 it can be noticed that the final setting time is

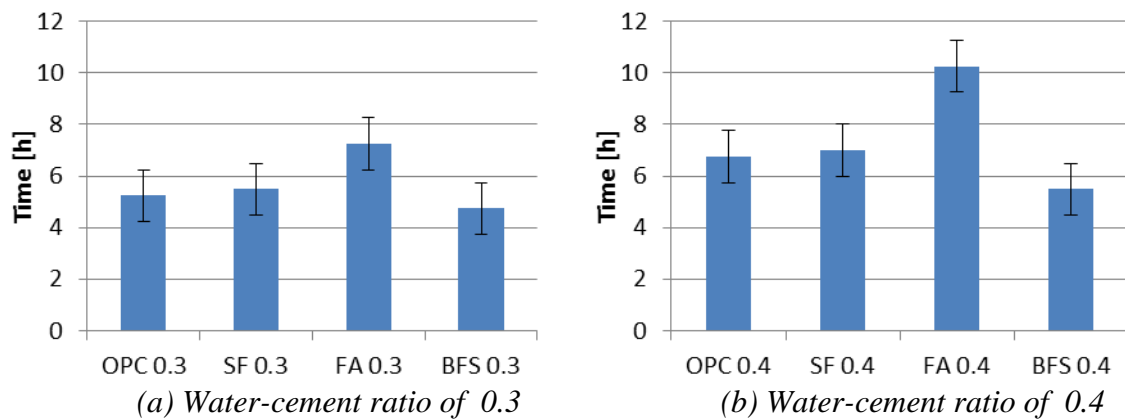


Figure 4.5 Final setting time of cement pastes with different supplementary materials.  
Code: See Table 4.3



longer for pastes with higher water-binder ratio for all kinds of cement paste. Fly ash cement paste has longer setting time than other cement pastes with the same water-binder ratio.

Some authors (Huang et al. 1985) reported that silica fume accelerates the reaction of  $C_3A$  and  $C_3S$  during the first hours of hydration. But as shown in Figure 4.5 the final setting times seem hardly influenced by the addition of silica fume. In these experiments silica fume was added in dry densified form. The silica fume used in other studies was often in slurry form. The phenomenon of accelerated hydration reported by other authors is due to the extreme fineness of silica fume they used. The commercial dry densified silica fume used in this thesis exists primarily in the form of clusters of spheres. The influence on the hydration process and final setting time is not as pronounced as that of silica fume added in slurry form. That coarse silica fume does not significantly influence the final setting time was also found by Rao (2003).

The addition of fly ash increases the final setting time of fly ash cement paste compared to that of ordinary Portland cement paste. This result is in line with the finding of Berg and Kukko (Berg et al. 1991). Compared with Portland cement, fly ash contains a higher amount of inactive minerals, such as quartz and mullite. As a consequence of this the fly ash reacts slower than cement at early age and results in longer final setting time.

Figure 4.5 shows that the final setting time of CEM III/B 42.5N is shorter than that of CEM I 42.5N. Shorter setting time of BFS cement paste has also been observed by Xiao et al. (2009). This, however, is contradictory to the common understanding that the setting time will increase with the addition of BFS. If the Portland cement and BFS cement are made with the same kind of clinker, the lower clinker content in BFS cement results in longer final setting time. According to the producer, CEM I 42.5N and CEM III/B 42.5N used in this study are made with different kind of clinker. CEM III/B 42.5N made with higher activity clinker may have shorter final setting time than that of CEM I 42.5N made with lower activity clinker.

#### **4.4.2 Non-evaporable water content**

The non-evaporable water contents (per gram of original powder) of different kinds of cement paste with water-binder ratio of 0.3 and 0.4 are displayed in Figures 4.6 and 4.7 as a function of time.

These figures show that the non-evaporable water content in fly ash cement pastes is lower than that in ordinary Portland cement pastes with the same water-binder ratio at the same curing age. This experimental result is in accordance with those reported by Zhang et al. (2000) and Lam et al. (2000).

The non-evaporable water content of the BFS cement paste is much lower than that of Portland cement paste with the same water-binder ratio and the same curing age. The lower non-evaporable water content of the BFS cement paste has two reasons. On one hand, the water binding capacity of BFS is lower than that of Portland cement. According to Gruyaert (2011), the water bound by Portland cement at complete hydration is about  $0.221 \text{ g H}_2\text{O} / \text{g cement}$ . The non-evaporable water content of BFS cement with 15% Portland cement and 85% BFS at complete hydration is about  $0.114 \text{ g H}_2\text{O} / \text{g cement}$ . On the other hand, the hydration rate of BFS during the first seven days is much slower than that of Portland cement. A lower degree of hydration of BFS results in a lower non-evaporable water content.

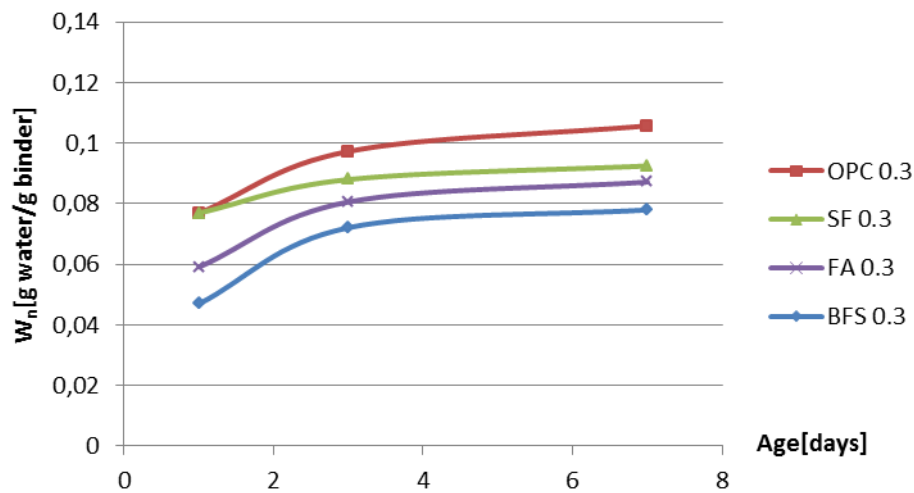


Figure 4.6 Non-evaporable water content as a function of age for different cement pastes with water-binder ratio of 0.3

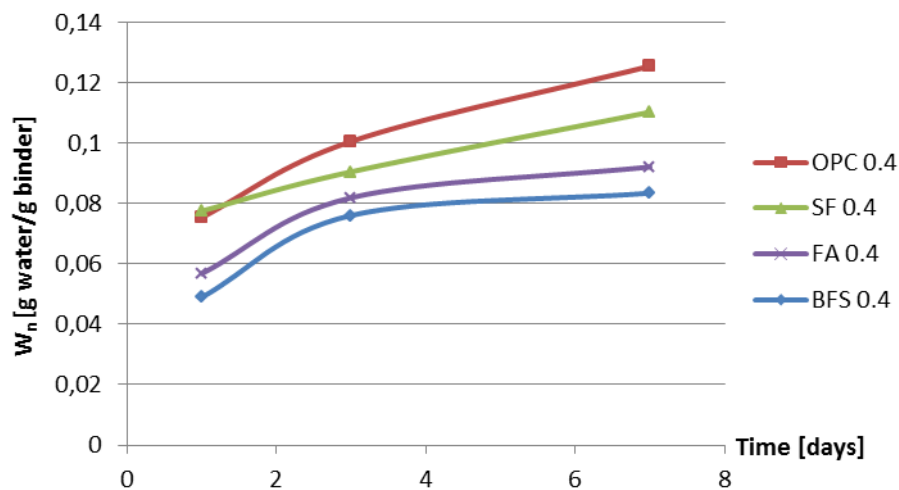


Figure 4.7 Non-evaporable water content as a function of age for different cement pastes with water-binder ratio of 0.4

Figures 4.6 and 4.7 show that the non-evaporable water content of the silica fume cement paste is lower than that of Portland cement paste with the same water-binder ratio at the same curing age. This result is in line with the finding of Gleize et al. (2003) and Huang et al. (1985). According to Taylor (1992) the reason of the lower non-evaporable water content of silica fume cement paste is similar to that of BFS cement paste, i.e. a lower quantity of water bound by silica fume than bound by Portland cement.

For all mixtures pastes with a higher water-binder ratio have higher non-evaporable water contents at the same curing age. At the same curing age, the degree of hydration of cement paste with higher water-binder ratio is higher than that of cement paste with lower water-binder ratio. Higher degree of hydration leads to a higher non-evaporable water content.

#### 4.4.3 Chemical shrinkage

Chemical shrinkage will be used for calculating degree of saturation of cement paste. Measured chemical shrinkage of four different types of cement is displayed in Figure 4.8. The mixture compositions of these cements are listed in Table 4.4.

Chemical shrinkage of fly ash cement paste is lower than that of other mixtures in the first week. Chemical shrinkage is proportional to the degree of hydration (Criado et al. 2007, Parrott et al. 1990). Compared with Portland cement, fly ash contains a higher amount of inactive minerals, such as quartz and mullite. As a consequence of this the fly ash reacts slower than cement and results in smaller chemical shrinkage at early age (Fang et al. 2011).

Chemical shrinkage of the BFS cement paste develops faster than that of Portland cement paste in the first 3 days. These results are in line with findings of Bentz (Thomas et al. 2012). According to Thomas et al. (2012) the density of hydration product of Portland cement and BFS cement paste is similar. The density of BFS particles is lower than that of Portland cement. Lower density of BFS results in bigger volume change between unhydrated BFS and hydration products.

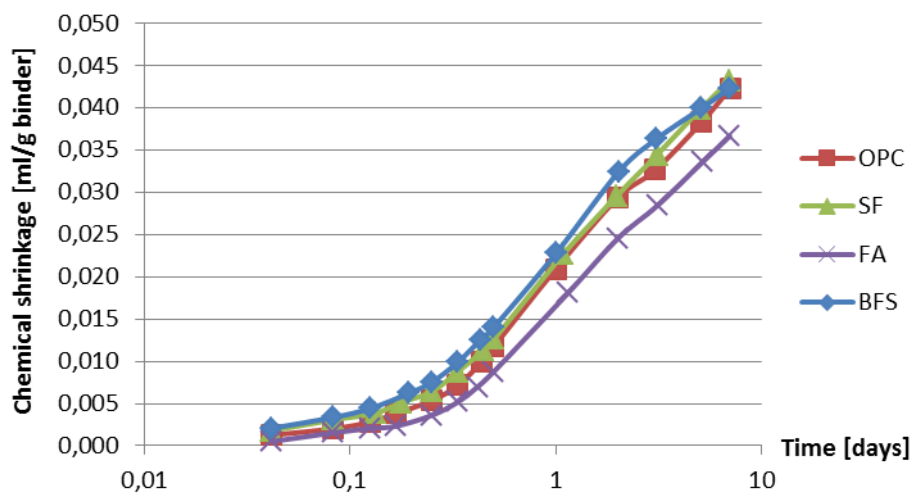


Figure 4.8 Chemical shrinkage as a function of age

Table 4.4: Mixture composition of Portland cement and blended cement (% by weight)

Name	CEM I 42.5N (%)	CEM III/B 42.5N (%)	Silica Fume (%)	Fly ash (%)
OPC	100	0	0	0
SF	90	0	10	0
FA	70	0	0	30
BFS	0	100	0	0

#### 4.4.4 Internal relative humidity

The internal relative humidity of the cement pastes mentioned in Table 4.3 was measured for a period of 7 days. For each series two specimens were tested. The difference between measured internal relative humidity of two specimens was less than 1%. The development of internal relative humidity with hydration time is provided in Figures 4.9, 4.10 and 4.11.

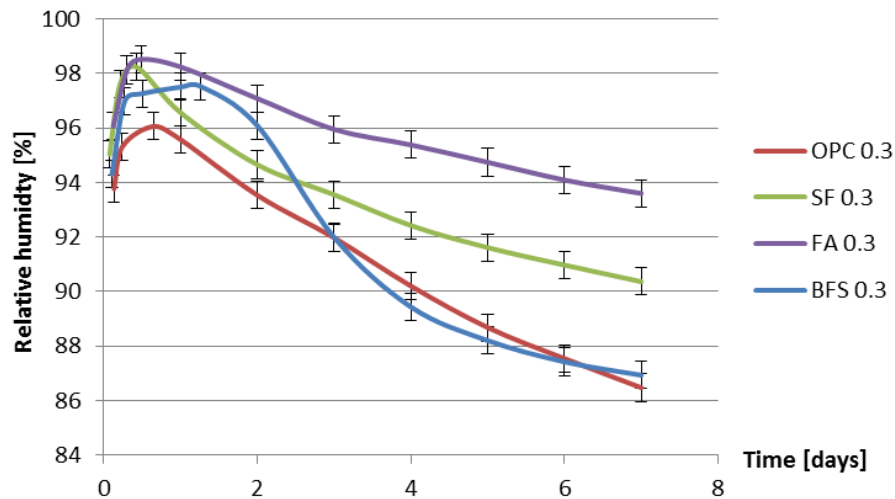


Figure 4.9 Internal relative humidity vs. age for different cement pastes with water-binder ratio of 0.3

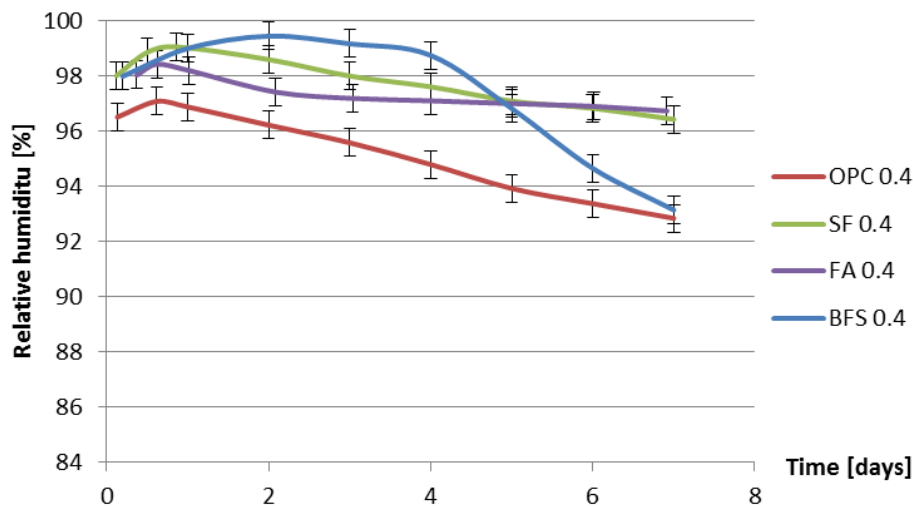


Figure 4.10 Internal relative humidity vs. age for different cement paste with water-binder ratio of 0.4

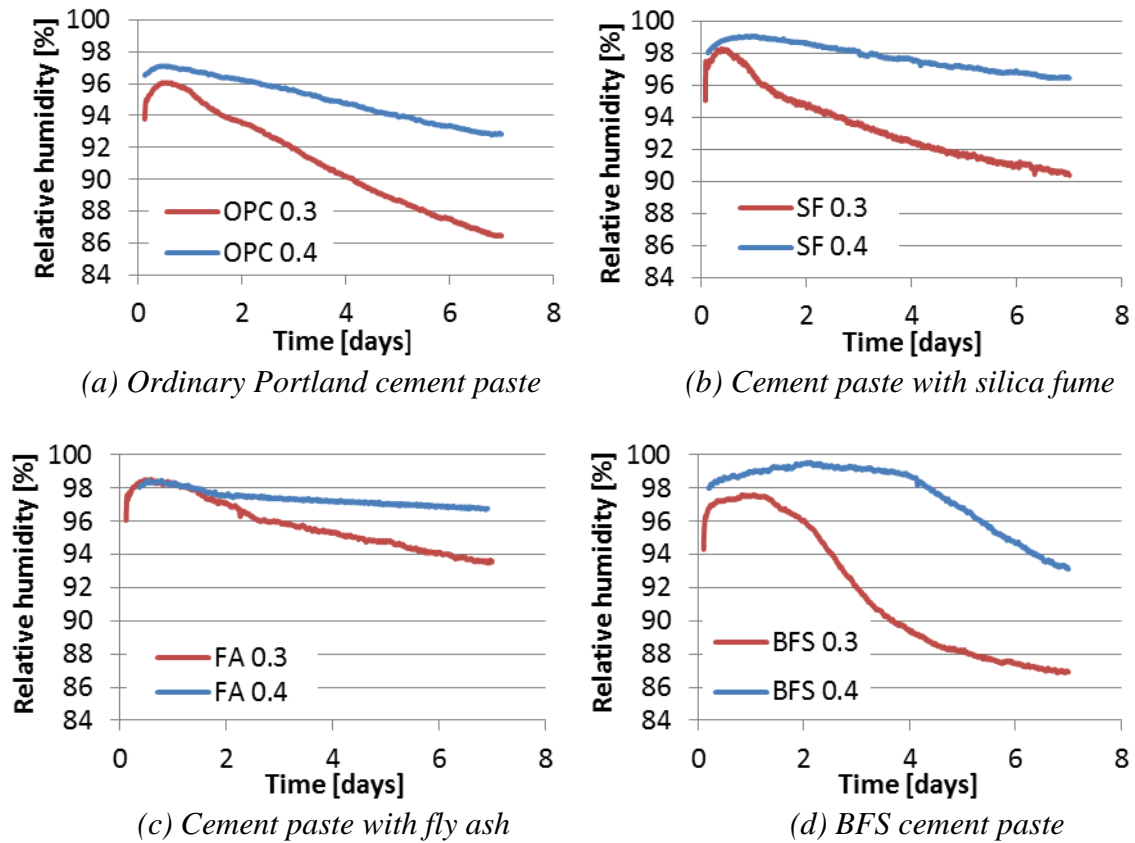


Figure 4.11 Internal relative humidity vs. age for different cement pastes with water-binder ratio of 0.3 and 0.4

Figures 4.9 and 4.10 show that the relative humidity of *fly ash* cement paste is higher than that of ordinary Portland cement paste with the same water-binder ratio. The higher relative humidity of *fly ash* cement paste is in accordance with the findings of Varga et al. (2012). Compared with Portland cement fly ash contains a higher amount of inactive minerals, such as quartz and mullite. Fly ash reacts slower than Portland cement. At the same curing age the non-evaporable water content in *fly ash* cement pastes is lower than that in ordinary Portland cement pastes with the same water-binder ratio as shown in Figures 4.6 and 4.7. More water is present in the pore structure of *fly ash* cement paste which results in higher relative humidity.

From Figures 4.9 and 4.10 it can be found that the moment that the relative humidity of BFS cement paste starts to drop significantly is later than that of Portland cement paste with the same water-binder ratio. For BFS cement paste with water-binder ratio 0.3 the relative humidity starts to drop 0.6 day later than that in the Portland cement paste with water-binder ratio 0.3. For BFS cement paste with water-binder ratio 0.4 the relative humidity starts to drop even 3.5 days later than that of Portland cement paste with water-binder ratio 0.4. A similar result can be found in Lura's thesis (Lura 2003). In his thesis the relative humidity of BFS cement paste with water-binder ratio 0.37 starts to drop 1 day later than in the Portland cement paste. The later starting moment of the RH drop of BFS cement paste can be attributed to the low activity of BFS after final setting. According to Taylor (1992) the hydration rate of BFS at early age is much slower than that of Portland cement. BFS cement (CEM III/B 42.5N) used in the test series contains BFS (66% by mass) and Portland

clinker (34% by mass). The large amount of low active BFS in CEM III/B 42.5N results in lower water consumption of BFS cement during the first few days of hydration and a later starting moment of RH drop of BFS cement paste.

#### 4.4.5 Compressive strength

The compressive strength of cement paste will be used (in Chapter 5) to calculate the elastic modulus. Elastic modulus of cement paste, on its turn, is an important factor in modelling of autogenous shrinkage. Figures 4.12 and 4.13 show the compressive strength as a function of age of four cement pastes with water-binder ratio of 0.3 and 0.4.

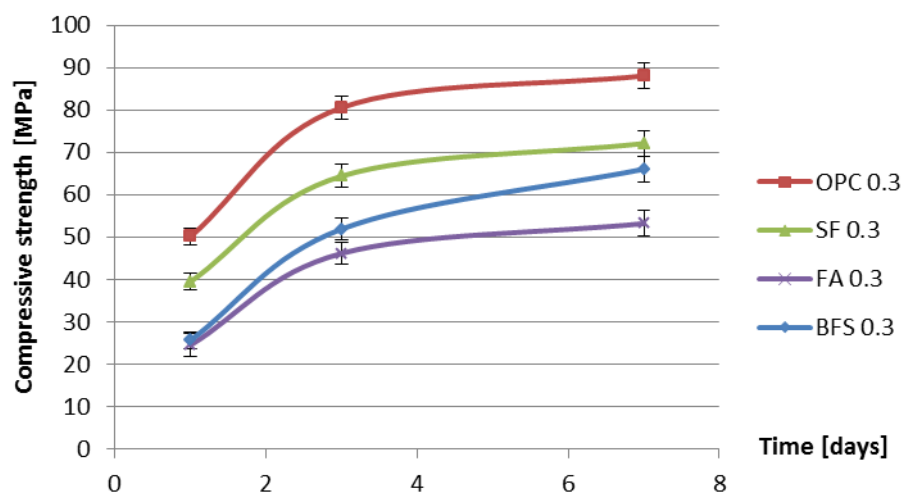


Figure 4.12 Compressive strength vs. age for different cement pastes with water-binder ratio of 0.3

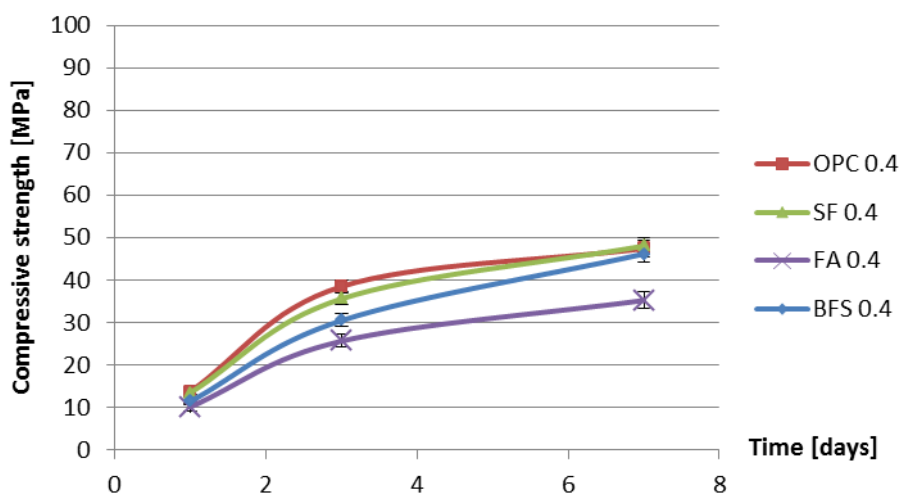


Figure 4.13 Compressive strength vs. age for different cement pastes with water-binder ratio of 0.4

Note that during the first 7 days the compressive strength of the samples with silica fume is lower than of the samples without silica fume. This is different from the common understanding that the addition of silica fume will increase the strength of concrete. Houssam and Tahar (Houssam et al. 1995) pointed out that the increase of strength of mortar and concrete with the incorporation of silica fume is due to the improvement of the aggregate-matrix bond. For the silica fume pastes, in the absence of ITZ, there is no substantial strengthening effect.

#### 4.4.6 Autogenous deformation as function of time

Figures 4.14 and 4.15 show the measured autogenous deformations as a function of age of different cement pastes with water-binder ratio of 0.3 and 0.4. Three samples were tested simultaneously. The final setting time is chosen as the starting time of the measurement. According to Standard ASTM 1698 the final setting time is determined by the Vicat apparatus. Before the final setting time the specimens were on a rotation machine to avoid bleeding.

For all mixtures a fast shrinkage can be noticed at the beginning. This fast shrinkage is followed by a short period of swelling. After the period of swelling the specimens steadily shrink.

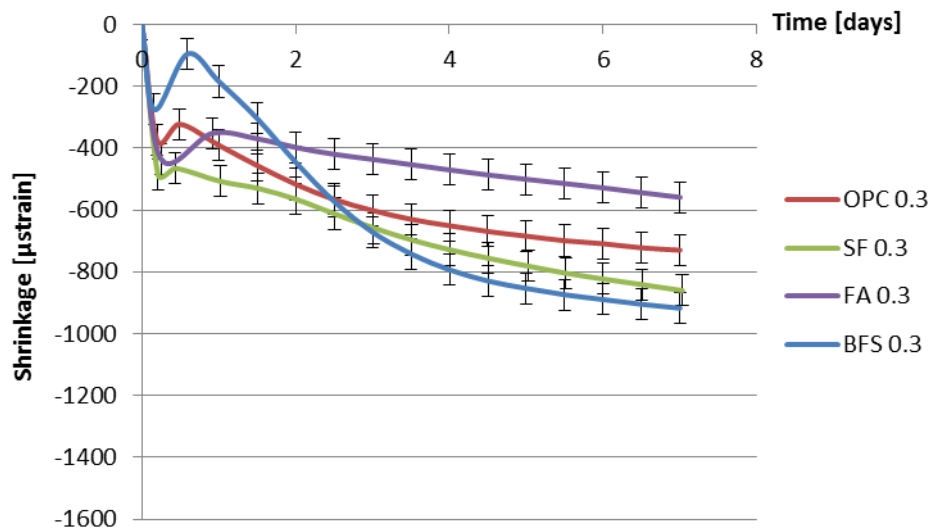


Figure 4.14 Autogenous deformation vs. age for different cement pastes with water-binder ratio of 0.3 (Starting time: final setting time)

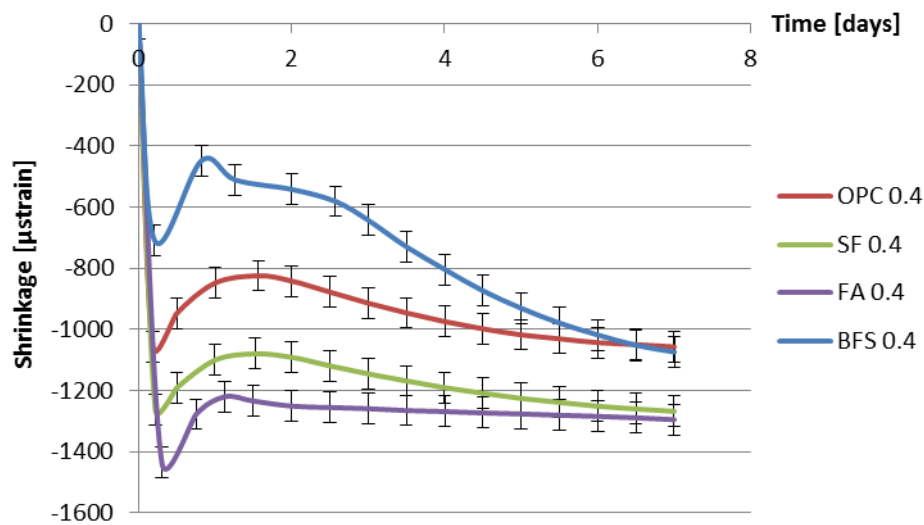


Figure 4.15 Autogenous deformation vs. age for different cement pastes with water- binder ratio of 0.4 (Starting time: final setting time)

From Figure 4.14 and Figure 4.15 a fast shrinkage can be noticed after final setting. After a short period of swelling the specimens shrink steadily. According to some researchers (Miao et al. 2007, Bentur 2002, Darquennes et al. 2011, Sant et al. 2006) taking the final setting time as the starting point of autogenous shrinkage is questionable. The starting time of autogenous shrinkage is roughly equal to the setting time but is not necessarily identical with it (Bentur 2003). A lot of researchers start counting autogenous shrinkage from ‘Time-zero’ which is defined as the duration between this instant when the water comes in contact with cement and the time at which the concrete develops sufficient structure to enable tensile stress transfer through the concrete (Weiss 2002, Kovler et al. 2007). According to Bjøntegaard (1999), the time when the maximum (macroscopically)

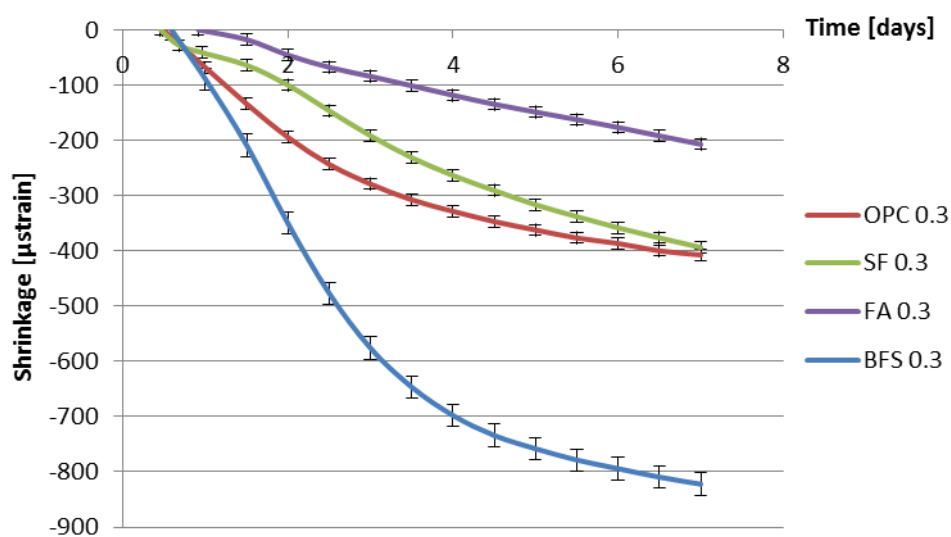


Figure 4.16 Autogenous deformation vs. age for different kinds of cement paste with water binder ratio of 0.3 (Starting time: after early-age swelling)



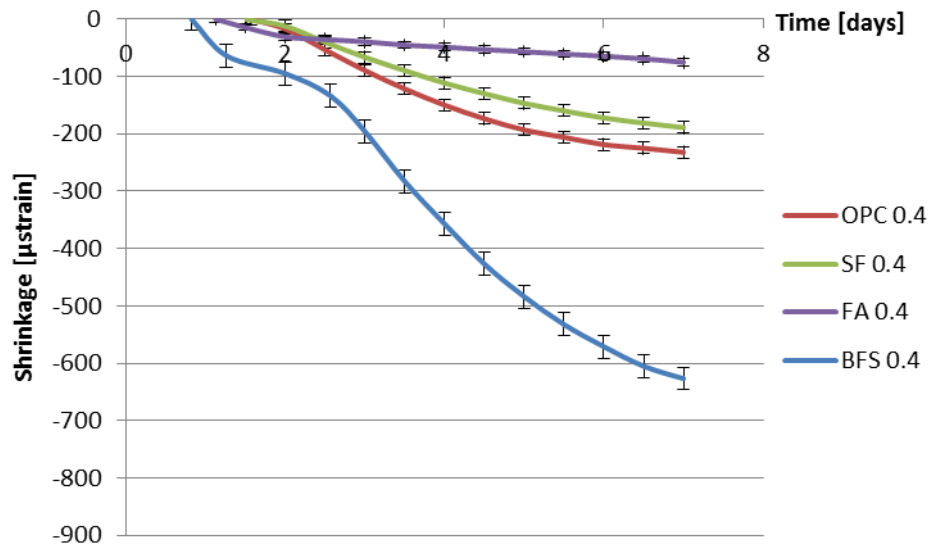


Figure 4.17 Autogenous deformation vs. age for different kinds of cement paste with water binder ratio of 0.4 (Starting time: after early-age swelling)

swelling is observed can be taken as the starting time of autogenous shrinkage ('Time-zero'). In this section the steady shrinkage after maximum (macroscopically) observed swelling is considered as autogenous shrinkage of the cement pastes.

Figures 4.16 and 4.17 show that in the first 7 days the addition of fly ash leads to smaller autogenous shrinkage of cement paste compared with that of ordinary Portland cement paste with same water-binder ratio. These results are in line with findings of Tangtermsirikul (1999). The lower activity of fly ash compared to ordinary Portland cement is considered the major reason of smaller autogenous shrinkage of fly ash cement paste (Fang et al. 2011). The low activity of fly ash led to slower hydration and resulted in a slower decrease of the internal relative humidity and smaller shrinkage at early age.

Figs 4.16 and 4.17 also show that in the first 7 days the addition of silica fume does not lead to bigger autogenous shrinkage of cement paste compared with that of ordinary Portland cement paste with same water-binder ratio. This result is contradictory to the finding reported by Jensen and Hansen (1996) that the addition of silica fume significantly increases the autogenous shrinkage of cement paste. The silica fume used by Jensen and Hansen is in slurry form which has large specific surface area and high activity at early age. High activity of silica fume results in larger chemical shrinkage and bigger drop of internal relative humidity which result in larger autogenous shrinkage of cement paste (Jensen et al. 1996). The silica fume used in this thesis is commercial dry densified silica fume produced by Elkem. The mean particle sizes of silica fume is not significantly smaller than Portland cement (as shown in Figure 4.1). The activity of dry densified silica fume at early age is not as high as that of silica fume in slurry form. The drop of internal relative humidity of cement paste dose not increase with the addition of dry densified silica fume (as shown in Figure 4.9 and Figure 4.10) and the autogenous shrinkage of silica fume cement paste is not significantly bigger than that of ordinary Portland cement paste with same water-binder ratio.

The measured autogenous shrinkage of BFS cement paste is much bigger than that of Portland cement paste with the same water-binder ratio. According to Chan et al. (1999), the autogenous deformation of concrete with 40% BFS is significantly higher than that of concrete without BFS. When the BFS content is higher, the autogenous deformation

decreases slightly, but it still remains higher than that of concrete without BFS. The bigger autogenous shrinkage of BFS cement paste has two reasons. First, the stiffness of BFS cement paste, e.g. elastic modulus, is lower than that of Portland cement paste with same water-binder ratio at the same curing age. Second, the drop of internal relative humidity of BFS cement paste is larger than that of ordinary Portland cement paste with the same water-binder ratio, as shown earlier in Figures 4.9 and 4.10. Similar results are also found by Lura and Ekaputri (Lura 2003, Ekaputri et al. 2016). According to Ishida et al. (2003), BFS cement pastes have a finer pore structure than Portland cement pastes. Finer pores of BFS cement paste result in a smaller radius of air-water meniscus and larger internal driving force of autogenous shrinkage, e.g. capillary tension.

#### 4.4.7 Autogenous deformation as function of relative humidity

Figures 4.18 and 4.19 show the measured autogenous deformations as a function of internal relative humidity of different cement pastes with water-binder ratio of 0.3 and 0.4. The starting time is after the maximum early-age swelling.

The Figures 4.18 and 4.19 show that the autogenous shrinkage of cement pastes with different supplementary materials follows a similar trend with decreasing internal relative humidity. This is consistent with the assumed existence of a relationship between autogenous deformation and relative humidity changes in the capillary pores of the hardening cement paste (L'Hermite 1960, Wittmann 1968, Powers 1968). The Figures 4.18 and 4.19 also show that the autogenous shrinkage of different cement pastes at the same relative humidity can differ significantly. The difference between the autogenous shrinkage of different cement pastes at the same relative humidity might be attributed to the different resistance to deformation, e.g. elastic modulus, of different cement pastes. Under the same internal load, the elastic deformation of different cement paste is different. The different capillary tension and resistance of cement paste to deformation will result in different autogenous shrinkage of different cement paste at the same relative humidity. In order to illustrate this, the Portland cement paste and BFS cement paste with water-binder ratio 0.3

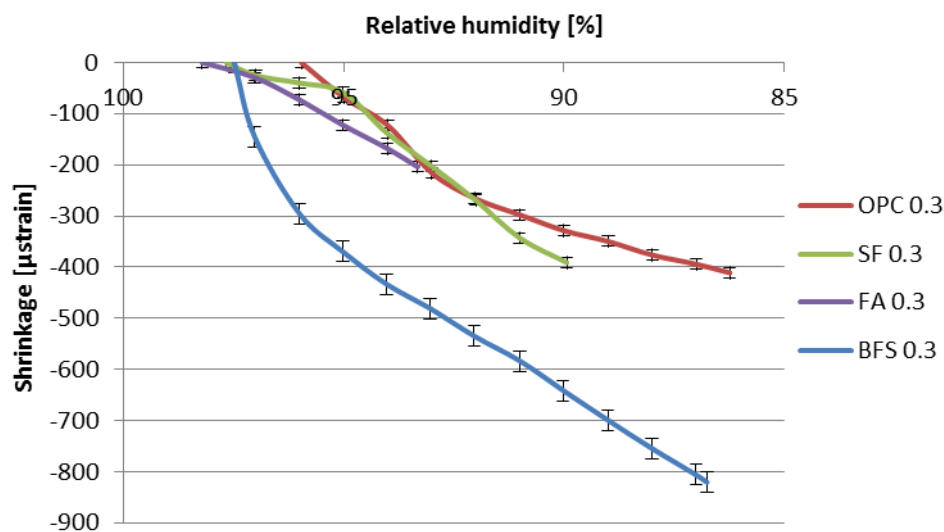


Figure 4.18 Autogenous deformation vs. internal relative humidity for different kinds of cement paste with water binder ratio of 0.3

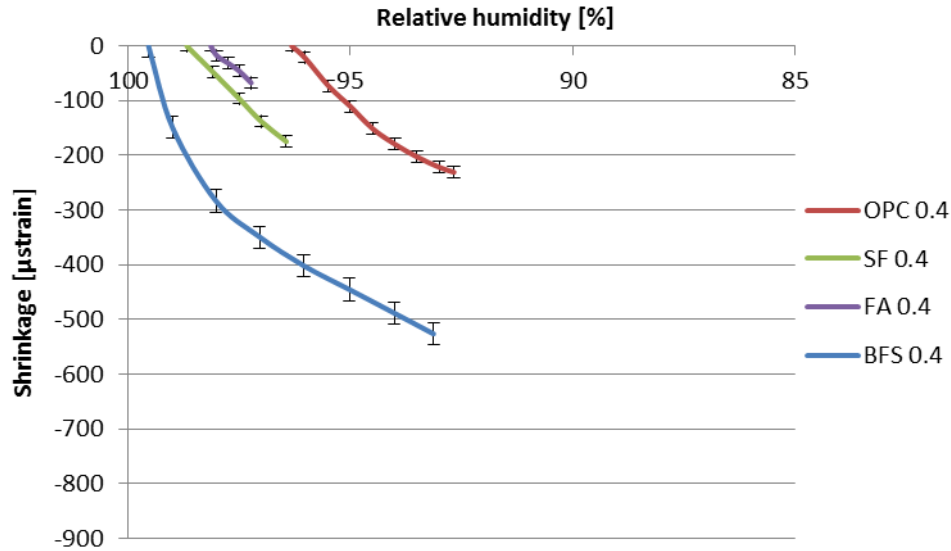


Figure 4.19 Autogenous deformation vs. internal relative humidity for different kinds of cement paste with water binder ratio of 0.4

is taken as an example. The elastic modulus of Portland cement paste and BFS cement paste with water-binder ratio 0.3 at seven days is 25 GP and 20 GP, respectively (see Figure 5.10). Under the same internal load, the elastic deformation of BFS cement paste is 1.25 times bigger than that of Portland cement paste. It should also be noticed that the cement paste is visco-elastic material. Under internal load, the autogenous shrinkage of different cement pastes includes an elastic part and creep part. Apart from the elastic part, the creep part of the autogenous shrinkage of different cement pastes are also different. In the following chapter, autogenous shrinkage of cement paste will be simulated with the model proposed in Chapter 3, which model includes an elastic part and a creep part and the role of elastic part.

## 4.5 Concluding remarks

In order to provide data for modeling autogenous shrinkage in the first week of hydration, measurements of setting time, internal relative humidity, non-evaporable water content, chemical shrinkage, compressive strength and autogenous deformation of cement paste are presented and discussed in this chapter. Pure Portland cement paste and three kinds of cement paste with different supplementary material, i.e. silica fume, fly ash and blast furnace slag, were considered. Water-binder ratios of these cement pastes are 0.3 and 0.4. The following conclusions can be drawn:

### 1) Final setting time

The final setting times seem hardly influenced by the addition of silica fume. The commercial dry densified silica fume used in this thesis is primarily present in the form of clusters of spheres. Its influence on the hydration process and final setting time is not as pronounced as that of silica fume added in slurry form. The addition of fly ash increases the final setting time of fly ash cement paste compared to that of ordinary Portland cement

paste. The chemical composition and slow reaction of fly ash is considered the main reason of the longer setting time of fly ash cement paste (Berg et al. 1991).

### *2) Non-evaporable water content*

The non-evaporable water content in fly ash cement pastes is lower than in ordinary Portland cement pastes with the same water-binder ratio and the same curing age. Fly ash contains a higher amount of inactive minerals compared with Portland cement. Fly ash reacts, therefore, slower than Portland cement, resulting in a lower non-evaporable water content at the same curing age.

The non-evaporable water content of the cement pastes with silica fume and BFS was lower than that of pure Portland cement paste at the same curing age. The reason of the lower non-evaporable water content of silica fume and BFS cement paste is the same, i.e. less water bound by silica fume and BFS than bound by Portland cement (Taylor 1992).

### *3) Chemical shrinkage*

Up to seven days the chemical shrinkage of the cement paste with fly ash was much smaller than that of Portland cement paste. Chemical shrinkage is proportional to the degree of hydration (Criado et al. 2007, Parrott et al. 1990). Because of the low reactivity of fly ash, the degree of hydration of fly ash cement paste is lower than that of Portland cement at the same curing age.

Chemical shrinkage of the BFS cement paste develops faster than that of Portland cement paste in the first 3 days. The density of hydration product of Portland cement and BFS cement paste is similar. According to Thomas et al. (2012) the density of BFS is lower than that of Portland cement. Lower density of BFS results in bigger volume change between unhydrated BFS and hydration products.

### *4) Internal relative humidity*

The moment that the relative humidity of BFS cement paste starts to drop significantly is later than that of Portland cement paste with the same water-binder ratio. The later start of the RH drop of BFS cement paste can be attributed to the low activity of BFS in CEM III/B 42.5N after final setting time.

### *5) Compressive strength*

For running the numerical simulation of autogenous shrinkage as proposed in Chapter 3, the evolution of the elastic modulus must be known. In this study, the elastic modulus of cement paste is calculated from the measured compressive strength of cement paste. The compressive strength of the samples with silica fume is lower than of the samples without silica fume. This is different from the common understanding that the addition of silica fume will increase the strength of concrete. Increasing strength of silica fume concrete is caused by the improvement of the aggregate-matrix bond (Houssam et al. 1995). For the silica fume pastes, in the absence of ITZ, there is no substantial strengthening effect.

### *6) Magnitude of autogenous shrinkage*

The measured autogenous deformations are the result of expansion and shrinkage processes which develop simultaneously. When shrinkage is dominant, the external volume will decrease, otherwise it will increase.

The type of cement has big effect on autogenous shrinkage. The addition of fly ash resulted in smaller autogenous shrinkage of cement paste compared with that of ordinary Portland cement paste with same water-binder ratio. The low activity of fly ash is

considered the major reason for this. The measured autogenous shrinkage of BFS cement paste is much bigger than that of Portland cement paste with same water-binder ratio. Lower elastic modulus and larger drop of relative humidity of BFS cement paste are considered as the two major reason.

The measurements also show that there is a relationship between autogenous deformation and relative humidity changes in the capillary pores of the hardening cement paste. The autogenous shrinkage of cement pastes with different supplementary materials follow a similar trend with decreasing internal relative humidity.



# Chapter 5

## Numerical simulation of autogenous shrinkage of ordinary Portland cement paste and cement paste with supplementary materials

### 5.1 Introduction

In chapter 3 a simulation model of autogenous shrinkage has been described. In that model autogenous shrinkage was divided into two parts, an elastic part and a time-dependent part. The elastic part and time-dependent part of autogenous shrinkage are calculated with Hooke's law and activation energy theory, respectively. Figure 5.1 shows a scheme of the formulas used in this simulation model of autogenous shrinkage. In this model, the degree of saturation, capillary tension and elastic modulus of cement paste are the inputs. In chapter 4 early-age properties of Portland cement pastes and cement pastes with supplementary materials were measured for providing input for modelling of the autogenous shrinkage. Non-evaporable water content and chemical shrinkage are used to calculate the degree of saturation. Internal relative humidity is used to calculate capillary tension. Compressive strength is used to calculate the elastic modulus of cement paste.

In this chapter, the degree of saturation, capillary tension and elastic modulus are calculated separately, using the experimental data generated in chapter 4. With these calculated results, the autogenous shrinkage of Portland cement pastes and cement pastes with supplementary materials are calculated with the proposed simulation model in chapter 3. The calculated autogenous shrinkages of different cement pastes are compared with the experimental results to evaluate the accuracy of the predictions with the proposed simulation model.

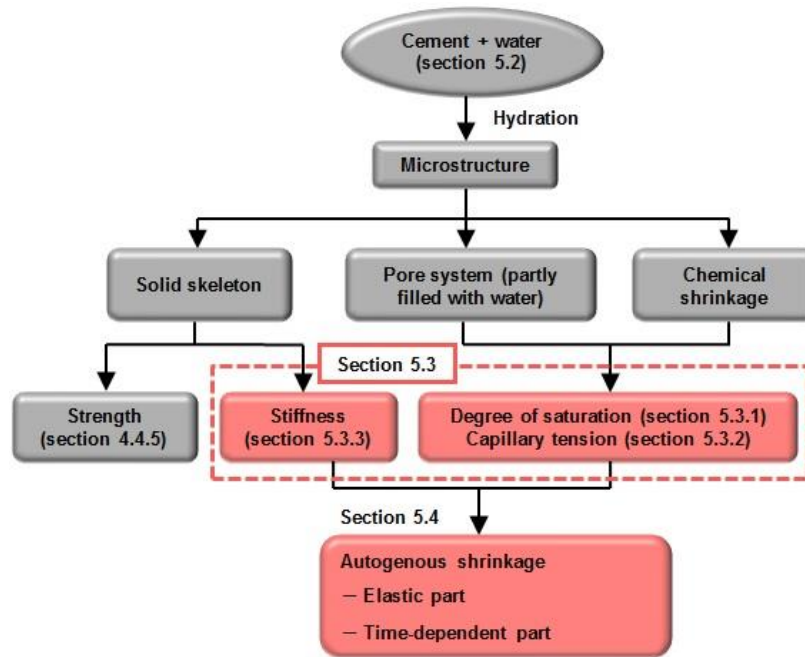


Figure 5.1 Scheme of autogenous shrinkage calculation

## 5.2 Mixture compositions of cement pastes used for verifying the numerical model

In order to validate the proposed numerical model of autogenous shrinkage presented in chapter 3, eight Portland cement and blended cement paste mixtures are studied, i.e. Portland cement paste, silica fume cement paste, fly ash cement paste and slag cement paste. The water/binder ratios are 0.3 and 0.4. The mixture compositions were listed in Table 4.3. More details of the materials were given in section 4.2.

## 5.3 Determination of material parameters used for numerical simulation of autogenous shrinkage

For calculating the autogenous shrinkage of cement paste with the numerical model proposed in chapter 3, the following materials parameters have to be determined (see Figure 5.1):

- 1) Degree of saturation
- 2) Capillary tension
- 3) Elastic modulus

### 5.3.1 Calculation of the degree of saturation

During the hydration process, a porous rigid microstructure forms while free water in the cement paste is consumed. The cement paste becomes partially saturated. The degree of saturation  $S_w$  can be calculated using Powers' model or directly from the non-evaporable



water content and the chemical shrinkage measurements, as mentioned in Chapter 3. In Powers' model, the degree of saturation  $S_w$  [-] is calculated based on the degree of hydration  $\alpha$  [-]. For blended cement pastes with supplementary materials, it is not easy to determine the degree of hydration. Therefore, in this chapter, the degree of saturation is calculated directly from the non-evaporable water content and chemical shrinkage measurements. It holds (Powers et al. 1948):

$$S_w = \frac{V_{ew}(\alpha)}{V_p(\alpha)} = \frac{V_{iw} - V_{new}}{V_{iw} - V_{new} + V_{cs}} \quad (5.1)$$

where  $V_{ew}$  [cm<sup>3</sup>/cm<sup>3</sup>] is the evaporable water content in the hardening paste,  $V_p$  [cm<sup>3</sup>/cm<sup>3</sup>] the pore volume of the paste,  $V_{iw}$  [cm<sup>3</sup>/cm<sup>3</sup>] the initial water content;  $V_{new}$  [cm<sup>3</sup>/cm<sup>3</sup>] the non-evaporable water content in the paste and  $V_{cs}$  [cm<sup>3</sup>/cm<sup>3</sup>] the volume of chemical shrinkage.

In order to calculate the degree of saturation with Equation 5.1, the non-evaporable water content  $V_{new}$  and the chemical shrinkage  $V_{cs}$  were measured as mentioned in Chapter 4. The measured non-evaporable water content  $V_{new}$  of different cement pastes with water-binder ratio 0.3 and 0.4 were shown in Figures 4.6 and 4.7 as a function of age. The chemical shrinkage  $V_{cs}$  of four different cement pastes was shown in Figure 4.8. The calculated degree of saturation of these four cement pastes with water-binder ratio of 0.3 and 0.4 are shown in Figures 5.2 and 5.3 as a function of age.

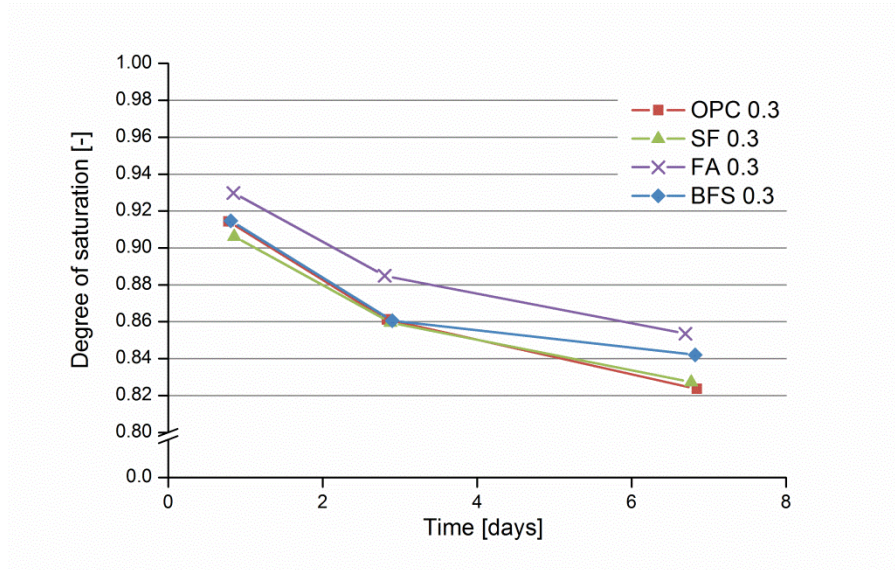


Figure 5.2 Calculated degree of saturation as a function of age for different cement pastes with water binder ratio of 0.3 (calculated with Equation 5.1)

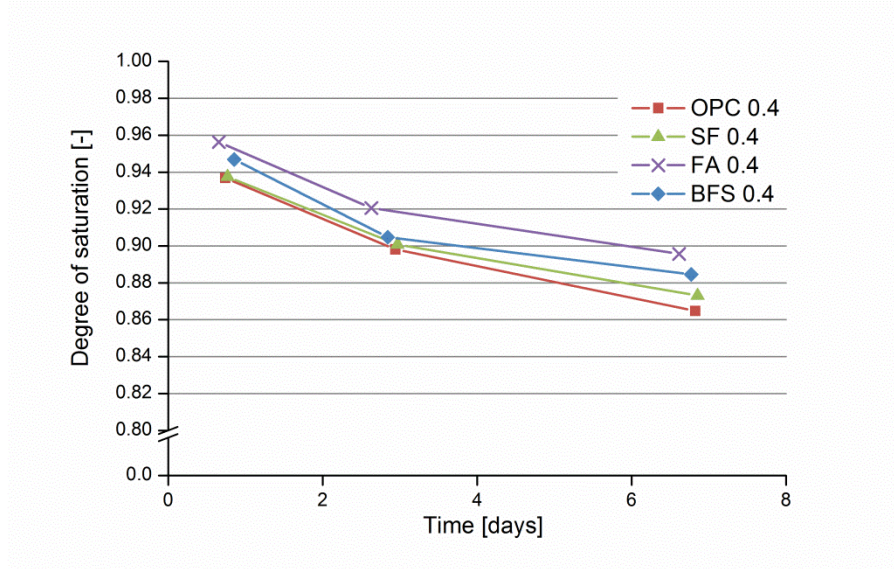


Figure 5.3 Calculated degree of saturation as a function of age for different cement pastes with water binder ratio of 0.4 (calculated with Equation 5.1)

These figures show that at the same age the degree of saturation of fly ash cement pastes is higher than that of other cement pastes. This is due to the fact that the chemical shrinkage of the fly ash cement paste is lower than that of other cement pastes in the first week, as shown in chapter 4. The magnitude of chemical shrinkage is proportional to the degree of reaction (Criado et al. 2007, Parrott et al. 1990). Compared with Portland cement, fly ash contains a higher amount of inactive minerals, such as quartz and mullite. The low reactivity of fly ash leads to a slower hydration rate than that of other cements and results in smaller shrinkage at early age (Fang et al. 2011). The lower chemical shrinkage leads to higher degree of saturation.

### 5.3.2 Capillary tension

The capillary tension  $\sigma_{cap}$  [MPa], in pores with radius  $r_k$  [m] can be calculated with the Laplace equation as (Defay et al. 1966):

$$\sigma_{cap} = -\frac{2\gamma}{r_k} \quad (5.2)$$

where  $\gamma$  [N/m] is the surface tension of the pore water;  $r_k$  [m] the radius of the largest capillary pore still filled with water. The radius  $r_k$  of the largest capillary pore still filled with water can be calculated as a function of the measured internal relative humidity with the classic Kelvin equation (von Helmholtz 1886):

$$r_k = -\frac{2\gamma V_w}{\ln \frac{RH}{RH_S} RT} \quad (5.3)$$

where  $\gamma$  [N/m] is the surface tension of the pore water;  $V_m$  [m<sup>3</sup>/mol] the molar volume of the pore water;  $RH_S$  [-] the drop of internal relative humidity due to effect of dissolved ions;

$RH$  [-] the measured internal relative humidity;  $R$  [J/(mol · K)] the universal gas constant and  $T$  [K] the absolute temperature. More details can be found in Section 3.2.3.

In order to calculate the capillary tension the relative humidity should be determined first. The measured internal relative humidity of different cement pastes with water-binder ratio 0.3 and 0.4<sup>1)</sup> are shown in Figure 5.4<sup>2)</sup>.

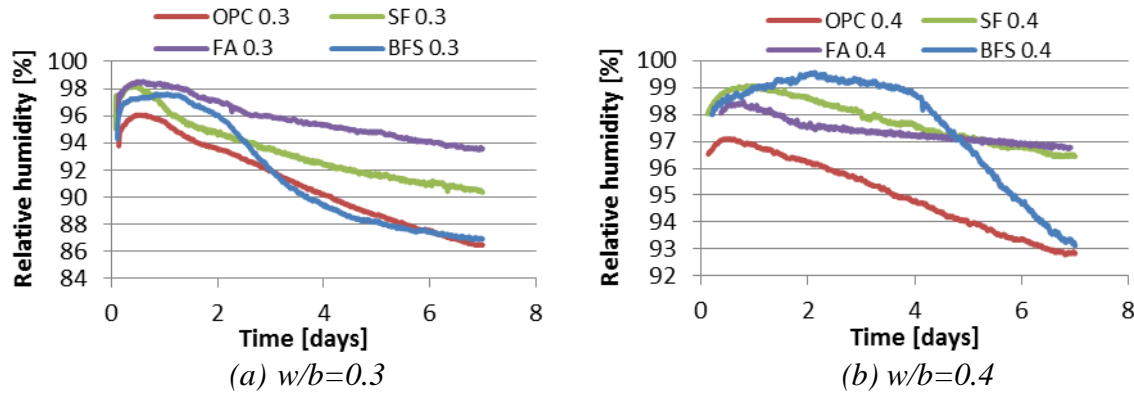


Figure 5.4 Measured internal relative humidity vs. age for different cement pastes (Section 4.4.4)

In order to calculate the capillary tension in the pore water with Equation 5.2, the radius of the largest pore still filled with water must be known. The values of the radius of the largest water-filled pore is calculated with Equation 5.3 as a function of the relative

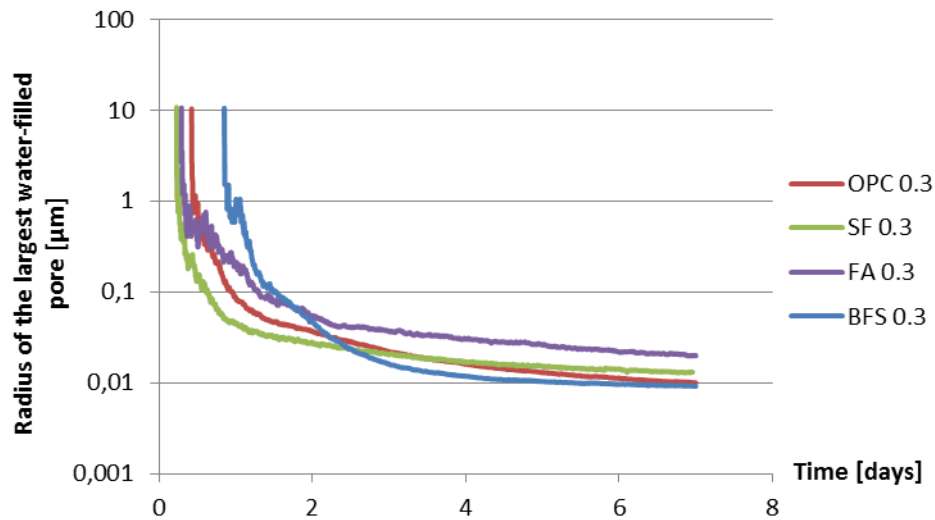


Figure 5.5 Calculated radius of the largest water-filled pore of different cement pastes with water-binder ratio of 0.3 (calculated with Equation 5.3)

1) The mixture compositions were listed in Table 4.3.

2) The experimental method and equipment were presented in Chapter 4.

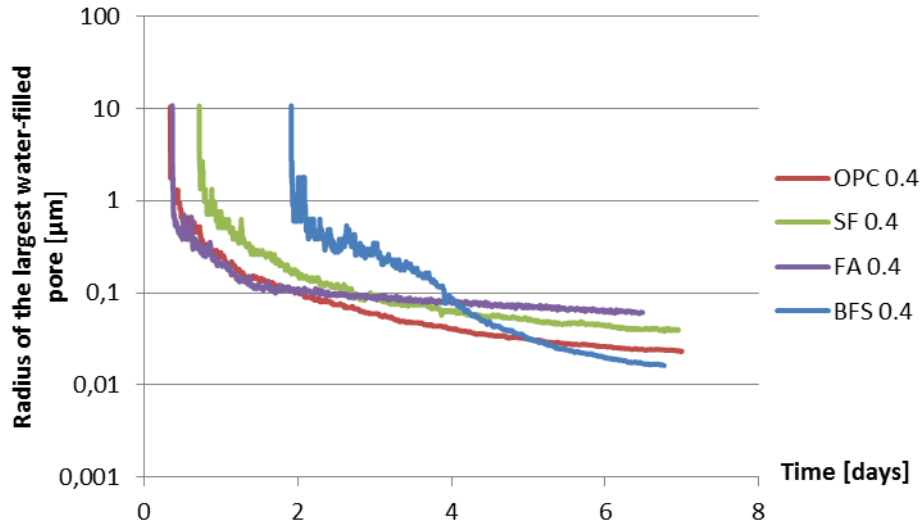


Figure 5.6 Calculated radius of the largest water-filled pore of different cement pastes with water-binder ratio of 0.4 (calculated with Equation 5.3)

humidity. The calculated values of the radius of the largest water-filled pore of cement pastes with water-binder ratio of 0.3 and 0.4 are shown in Figures 5.5 and 5.6, respectively. The starting point of calculation is the time when the measured internal relative humidity reaches its peak (see Figure 5.4) and starts to decrease. The calculated capillary tension of different cement pastes with water-binder ratio 0.3 and 0.4 is shown as a function of age in Figures 5.7 and 5.8.

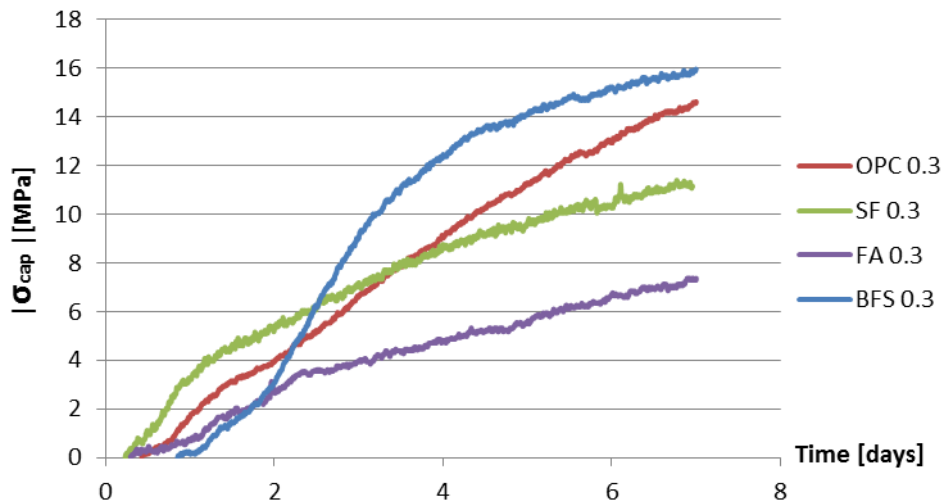


Figure 5.7 Calculated capillary tension in the pore water for different cement pastes with water-binder ratio of 0.3 as a function of age (calculated with Equation 5.2)

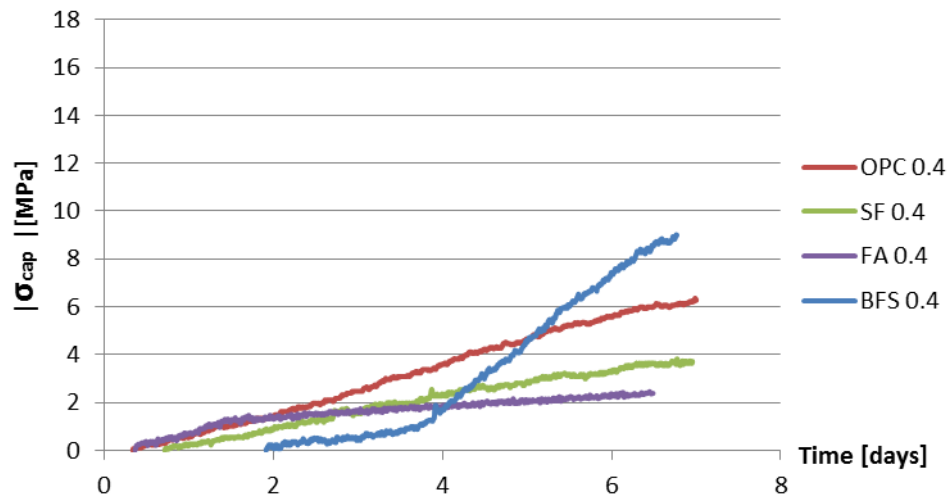


Figure 5.8 Calculated capillary tension in the pore water for different cement pastes with water-binder ratio of 0.4 as a function of age (calculated with Equation 5.2)

By comparing Figures 5.7 and 5.8 it is clear that for the same curing age the capillary tension in cement pastes with lower water-binder ratio is larger than that of cement paste with higher water-binder ratio. The reason for this is that the relative humidity of cement paste with lower water-binder ratio will decrease faster with elapse of time than that of cement paste with higher water-binder ratio.

Similar calculated results of capillary tension can be found in Lebental's paper (Lebental et al. 2012). In that paper the calculated capillary pressure and water saturation were plotted against relative humidity and shown in Figure 5.9. That figure shows that the capillary pressure (tension) increases from 0 MPa to 20 MPa when the relative humidity drops from 100% to 85%. In BFS cement pastes with water-binder ratio 0.3, the calculated capillary tension increases from 0 MPa to 16 MPa in the first 7 days after casting (Figure 5.7). In these 7 days the measured internal relative humidity drops from 98% to 87% (Figure 5.4). This result is in accordance with that reported by Lebental.

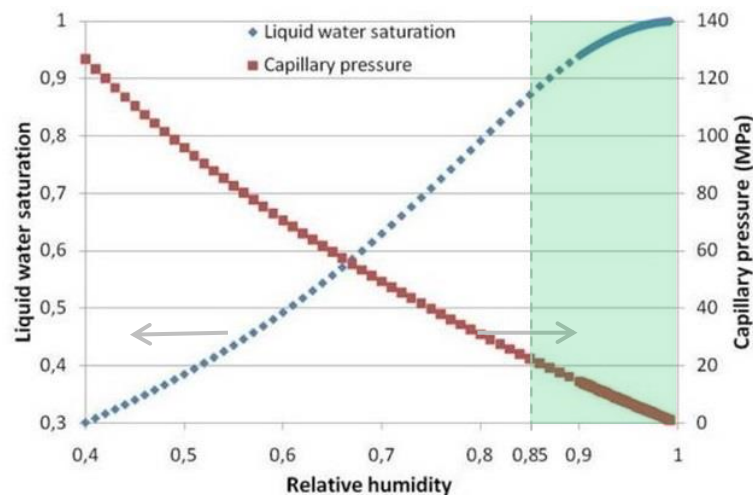


Figure 5.9 Calculated capillary pressure (tension) using Kelvin's equation and calculated water saturation, both as function of relative humidity (w/c:0.3) (after Lebental et al. 2012)

### 5.3.3 Elastic modulus

For calculating the elastic part of the autogenous deformation of cement paste the evolution of the elastic modulus is needed. In the past, several equations for predicting the elastic modulus  $E$  of cementitious materials as a function of compressive strength  $f_c$  have been proposed (ACI Committee 363, AIJ 1985, Takafumi et al. 2009). Among these equations, the equation proposed by Takafumi et al. (2009) takes the effect of type of supplementary material on the elastic modulus into consideration. In this thesis, this equation is adopted to calculate the elastic modulus  $E$  [MPa]. It holds:

$$E = k_1 k_2 \varphi f_c^{1/3} \rho^2 \quad (5.4)$$

where  $k_1$  [-] is the correction factor related to the type of aggregate. For cement paste,  $k_1$  is taken as 1 because there is no effect of aggregate on the elastic modulus of cement paste.  $k_2$  [-] is a correction factor related to the type of supplementary material.  $\varphi$  [-] is a fitting coefficient, its value is taken as  $\approx 0.0015$  (Takafumi et al. 2009).  $\rho$  [N/m<sup>3</sup>] the unit weight of the cement paste or concrete.

From experimental results Takafumi found that when fly ash is used as a supplementary material, the value of  $k_2$  is generally larger than 1. Conversely, when silica fume and ground-granulated blast furnace slag are added to concrete, the correction factor  $k_2$  is usually smaller than 1. The values of  $k_2$  for different supplementary materials are shown in Table 5.1 (Takafumi et al. 2009). The values of the compressive strength  $f_c$  were shown in Figures 4.12 and 4.13. The elastic modulus of different kinds of cement paste, calculated with Equation 5.4, are shown in Figure 5.10.

*Table 5.1: Practical values of correction factor  $k_2$  for pastes made with different binders*

Type of addition	$k_2$
Silica fume, ground-granulated blast-furnace slag, fly ash fume	0.95
Fly ash	1.1
Addition other than above	1.0

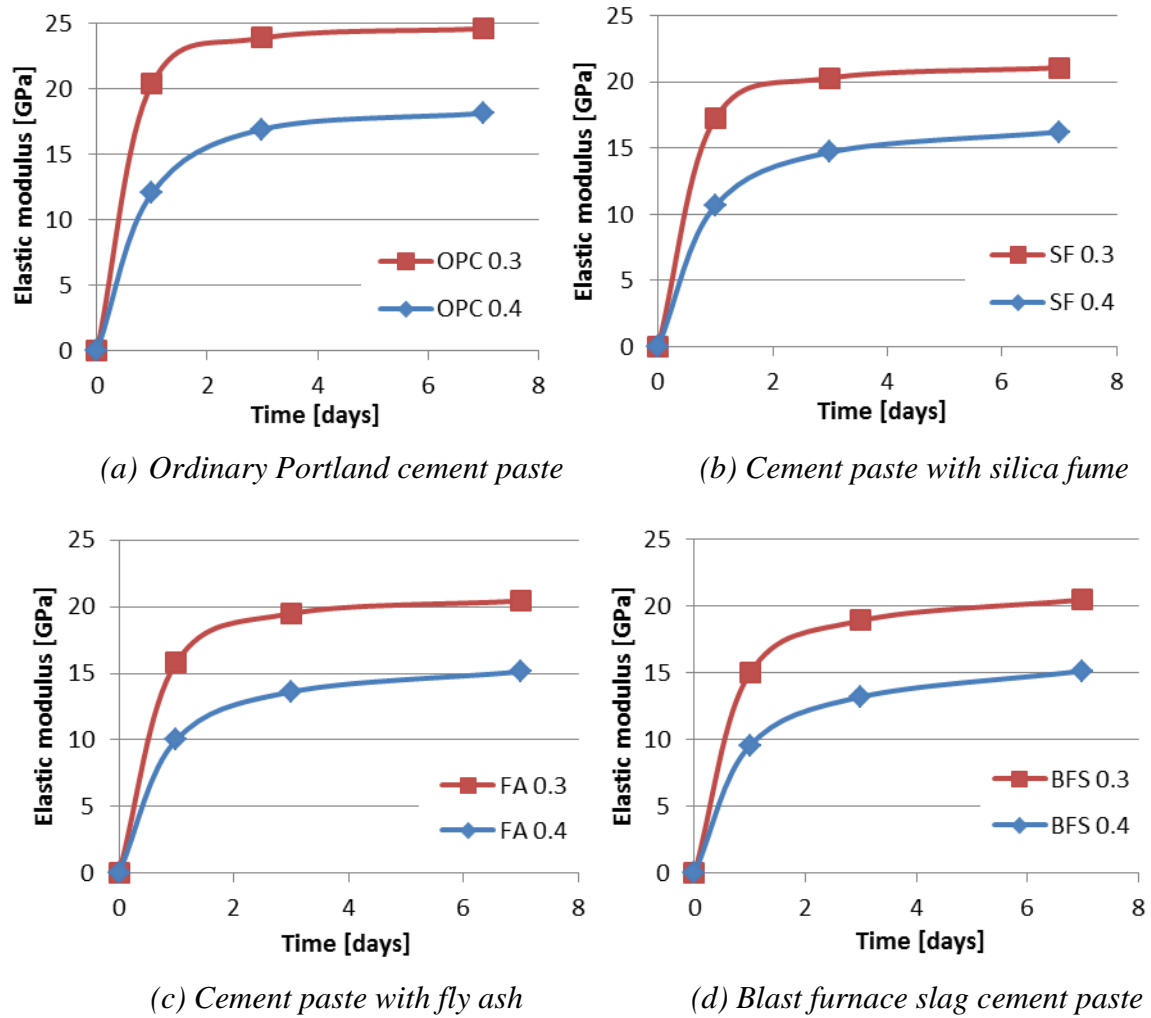
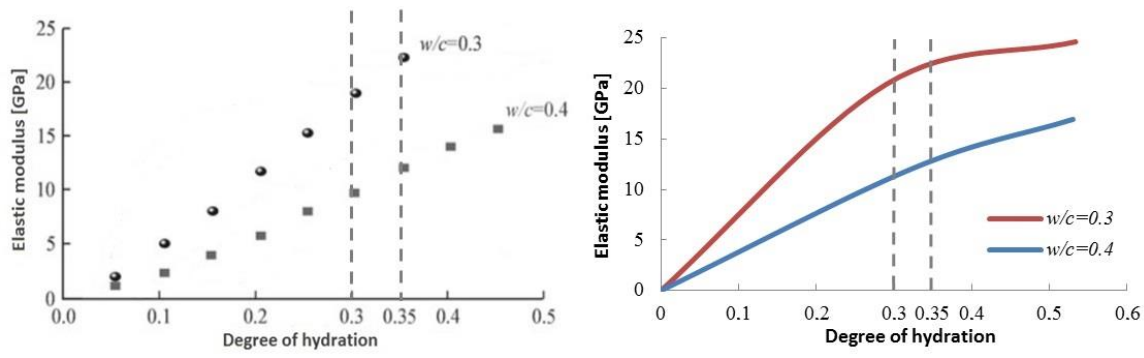


Figure 5.10 Calculated elastic modulus vs. age of different cement pastes with water-binder ratio of 0.3 and 0.4 (calculated with Equation 5.4)

Similar results can be found in Tian's paper (Tian et al. 2013). In that paper, the measured elastic modulus of Portland cement pastes with water-binder ratio 0.3 and 0.4 is presented as a function of the degree of hydration  $\alpha$ , as shown in Figure 5.11(a). Figure 5.11(b) shows the elastic modulus of Portland cement pastes with water-binder ratio of 0.3 and 0.4, calculated with Equation 5.4, also as a function of the degree of hydration  $\alpha^3$ . Figure 5.11b shows that at a degree of hydration of 0.3 the *calculated* elastic modulus of cement paste with water-binder ratio 0.3 and 0.4 is 20 GPa and 11 GPa, respectively. The *measured* elastic modulus of cement paste with water-binder ratio 0.3 and 0.4 is 20 GPa and 10 GPa, respectively. At a degree of hydration of 0.35, the *calculated* elastic modulus of cement paste with water-binder ratio 0.3 and 0.4 is 23 GPa and 13 GPa. The *measured* elastic modulus of cement paste with water-binder ratio 0.3 and 0.4 is 22 GPa and 12 GPa. Comparison of Figures 5.11(a) and 5.11(b) shows that the calculated elastic modulus is in good agreement with the measurement result.

3) The degree of hydration  $\alpha$  of Portland cement paste is simulated with HYMOSTRUC. See footnote Section 3.2.3.





(a) Measured elastic modulus (b) Elastic modulus calculated with Eq. 5.4

Figure 5.11 Measured elastic modulus (after Tian et al. 2013) and calculated elastic modulus vs. degree of hydration for Portland cement paste with water binder ratio of 0.3 and 0.4

#### 5.4 Autogenous deformation – Elastic plus time-dependent part

In the simulation model for autogenous shrinkage presented in Chapter 3, the deformation of cement paste has been divided into two parts, an elastic and time-dependent part, as shown in Figure 5.12 and Equation 5.5:

$$\varepsilon(t, \tau) = \varepsilon_{el}(\tau) + \varepsilon_{cr}(t, \tau) \quad (5.5)$$

where  $\varepsilon(t, \tau)$  is the total deformation at time  $t$ ;  $\varepsilon_{el}(\tau)$  the elastic deformation at time  $\tau$ ;  $\varepsilon_{cr}(t, \tau)$  the creep at time  $t$ ;  $\tau$  the time at loading.

The elastic part of the shrinkage,  $\varepsilon_{el}(\tau)$ , can be calculated with Hooke's law as (Bentz et al. 1998):

$$\varepsilon_{el}(\tau) = \frac{\kappa S_w(\tau) \sigma_{cap}(\tau)}{3K_P(\tau)} = \frac{S_w(\tau) \sigma_{cap}(\tau)}{3} \left( \frac{1-2\vartheta}{E(\tau)} - \frac{1}{K_S} \right) \quad (5.6)$$

where  $S_w$  is the degree of saturation;  $\sigma_{cap}$  is the capillary tension;  $K_P$  is the bulk modulus of the cement paste;  $\kappa$  is Biot coefficient;  $E$  is the elastic modulus of cement paste;  $\vartheta$  is the Poisson ratio of cement paste;  $K_S$  is the bulk modulus of the solid material.

For the time-dependent part of autogenous shrinkage,  $\varepsilon_{cr}(t, \tau)$ , can be calculated with (see Section 3.3.3):

$$\varepsilon_{cr}(t, \tau) = \omega \eta \kappa S_w(\tau) \sigma_{cap}(\tau) \exp\left(-\frac{Q}{RT}\right) (1-2\vartheta) \Delta\tau + \sum_{k=1}^{n-1} \Delta\varepsilon_{cr}(t_k, \tau_k) \quad (5.7)$$

where  $Q$  is the activation energy of the cement paste;  $\omega$  and  $\eta$  are structure dependent parameters;  $R$  is the universal gas constant and  $T$  is the absolute temperature. More details were given in section 3.3.3.



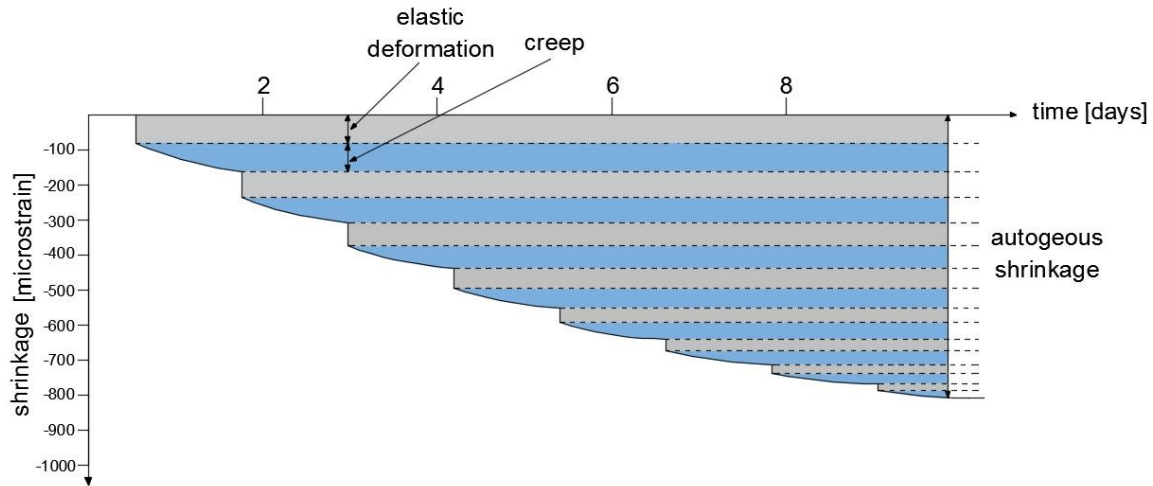


Figure 5.12 Schematic representation of autogenous shrinkage of cement paste

#### 5.4.1 Portland cement pastes with w/b ratio 0.3 and 0.4

Figures 5.13(a) and 5.14(a) show the measured and calculated autogenous deformation of ordinary Portland cement pastes with water-binder ratio 0.3 and 0.4 *after* the final setting time. The measured values of autogenous shrinkage are shown from the moment of final setting time. A fast shrinkage can be noticed after final setting. As explained in Chapter 4, taking the moment of final setting as the starting point of autogenous shrinkage is questionable. Therefore, in this section the measured autogenous shrinkage after maximum swelling of the cement paste is used for comparison with the simulation results. In Figures 5.13(b) and 5.14(b), autogenous shrinkages of Portland cement pastes with water-binder ratio 0.3 and 0.4 after the short period of swelling are presented. In the latter figures, the contributions of elastic and time-dependent part of autogenous deformation to autogenous shrinkage are shown as well.

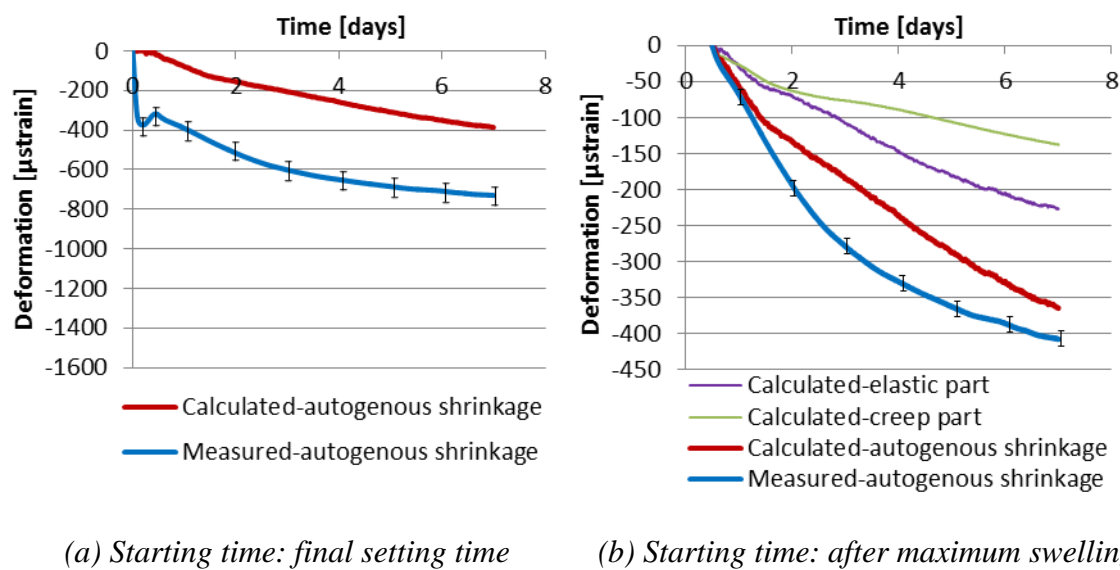


Figure 5.13 Measured and calculated autogenous deformation of Portland cement paste with water-binder ratio 0.3 (Note: Vertical scales are different)

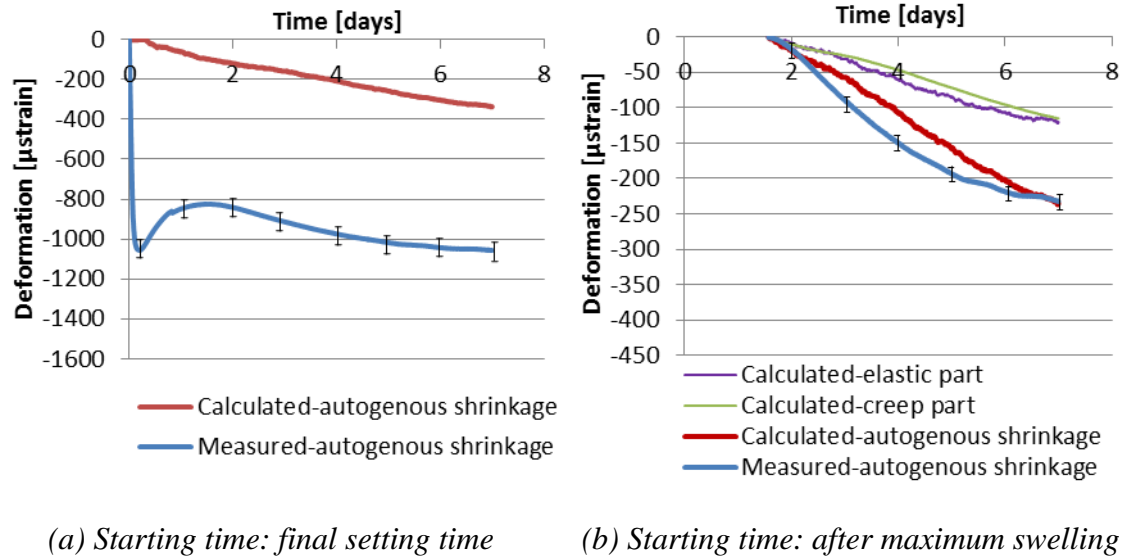


Figure 5.14 Measured and calculated autogenous deformation of Portland cement paste with water-binder ratio 0.4 (Note: Vertical scales are different)

#### 5.4.2 Portland cement pastes with 10% silica fume and w/b ratio 0.3 and 0.4

Figures 5.15 and 5.16 show the measured and calculated autogenous shrinkage of Portland cement pastes blended with 10% silica fume and water-binder ratio 0.3 and 0.4.

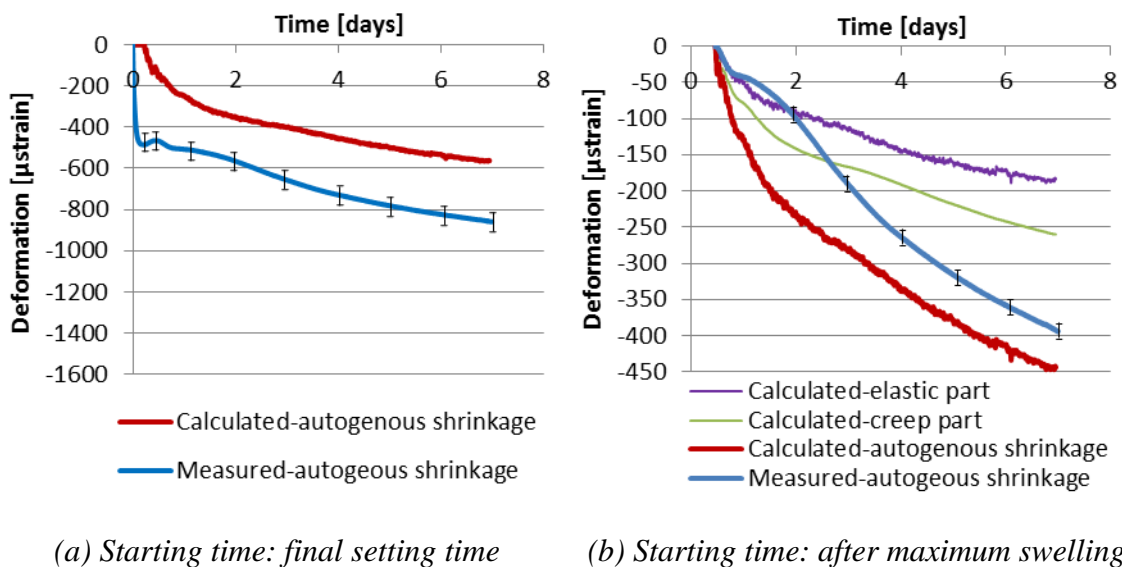


Figure 5.15 Measured and calculated autogenous deformation of silica fume cement paste (10% silica fume by weight of cement) with water-binder ratio 0.3 (Note: Vertical scales are different)

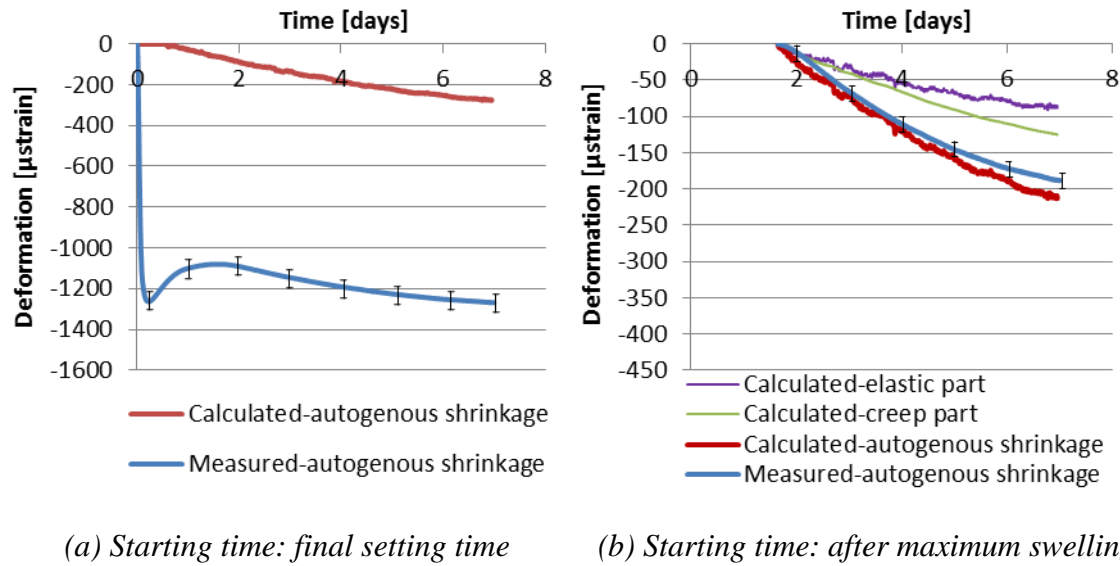


Figure 5.16 Measured and calculated autogenous deformation of silica fume cement paste (10% silica fume by weight of cement) with water-binder ratio 0.4 (Note: Vertical scales are different)

Figures 5.15(a) and 5.16(a) show the measured and calculated autogenous deformation of Portland cement pastes with 10% silica fume and water-binder ratio of 0.3 and 0.4 *after* final setting. In Figures 5.15(b) and 5.16(b), autogenous shrinkage of Portland cement pastes with 10% silica fume and water-binder ratio of 0.3 and 0.4 *after* the short period of swelling are presented. The contributions of elastic and time-dependent part of autogenous deformation to autogenous shrinkage are explicitly shown. Figure 5.15(b) shows that the measured autogenous shrinkage of SF-blended cement paste is smaller than the calculated autogenous shrinkage. After the short period of swelling, the calculated autogenous shrinkage develops faster than the measured autogenous shrinkage. This might be caused by the fact that the influence of any expansion mechanism on autogenous shrinkage has not been taken into consideration in the simulation model. The early-age deformations observed on macroscale are determined by expansion and shrinkage processes, which develop simultaneously. When the shrinkage is bigger than expansion, the external volume of cement paste will decrease. But the mechanism of expansion, i.e. crystal pressure, might still be active and will mitigate the measured shrinkage.

#### 5.4.3 Portland cement pastes with 30% fly ash and w/b ratio 0.3 and 0.4

Figures 5.17(a) and 5.18(a) show the measured and calculated autogenous deformation of the cement pastes with 30% fly ash and water-binder ratio 0.3 and 0.4 *after* final setting time.

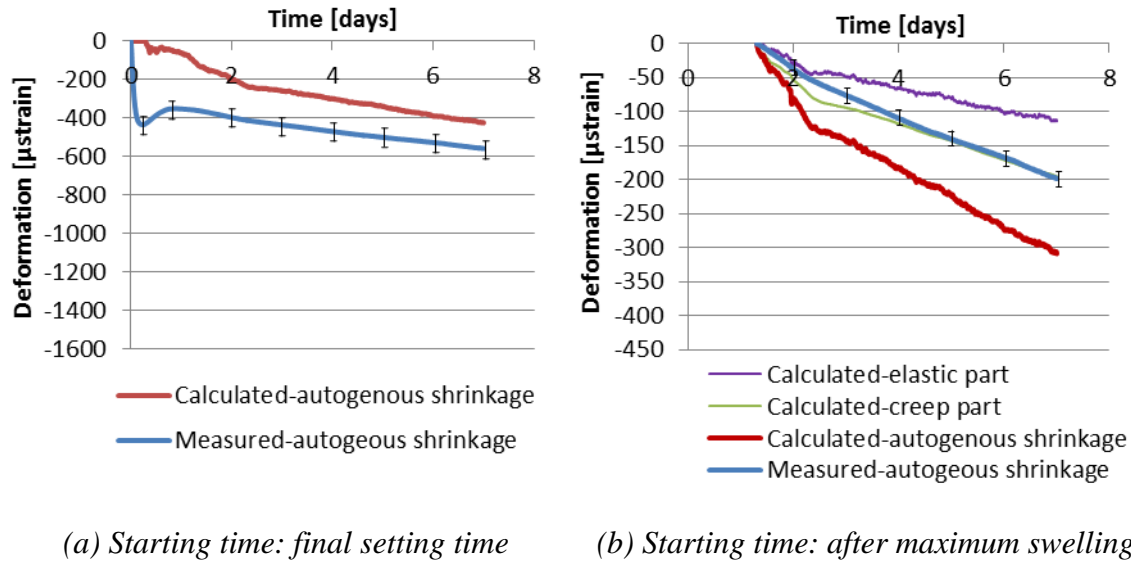


Figure 5.17 Measured and calculated autogenous deformation of fly ash cement paste (30% fly ash by weight of cement) with water-binder ratio 0.3 (Note: Vertical scales are different)

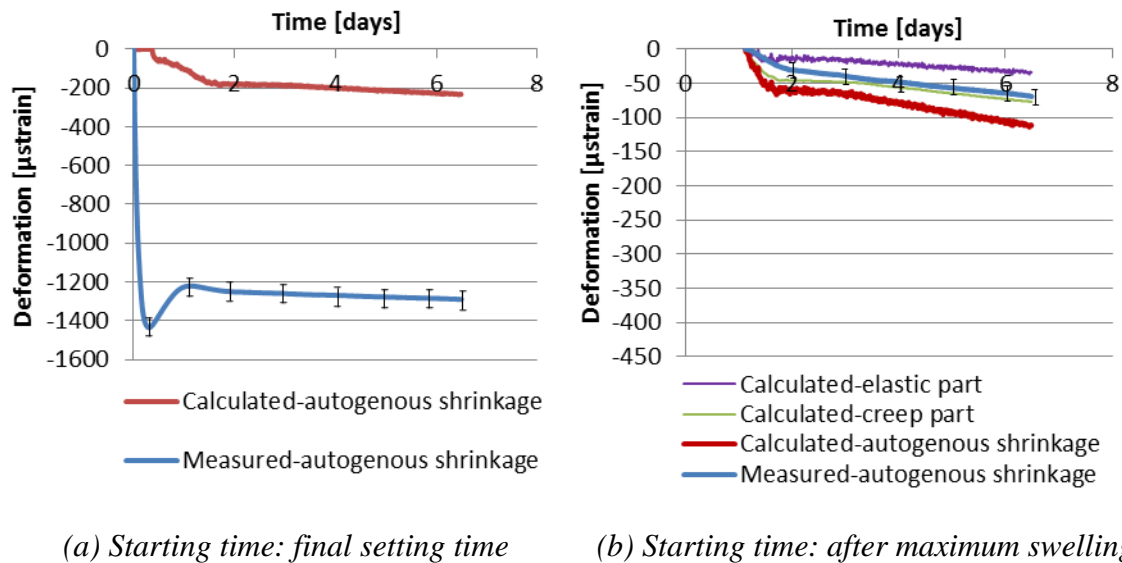


Figure 5.18 Measured and calculated autogenous deformation of fly ash cement paste (30% fly ash by weight of cement) with water-binder ratio 0.4 (Note: Vertical scales are different)

In Figures 5.17(b) and 5.18(b), autogenous shrinkage of Portland cement pastes with 30% fly ash and water-binder ratio 0.3 and 0.4 after the short period of swelling are presented. In Figures 5.17(b) and 5.18(b), a significant difference between the measured and calculated autogenous shrinkage after maximum swelling at seven days can be noticed. The difference between the measured and calculated autogenous shrinkage attention might be caused by inaccurate estimation of capillary tension. As mentioned in Section 5.3.2 capillary tension in cement paste is calculated as function of the surface tension of the pore water. In these calculation the surface tension of pore water is taken as the value of pure

water, i.e. 0.072 N/m. But in a cement paste the value of surface tension of pore water is affected by the dissolved ion concentration. The change of surface tension on the autogenous shrinkage might be a reason of the difference between the measured and calculated autogenous shrinkage.

The ion concentration will also affect the calculated capillary tension. As explained in Section 3.2.3, the value of calculated capillary tension is affected by the measured relative humidity and dissolved ions. The effect of dissolved ions in the pore solution on the calculated capillary tension changes with the ion concentration. In this thesis, the change of effect of dissolved ions on the calculated capillary tension is ignored. In fact the ion concentration of pore water of fly ash cement paste increases with time during the first 28 days *after* mixing (Taylor 1992). Its influence on the the calculated capillary tension also increases with time. Without taking the increasing ion concentration of pore water into consideration, the capillary tension is overestimated. As shown in Figure 5.4, the drop of measured relative humidity of fly ash cement paste with water-binder ratio 0.3 and 0.4 is 4% and 2% at 7 days. According to measurements of Hu (2017), the drop of relative humidity of fly ash cement paste (water-binder ratio 0.35) due to the increasing ion concentration in pore water is 1% at 7 days. By taking the effect of ion concentration of pore water into account, the calculated capillary tension of fly ash cement paste (water-binder ratio 0.3 and 0.4) is 5.25 MPa and 1.15 MPa at 7 days respectively. The calculated autogenous shrinkage of fly ash cement paste (water-binder ratio 0.3 and 0.4) is 225  $\mu$ strain and 56  $\mu$ strain at 7 days respectively (purple line in Figure 5.19). This calculated autogenous shrinkage of fly ash cement paste is close to the measured results, 200  $\mu$ strain and 65  $\mu$ strain respectively (blue line in Figure 5.19).

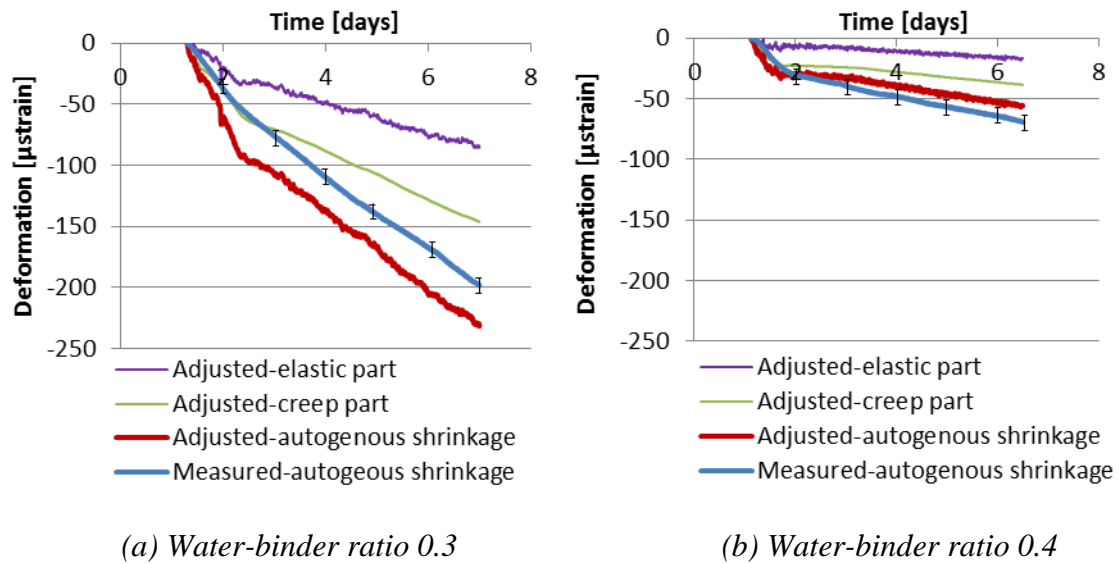


Figure 5.19 Measured and calculated autogenous deformation of fly ash cement paste (taking change of ion concentration into account) with water-binder ratio 0.3 and 0.4

#### 5.4.4 Blast furnace slag cement pastes with w/b ratio 0.3 and 0.4

Figures 5.20 and 5.21 show the measured and calculated autogenous shrinkage of BFS cement pastes with water-binder ratio 0.3 and 0.4. Figures 5.20(a) and 5.21(a) show the measured and calculated autogenous deformation of BFS cement paste with water-binder ratio 0.3 and 0.4 after the final setting time. The calculated autogenous shrinkage of BFS cement paste after early-age swelling is shown in Figures 5.20(b) and 5.21(b), subdivided in an elastic part and a creep part.

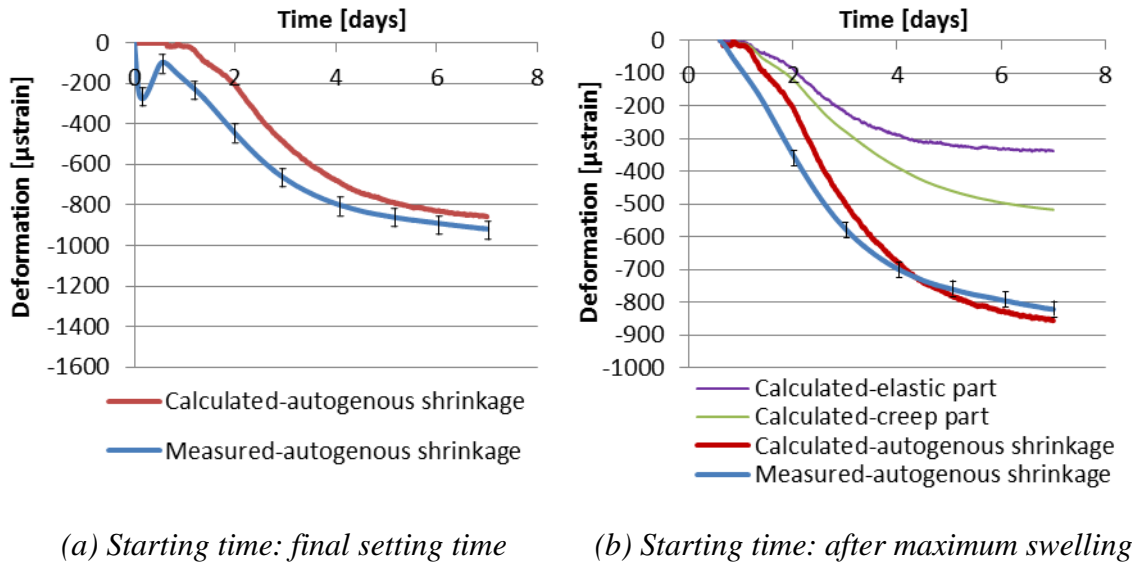


Figure 5.20 Measured and calculated autogenous deformation of blast furnace slag cement paste with water-binder ratio 0.3 (Note: Vertical scales are different)

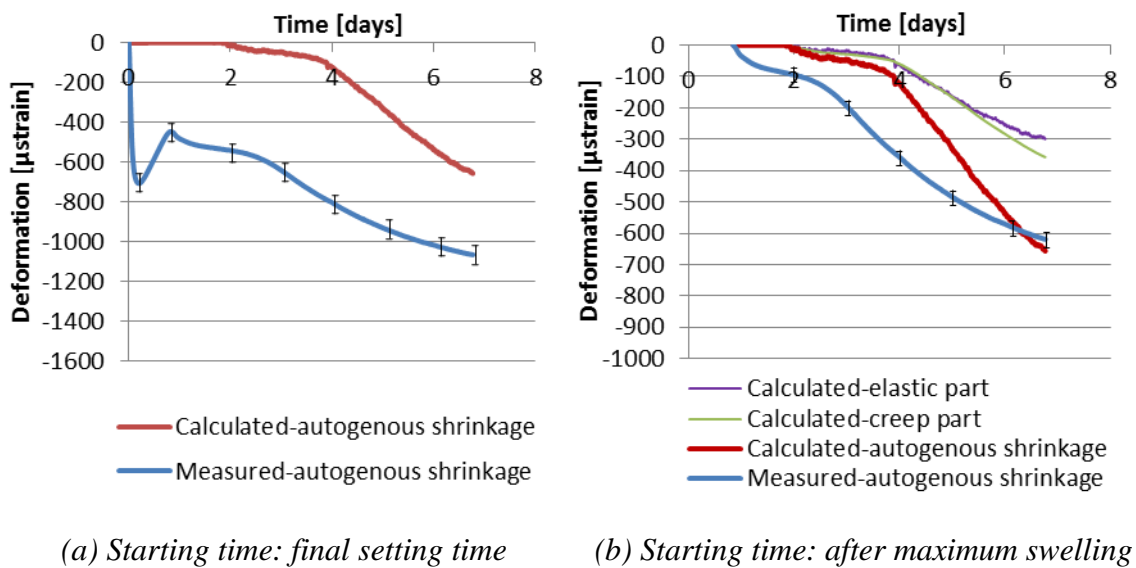


Figure 5.21 Measured and calculated autogenous deformation of blast furnace slag cement paste with water-binder ratio 0.4 (Note: Vertical scales are different)

The calculated autogenous shrinkage of BFS cement paste is much bigger than that of plain Portland cement paste with the same water-binder ratio at the same curing age (See Figures 5.13 and 5.20). The bigger calculated autogenous shrinkage of BFS cement paste may have two reasons. First, the calculated elastic modulus of BFS cement paste is lower than that of Portland cement paste with same water-binder ratio at the same curing age, as shown in Figure 5.10. In this study the elastic modulus of cement paste is calculated from the measured compressive strength. As shown in Figures 4.12 and 4.13, the compressive strength of BFS cement paste is lower than that of Portland cement paste with same water-binder ratio. A lower compressive strength results in a lower calculated elastic modulus. Under the same load cement paste with lower elastic modulus will have larger deformation than the cement paste with higher elastic modulus. Second, the calculated capillary tension in BFS cement paste is bigger than in Portland cement paste with same water-binder ratio at the same curing age. As shown in Figure 5.4, the change of internal relative humidity of BFS cement pastes is much bigger than that of Portland cement pastes with same water-binder ratio at the same curing age. A bigger change of relative humidity of BFS cement paste results in bigger capillary tension and bigger calculated autogenous shrinkage.

#### 5.4.5 Discussion

As mentioned in the section 5.4.1, taking the final setting time as the start of autogenous shrinkage is questionable. Therefore, only the measured autogenous shrinkage *after* maximum swelling of the cement paste is used for comparison with the simulation results. Measurements start from the maximum early-age swelling and continue until seven days after casting, as shown schematically in Figure 5.22. Since for different cement pastes the moment of maximum swelling ( $t_s$  in Figure 5.22) is different, the period during which autogenous shrinkage is measured is different as well. This complicates the comparison of the measured autogenous shrinkage after maximum swelling of the cement pastes considered in this study.

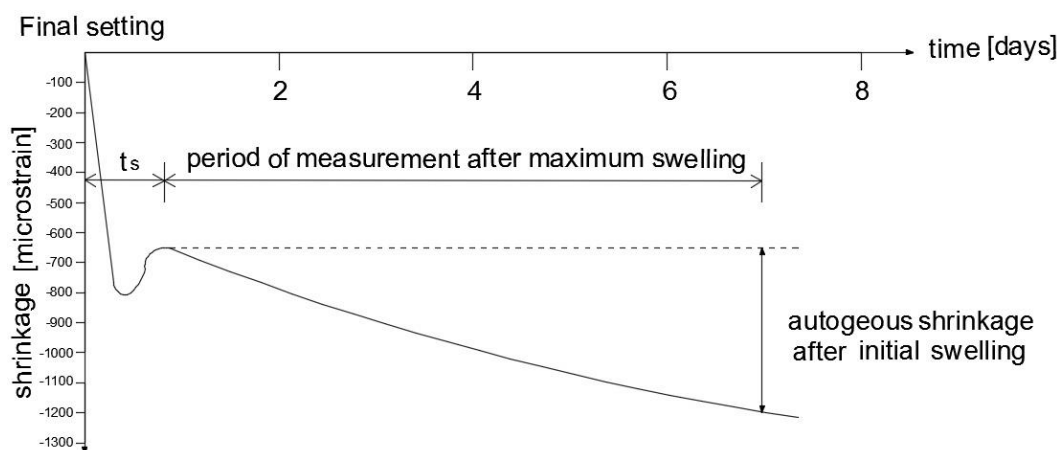


Figure 5.22 Schematic representation of autogenous shrinkage of hardening cement paste

As shown in the previous section the autogenous shrinkage of cement paste is influenced by the water-binder ratio. In order to verify the prediction of autogenous shrinkage of cement pastes with different water-binder ratio with the simulation model proposed in Chapter 3, the ratios between the autogenous shrinkage of different cement pastes with water-binder ratio 0.3 and 0.4 *after* maximum swelling at 7 days,  $\varepsilon_{0.3}/\varepsilon_{0.4}$ , is studied. The measured ratios  $\varepsilon_{0.3}/\varepsilon_{0.4}$  of different cement pastes are given in Table 5.2.

*Table 5.2: Measured autogenous shrinkages  $\varepsilon_{0.3}$  and  $\varepsilon_{0.4}$  after maximum swelling of Portland cement pastes and cement pastes with supplementary materials with water-binder ratio 0.3 and 0.4 (measurements continued up to seven days)*

Name	w/b=0.3		w/b=0.4		$\varepsilon_{0.3}/\varepsilon_{0.4}$ (measured)
	duration of measurement (days)	$\varepsilon_{0.3}$ (measured) ( $\mu$ strain)	duration of measurement (days)	$\varepsilon_{0.4}$ (measured) ( $\mu$ strain)	
OPC	6.5	407	5.5	232	1.75
SF	6.5	393	5.3	176	2.23
FA	5.8	198	5.7	69	2.87
BFS	6.4	822	6.2	618	1.33

*Table 5.3: Calculated autogenous shrinkages  $\varepsilon_{0.3}$  and  $\varepsilon_{0.4}$  after maximum swelling of Portland cement pastes and cement pastes with supplementary materials with water-binder ratio of 0.3 and 0.4 (calculations continued up to seven days)*

Name	w/b:0.3		w/b:0.4		$\varepsilon_{0.3}/\varepsilon_{0.4}$ (Calculated)
	duration of Calculation (days)	$\varepsilon_{0.3}$ (Calculated) ( $\mu$ strain)	duration of Calculation (days)	$\varepsilon_{0.4}$ (Calculated) ( $\mu$ strain)	
OPC	6.5	364	5.5	235	1.55
SF	6.5	444	5.3	213	2.08
FA	5.8	309	5.7	112	2.76
BFS	6.4	857	6.2	656	1.31

The *calculated* autogenous shrinkage after maximum swelling of different cement pastes at seven days and the ratio  $\varepsilon_{0.3}/\varepsilon_{0.4}$  are shown in Table 5.3. A comparison between values presented in Tables 5.2 and 5.3 shows a difference between the *absolute* values of the measured and calculated autogenous shrinkage of cement paste. The difference in *absolute* autogenous shrinkage values may be caused by several factors:

- The influence of any expansion process on the autogenous shrinkage is not taken into consideration in the simulation model. The early-age deformations observed on macroscale are determined by the expansion and shrinkage processes, which develop simultaneously. The ignorance of any influence of expansion mechanism in the simulation model might lead to an overestimated autogenous shrinkage.
- The change of dissolved ions in the pore solution is not taken into consideration in the calculations. The capillary tension is calculated based on the Kelvin radius and surface tension of pore water. The dissolved ions in the pore solution affect the value of surface



tension and the Kelvin radius. Ignoring the change of dissolved ions in the pore solution leads to an overestimated autogenous shrinkage.

In Figure 5.23 the comparison between the measured and calculated ratios,  $\varepsilon_{0.3}/\varepsilon_{0.4}$ , of the autogenous shrinkages of different pastes with water-binder ratio 0.3 and 0.4 is shown. Figure 5.23 shows that the proposed simulation model can predict the effect of water-binder ratio on the autogenous shrinkage of cement paste quite well.

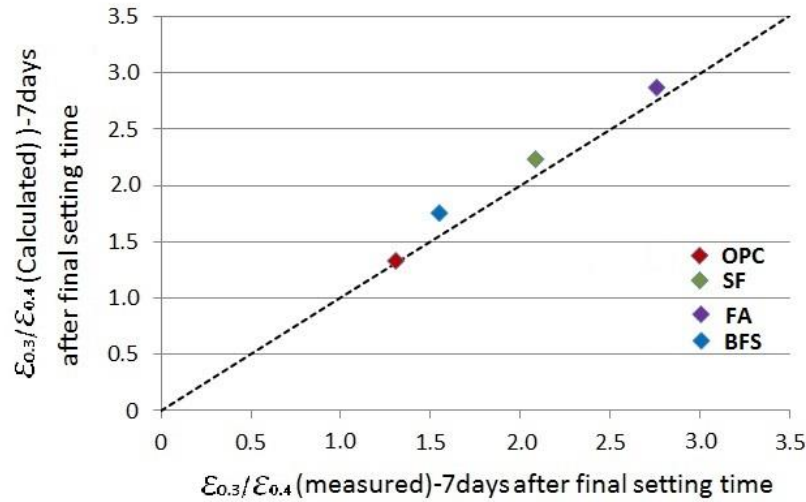


Figure 5.23 Comparison between the measured and calculated ratio  $\varepsilon_{0.3}/\varepsilon_{0.4}$  of different cement pastes

In the simulation model cement paste is considered as a visco-elastic material and creep is taken into consideration. In order to illustrate the importance of the creep part of

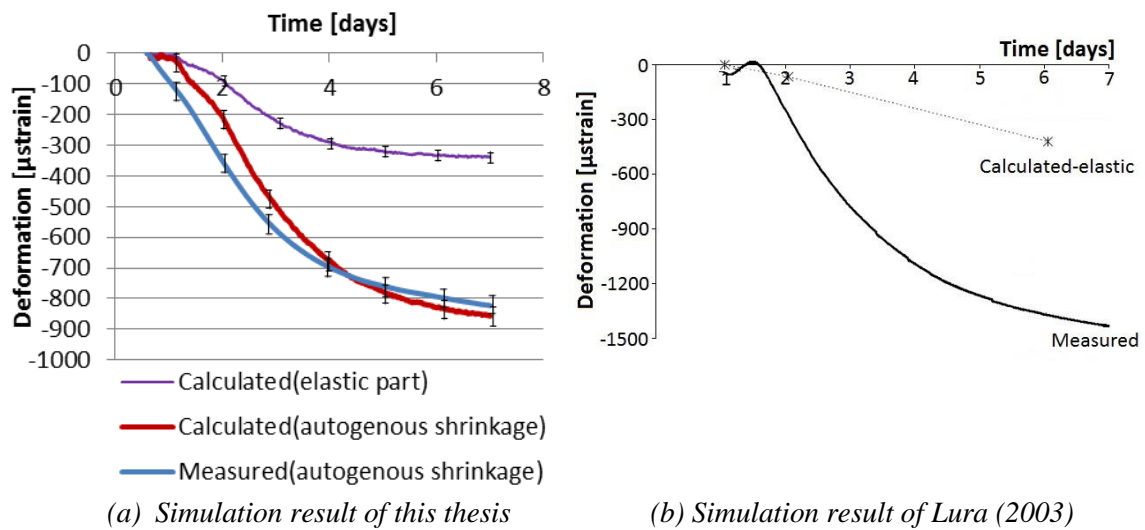


Figure 5.24 Measured and calculated autogenous deformation of blast furnace slag cement paste with water binder ratio of 0.3

autogenous shrinkage, blast furnace slag cement paste with water-binder ratio of 0.3 is taken as an example. As shown in Figure 5.24(a), the simulation model predicts the autogenous shrinkage of BFS cement paste with water-binder ratio of 0.3 quite well. If only the elastic part is considered and the creep part is neglected, the calculated autogenous shrinkage is much smaller than the measured autogenous shrinkage as shown in Figure 5.24(a). This result is in line with the finding reported by Lura (2003). In Lura's thesis, the autogenous shrinkage of the BFS cement paste with water-binder ratio of 0.37 was studied. Lura simulated the autogenous shrinkage of BFS cement paste assuming the cement paste to perform as an elastic material. The calculated and measured autogenous shrinkage are shown in Figure 5.24(b).

It also should be noted that there is a scatter of the measurement results which are used to calculate the autogenous shrinkage, e.g. the relative humidity which is used to calculate the capillary tension and the compressive strength which is used to calculate the modulus of elasticity. The scatter of inputs will result in a range of the calculated autogenous shrinkage. Taking the Portland cement paste with water-binder ratio 0.3 and 0.4 as examples, the range of the calculated autogenous shrinkage is shown in Figure 5.25 in the form of error bar. Figure 5.25 shows the range of the calculated autogenous shrinkage due to the scatter of inputs is about 10%.

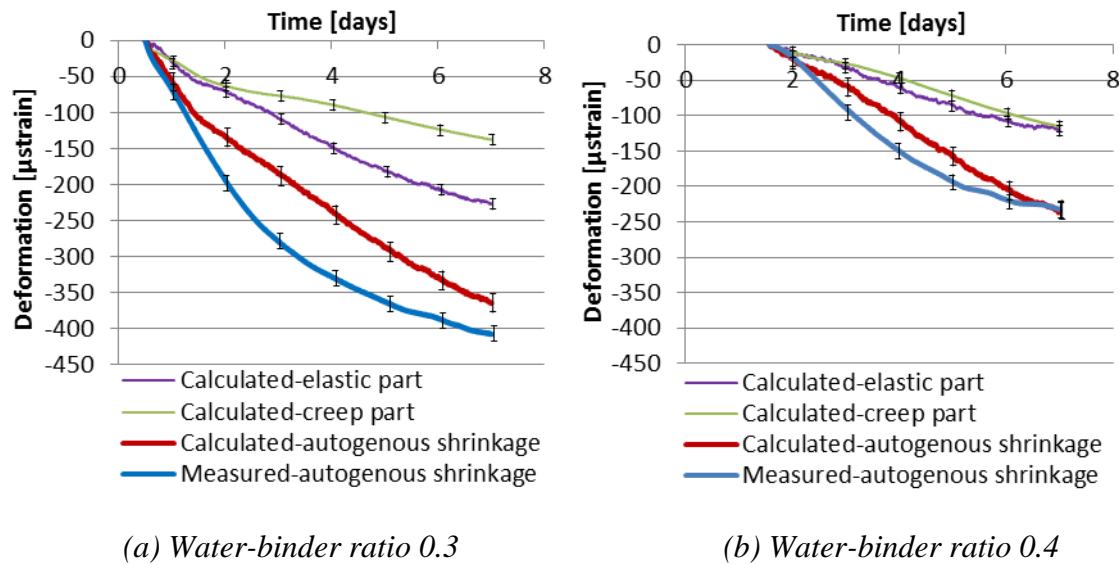


Figure 5.25 Measured and calculated autogenous deformation of Portland cement paste with water-binder ratio 0.3 and 0.4

## 5.5 Conclusions

In this chapter the degree of saturation, capillary tension and elastic modulus of Portland cement pastes and cement pastes with supplementary materials with water-binder ratio of 0.3 and 0.4 were simulated. The results of these simulations were used as inputs for the simulation model of autogenous deformation (proposed in Chapter 3). The autogenous shrinkage of eight mixtures was simulated. Numerical results were compared with measured autogenous shrinkage. The following conclusions can be drawn:

*1) Degree of saturation*

At the same age the degree of saturation of fly ash cement pastes is higher than that of Portland cement pastes. The degree of saturation is calculated from the non-evaporable water content and chemical shrinkage (Equation 5.1). The non-evaporable water content in fly ash cement pastes is lower than that in ordinary Portland cement pastes with the same water-binder ratio at the same curing age (as shown in Figures 4.6 and 4.7). The chemical shrinkage of fly ash cement paste is lower than that of ordinary Portland cement paste in the first week. Both factors result in higher degree of saturation of fly ash cement pastes during the first 7 days.

*2) Capillary tension*

The capillary tension of cement pastes with lower water-binder ratio is larger than that of cement paste with higher water-binder ratio at the same curing age. This is due to the fact that the relative humidity of cement paste with lower water-binder ratio will decrease faster with elapse of time than that of cement paste with higher water-binder ratio. Larger drop of relative humidity results in bigger capillary tension.

*3) Prediction of autogenous shrinkage using proposed simulation model*

The simulation model predicts the trend of autogenous shrinkage of Portland and BFS cement pastes quite well. But there is difference between the measured and calculated autogenous shrinkage of fly ash cement paste. The differences may be caused by the ignorance of the change of ion concentration of pore water. By taking changes of the ion concentration of pore water during hydration into account, the calculated autogenous shrinkage of fly ash cement paste is close to the measured results.

The comparison between the calculated autogenous shrinkage of cement paste (including elastic part and creep) and the measured result shows that creep plays an important role in autogenous shrinkage and should not be neglected.



# Chapter 6

## Restraining effect of sand on shrinking cement mortar and concrete

### 6.1 Introduction

Shrinkage of the cement paste in hardening concrete is restrained by the non-shrinking coarse aggregates. The interaction between the shrinking cement paste and the non-shrinking sand and coarse aggregate may lead to micro cracking in the concrete.

In literature different models for shrinkage of mortar and concrete have been proposed. These models can be classified as finite element model (Xiong et al. 2015, Maruyama et al. 2014), lattice discrete particle model (Abdellatef et al. 2015) and classic mechanical model (also called composite models) (Pickett 1956, Hansen et al. 1965, Hobbs 1969, Tazawa et al. 2000, Hammer et al. 2002), etc. Compared with finite element model and lattice discrete particle model which requires a few hours up to several days of calculation, classic mechanical model is less time-consuming (only a few minutes of calculation) and can still provide satisfactory results.

In this chapter autogenous shrinkage of hardening cement mortars with fine sand (0.125~0.25 mm) is calculated based on the autogenous shrinkage of the cement paste and the restraining effect of the sand particles using an extended Pickett model. Pickett's model (Pickett 1956) was originally developed for predicting the drying shrinkage of concrete as a function of shrinkage of cement paste and the aggregate content. The cement paste and inert inclusions were considered as elastic material. In this chapter Pickett's model will be extended by taking the effect of creep on shrinkage of the cement paste into consideration. The autogenous shrinkage of mortar with fine sand (0.125~0.25 mm) is simulated by this model and compared with experimental results to evaluate the accuracy of the predictions with the extended Pickett model. The extended Pickett model is also used to predict the early-age autogenous shrinkage of OPC concrete and BFS concrete with high aggregate content.

### 6.2 Background

Cement mortar and concrete are assumed to consist of two phases, i.e. sand/aggregate particles and the cement paste matrix. The autogenous shrinkage only takes place in the cement phase. Aggregate particles in mortar and concrete mixtures will cause a reduction of the autogenous shrinkage due to their restraining effect (Pickett 1956, Holt 2002). Examples of measured autogenous deformations of cement paste and concretes (mixture with w/c 0.35 and 0.45) with different aggregate contents are shown in Figure 6.1 (Wei 2008). This figure shows that there is a period of expansion before the specimens start to shrink steadily. After the period of expansion, the deformation will turn into shrinkage. The

autogenous shrinkage of concrete decreases dramatically with the increase of aggregate content. The expansion period of concrete was found to be longer than that of cement paste. The higher the aggregate content, the longer the expansion period was. According to Wei (2008), the expansion of concrete is due to changes of the water distribution in the pore structure of the concrete caused by the addition of aggregates. The small pores in aggregates adsorb water during mixing. The adsorbed water is released to the surrounding cement paste during the hydration process. The water released from aggregate will slightly increase the relative humidity in the cement paste and consequently reduce and delay the shrinkage. This is a form of internal curing.

Another explanation of the expansion of concrete is the occurrence of micro-cracks in the concrete. Due to the restraining effect of the non-shrinking aggregate the cement paste in concrete is under tension. Due to the tension and low tensile strength of the cement paste, cracks perpendicular to the interface between matrix and aggregate may form in the paste (see also Figure 6.7) (Goltermann 1994). Microcracking will lead to the macroscopic expansion of concrete structures (Charpin et al. 2012).

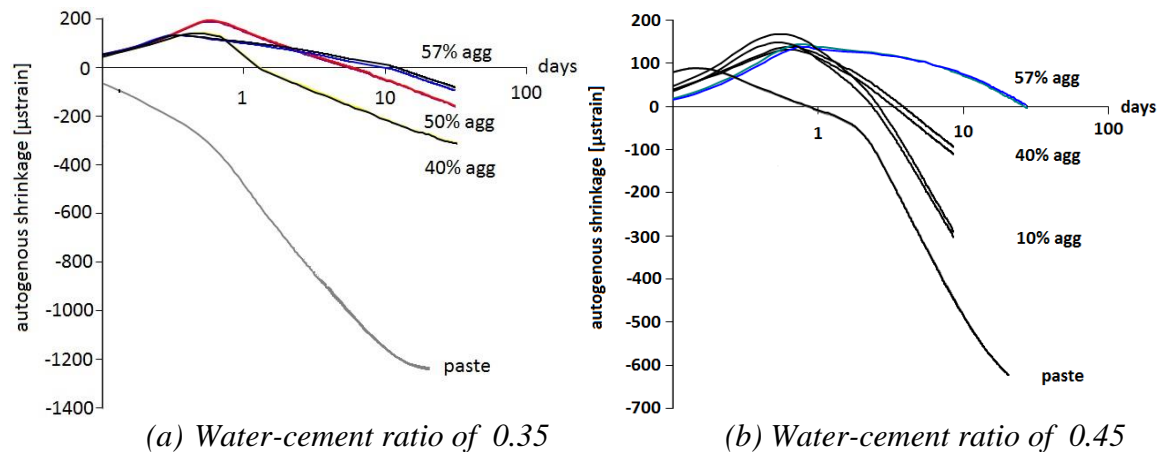


Figure 6.1 Measured autogenous shrinkage of ordinary Portland cement paste and concrete with different aggregate contents (by volume) (Wei 2008)

## 6.3 Simulation models of autogenous shrinkage of cement mortar

### 6.3.1 General introduction of composite models

In past decades different composite models (Pickett 1956, Hansen et al. 1965, Hobbs 1969) have been proposed to determine the autogenous shrinkage of mortar and concrete based on the shrinkage of the matrix and the aggregate volume concentration and the properties of the constituents, i.e. series model, parallel model, Hobb's model and Pickett's model. Tazawa et al. (2000) compared different composite models for calculating autogenous shrinkage of concrete, i.e. the series model and the parallel model. The series model is expressed as:

$$\varepsilon_{sh,c} = (1 - \Phi_A)\varepsilon_{sh,p} \quad (6.1)$$

where  $\varepsilon_{sh,c}$  [m/m] is the the shrinkage of concrete;  $\varepsilon_{sh,p}$  [m/m] the shrinkage of the cement paste;  $\Phi_A$  [m<sup>3</sup>/m<sup>3</sup>] the volume fraction of aggregates.

According to the series model the ratio between the autogenous shrinkage of concrete and cement paste is equal to the volume fraction of cement paste, i.e.  $1 - \Phi_A$ . In reality, the aggregate has a restraining effect on autogenous shrinkage of the surrounding cement paste. The restraining effect of aggregate on shrinkage of concrete can be very important. In Equation 6.1, however, this restraining effect of aggregate is not considered.

The parallel model is expressed as:

$$\varepsilon_{sh,c} = \frac{1 - \Phi_A}{1 + (E_A/E_p - 1)\Phi_A} \varepsilon_{sh,p} \quad (6.2)$$

where  $E_A$  [MPa] and  $E_p$  [MPa] the elastic modulus of aggregate and cement paste, respectively.

Hobbs' model (Hobbs 1969,1974) was developed for drying shrinkage. In his model the elastic modulus of the cement paste was assumed constant and the shrinkage of concrete,  $\varepsilon_{sh,c}$  [m/m], can be expressed as:

$$\varepsilon_{sh,c} = \frac{\varepsilon_{sh,p}(1 - \Phi_A)(G_p + G_A) + 2\varepsilon_{sh,a}\Phi_A G_A}{G_p + G_A + \Phi_A(G_A - G_p)} \quad (6.3)$$

where  $\varepsilon_{sh,p}$  [m/m] is the shrinkage of the cement paste;  $\varepsilon_{sh,a}$  [m/m] the shrinkage of the aggregates;  $G_A$  [MPa] the shear modulus of the aggregates and  $G_p$  [MPa] the shear modulus of the paste.

In 1956 Pickett (1956) derived an expression for the restraining effects of aggregates on concrete shrinkage. The formula accounts for the restraining effect of small spherical aggregate particles embedded in a large body of shrinking paste. The cement paste surrounding the aggregate particle is considered as a homogeneous material and both the aggregate particle and the cement paste are assumed to be elastic.

Aforementioned composite models are proposed for calculating shrinkage of concrete based on the shrinkage of cement paste and the restraining effect of the aggregate particles. All these models have common assumptions (Hobbs 1974):

- Concrete consists of two homogenous phases, i.e. aggregates and cement paste matrix.
- Aggregate and cement matrix behave elastically and creep is not considered.
- Elastic properties of the shrinking cement paste matrix are not influenced by the microcracking caused by the restraining aggregate.

With these assumptions the shrinkage of concrete can be approximated with these composite models. In order to obtain a better prediction of autogenous shrinkage of cement mortar, microcracking caused by the restraining sand particles and the creep of hydrating cement paste should be taken into consideration. In this chapter, the theoretical basis of Pickett's model is presented first. Then the probability of microcracking caused by restraining sand particles is evaluated for the original Pickett model. Finally, the extended Pickett model which takes creep into account is proposed.

### 6.3.2 Theoretical basis of Pickett's model

#### 6.3.2.1 One particle restraint

Many researchers have used Pickett's model to predict autogenous shrinkage of concrete (Tazawa et al. 2000, Hammer et al. 2002, Lura 2003, Grasley 2006, Akcay 2007, Wei 2008). In Pickett's model the restraining effect of one small spherical aggregate particle on the shrinking cement paste is calculated first. The cement paste in the mixture is represented as one single shell surrounding the aggregate particle (Pickett 1956).

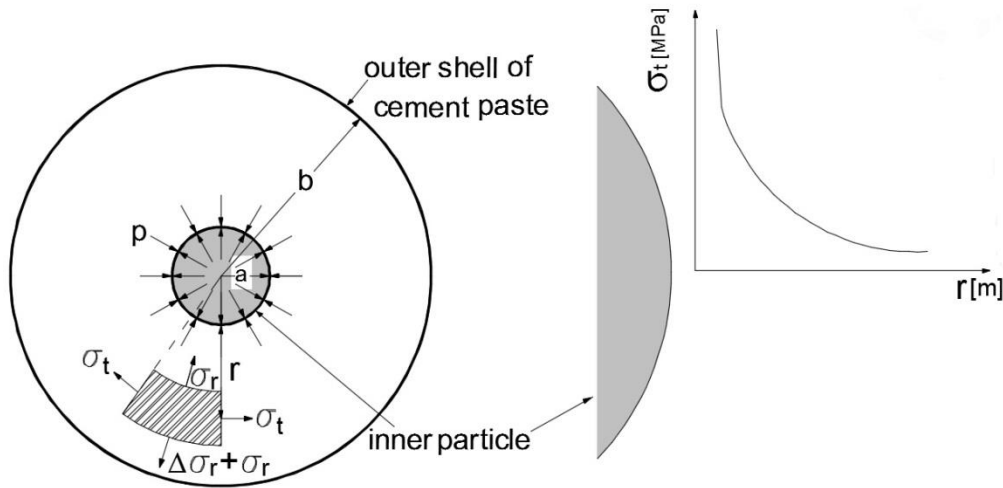
The restraint exerted by a small spherical particle on the shrinkage of the surrounding outer shell of cement paste will cause the following stresses in the shell as shown in Figure 6.2 (Timoshenko 1951, Jones 2009):

$$\sigma_r = -\frac{pa^3}{r^3} \frac{b^3 - r^3}{b^3 - a^3} \quad (6.4)$$

$$\sigma_t = \frac{pa^3}{2r^3} \frac{b^3 + 2r^3}{b^3 - a^3} \quad (6.5)$$

$$p = \frac{r^3 \varepsilon_p E_p (b^3 - a^3)}{a^3 [(1 - 2\nu_p)r^3 - (1 + \nu_p)b^3]} \quad (6.6)$$

where  $\sigma_r$  [MPa] is the normal stress in the radial direction;  $\sigma_t$  [MPa] the normal stress perpendicular to the radius;  $r$  [m] the radial coordinate;  $p$  [MPa] the pressure exerted by the shrinking outer shell at the interface between aggregate particle and outer shell;  $a$  [m] the radius of the inner aggregate particle;  $b$  [m] radius of outer shell;  $\varepsilon_p$  [m/m] the strain in the radial direction caused by the pressure  $p$ ;  $E_p$  [MPa] and  $\nu_p$  [-] are Young's modulus and Poisson ratio of the shell of cement paste, respectively.



(a) Restraining effect of aggregate particle (b) Stress perpendicular to the radius  $\sigma_t$

Figure 6.2 Schematic representation of mechanism for (a) restraining effect of aggregate particle on shrinking cement paste (after Hansen et al. 1965) and (b) relationship between stress  $\sigma_t$  and radius  $r$



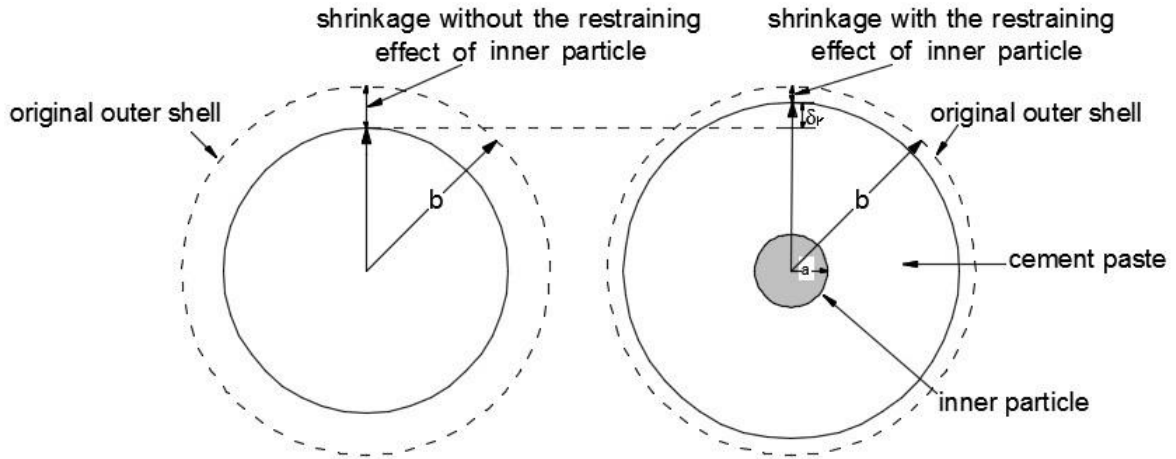


Figure 6.3 Schematic representation of restraining effect of an aggregate particle on the volume shrinkage of the outer shell of cement paste (after Hansen et al. 1965)

Under conditions of spherical symmetry, as shown in Figure 6.3, the change of radius  $\delta_r$  of the outer shell caused by the restraining effect of the aggregate particle is calculated as:

$$\delta_r = \frac{r}{E_p} [(1 - \nu_p)\sigma_t - \nu_p\sigma_r] \quad (6.7)$$

where  $r$  is the radial coordinate.

The restraint of the aggregate particle reduces the volume shrinkage of the total body by the amount:

$$4\pi b^2 \delta_r \big|_{r=b} = \frac{3pV_s}{E_p} \left( \frac{1-\nu_p}{2} \right) \frac{3b^3}{b^3-a^3} \quad (6.8)$$

where  $V_s = 4\pi a^3/3$  is the volume of the rigid aggregate particle.

If there were no restraint, the outer shell would have reduced in volume by  $3\varepsilon V$ , where  $V$  [m<sup>3</sup>] is the volume of the mixture, i.e.  $4\pi b^3/3$ , and  $\varepsilon$  [m/m] is the linear deformation. The reduction in volume shrinkage due to restraint by the aggregate particle can be designated as  $-3\Delta\varepsilon V$ , where  $\Delta\varepsilon$  is the reduction in the linear deformation:

$$-3\Delta\varepsilon V = 4\pi b^2 \delta_r \big|_{r=b} = \frac{3pV_s}{E_p} \left( \frac{1-\nu_p}{2} \right) \frac{3b^3}{b^3-a^3} \quad (6.9)$$

The aggregate particle restrains the shrinkage of the outer shell, while the shrinking cement paste generates a pressure  $p$  on the aggregate particle. This pressure causes a volume reduction of the aggregate particle as shown in Figure 6.4. The volume reduction of the aggregate particle is “filled up” with shrinking surrounding cement paste. The volume reduction of the aggregate particle can be calculated as:

$$\frac{3(1-2\nu_s)pV_s}{E_s} = 3\varepsilon V_s - 4\pi a^2 \delta_r \big|_{r=a} \quad (6.10)$$

where  $E_s$  and  $\nu_s$  are the Young's modulus and the Poisson ratio of the aggregate particle, respectively.

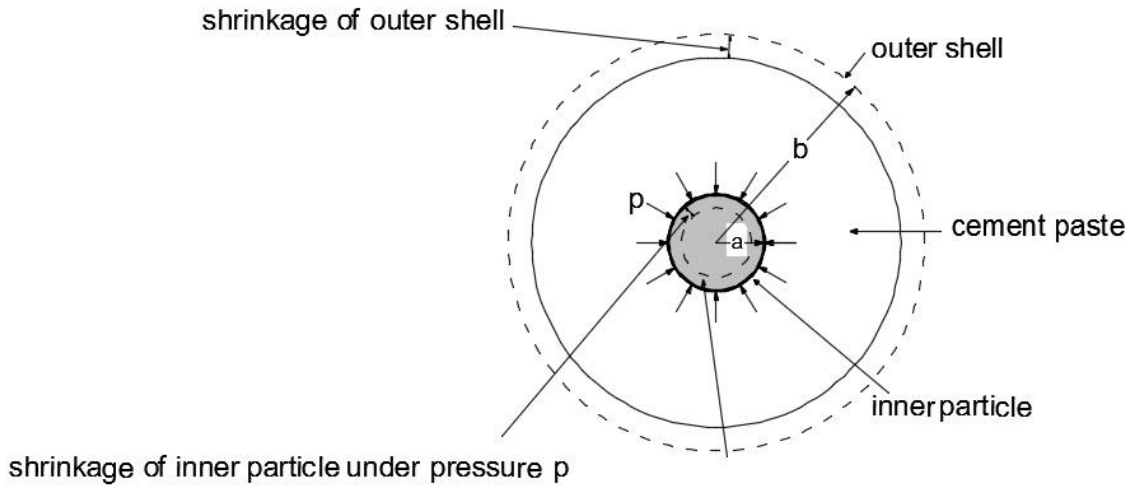


Figure 6.4 Schematic representation of restraining inner aggregate particle (after Pickett 1956)

Eliminating  $p$  from equation 6.9 and 6.10 gives:

$$-\Delta\epsilon V = \beta \epsilon V_s \quad (6.11)$$

where

$$\beta = \frac{3(1-\nu_p)}{1+\nu_p+2(1-\nu_s)E_p/E_s} \quad (6.12)$$

#### Discussion

The factor  $\beta$  (Equation 6.12) is a function of the ratio between the elastic moduli of cement paste and aggregate particle,  $E_p/E_s$  (see Equation 6.12). The relationship between factor  $\beta$  and the ratio  $E_p/E_s$  is shown in Figure 6.5<sup>1)</sup>. Figure 6.5 shows that the factor  $\beta$  decreases with increasing  $E_p/E_s$  ratio.

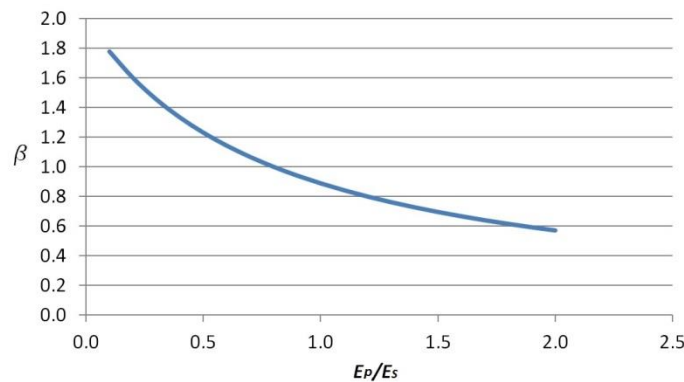


Figure 6.5 Empirical relationship between factor  $\beta$  and ratio  $E_p/E_s$

1) The Poisson ratio of cement paste is taken as 0.2 (Nielsen 1991) and the Poisson ratio of aggregate is taken as 0.25 (Zhu 2012).

### 6.3.2.2 Multi particles restraint

The previous text describes the restraining effect of one aggregate particle on the shrinkage of the cement paste shell. The restraining effect of all aggregate particles in the cement mortar on the shrinkage can be calculated with the following formulas. Let the volume ratio of the aggregate be  $\Phi_A$ [-]. As one more aggregate particle with volume  $V_s$  is added into the mixture, the change of  $\Phi_A$  can be expressed as (Pickett 1956):

$$\Delta\Phi_A = \frac{\Phi_A V + V_s}{V + V_s} - \Phi_A = (1 - \Phi_A) \frac{V_s}{V + V_s} \quad (6.13)$$

From Equation 6.11 and 6.13 we get:

$$\frac{\Delta\varepsilon}{\varepsilon} = - \frac{\beta \Delta\Phi_A}{1 - \Phi_A} \frac{V + V_s}{V} \quad (6.14)$$

In differential form,

$$\frac{d\varepsilon}{\varepsilon} = - \frac{\beta d\Phi_A}{1 - \Phi_A} \quad (6.15)$$

Then integrate it,

$$\varepsilon_{sh,m} = \varepsilon_{sh,p} (1 - \Phi_A)^\beta \quad (6.16)$$

where  $\varepsilon_{sh,m}$  [m/m] is the shrinkage of mortar;  $\varepsilon_{sh,p}$  [m/m] is the shrinkage of corresponding paste.

### 6.3.2.3 Autogenous shrinkage of cementitious material as a function of aggregate content

Figure 6.6 shows the calculated autogenous shrinkage (using the simulation model for autogenous shrinkage presented in Chapter 3) of blast furnace slag cement paste (CEM III 42.5N) with water-cement ratio of 0.3. The restraining effect of rigid sand particles on the autogenous shrinkage of BFS cement mortar has been predicted with Pickett's model (Equation 6.16). The predicted autogenous shrinkage of BFS cement mortars with sand-solid phase (cement and sand) weight ratio 0.1, 0.3, 0.5 and 0.7 is shown in Figure 6.6 as well. The figure shows that with increasing volume of sand, the calculated autogenous shrinkage of cement mortar decreases due to the larger restraining effect of the sand particles.

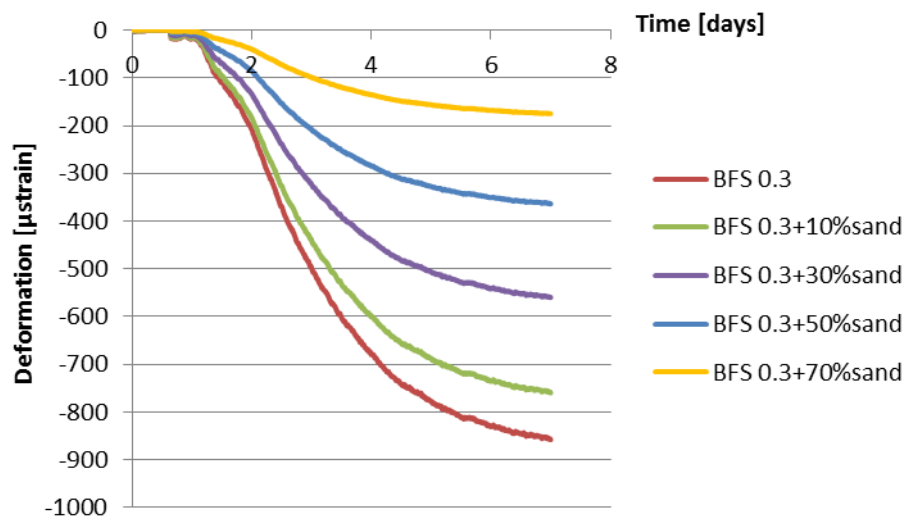


Figure 6.6 Calculated autogenous deformation of BFS cement paste and mortar (sand-solid phase (cement and sand) weight ratio is 0.1, 0.3, 0.5 and 0.7) with Pickett's model (Equation 6.16) with water-binder ratio of 0.3

### 6.3.3 Evaluation of microcracking of cement mortar

According to Wei (2008), there is difference between the measured autogenous shrinkage of concrete and calculated autogenous shrinkage of concrete using Pickett's model, especially for concrete with high aggregate contents and low water-cement ratio. This difference can be attributed to several factors, e.g. microcracking and creep.

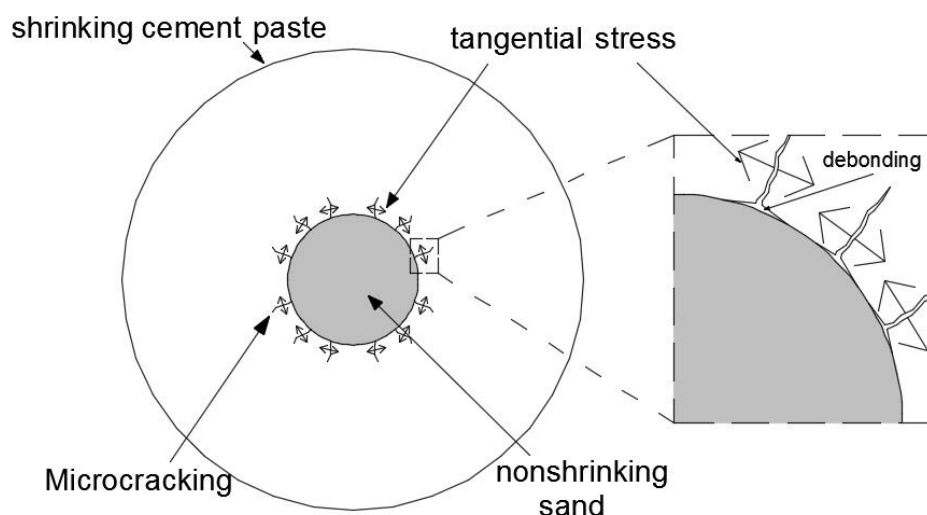


Figure 6.7 Schematic representation of the microcracking generated on the interface of the shrinkage cement paste and inert particle (after Wei 2008)

Due to the restraining effect of the non-shrinking aggregate in concrete, cement paste in concrete is under tension. At the interface between the cement paste and inert particle the tension is the largest. Due to the tension and low tensile strength of the cement paste, cracks perpendicular to the surface of the aggregate particle may form in the paste phase as demonstrated in Figure 6.7 (Goltermann 1994). Microcracking results in debonding of cement paste from sand particles and a reduction of the shrinkage and stiffness of mortar and concrete. In the following section, the tangential tensile stress and tensile strength of cement mortar will be calculated and the possibility of microcracking of cement mortar will be evaluated.

#### 6.3.3.1 Calculation of tangential tensile stress

Stresses caused by a restraining particle are the stress in radial direction  $\sigma_r$  and the stresses perpendicular to the radius  $\sigma_t$ . The stress  $\sigma_t$  is the tensile stress that causes micro-cracks in the cement paste. This stress decreases with increasing radial coordinate  $r$ . At the surface of the sand grain, i.e.  $r = a$ , the tangential tension  $\sigma_t$  is largest. Micro-cracks firstly appear in this zone. The largest tangential tension  $\sigma_t$  can be calculated with equations 6.5 and 6.6 as ( $r = a$ , see Figure 6.2):

$$\sigma_t = \frac{\varepsilon_p E_p (b^3 + 2a^3)}{2[(1 - 2\nu_p)a^3 - (1 + \nu_p)b^3]} \quad (6.17)$$

where  $a$  [m] is the radius of the sand particle;  $b$  [m] the radius of outer shell;  $E_p$  [MPa] and  $\nu_p$  [-] are Young's modulus and Poisson ratio of the outer shell, respectively;  $\varepsilon_p$  [m/m] the strain in the radial direction caused by the pressure  $p$ , i.e.  $r = a$ ;  $p$  [MPa] is the pressure exerted by the shrinking outer shell at the surface of the sand particle as shown in Figure 6.2.

Figure 6.8 shows an example of the calculated tangential tensile stress at the surface of sand particle (Equation 6.17) in cement pastes of blast furnace slag cement mortars (CEM III 42.5N) with water-cement ratio of 0.3 and sand-solid phase (cement and sand) weight ratios 0.1, 0.3, 0.5 and 0.7. The size of the sand particles is 0.125~0.25 mm. Figure 6.8 shows how the tangential tensile stress in cement paste (at the surface of sand) increases with increasing sand content (see also Moon et al. (2005)).

In fact the tangential tensile stress fields around adjacent restraining aggregates in concrete will overlap. In Pickett's model, this overlap is not taken into consideration. If the overlap is taken into account, the calculated tangential tensile stress will be bigger. However, the tangential tensile stress  $\sigma_t$  around different restraining aggregates will decrease with the increase of the radial coordinate  $r$  (Equation 6.5). When  $r$  increases from  $a$  to  $2a$  or  $3a$ , i.e. from the surface of sand particle to two or three times the radius of the sand particle, the tangential tensile stress  $\sigma_t$  will decrease to one eighth and one-seventeenth of the value at the surface. For cement mortars with water-cement ratio of 0.3 and sand-solid phase weight ratios of 0.7, the average distance between sand particles is 0.63 mm. This distance is larger than two times of the radius of sand particle (0.125~0.25 mm) and the overlap of tangential tensile stress around different restraining aggregates will not affect the calculated result significantly.

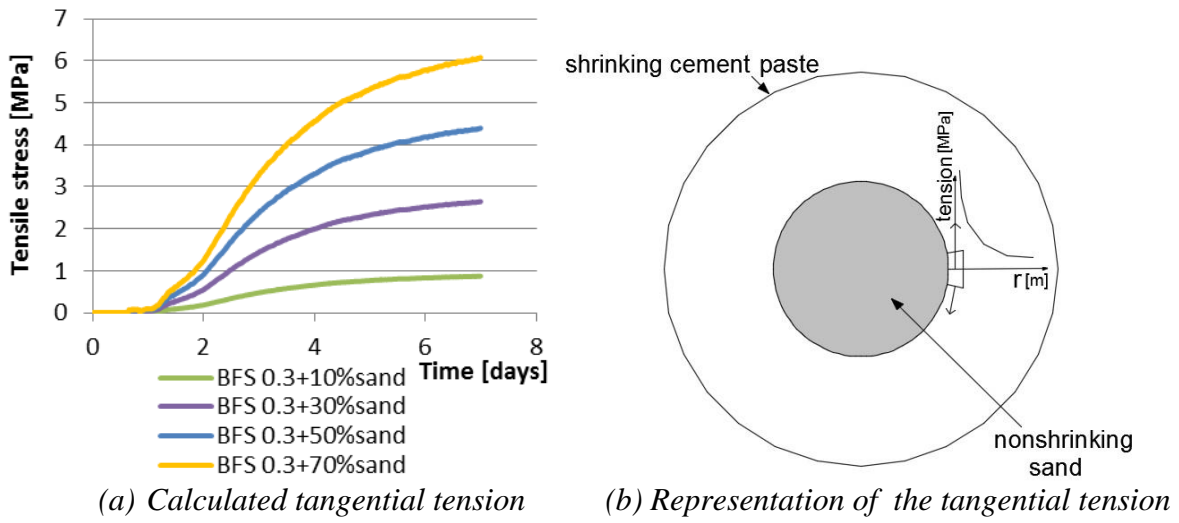


Figure 6.8 Calculated tangential tensile stress (Equation 6.17) in different BFS cement mortars and schematic representation of the tangential tensile stress

#### 6.3.3.2 Estimation of tensile strength of mortars

In order to evaluate the probability of microcracking, the tensile strength  $f_{t,p}$  [MPa] of cement paste should be known. Gardner et al. (1976) proposed an expression for the relationship between the tensile and compressive strength of concrete. In this study Gardner's equation is assumed to be also applicable for estimating the tensile strength of cement paste  $f_{t,p}$  as function of the compressive strength  $f_{c,p}$  of cement paste, viz:

$$f_{t,p} = 0.3f_{c,p}^{2/3} \quad (6.18)$$

This relationship is assumed to hold for a wide range of strengths and is supposed not to depend on the magnitude of the degree of hydration (i.e. on the strength level). Figure 6.9

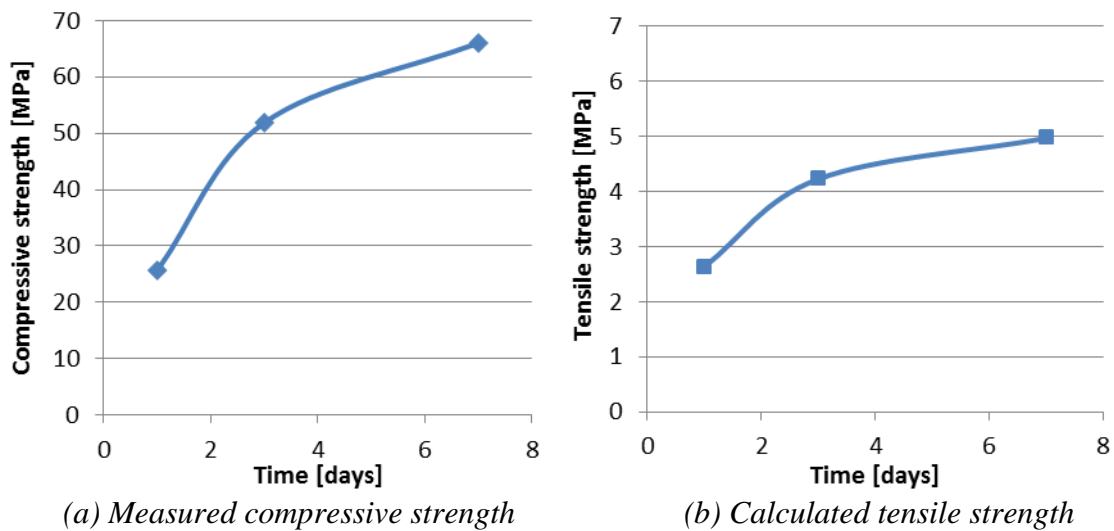


Figure 6.9 Measured compressive strength and calculated tensile strength of BFS cement paste (Equation 6.18) with water-binder ratio of 0.3 (Note: Vertical scales are different)

shows the calculated tensile strength of blast furnace slag cement paste (CEM III 42.5N) with water-binder ratio of 0.3.

### 6.3.3.3 Evaluation of microcracking of cement mortar

When the tangential tensile stress in the cement paste,  $\sigma_t$ , at the surface of a sand particle exceeds the tensile strength  $f_{t,p}$  of the cement paste, microcracking will occur. Figure 6.10 schematically shows the probability of micro cracking of the BFS cement mortars. For BFS cement mortars with low sand content (sand-solid phase weight ratio is 0.1 and 0.3), the probability of micro cracking is still low. The probability of cracking will increase with the sand content. When the sand-solid phase weight ratio is 0.5 and 0.7 (volume ratio of sand is 0.4 and 0.61), the probability of microcracking after the first few (three) days of hydration is quite high. Similar results are reported by Moon et al. (2005). Moon used finite element analyses (FEA) to study the development of tensile stress (caused by the restraining effect of aggregate) in concrete undergoing autogenous shrinkage.

Note the calculated tangential tensile stress shown in Figure 6.10 is overestimated because the effect of relaxation on the tangential stresses is not taken into consideration. If the relaxation is considered, the probability of microcracking of the BFS cement mortars will be lower.

For cement mortar, the sand content is low (sand-solid phase weight ratio is 0.1 and 0.3, i.e. volume fraction of sand is 0.07 and 0.22). For these mixtures, the influence of microcracking on autogenous shrinkage of cement mortar is negligible. For concrete, the aggregate content is high (volume fraction of sand is 0.7). In that case, the influence of microcracking on autogenous shrinkage of concrete should be taken into consideration.

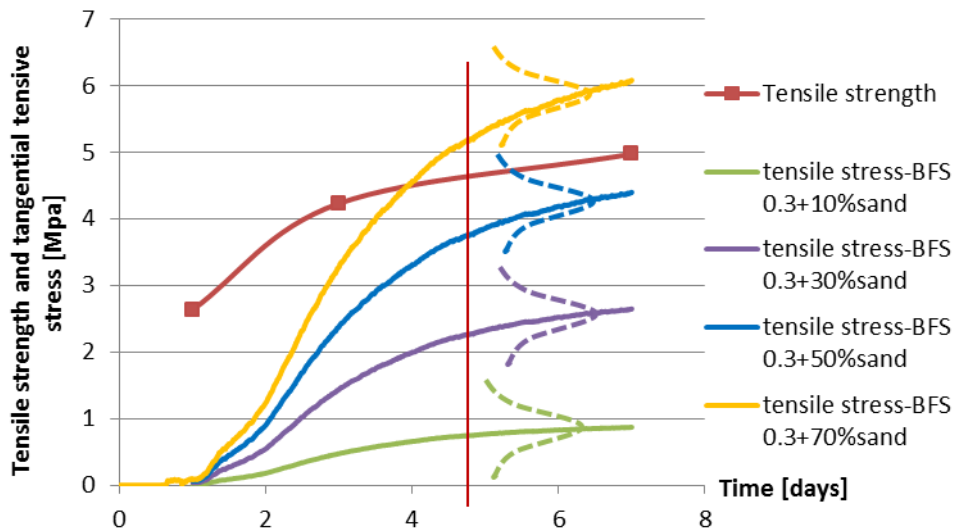


Figure 6.10 Calculated tangential tension (Equation 6.17) at the surface between the sand and cement paste in BFS cement mortars and tensile strength (Equation 6.18) of BFS cement paste (sand-solid phase weight ratio is 0.1, 0.3, 0.5 and 0.7, water-binder ratio is 0.3)

### 6.3.4 Extended Pickett model considering the effect of creep of cement paste on autogenous shrinkage of cement mortar

Besides microcracking, another factor often mentioned to explain the difference between the measured autogenous shrinkage and calculated autogenous shrinkage using Pickett's model is the ignorance of creep of cement paste. Therefore, in order to predict the autogenous shrinkage of cement mortar more accurately, Pickett's model will be extended by taking the effect of creep into account. The sand particle is assumed to perform elastic. The cement paste surrounding the sand particle is considered a homogeneous and visco-elastic material. The deformation of cement paste is supposed to consist of two parts, i.e. an elastic part and a time-dependent part. The time-dependent part is simulated with the activation energy theory.

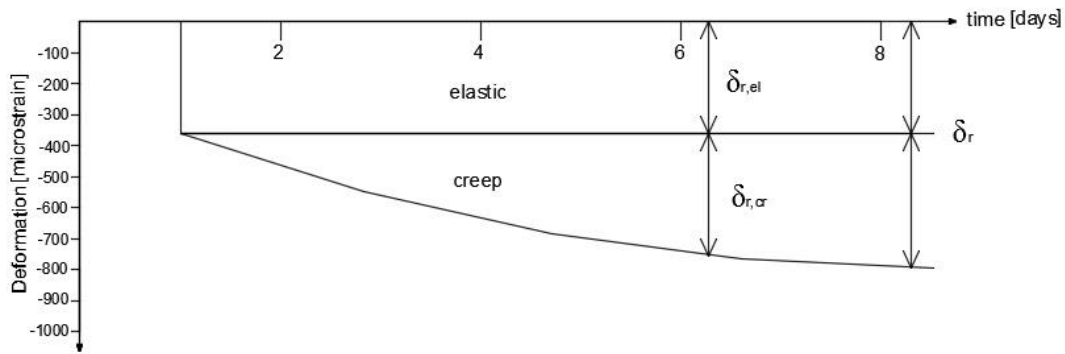


Figure 6.11 Schematic representation of change of radius of the outer shell  $\delta_r$

#### 6.3.4.1 One particle restraint

As mentioned in section 6.3.2, an aggregate particle will restrain the shrinkage of cement paste surrounding it. As shown in Figure 6.3, there is a change of radius of the outer shell  $\delta_r$ , caused by the restraining effect of the aggregate particle. The change of radius of the outer shell  $\delta_r$ , is supposed to consist of an elastic and a time-dependent part as shown in Figure 6.11.

For the elastic part  $\delta_{r,el}$ , it holds (see Equation 6.7):

$$\delta_{r,el} = \frac{r}{E_p} [(1 - \nu_p)\sigma_t - \nu_p\sigma_r] \quad (6.19)$$

For the time-dependent part  $\delta_{r,cr}$ , i.e. creep in radial direction, it holds (Equation 3.22):

$$\delta_{r,cr} = \frac{2r}{E_p} [(1 - \nu_p)\sigma_t - \nu_p\sigma_r] \left\{ 1 - \exp \left( - \frac{\omega\eta[(1-\nu_p)\sigma_t - \nu_p\sigma_r]E_p}{2[(1-\nu_p)\sigma_t - \nu_p\sigma_r] \exp\left(\frac{Q(t)}{RT}\right)} t \right) \right\} \quad (6.20)$$

where  $r$  is the radial coordinate;  $Q(t)$  is the activation energy of the cement paste;  $\omega$  and  $\eta$  are structure dependent parameters;  $R$  the universal gas constant and  $T$  the absolute temperature;  $E_p$  and  $\nu_p$  are Young's modulus and Poisson ratio of the cement paste, respectively. More details of these parameters were given in Section 3.3.



From Equations 6.4, 6.5, 6.19 and 6.20, the change of radius of the outer shell  $\delta_r$  can be expressed as the sum of  $\delta_{r,el}$  and  $\delta_{r,cr}$  (a and b as in Figure 6.2):

$$\delta_r = \frac{pa^3}{E_p r^2} \left[ \frac{1-\vartheta_p}{2} \frac{b^3+2r^3}{b^3-a^3} + \vartheta_p \frac{b^3-r^3}{b^3-a^3} \right] \left[ 1 + 2 \left\{ 1 - \exp \left( - \frac{\omega \eta [(1-\vartheta_p)\sigma_t - \vartheta_p \sigma_r] E_p}{2[(1-\vartheta_p)\sigma_t - \vartheta_p \sigma_r] \exp(\frac{Q(t)}{RT})} t \right) \right\} \right] \quad (6.21)$$

The restraint by the aggregate particle reduces the volume shrinkage of the total body by the amount:

$$4\pi b^2 \delta_r \Big|_{r=b} = \frac{3pV_s}{E_p} \left( \frac{1-\vartheta_p}{2} \right) \frac{3b^3}{b^3-a^3} \left[ 1 + 2 \left\{ 1 - \exp \left( - \frac{\omega \eta [(1-\vartheta_p)\sigma_t - \vartheta_p \sigma_r] E_p}{2[(1-\vartheta_p)\sigma_t - \vartheta_p \sigma_r] \exp(\frac{Q(t)}{RT})} t \right) \right\} \right] \quad (6.22)$$

where  $V_s = 4/3\pi a^3$  is the volume of the aggregate particle.

If there were no restraint, the outer shell would have reduced in volume by  $3\varepsilon V$ , where  $V$  is the volume of the mixture and  $\varepsilon$  is the linear deformation. The reduction in volume shrinkage due to restraint by the aggregate particle will, therefore, be designated as  $-3\Delta\varepsilon V$ , where  $\Delta\varepsilon$  is the reduction in the linear deformation:

$$-3\Delta\varepsilon V = \frac{3pV_s}{E_p} \left( \frac{1-\vartheta_p}{2} \right) \frac{3b^3}{b^3-a^3} \left[ 1 + 2 \left\{ 1 - \exp \left( - \frac{\omega \eta [(1-\vartheta_p)\sigma_t - \vartheta_p \sigma_r] E_p}{2[(1-\vartheta_p)\sigma_t - \vartheta_p \sigma_r] \exp(\frac{Q(t)}{RT})} t \right) \right\} \right] \quad (6.23)$$

As explained in Section 6.3.2, reduction in volume of the aggregate particle caused by pressure  $p$  can be calculated as (Equation 6.10):

$$\frac{3(1-2\vartheta_s)pV_s}{E_s} = 3\varepsilon V_s - 4\pi a^2 \delta_r \Big|_{r=a} \quad (6.24)$$

where  $E_s$  and  $\vartheta_s$  are Young's modulus and Poisson ratio for the aggregate particle.

Eliminating  $p$  in equation 6.23 and 6.24 (According to Pickett, the  $b/a$  is taken as  $\infty$  (Pickett 1956)):

$$-\Delta\varepsilon V = \beta_\emptyset \varepsilon V_s \quad (6.25)$$

where

$$\beta_\emptyset = \frac{3(1-\vartheta_p)}{1+\vartheta_p+2(1-\vartheta_s)(E_p/E_s) \left/ \left[ 1+2 \left\{ 1 - \exp \left( - \frac{\omega \eta [(1-\vartheta_p)\sigma_t - \vartheta_p \sigma_r] E_p}{2[(1-\vartheta_p)\sigma_t - \vartheta_p \sigma_r] \exp(\frac{Q(t)}{RT})} t \right) \right\} \right] \right.} \quad (6.26)$$

### Discussion

In the extended Pickett model, the restraining effect of aggregate on autogenous shrinkage of surrounding cement paste is calculated with a factor  $\beta_\emptyset$  (see Equation 6.26), which takes the effect of creep into consideration. The factor  $\beta_\emptyset$  is a function of the ratio between the elastic modulus of cement paste and aggregate particle,  $E_p/E_s$  (see Equation 6.26).

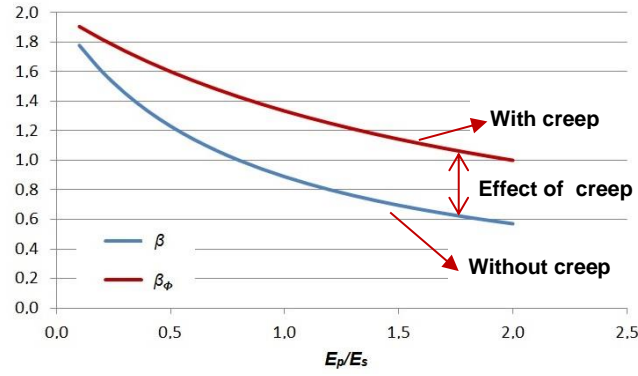


Figure 6.12 Relationships between the ratio  $E_p/E_s$  and the factors  $\beta$  and  $\beta_\phi$  (Equation 6.12 and Equation 6.26)

The relationship between factor  $\beta_\phi$  and ratio  $E_p/E_s$  is shown in Figure 6.12<sup>3)</sup>. The factor  $\beta_\phi$  decreases with increasing ratio  $E_p/E_s$ . With the same ratio  $E_p/E_s$ , the factor  $\beta_\phi$  in the extended Pickett model is bigger than the factor  $\beta$  in the original Pickett model. This means that due to the effect of creep the autogenous shrinkage calculated with the extended Pickett model is smaller than that with the original Pickett model.

#### 6.3.4.2 Multi particles restraint

Let the volume ratio of the aggregate in the mixture be  $\Phi_A$ , then the relationship between the shrinkage of cement paste and mortar can be expressed as:

$$\varepsilon_{sh,m} = \varepsilon_{sh,p}(1 - \Phi_A)^{\beta_\phi} \quad (6.27)$$

where  $\varepsilon_{sh,m}$  is the shrinkage of mortar;  $\varepsilon_{sh,p}$  is the shrinkage of corresponding paste.

#### 6.3.4.3 Autogenous shrinkage of cementitious material as a function of aggregate content

Figure 6.13 shows the autogenous shrinkage of blast furnace slag cement mortars (CEM III 42.5N) with water-cement ratio 0.3 and different sand-solid phase weight ratio, i.e. 0.1, 0.3, 0.5 and 0.7, calculated with the original Pickett model and the extended Pickett model. This figure shows that the autogenous shrinkage calculated with the extended Pickett model is smaller than that with the original Pickett model. The difference between the calculated autogenous shrinkage with Pickett's model and the extended Pickett model of cement mortar increases with increasing sand content. For example, due to creep the calculated autogenous shrinkage of a BFS cement mortar with water-binder ratio 0.3 and the sand-solid phase ratio 0.7 at 7 days changes from 180  $\mu$ strain to 120  $\mu$ strain, so decreasing by 60  $\mu$ strain (yellow dotted line and yellow solid line in Figure 6.13). This is in line with results reported by Grasley et al. (2005), who studied the autogenous shrinkage of fly ash concrete with water-binder ratio of 0.33. The fly ash dosage in blended mixtures was 35% by weight of the binder. The sand-solid phase (cement and sand) weight ratio was 0.74. According to Grasley, by taking creep into consideration, the calculated autogenous shrinkage of concrete at 10 days changed from 144  $\mu$ strain to 94  $\mu$ strain, decreasing 50  $\mu$ strain.

3) The Poisson ratio of cement paste is taken as 0.2 (Nielsen 1991) and the Poisson ratio of aggregate is taken as 0.25 (Zhu 2012).

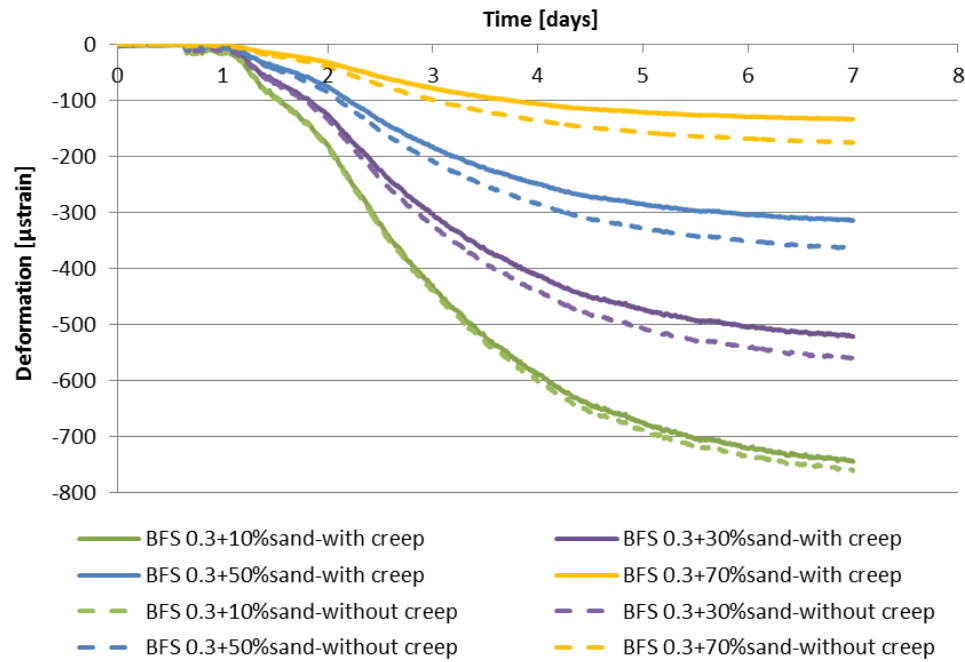


Figure 6.13 Calculated autogenous deformation of BFS cement paste and mortar (sand-solid phase (cement and sand) weight ratio is 0.1, 0.3, 0.5 and 0.7) with Pickett model (Equation 6.16) and the extended Pickett model (Equation 6.27) with water-binder ratio of 0.3

## 6.4 Experimental program of autogenous shrinkage of cement mortar

In this section, measurements of final setting time and autogenous deformation of cement mortar are presented and discussed. Portland cement mortar and slag cement mortar are studied. Mortar with pure Portland cement blended with different supplementary material, i.e. silica fume and fly ash, are also studied. In all cases, the water-binder ratios are 0.3 and 0.4. The sand-solid phase (cement and sand) weight ratios are 0.1 and 0.3.

### 6.4.1 Materials

#### Material information

The materials used in this study are Portland cement (CEM I 42.5N), silica fume, fly ash, slag cement (CEM III/B 42.5N), water and quartz sand. The mineral composition of Portland cement and chemical compositions of the supplementary materials were given in Table 4.1 and Table 4.2. Quartz sand with size of 0.125~0.25 mm was added.

#### Mixture design

Sixteen mortar mixtures are considered to study autogenous shrinkage of cement mortar. The Portland cement pastes made with CEM I 42.5N serve as reference. The silica fume and fly ash dosages in blended mixtures are 10% and 30% by weight of the binder. CEM III/B 42.5N is used to prepare slag cement paste. In both cases, the water-binder ratios are 0.3 and 0.4. The mortars are made of the same pastes, with the sand-solid phase (cement and sand) weight ratios 0.1 and 0.3. The mixture compositions of pastes and mortars are

*Table 6.1: Mixture composition of different cement pastes and mortars (% by weight)*

Name	Binder					Volume fraction of sand (%)	
	CEM I 42.5N (%)	CEM III/B 42.5N (%)	Silica Fume (%)	Fly ash (%)	Sand (%)	W/b	
OPC 0.3	100	0	0	0	0	0.3	0
OPC 0.3+10% sand	90	0	0	0	10	0.3	7
OPC 0.3+30% sand	70	0	0	0	30	0.3	23
OPC 0.4	100	0	0	0	0	0.4	0
OPC 0.4+10% sand	90	0	0	0	10	0.4	6
OPC 0.4+30% sand	70	0	0	0	30	0.4	21
SF 0.3	90	0	10	0	0	0.3	0
SF 0.3+10% sand	81	0	9	0	10	0.3	7
SF 0.3+30% sand	63	0	7	0	30	0.3	23
SF 0.4	90	0	10	0	0	0.4	0
SF 0.4+10% sand	81	0	9	0	10	0.4	6
SF 0.4+30% sand	63	0	7	0	30	0.4	20
FA 0.3	70	0	0	30	0	0.3	0
FA 0.3+10% sand	63	0	0	27	10	0.3	7
FA 0.3+30% sand	49	0	0	21	30	0.3	22
FA 0.4	70	0	0	70	0	0.4	0
FA 0.4+10% sand	63	0	0	63	10	0.4	6
FA 0.4+30% sand	49	0	0	49	30	0.4	20
BFS 0.3	0	100	0	0	0	0.3	0
BFS 0.3+10% sand	0	90	0	0	10	0.3	7
BFS 0.3+30% sand	0	70	0	0	30	0.3	22
BFS 0.4	0	100	0	0	0	0.4	0
BFS 0.4+10% sand	0	90	0	0	10	0.4	6
BFS 0.4+30% sand	0	70	0	0	30	0.4	20

listed in Table 6.1. Mortar is mixed in a 5 l epicyclic Hobart mixer. De-ionized water is used and added in two steps to ensure homogeneity of the mortar. Total mixing time is 3 minutes.

## 6.4.2 Experimental methods and equipment

The final setting time of cement mortars was measured by the Vicat needle method. The cement mortar was cast into corrugated plastic molds. After the final setting time, the specimens were placed in a dilatometer and immersed into a temperature controlled glycol bath at  $20 \pm 0.1^\circ\text{C}$ . The longitudinal autogenous deformation was measured every 5 minutes. More details of the experimental set-up were given in Chapter 4.

## 6.5 Experimental results

### 6.5.1 Final setting time

Figure 6.14, 6.15, 6.16 and 6.17 show the measured final setting times of different cement pastes and mortars with water-binder ratio of 0.3 and 0.4, cured at  $20^\circ\text{C}$ . From Figure 6.14 to 6.17 it can be seen that the addition of micro-sized sand will not affect the final setting

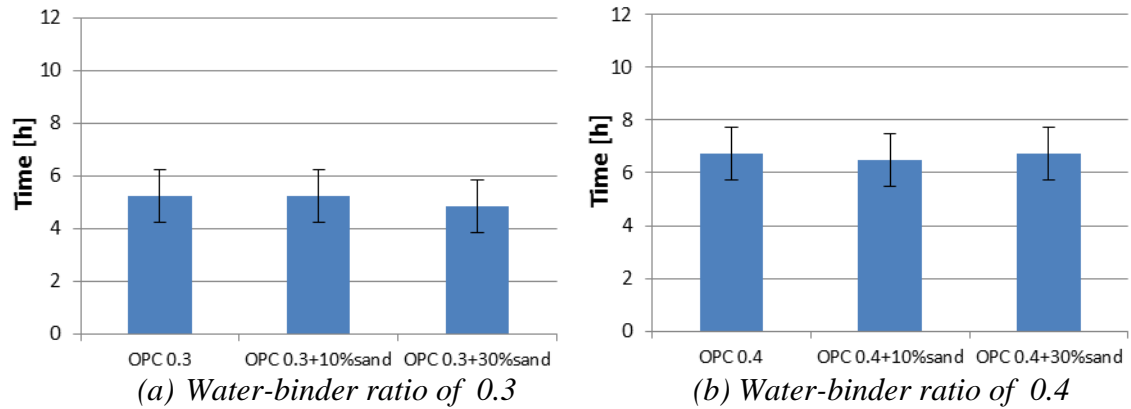


Figure 6.14 Final setting time of Portland cement pastes and mortars. Specimen code: See Table 6.1

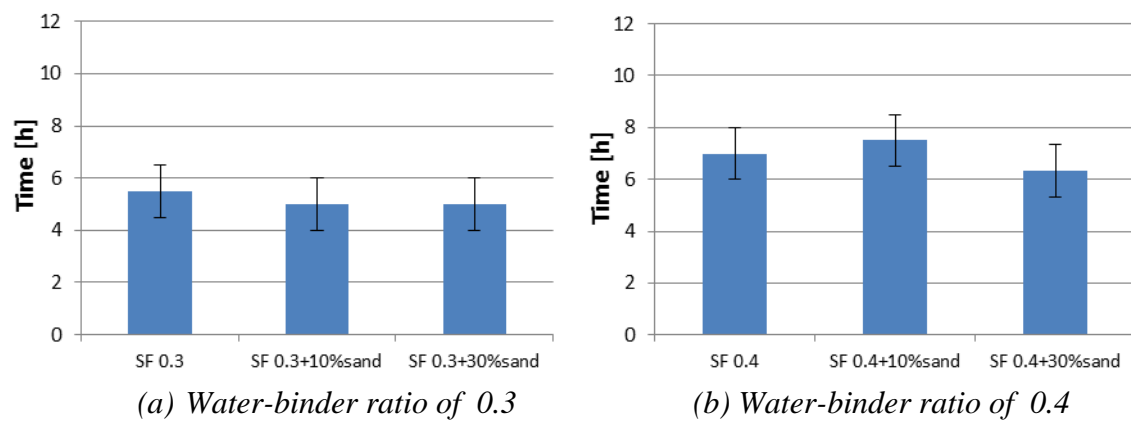


Figure 6.15 Final setting time of cement pastes and mortars with silica fume. Specimen code: See Table 6.1

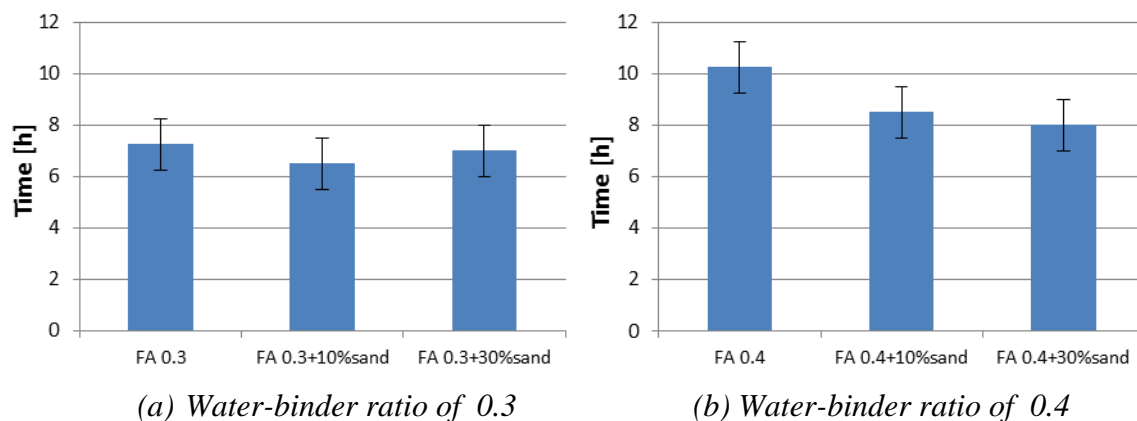


Figure 6.16 Final setting time of cement pastes and mortars with fly ash. Specimen code: See Table 6.1

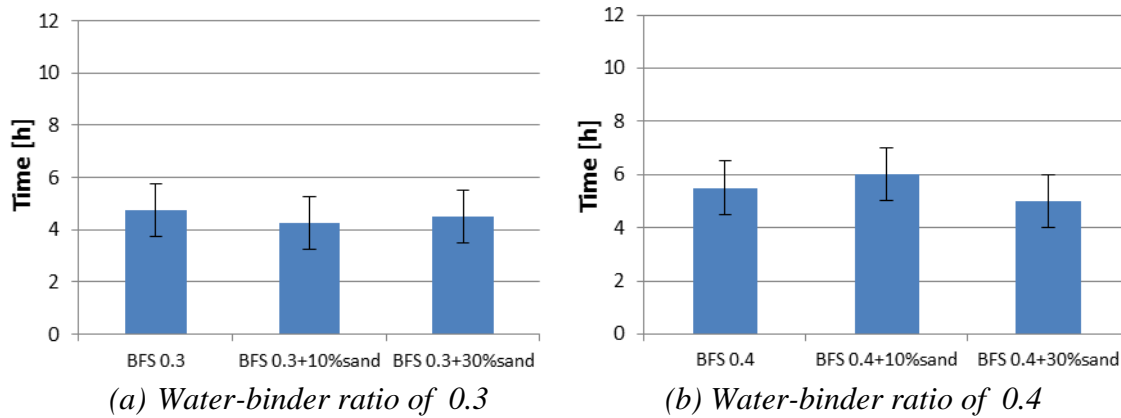


Figure 6.17 Final setting time of BFS cement pastes and mortars. Specimen code: See Table 6.1

time of cement mortar significantly. The final setting time reflects the time that a stable microstructure of cement paste and mortars has been formed. The formation of a microstructure of cement mortar is determined by the hydrating cement matrix. The effect of micro-sized sand on the microstructure of the cement matrix is not significant. For cement paste and mortar with the same water-binder ratio, the microstructure of cement paste and cement matrix in mortar is similar. Therefore, the final setting time of cement paste and mortar with the same water-binder ratio is almost similar.

### 6.5.2 Autogenous deformation

Figures 6.18, 6.19, 6.20 and 6.21 show the measured autogenous deformations of different cement pastes and mortars with water-binder ratio 0.3 and 0.4. The starting time of the measurements is the final setting time.

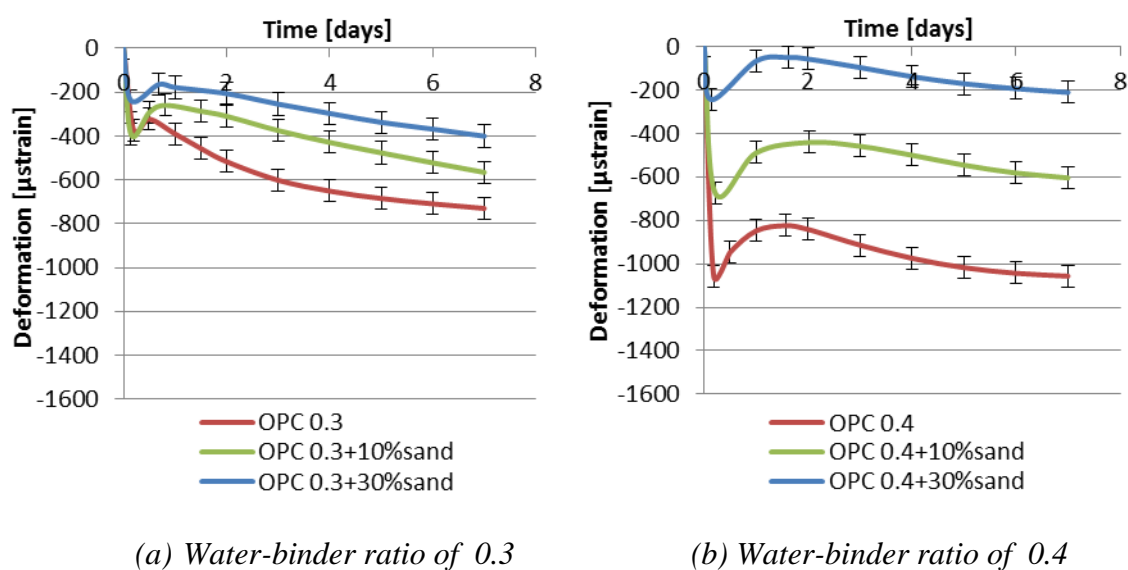


Figure 6.18 Autogenous deformation as a function of age for Portland cement pastes and mortars (The starting time of the measurement is the final setting time)

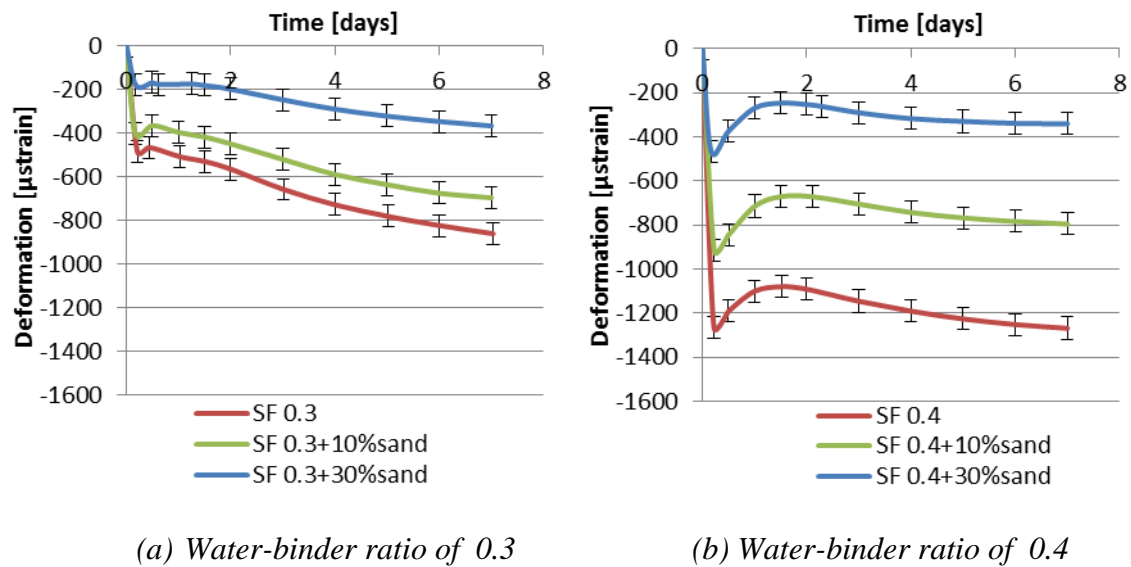


Figure 6.19 Autogenous deformation as a function of age for silica fume cement pastes and mortars (The starting time of the measurement is the final setting time)

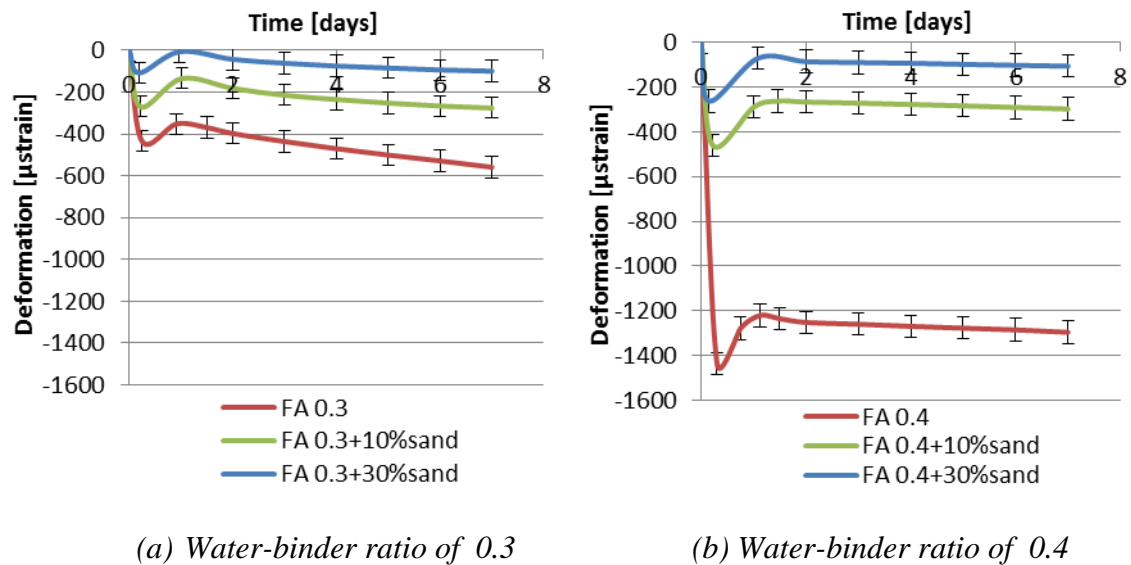


Figure 6.20 Autogenous deformation as a function of age for fly ash cement pastes and mortars (The starting time of the measurement is the final setting time)

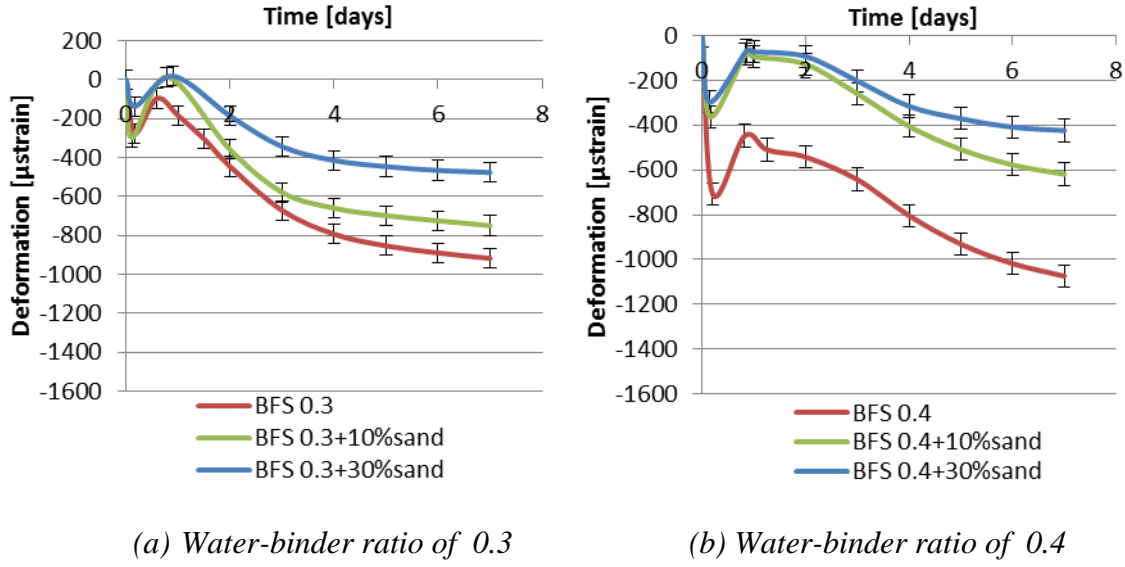


Figure 6.21 Autogenous deformation as a function of age for BFS cement pastes and mortars (The starting time of the measurement is the final setting time)

These figures show that the autogenous shrinkage of cement mortars will change with the sand content. For the same types of cement, a higher sand dosage will lead to smaller autogenous shrinkage of the mortars. The autogenous shrinkage of cement mortar with different dosage of sand will be simulated in the following section.

## 6.6 Simulation results of autogenous deformation and discussion

In this section the prediction of autogenous shrinkage with the proposed extended Pickett model is evaluated by comparing the calculated and measured autogenous shrinkage of different cement mortars.

### 6.6.1 Calculation procedure

In the extended Pickett model the autogenous shrinkage of cement mortar is calculated, as function of the autogenous shrinkage of cement paste, viz. Equation 6.27:

$$\varepsilon_{sh,m} = \varepsilon_{sh,p}(1 - \Phi_A)^{\beta_\phi} \quad (6.31)$$

where  $\varepsilon_{sh,m}$  is the shrinkage of mortar;  $\varepsilon_{sh,p}$  is the shrinkage of corresponding paste;  $\Phi_A$  is the volume ratio of the sand;  $\beta_\phi$  is a factor considering the restraining effect of sand. More details were given in section 6.3.4.



### 6.6.2 Portland cement mortars (sand-solid phase (cement and sand) weight ratio = 0.1 and 0.3, water-binder ratio = 0.3 and 0.4)

Figures 6.22 and 6.23 show the calculated and measured autogenous shrinkage of the Portland cement mortars with water-binder ratio of 0.3 and sand-solid phase (cement and sand) weight ratio 0.1 and 0.3. The starting time of the measurement is the final setting time. A fast shrinkage occurs after final setting. This fast shrinkage is followed by a short period of swelling. After the period of swelling the specimens will shrink steadily. As discussed in Chapter 4, the early-age deformations observed on macroscale are determined by expansion

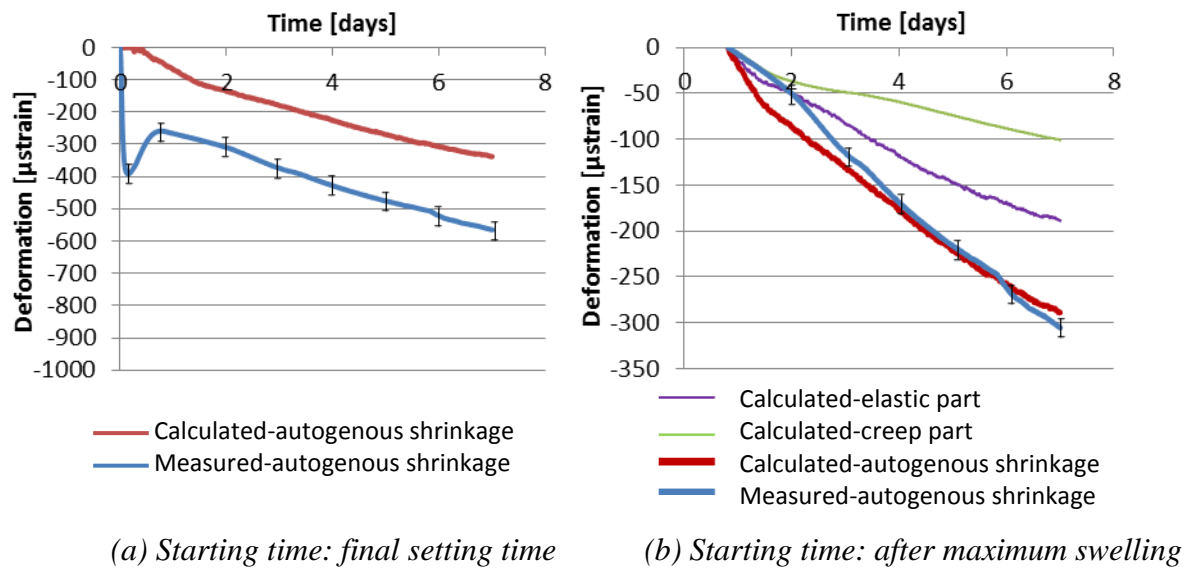


Figure 6.22 Measured and calculated autogenous deformation of Portland cement mortar (10% sand) with water-binder ratio of 0.3

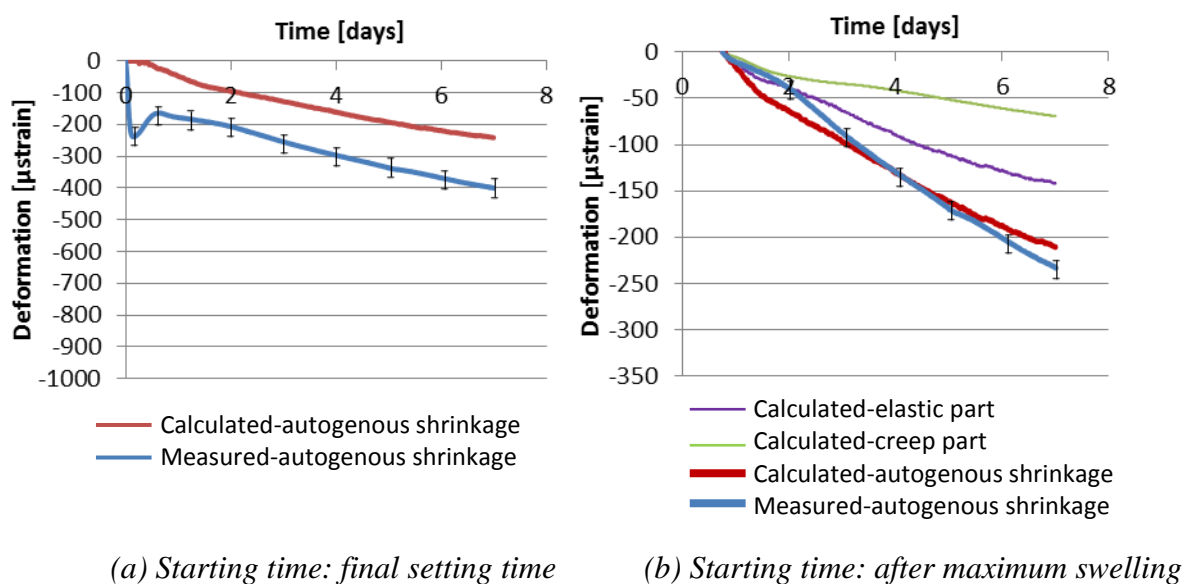


Figure 6.23 Measured and calculated autogenous deformation of Portland cement mortar (30% sand) with water-binder ratio of 0.3

and shrinkage processes, which develop simultaneously. The influence of the expansion process on the autogenous shrinkage has not been taken into consideration in the proposed simulation model of autogenous shrinkage. In this section, the measured autogenous shrinkages after maximum swelling of different cement pastes are used to validate the simulation results. In Figures 6.22(b) and 6.23(b), autogenous shrinkage of these Portland cement mortars after maximum swelling are presented.

Figures 6.24 and 6.25 show the measured and calculated autogenous shrinkage of the Portland cement mortars with water-binder ratio of 0.4 and sand-solid phase (cement and sand) weight ratio 0.1 and 0.3. After maximum swelling, the calculated autogenous

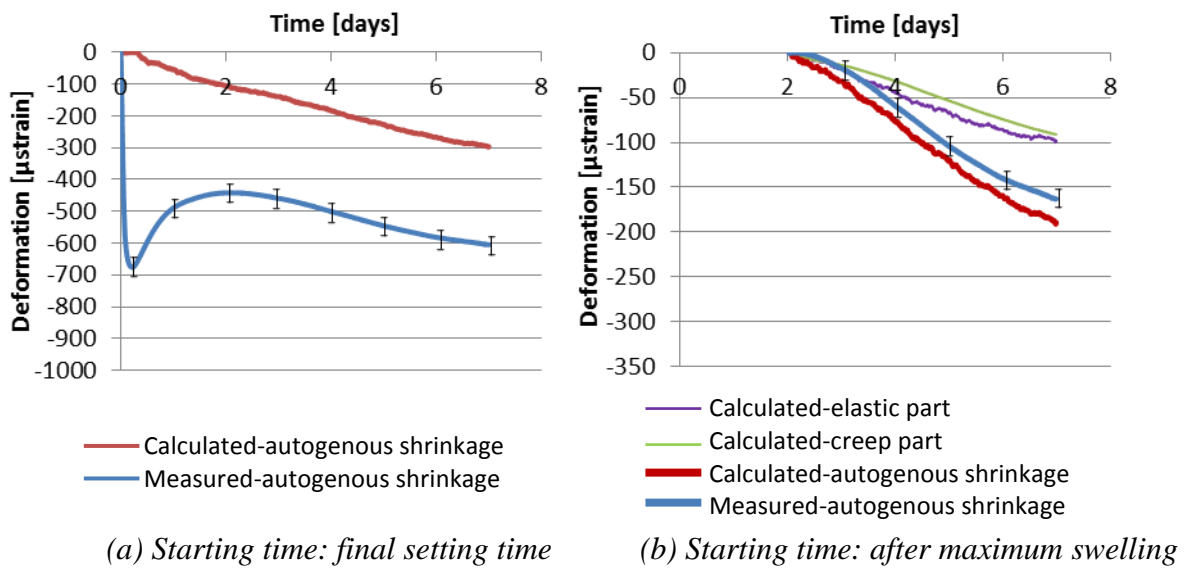


Figure 6.24 Measured and calculated autogenous deformation of Portland cement mortar (10% sand) with water-binder ratio of 0.4

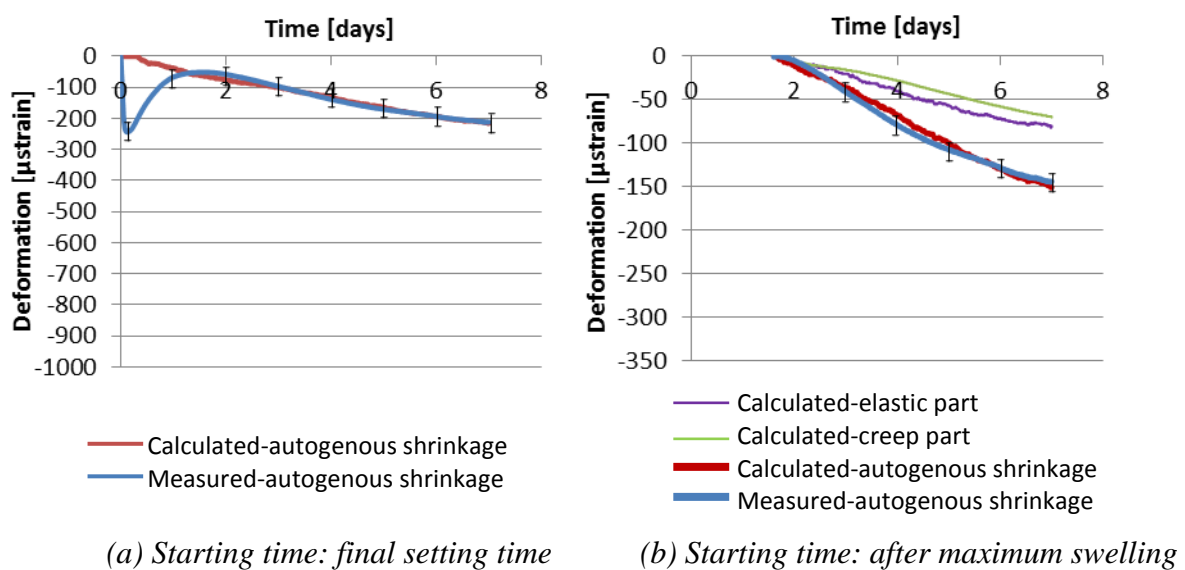


Figure 6.25 Measured and calculated autogenous deformation of Portland cement mortar (30% sand) with water-binder ratio of 0.4

shrinkage of cement pastes is shown in Figures 6.24(b) and 6.25(b), separated in an elastic part and a creep part. As shown in Figures 6.24 and 6.25, the autogenous shrinkage of cement mortar with higher sand-solid phase (cement and sand) weight ratio is smaller than that of cement mortar with lower sand-solid phase (cement and sand) weight ratio, clearly showing the restraining effect of sand on shrinking cement mortar.

### 6.6.3 Silica fume cement mortars (silica fume addition = 10%, sand-solid phase (cement and sand) weight ratio = 0.1 and 0.3, water-binder ratio = 0.3 and 0.4)

Figures 6.26 and 6.27 show the measured and calculated autogenous shrinkage of the silica fume cement mortars. The water-binder ratio is 0.3 and sand-solid phase (cement and sand) weight ratios are 0.1 and 0.3. In Figures 6.26(b) and 6.27(b), autogenous shrinkage of silica fume cement mortars after maximum swelling is presented. The contributions of the elastic and time-dependent part of autogenous deformation to autogenous shrinkage are shown explicitly. Figures 6.26(b) and 6.27(b) show that the measured autogenous shrinkage after maximum swelling is smaller than calculated. After the maximum swelling, the calculated autogenous shrinkage develops faster than the measured autogenous shrinkage. As discussed in Chapter 5, the early-age deformations observed on macroscale are determined by both expansion and shrinkage processes, which develop simultaneously. When the shrinkage is bigger than the expansion, the external volume of cement paste will decrease. But the mechanism of expansion, i.e. crystal pressure, might still be active and will reduce the measured shrinkage. The ignorance of the influence of any expansion process on the autogenous shrinkage may result in the overestimation of early-age autogenous shrinkage.

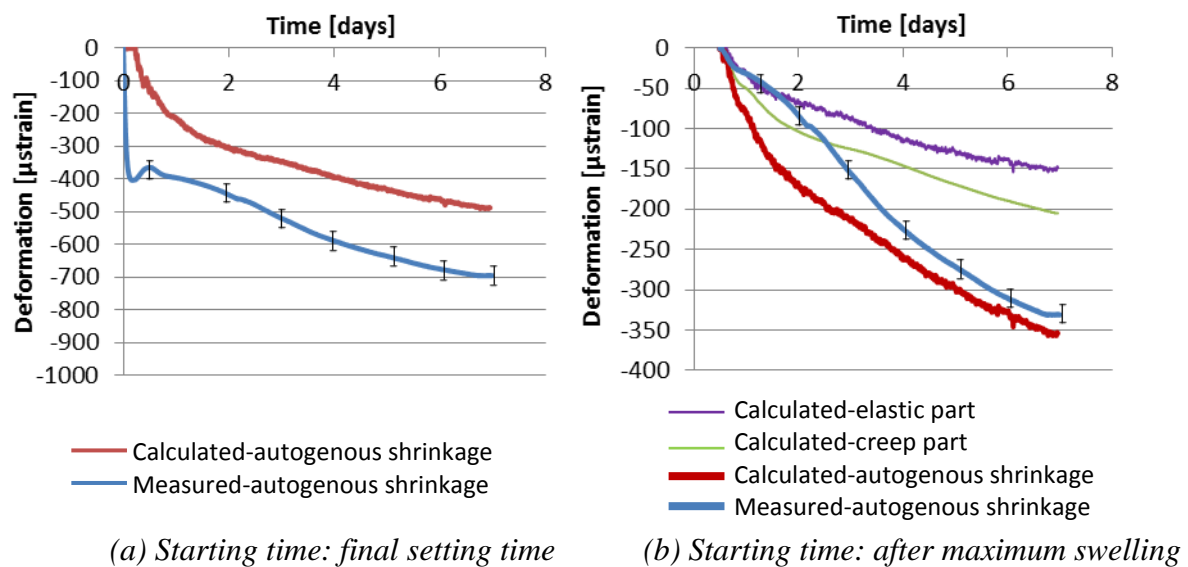


Figure 6.26 Measured and calculated autogenous deformation of silica fume cement mortar (10% sand) with water-binder ratio of 0.3

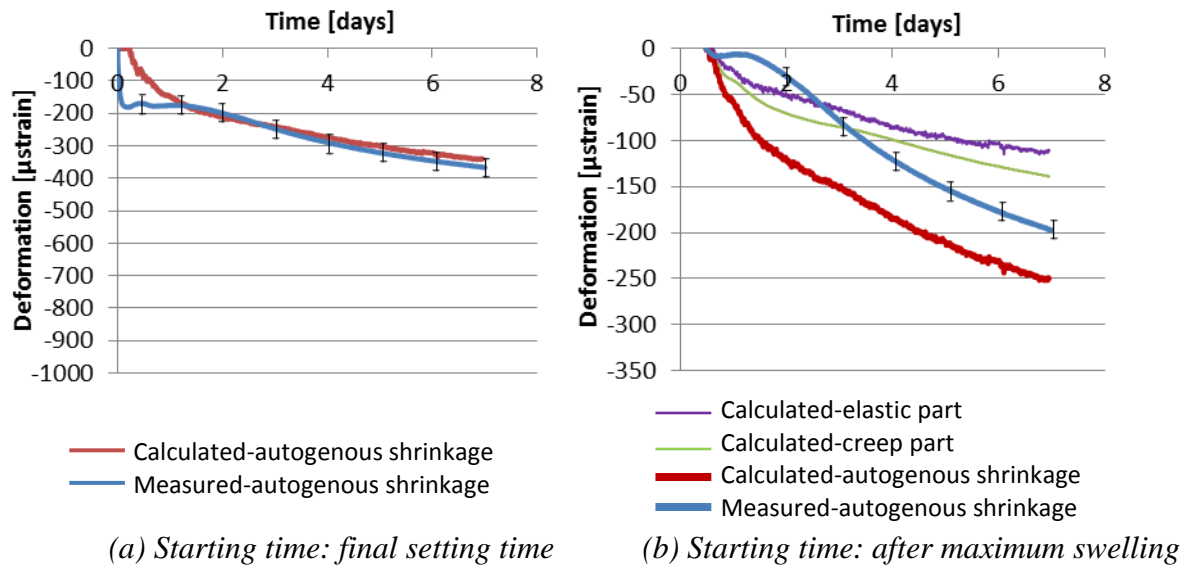


Figure 6.27 Measured and calculated autogenous deformation of silica fume cement mortar (30% sand) with water-binder ratio of 0.3

Figures 6.28 and 6.29 show the measured and calculated autogenous shrinkage of the silica fume cement mortars. The water binder ratio is 0.4 and sand-solid phase (cement and sand) weight ratios are 0.1 and 0.3. Figures 6.28(b) and 6.29(b) show the autogenous shrinkage of the silica fume cement mortars after maximum swelling.

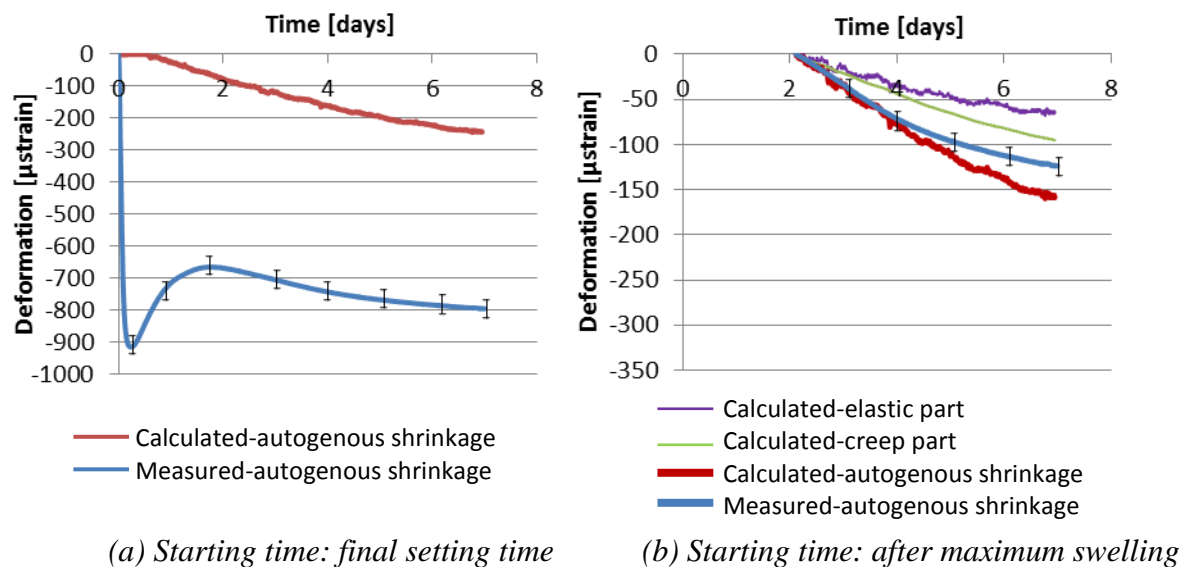


Figure 6.28 Measured and calculated autogenous deformation of silica fume cement mortar (10% sand) with water-binder ratio of 0.4

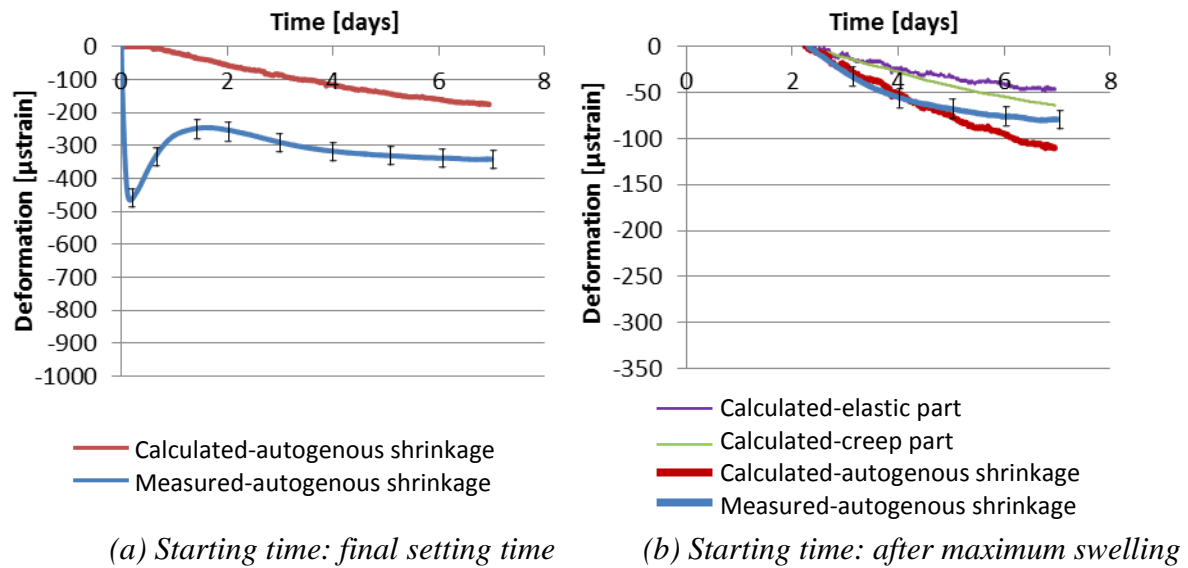


Figure 6.29 Measured and calculated autogenous deformation of silica fume cement mortar (30% sand) with water-binder ratio of 0.4

Figures 6.28(b) and 6.29(b) show that autogenous shrinkage of silica fume cement mortar decreases with the increase of water-binder ratio. The autogenous shrinkage of silica fume cement mortar with higher sand-solid phase (cement and sand) weight ratio is smaller than that of silica fume cement mortar with lower sand-solid phase weight ratio. The measured autogenous shrinkage of silica fume cement mortar with water-binder ratio of 0.4 is also smaller than the calculated autogenous shrinkage. The ignorance of the influence of expansion process on the autogenous shrinkage is an important reason for the overestimation of the measured autogenous shrinkage.

#### 6.6.4 Fly ash cement mortars (fly ash addition = 30%, sand-solid phase (cement and sand) weight ratio = 0.1 and 0.3, water-binder ratio = 0.3 and 0.4)

##### 6.6.4.1 Fly ash cement mortars with water-binder ratio 0.3

Figures 6.30 and 6.31 show the measured and calculated autogenous shrinkage of the fly ash cement mortars with water-binder ratio 0.3 and sand-solid phase (cement and sand) weight ratios 0.1 and 0.3. In Figures 6.30(b) and 6.31(b) the autogenous shrinkage of fly ash cement mortars after the maximum swelling are shown. From Figure 6.30 and 6.31, it can be noticed that the magnitude of creep is bigger than the magnitude of elastic deformation at seven days. Similar results can be found in Hu's thesis (Hu 2017). In her thesis the elastic part and the creep part of the autogenous shrinkage of fly ash cement paste with water-binder ratio 0.35 were calculated separately. The elastic part was calculated with Hooke's law and the creep part was calculated with solidification theory (Bažant et al. 1989). The fly ash cement paste was made with CEM I 42.5 N and fly ash. The fly ash dosages in blended mixtures is 40% by weight of the binder. According to Hu the time-dependent part of autogenous shrinkage of fly ash cement paste at seven days was twice as big as the elastic part of autogenous shrinkage. The larger creep of fly ash cement mortar was attributed to the higher porosity of fly ash cement paste at early age (Wei et al. 2017). Wei investigated the relationship between creep and porosity of cementitious materials

experimentally. According to Wei the ratio between creep and elastic deformation increases with porosity of cementitious materials. As discussed in Chapter 4, the degree of hydration of fly ash cement during the first seven days is lower than that of Portland cement. The lower degree of hydration of fly ash cement results in higher porosity of fly ash cement paste.

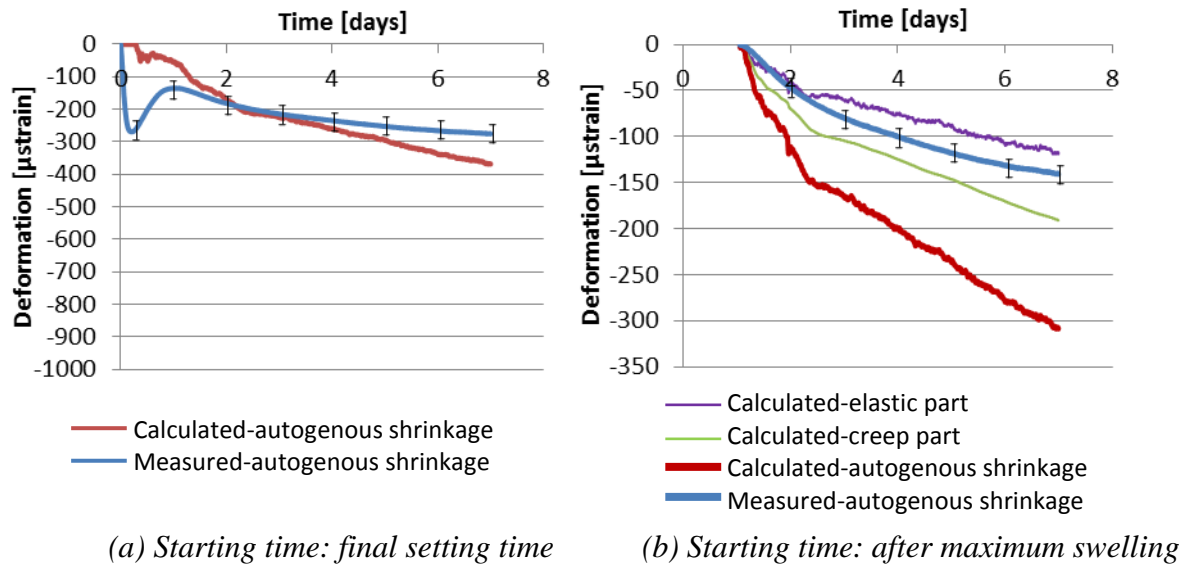


Figure 6.30 Measured and calculated autogenous deformation of fly ash cement mortar (10% sand) with water-binder ratio of 0.3

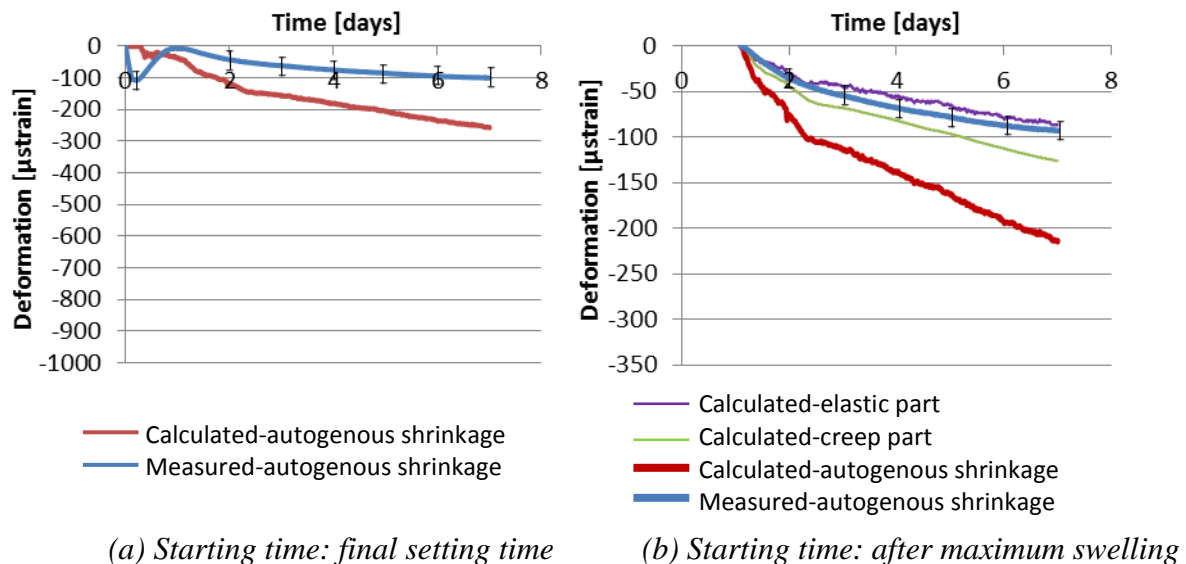


Figure 6.31 Measured and calculated autogenous deformation of fly ash cement mortar (30% sand) with water-binder ratio of 0.3

#### 6.6.4.2 Fly ash cement mortars with water-binder ratio 0.4

Figures 6.32 and 6.33 show the measured and calculated autogenous shrinkage of the fly ash cement mortars with water-binder ratio is 0.4 and the sand-solid phase ratios are 0.1 and 0.3. In Figures 6.32(b) and 6.33(b) the autogenous shrinkage of fly ash cement mortars after the maximum swelling are shown.

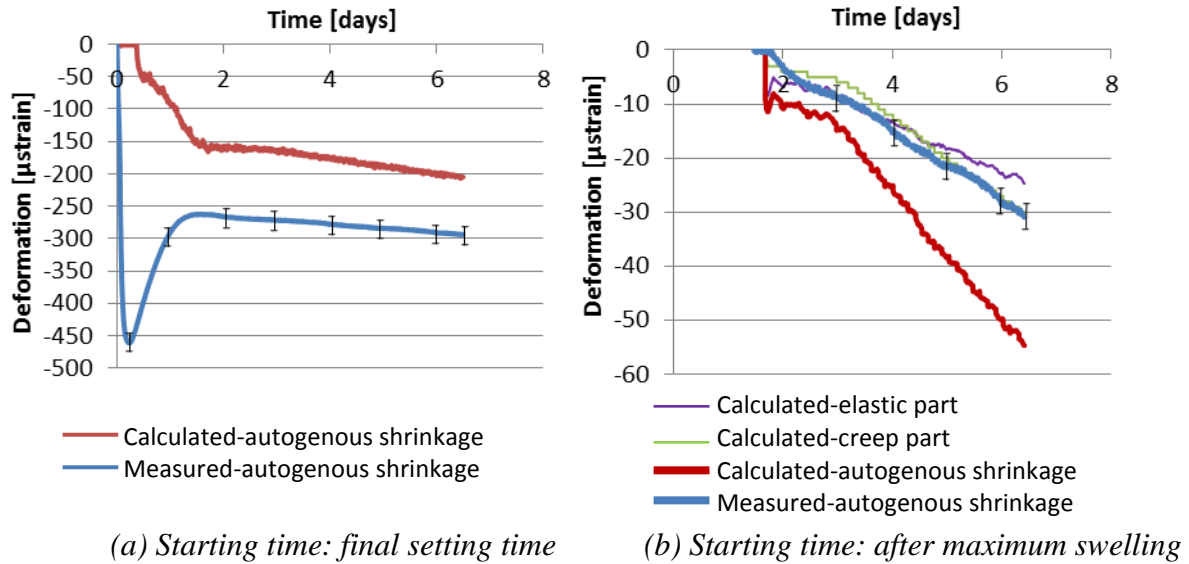


Figure 6.32 Measured and calculated autogenous deformation of fly ash cement mortar (10% sand) with water binder ratio of 0.4

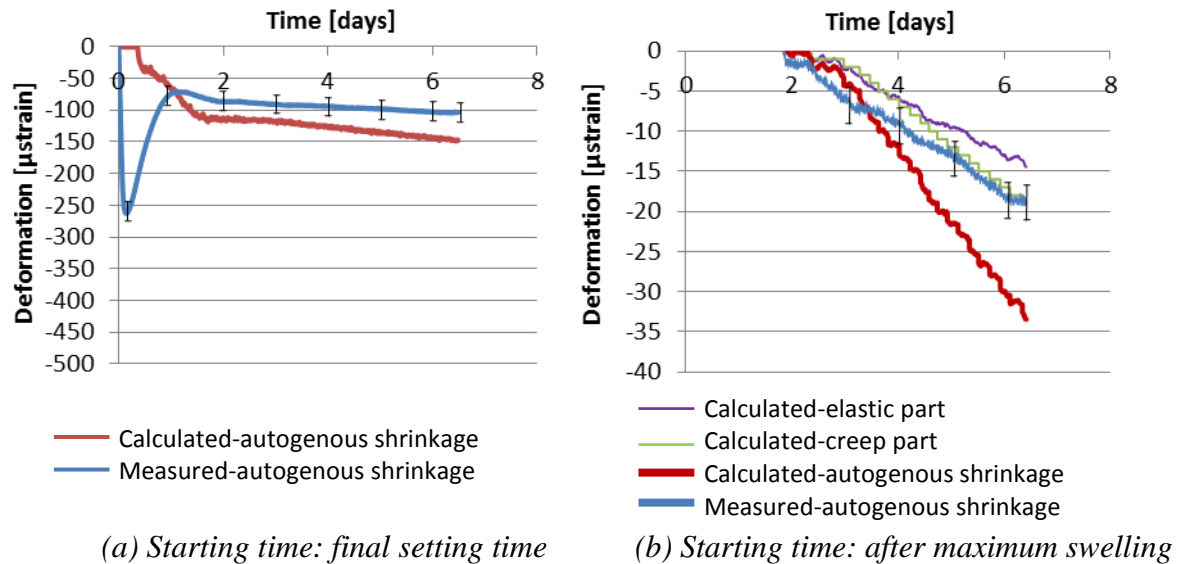


Figure 6.33 Measured and calculated autogenous deformation of fly ash cement mortar (30% sand) with water binder ratio of 0.4



### 6.6.4.3 Effect of change of ion concentration on the calculated autogenous shrinkage of fly ash mortars

Figures 6.30, 6.31, 6.32 and 6.33 show that the calculated autogenous shrinkage of fly ash cement mortar is significantly bigger than the measured value. As discussed in Chapter 5, this is due to the fact that the increasing ion concentration of pore water is not taken into account and the capillary tension is overestimated. The overestimation of capillary tension might result in an overestimation of autogenous shrinkage. By taking the increasing ion concentration of pore water into account, the calculated autogenous shrinkage of the fly ash cement mortars with water-binder ratio 0.3 and sand-solid phase (cement and sand) weight

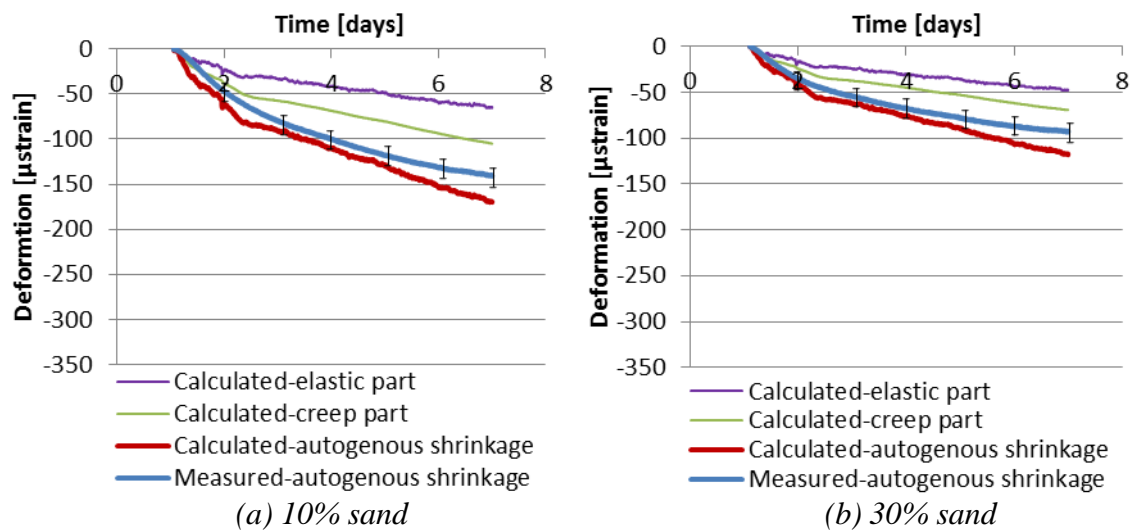


Figure 6.34 Measured and calculated autogenous deformation of fly ash cement mortar (taking change of ion concentration into account) with water-binder ratio of 0.3

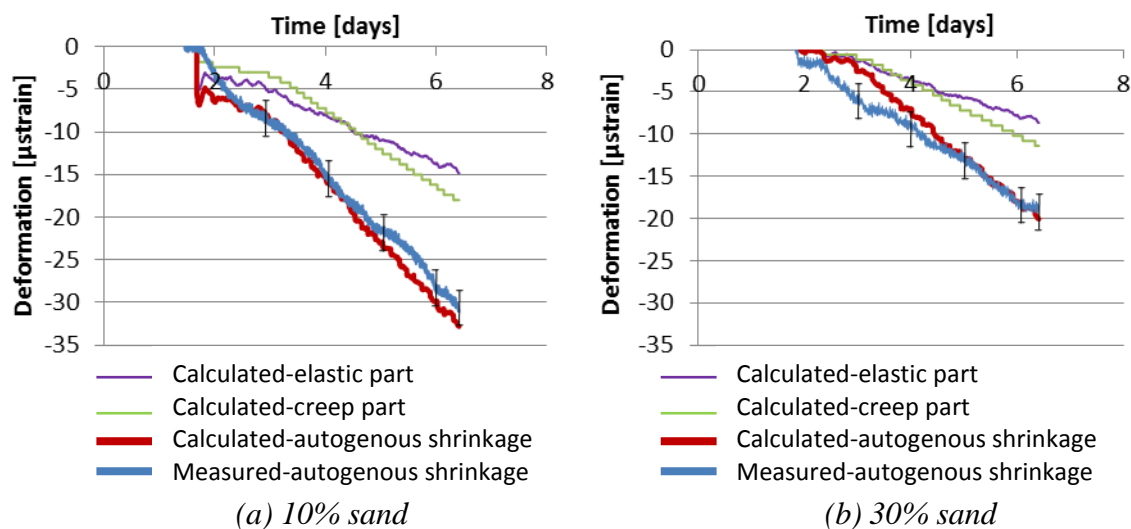


Figure 6.35 Measured and calculated autogenous deformation of fly ash cement mortar (taking change of ion concentration into account) with water-binder ratio of 0.4



ratios 0.1 and 0.3 is shown in Figure 6.34 and the calculated autogenous shrinkage of the fly ash cement mortars with water-binder ratio 0.4 and sand-solid phase (cement and sand) weight ratios 0.1 and 0.3 is shown in Figure 6.35. In Figure 6.34 and Figure 6.35 the calculated autogenous shrinkage is close to the measurements. More detailed discussion about the effect of change of ion concentration on the calculated autogenous shrinkage was given in Section 5.4.3.

#### 6.6.5 BFS cement mortars (sand-solid phase (cement and sand) weight ratio = 0.1 and 0.3, water-binder ratio = 0.3 and 0.4)

Figures 6.36 and 6.37 show the measured and calculated autogenous shrinkage of the BFS cement mortars with sand-solid phase (cement and sand) weight ratio of 0.1 and 0.3 and water-binder ratio of 0.3. Figures 6.38 and 6.39 show the measured and calculated autogenous shrinkage of the BFS cement mortars with sand-solid phase (cement and sand) weight ratio of 0.1 and 0.3 and water binder ratio of 0.4. The calculated autogenous shrinkage of BFS cement mortar after maximum swelling is shown in Figures 6.36(b), 6.37(b), 6.38(b) and 6.39(b), separated in an elastic part and a creep part. Compared with Figures 6.22(b), 6.23(b), 6.24(b), and 6.25(b), the autogenous shrinkage of BFS cement mortar is much bigger than that of plain Portland cement mortar with same water-binder ratio and sand-solid phase (cement and sand) weight ratio. This can be the result of two mechanisms. First, at the same curing age, BFS cement pastes have lower elastic modulus than plain Portland cement pastes with the same water-binder ratio. This will lead to bigger autogenous shrinkage of cement paste for the same magnitude of internal driving force, i.e. capillary tension. Second, the drop of internal relative humidity of BFS cement pastes is much bigger than in plain Portland cement pastes at the same curing age. This will lead to a higher value of the capillary tension. Both mechanisms result in bigger autogenous shrinkage of BFS cement paste.

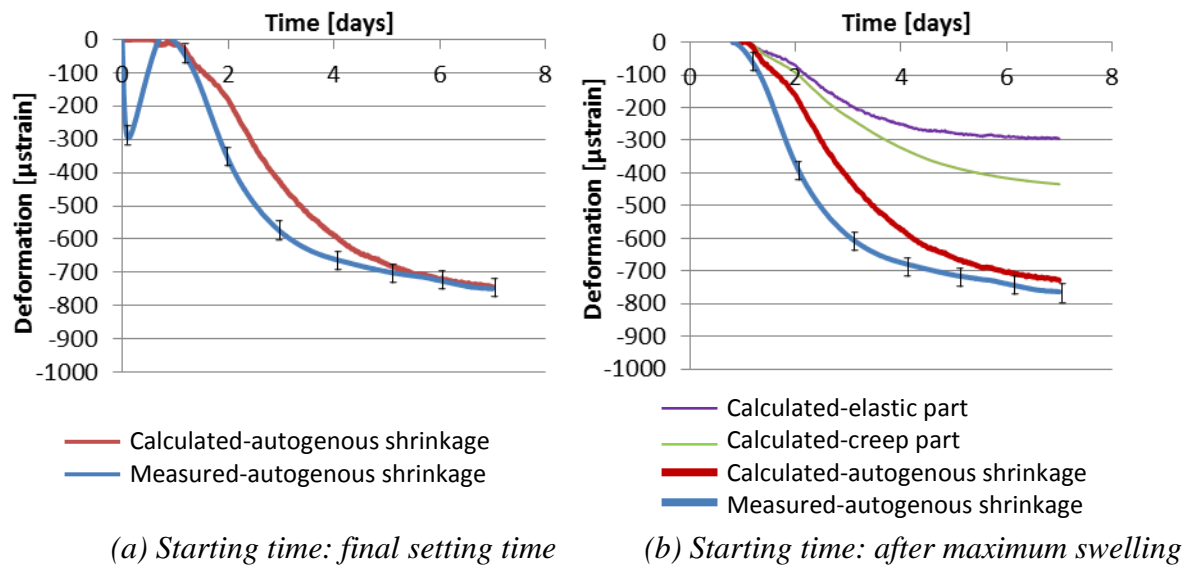


Figure 6.36 Measured and calculated autogenous deformation of BFS cement mortar (10% sand) with water-binder ratio of 0.3

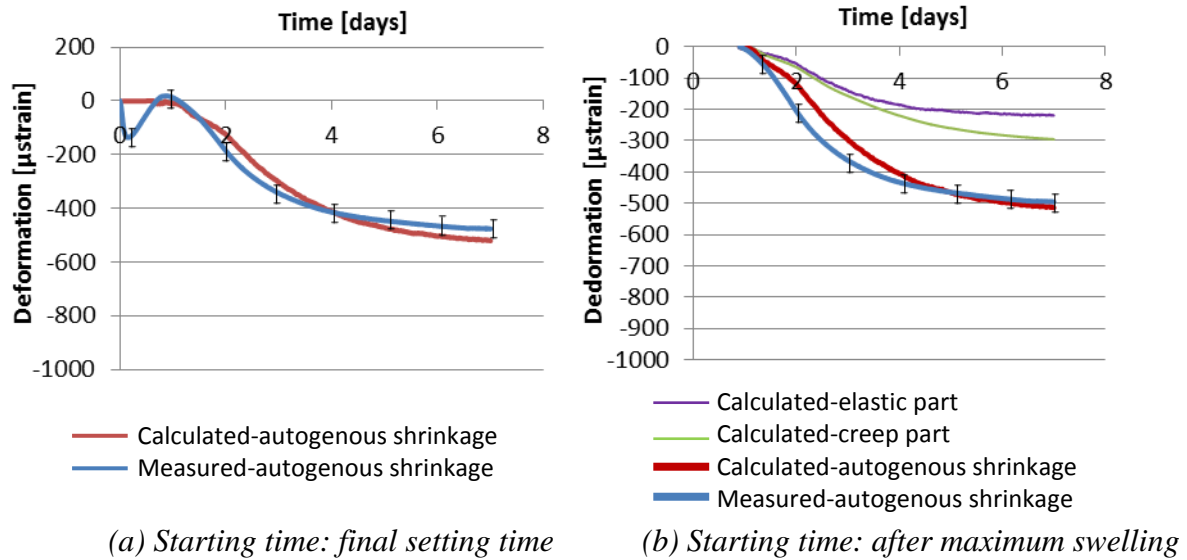


Figure 6.37 Measured and calculated autogenous deformation of BFS cement mortar (30% sand) with water-binder ratio of 0.3

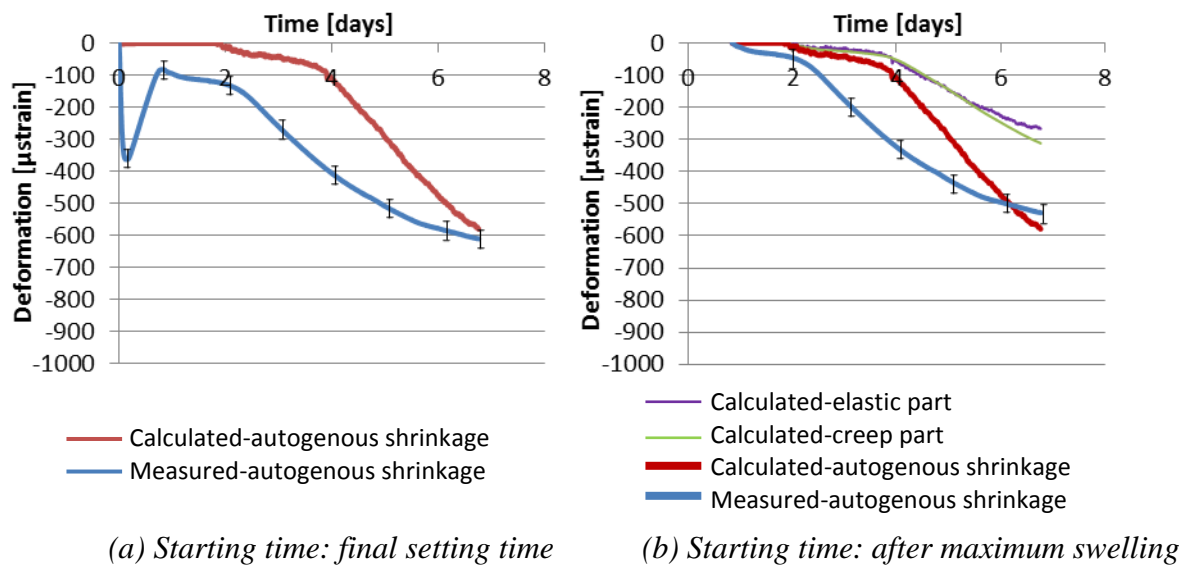


Figure 6.38 Measured and calculated autogenous deformation of BFS cement mortar (10% sand) with water-binder ratio of 0.4

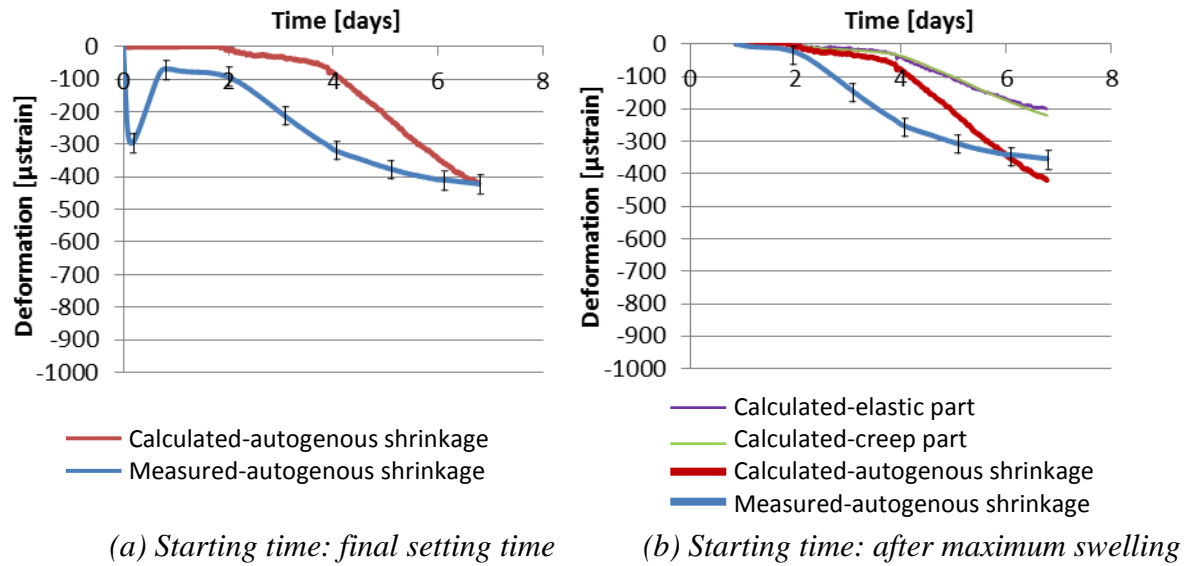


Figure 6.39 Measured and calculated autogenous deformation of BFS cement mortar (30% sand) with water-binder ratio of 0.4

#### 6.6.6 Effect of change of ion concentration on the calculated autogenous shrinkage of Portland and BFS cement mortars

As discussed in Section 6.6.4, a change of ion concentration of pore water will influence the calculated capillary tension and the calculated autogenous shrinkage. In that section it was shown that the effect of change of ion concentration on the calculated autogenous shrinkage of fly ash cement mortar was not negligible. For Portland and BFS cement mortar with water-binder ratio 0.4, the calculated autogenous shrinkage (with and without taking the change of ion concentration into account) is shown in Figure 6.40 and 6.41. Figure 6.40

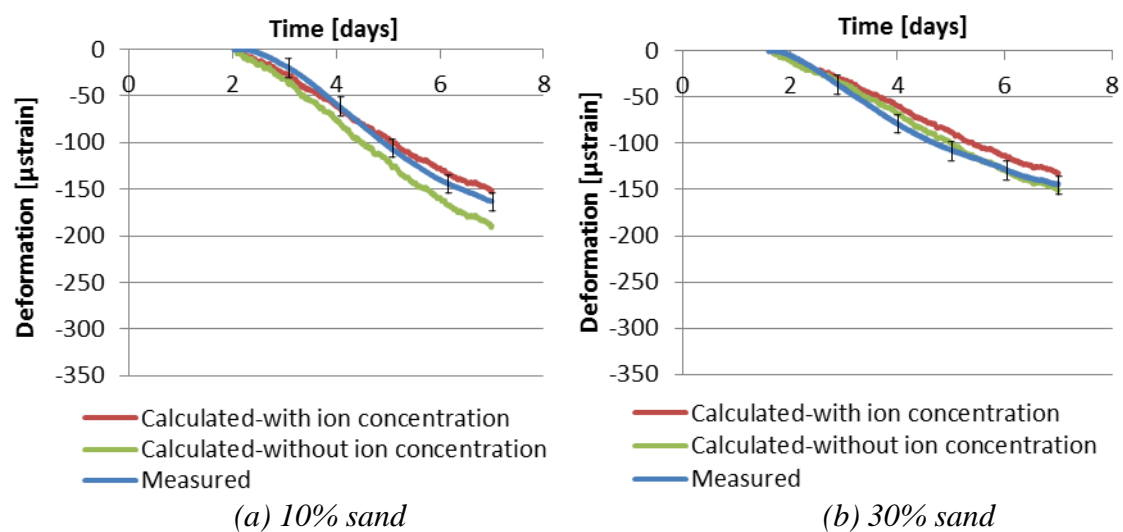


Figure 6.40 Measured and calculated autogenous deformation of Portland cement mortar (with and without taking the change of ion concentration into account) with water-binder ratio of 0.4

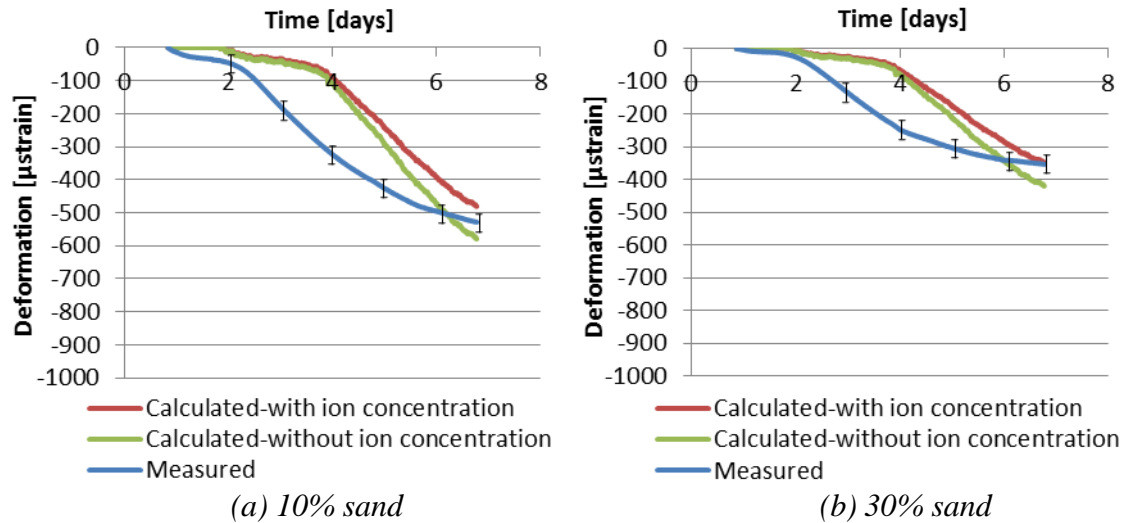


Figure 6.41 Measured and calculated autogenous deformation of BFS cement mortar (with and without taking the change of ion concentration into account) with water-binder ratio of 0.4

and 6.41 shows that the change of ion concentration of pore water does not influence the calculated autogenous deformation of Portland and BFS cement mortar significantly. This is due to the fact that the drop of the relative humidity of Portland and BFS cement paste is much bigger than that of fly ash cement paste with the same water-binder ratio (as shown in Figure 4.10). The effect of the same change of ion concentration on the calculated capillary tension (Equation 5.2 and 5.3) and calculated autogenous shrinkage (Equation 5.6, 5.7 and 6.31) of Portland and BFS cement mortar is, therefore, much smaller than that of fly ash cement paste and mortar.

## 6.7 Prediction of autogenous shrinkage of concrete at 28 days

In section 6.6 the extended Pickett model was used for predicting early-age autogenous shrinkage of different cement mortars with fine sand (0.125~0.25 mm) and a relatively low aggregate fraction. For real concrete larger aggregate particles are used and the aggregate volume ratio is higher, up to 70%. In this section, the early-age autogenous shrinkage of one OPC concrete and two BFS concretes were studied to see whether the extended Pickett model will also give reasonable results for concrete, i.e. mixtures with high aggregate content.

### 6.7.1 Mixture design

Three concrete mixtures are considered for studying the autogenous shrinkage of concrete. The mixtures are OPC concrete and two BFS concretes.

The measured autogenous shrinkage of OPC concrete is taken from Zhang's paper (Zhang et al. 2003). The concrete was made with Type I (ASTM) normal Portland cement. The water-binder ratio was 0.3. The coarse aggregate used was crushed granite with a maximum size of 20 mm. The fine aggregate used was natural sand. The density of both

the coarse and fine aggregates was  $2650 \text{ kg/m}^3$ . The volume fraction of aggregate of concrete is 71%.

The measured autogenous shrinkage of the two BFS concretes is taken from Mors (Mors 2011). The BFS concretes were made with CEM III/B 42.5N. The water-binder ratio was 0.44 and 0.5. The fine aggregate used was sand with size of 0-4 mm. The coarse aggregate used was gravel with size 4-8 mm and 8-16 mm. The volume fraction of aggregate of concrete was 70%.

The mixture compositions of OPC concrete and BFS concrete are listed in Table 6.2.

Table 6.2: Mixture composition of different concrete (% by weight)

Name	Reference	Binder		Mixture composition	
		Type I normal Portland cement (%)	CEM III/B 42.5N (%)	W/b	Volume fraction of aggregate (%)
OPC 0.3	Zhang et al. 2003	100	0	0.3	71
BFS 0.44	Mors 2011	0	100	0.44	70
BFS 0.5	Mors 2011	0	100	0.5	70

## 6.7.2 Portland cement-based concrete (Zhang et al. 2003)

### 6.7.2.1 Testing method (used by Zhang et al. 2003)

The concrete was mixed in a laboratory pan mixer. The fine and coarse aggregates were mixed first, followed by the addition of cement, mixing and adding water. Two prisms of  $400 \times 100 \times 100 \text{ mm}^3$  were cast for measuring the total shrinkage. The strain transducers were embedded in the concrete prism and connected to a computer-controlled data logger right after casting of the concrete specimen. Immediately after casting, each prism was sealed for the entire period of the experiment. The weight change of each prism was

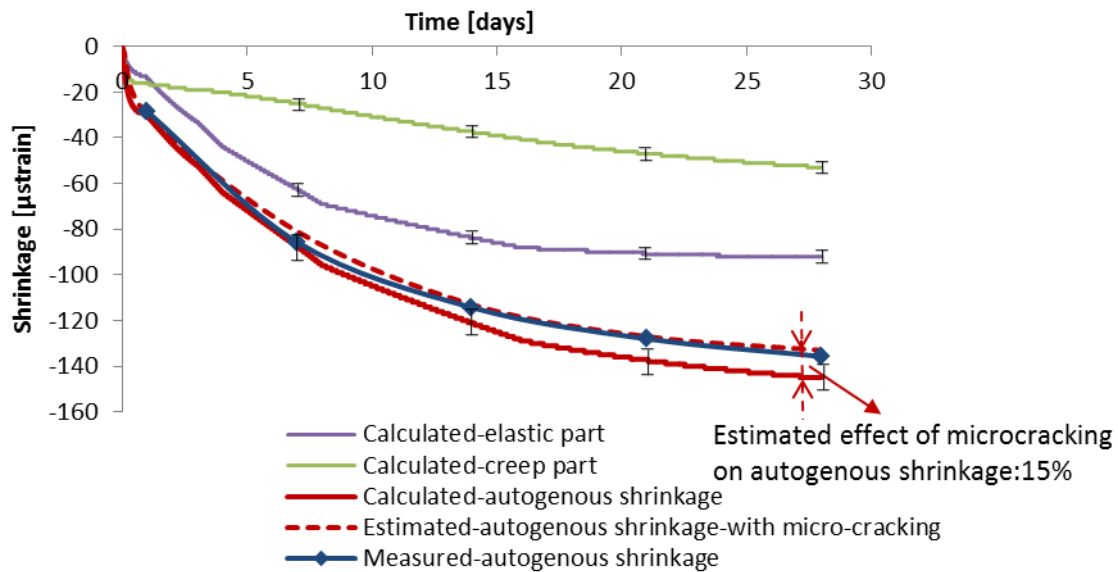


Figure 6.42 Measured autogenous deformation of OPC concrete (Zhang et al. 2003) and calculated autogenous deformation of concrete with the extended Pickett's model (water-binder ratio: 0.3, volume fraction of aggregate: 71%)

measured. The autogenous shrinkage was measured during 28 days after casting and shown in Figure 6.42.

#### 6.7.2.2 Numerical simulation of autogenous shrinkage

For simulating the autogenous shrinkage of the OPC concrete with the extended Pickett model, a few parameters are needed, viz.: the evolution of relative humidity, degree of saturation and elastic modulus of the concrete, is simulated with HYMOSTRUC<sup>4)</sup> (van Breugel 1991). Capillary tension is calculated from the simulated relative humidity using Kelvin equation (Equation 3.8). The simulated results are shown in Figures 6.43 and 6.44. The calculated autogenous shrinkage of OPC concrete is shown in Figure 6.42. The contributions of both the elastic and time-dependent part of autogenous deformation to autogenous shrinkage are shown.

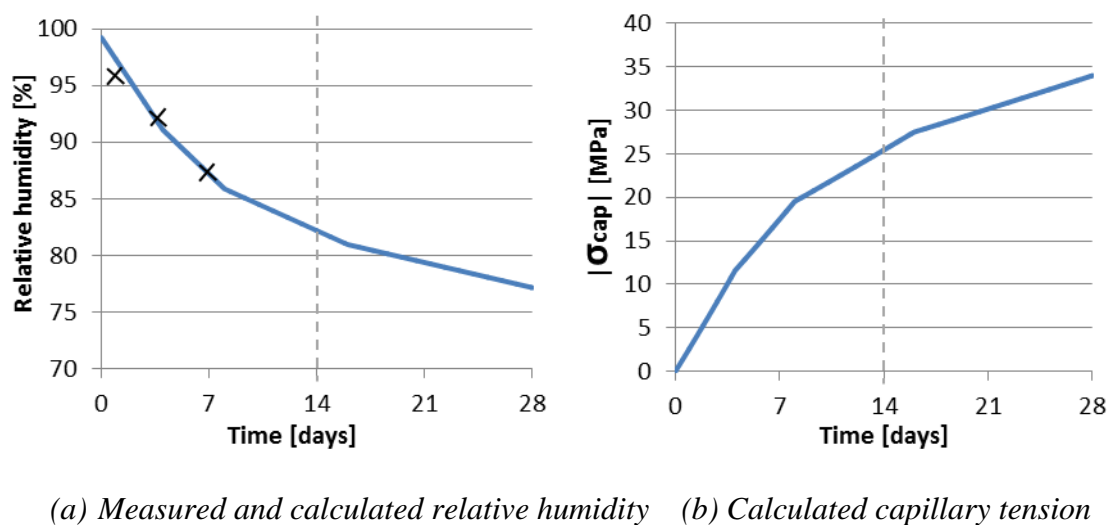


Figure 6.43 Measured and calculated relative humidity (black cross: measured relative humidity; blue line: calculated relative humidity) and capillary tension of OPC concrete (water-binder ratio: 0.3)

4) In HYMOSTRUC the degree of hydration  $\alpha$  of cement is simulated as a function of the particle size distribution and of the chemical composition of the cement, the water/cement ratio and the reaction temperature. The evolution of relative humidity and degree of saturation of the concrete are simulated based on the degree of hydration  $\alpha$ . Elastic modulus is calculated using the composite model (Lokhorst 1998). All the inputs of Lokhorst's composite model are determined by HYMOSTRUC. In this case, the Type I (ASTM) normal Portland cement used by Zhang et al. (2003) has the similar physical properties and chemical composition as that of Portland cement (CEM I 42.5N). The particle size distribution and the chemical composition of the Portland cement (CEM I 42.5N) are used as the input of HYMOSTRUC to calculate the evolution of relative humidity, capillary tension, degree of saturation and elastic modulus of OPC concrete. The water-binder ratio is 0.3 and curing temperature is 20°C.

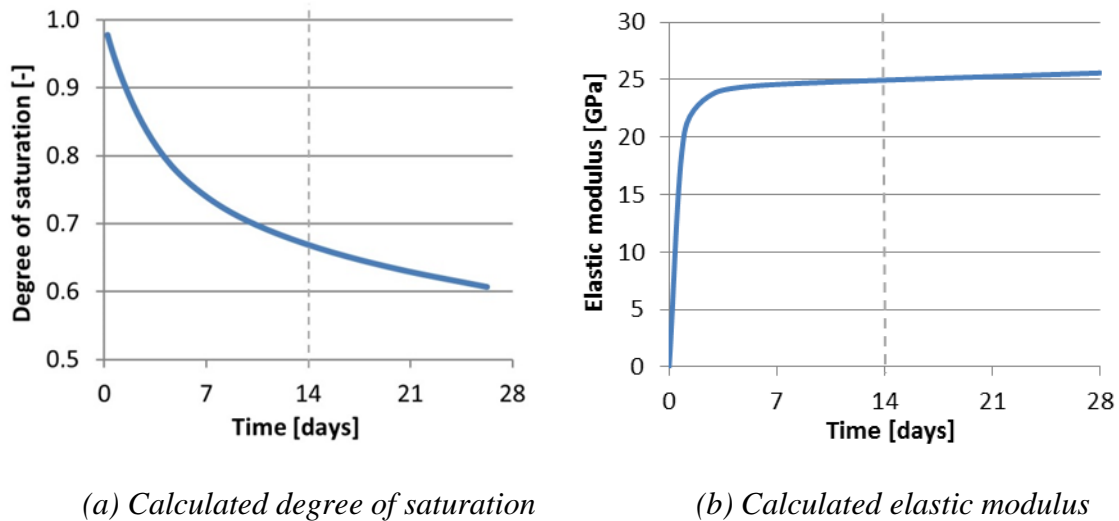


Figure 6.44 Calculated degree of saturation and elastic modulus (with *HYMOSTRUC*) of OPC concrete (water-binder ratio: 0.3)

Figure 6.42 shows that the prediction of the autogenous shrinkage of OPC concrete with the extended Pickett model is in very good agreement with the measurements. At 28 days, the autogenous shrinkage of concrete is about 140  $\mu\text{m}/\text{m}$ . Figure 6.42 also shows that the elastic part of autogenous shrinkage is almost constant after the first 14 days. After the first 14 days, the increase of capillary tension is slow and the degree of saturation still decreases (see Figures 6.43b and 6.44a). The combined effect of capillary tension and degree of saturation result in a constant elastic part of autogenous shrinkage. After the first 14 days the creep part still increases with time and plays a more and more important role in autogenous shrinkage.

It must be mentioned that the microcracking is not taken into consideration in the calculation with the extended Pickett model. As discussed in section 6.3.2, there is high probability of microcracking in cement mortars after the first few days if the aggregate volume fraction is higher than 0.5. In this mixture the aggregate volume fraction is 0.71. Microcracks probably occur inside these concretes after the first few days. Microcracking results in debonding between cement paste and sand particles and a *reduction* of the autogenous shrinkage. Maruyama et al. (2006) calculated the autogenous shrinkage of concrete using finite element analysis. According to Maruyama the value of calculated autogenous shrinkage of concrete may decrease by about 15% when the microcracking caused by internal restraint is taken into consideration. The adjusted autogenous shrinkage of OPC concrete by taking the microcracking into consideration (decrease by 15%) is indicated with the dashed line in Figure 6.42. After adjusting the calculated autogenous shrinkage for the effect of microcracking the measured and predicted shrinkage curves are very close.



### 6.7.3 Blast furnace slag concrete (Mors 2011)

#### 6.7.3.1 Testing method (used by Mors, 2011)

Two prisms of  $400 \times 100 \times 100 \text{ mm}^3$  were cast for measuring the autogenous shrinkage. After demoulding the prisms are directly wrapped in plastic foil and sealed with aluminium foil to prevent moisture exchange with the surrounding environment. A dial gauge was attached at two opposite sides of the prism to measure the autogenous shrinkage. The

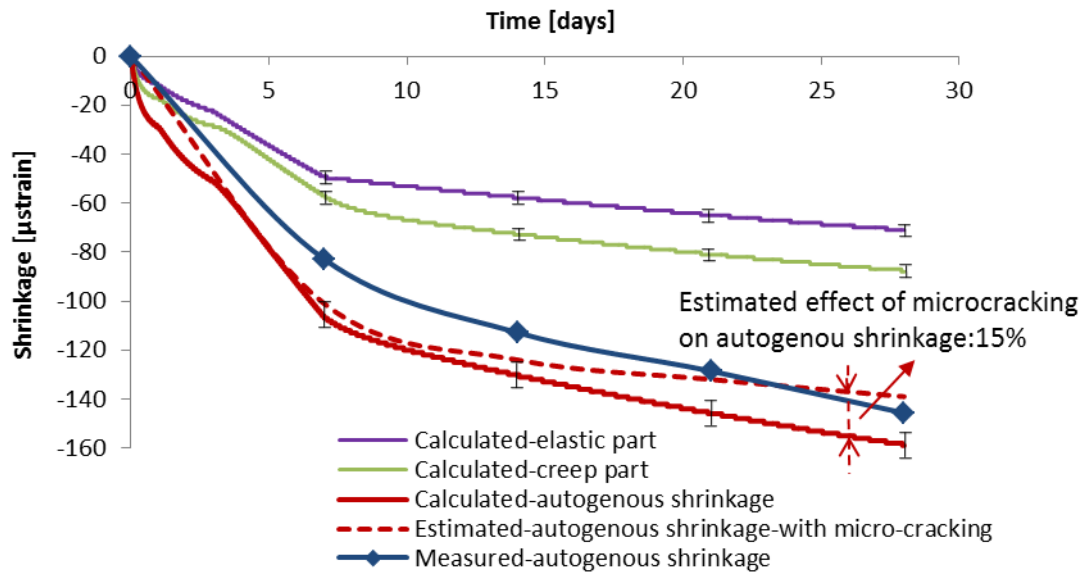


Figure 6.45 Measured autogenous deformation of BFS concrete (w/b:0.44) (Mors 2011) and calculated autogenous deformation of BFS concrete with the extended Pickett model

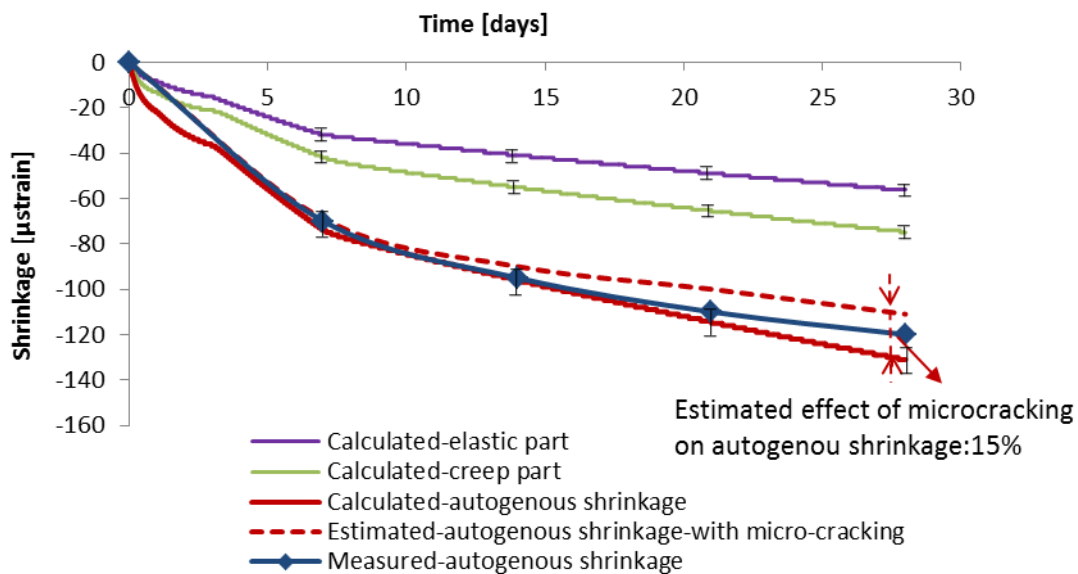


Figure 6.46 Measured autogenous deformation of BFS concrete (w/b:0.5) (Mors 2011) and calculated autogenous deformation of BFS concrete with the extended Pickett model



measuring length of the dial gauge is 20 cm and the accuracy of the dial gauge is 1  $\mu\text{m}$ . The weight loss of each prism was measured. The measured weight loss was used to correct the autogenous shrinkage measurement for minor leakage through the sealing. The corrected autogenous shrinkage of BFS concrete with water-binder ratio 0.44 and 0.5 are shown in Figures 6.45 and 6.46.

#### 6.7.3.2 Numerical simulation of autogenous shrinkage

The calculated autogenous shrinkage of BFS concrete with water-binder ratio 0.44 and 0.5 using the extended Pickett model are shown in Figures 6.45 and 6.46. The inputs of the model, i.e. the evolution of relative humidity, capillary tension, degree of saturation and elastic modulus of the BFS concrete are shown in Figures 6.47 and 6.48. These inputs are estimated from the simulation results of Portland concrete (CEM I 42.5N) with the same water-binder ratio using HYMOSTRUC<sup>5)</sup> (as shown in Figures 6.47 and 6.48). According to the simulation with HYMOSTRUC the drop of relative humidity of Portland concrete with water-binder ratio 0.44 and 0.5 at 7 days is 4.6% and 2.6%. As shown in Figure 4.10 the measured drop of relative humidity of BFS cement paste at seven days is larger than that of Portland cement paste with the same water-binder ratio. The ratio between the measured drop of relative humidity of BFS cement paste and that of Portland cement paste at 7 days is almost 1.5. Therefore, the drop of relative humidity of BFS concrete with water-binder ratio 0.44 and 0.5 at 7 days is taken as 7% ( $\approx 1.5 \times 4.6\%$ ) and 4% ( $\approx 1.5 \times 2.6\%$ ). During the period from 7 days to 28 days, the ratio between the drop of relative humidity of BFS concrete and the drop of relative humidity of Portland concrete with same water-binder ratio is also taken as 1.5. The estimated relative humidity of BFS concrete with water-binder ratio 0.44 and 0.5 is shown in Figure 6.47(a). The capillary tension is

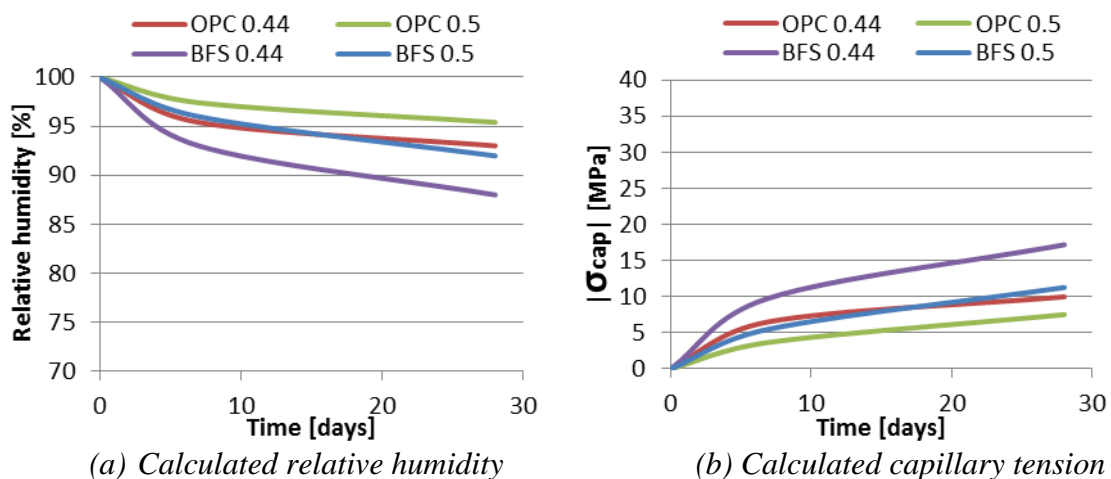


Figure 6.47 Estimated relative humidity and capillary tension of BFS concrete with water-binder ratio 0.44 and 0.5 (Estimation based on the simulation results of Portland concrete (CEM I 42.5N) with same water-binder ratio using HYMOSTRUC)

5) The particle size distribution and the chemical composition of the Portland cement (CEM I 42.5N) are used as the input of HYMOSTRUC to calculate the evolution of relative humidity and degree of saturation of OPC concrete. Elastic modulus is calculated using the composite model (Lokhorst 1998). All the inputs of composite model are determined by HYMOSTRUC. The water-binder ratio is 0.44 and 0.5. The curing temperature is 20°C.

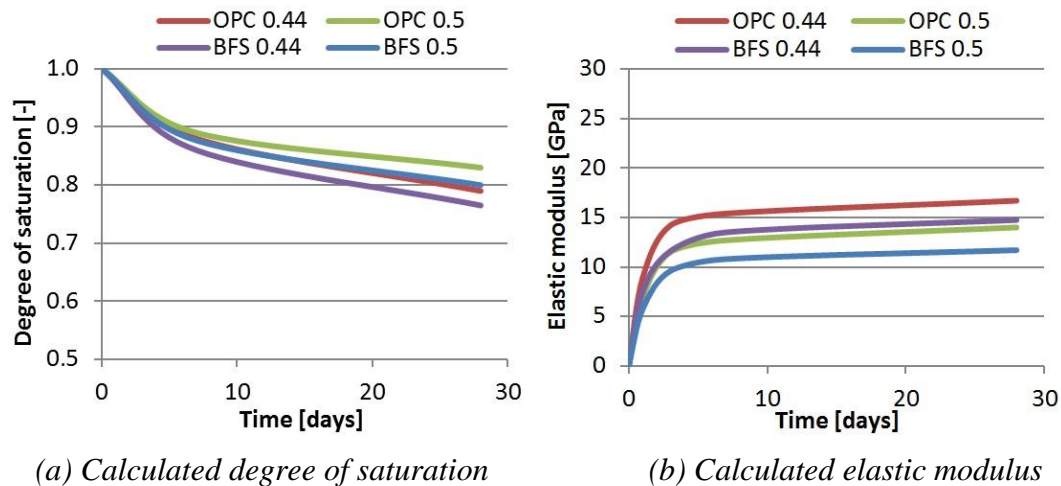


Figure 6.48 Estimated degree of saturation and elastic modulus of BFS concrete with water-binder ratio 0.44 and 0.5 (Estimation based on the simulation results of Portland cement concrete (CEM I 42.5N) with same water-binder ratio using HYMOSTRUC)

calculated from the predicted relative humidity using Kelvin equation (Equation 3.8) and shown in Figure 6.48(b). The degree of saturation and elastic modulus of BFS concrete are also estimated based on the simulation results using HYMOSTRUC.

Figures 6.45 and 6.46 show the predictions of the autogenous shrinkage of the BFS concrete mixtures with the extended Pickett model. As discussed in Section 6.3.3, the microcracking should be taken into consideration in the extended Pickett model when the aggregate volume fraction of concrete is higher than 50%. By taking an assumed effect of microcracking into consideration, the estimated autogenous shrinkages of BFS concretes decrease about 15%. The estimated autogenous shrinkage of BFS concretes are shown in Figures 6.45 and 6.46. Figures 6.45 and 6.46 show that the autogenous shrinkage of BFS concrete will be simulated slightly better by taking the effect of microcracking into consideration.

#### 6.7.4 Evaluation of prediction of autogenous shrinkage of concrete

In this section, the extended Pickett model was used to predict the autogenous shrinkage of concrete with high aggregate content. A comparison of the calculated and measured autogenous shrinkage of OPC concrete and two BFS concretes reveals that the extended Pickett model predicts the trend of autogenous shrinkage of concrete quite well, even without taking any effect of microcracking into account. By taking an assumed effect of microcracking into consideration (decrease by 15% according to Maruyama et al. (2006)), the prediction of the autogenous shrinkage of OPC concrete was not worse, while that of BFS concretes was even better.

It should also be noted that the inputs of the extended Pickett model, i.e. the evolution of relative humidity, capillary tension, degree of saturation and elastic modulus of the BFS concrete, are estimations. These inputs are predicted based on the simulation results for Portland concrete (CEM I 42.5N) with the same water-binder ratio using HYMOSTRUC. Figure 6.43 (a) shows a good agreement between the measured and the calculated relative humidity. There is a scatter of the measured relative humidity (as shown in Figure 4.9 and

4.10). The scatter of measured relative humidity along with the scatters of other inputs will result in a range of the calculated autogenous shrinkage. The range of the calculated autogenous shrinkage of concretes is about 10% and shown in Figure 6.42, 6.45 and 6.46 in the form of error bar.

## 6.8 Discussion and conclusion

In this chapter, the autogenous deformation of sixteen cement mortars were experimentally and numerically studied. Pure Portland cement mortars and mortars made with three blended cements, i.e. cements blended with silica fume, fly ash and blast furnace slag, were studied. The water-binder ratios were 0.3 and 0.4. The sand-solid phase (cement and sand) weight ratios were 0.1 and 0.3. Also the autogenous shrinkage of three concretes was studied, i.e. an OPC concrete and two BFS concretes.

In this chapter the original Pickett model is presented first. Pickett's model overestimates autogenous shrinkage of concrete, especially for concrete with higher aggregate contents and lower water-cement ratio. The factors causing the discrepancy between the calculated and measured autogenous shrinkage are microcracking and the ignorance of creep. According to the calculated results, there is a low probability of microcracking in the concrete with low sand weight ratio, i.e. sand-solid phase (cement and sand) weight ratio as low as 0.1 to 0.3. The probability of cracking will increase with increasing amount of sand in the mixture. When the sand weight ratio is higher than 0.5, the probability of cracking after the first few days is quite high. In the mortar experiments considered in this thesis the sand-solid phase (cement and sand) weight ratios of cement mortar is low, i.e. 0.1 and 0.3. For these mixtures the influence of microcracking on autogenous shrinkage of cement mortar is negligible.

The original Picket model has been extended by taking creep into consideration. In this model, creep is simulated with formulas based on the activation energy theory. The predictions of autogenous shrinkage with the extended Pickett model are evaluated by comparing the calculated and measured autogenous shrinkage of different cement mortars. A comparison of the measured autogenous shrinkage with the autogenous shrinkage calculated with the extended Pickett model reveals that the extended Pickett model predicts the trend of autogenous shrinkage of Portland and BFS cement mortars quite well. But there is a large difference between the measured and calculated autogenous shrinkage of fly ash cement mortar. The calculated autogenous shrinkage of fly ash cement mortar is much bigger than the measured autogenous shrinkage. This difference is possibly caused by an overestimation of the capillary tension. Capillary tension is calculated as function of the relative humidity. The dissolved ions in the pore solution decrease the value of relative humidity. In this study the effect of dissolved ions on the relative humidity is assumed constant. But in fact the ion concentration of the pore solution of fly ash cement paste increases with time during the first 28 days *after* mixing (Taylor 1992). Its influence on the measured relative humidity will also increase with time. Without taking the increasing ion concentration of pore solution into consideration, the calculated capillary tension is overestimated. Overestimation of capillary tension results in overestimation of calculated autogenous shrinkage. By taking changes of the ion concentration of pore water during hydration into account, the calculated autogenous shrinkage of fly ash cement mortars is close to the measured results. The influence of the changes of the ion concentration of pore water on the calculated autogenous shrinkage of Portland and BFS cement mortar is not as significant as that of Fly ash. This is due to the fact that the drop of the relative humidity of

Portland and BFS cement pastes is much bigger than that of fly ash cement paste. The effect of the same change of ion concentration on the calculated capillary tension and autogenous shrinkage of Portland and BFS cement pastes and mortars is, therefore, much smaller than that of fly ash cement pastes and mortars.

The extended Pickett model was also used to predict the autogenous shrinkage of OPC and BFS *concretes* with high aggregate content. From the comparison between the calculated and measured results it was found that the extended Pickett model predicts the trend of autogenous shrinkage of the investigated concretes quite well, even without taking any effect of microcracking into account. By taking an assumed effect of microcracking into consideration (according to Maruyama et al. (2006) causing a decrease of autogenous shrinkage by 15%), the prediction of the autogenous shrinkage of OPC concrete was not worse, while that of BFS concretes was even better.

# Chapter 7

## Retrospection, Conclusions and Prospects

### 7.1 Retrospection

With the increasing use of concretes with low water-binder ratio an increasing proneness to shrinkage-induced cracking has been observed in highway pavements, bridge decks, airport pavements and industrial floors soon after construction, i.e. in the first few weeks after casting. Cracks accelerate the ingress of water and corrosive agents and can reduce the overall performance. Autogenous shrinkage, as an important component of early-age concrete shrinkage, is a consequence of the self-desiccation during the cement hydration process. As hydration progresses, the internal relative humidity drops and capillary tension develops. Capillary tension is considered to be the major internal driving force of autogenous shrinkage, will lead to volume changes of concrete. Autogenous shrinkage is quite pronounced in high-performance concrete with low water-cementitious ratio.

Quantifying autogenous shrinkage of cementitious systems, especially given the widespread and increasing utilization of high-performance concrete containing supplementary materials, becomes more and more important for evaluating the probability of premature cracking in concrete structures. During the past few years, many researchers have worked on models for prediction of autogenous shrinkage of hydrating cementitious material. However, different proposed mechanisms, inaccurate description of mechanical properties of early-age hardening cement paste and lack of widely accepted experimental data due to absence of standard test methods have slowed down the progress of the search for reliable predictive models of autogenous shrinkage, particularly for non-traditional mixtures.

This thesis focuses on the modelling of the autogenous shrinkage in cementitious systems blended with different kinds of supplementary materials. A simulation model is proposed for autogenous shrinkage of cement paste. In this model, capillary tension which causes compression of solid skeleton of cement paste, is considered as the major driving force of autogenous shrinkage. Autogenous shrinkage of cement paste is divided into two parts, i.e. an elastic part and a time-dependent part. The time-dependent part is analysed with formulas based on the activation energy theory.

Various experimental methods are presented for measuring of early-age properties of cement pastes. These experimental results are used as input of the proposed model to predict the autogenous shrinkage of cement paste. The simulation results are compared with measured autogenous shrinkage. The accuracy of the predictions of autogenous shrinkage with the proposed model is evaluated.

Finally, an extended Pickett model, which takes the visco-elastic behavior of the cement matrix into consideration, is proposed for predicting the autogenous shrinkage of cement mortar and concrete. The predicted autogenous shrinkage of cement mortar is compared with measurement results (first 7 days after casting) to evaluate the accuracy of the predictions with the extended Pickett model. The extended Pickett model is also used to

predict the autogenous shrinkage of concrete with high aggregate content. The simulated autogenous shrinkage of concrete is compared with data (first 28 days after casting) from literature.

## 7.2 Conclusions

The general conclusions of this research are:

- The early-age autogenous shrinkage of cement paste is supposed to include an elastic part and a time-dependent part in this thesis. The proposed numerical model, which calculates the elastic part and the time-dependent part separately, can simulate the trend of the autogenous shrinkage of Portland cement pastes and Portland cement pastes blended with different supplementary materials quite well.
- By taking the restraining effect of sand particles and time-dependent behaviour of heterogeneous mixtures into account, the autogenous shrinkage of hardening cement mortar (fine sand, 0.125~0.25 mm) can be estimated by using the extended Pickett model. The autogenous shrinkage of concrete with larger aggregate particles and higher aggregate volume ratio can also be estimated with the extended Pickett model.

In order to evaluate the accuracy of the prediction of autogenous shrinkage by using the proposed model, the autogenous shrinkage of Portland cement pastes and Portland cement pastes blended with different supplementary materials is measured and simulated. Based on the simulation and experimental results, the following conclusions can be drawn:

- The addition of fly ash leads to smaller autogenous shrinkage of cement paste compared with that of ordinary Portland cement paste with the same water-binder ratio. The smaller autogenous shrinkage of fly ash cement paste is supposed to be caused by a higher humidity of the fly ash cement paste than that of ordinary Portland cement paste with the same water-binder ratio during the first seven days of hydration. Fly ash contains higher amount of inactive minerals compared with Portland cement. Because of its low reactivity the fly ash hydrates slower than cement and less water is consumed in fly ash cement paste. The higher internal relative humidity leads to smaller capillary tension and autogenous shrinkage of fly ash cement paste than that of Portland cement paste with same water-binder ratio.
- The measured autogenous shrinkage of BFS cement paste is much bigger than that of Portland cement paste with same water-binder ratio. The bigger autogenous shrinkage of BFS cement paste has two reasons. On one hand, the resistance to deformation of BFS cement paste is lower than that of Portland cement paste with same water-binder ratio at the same curing age. On the other hand, the change of internal relative humidity of BFS cement pastes is much bigger than that of Portland cement pastes with same water-binder ratio at the same curing age. Bigger drop of relative humidity of BFS cement paste results in bigger capillary tension. The bigger capillary tension and smaller resistance to deformation result in bigger autogenous shrinkage of BFS cement paste.
- The autogenous shrinkage of cement pastes with different supplementary materials follow a similar trend with decreasing internal relative humidity. This phenomenon is consistent with the assumed existence of a relationship between autogenous

deformation and relative humidity changes in the capillary pores of the hardening cement paste.

- For concrete with high aggregate content, micro-cracks probably occur inside concrete after the first few days. Microcracking results in a reduction of the autogenous shrinkage. The effect of microcracking on autogenous shrinkage was estimated to be 15%.

### **7.3 Contribution of this study to autogenous shrinkage of cementitious material**

With this research, the mechanisms of autogenous shrinkage of cement paste, i.e. disjoining pressure and capillary tension, were discussed. The capillary tension which puts the solid skeleton in compression is considered the driving force of autogenous shrinkage. The autogenous shrinkage of cement paste and mortar with different supplementary material was studied. A simulation model for autogenous shrinkage of blended cement paste was proposed. Furthermore an extended Pickett model, which takes the visco-elastic behavior of the cement matrix into consideration, was proposed. The main contribution of this study are listed:

- In this research, the mechanism of autogenous deformation is studied. Two mechanisms for autogenous deformation of early-age hydrating cement paste, i.e. disjoining pressure and capillary tension, are studied quantitatively. For the conditions considered in this chapter, the disjoining pressure separates the adjacent cement particles in cement paste and it has a significant value in small gel pores where reaction products are densely packed. Meanwhile, the pore water in capillary pores is in tension and puts the solid skeleton of cement paste, including the water between reaction products, in compression, which results in the external volume reduction of the cement paste, i.e. autogenous shrinkage. Capillary tension increases with decreasing internal relative humidity. In cement paste the compressive forces must be in equilibrium with tensile forces. This equilibrium requirement somehow links the (compressive) disjoining pressure to the capillary tension.
- In studies on the autogenous shrinkage cement paste is normally considered as a continuously changing elastic material. However, the early-age cement paste is a visco-elastic material. The time-dependent behaviour of the material, i.e. creep, plays a significant role in the early-age autogenous shrinkage as well. The contribution of creep to autogenous shrinkage increases with time. In this research, the effect of creep on autogenous shrinkage of cement paste is studied. The calculated autogenous shrinkage (with creep) of cement paste is compared with measurements. The comparison between the calculated autogenous shrinkage of cement paste and the measured result shows the simulation model predicts the trend of autogenous shrinkage of cement pastes quite well.
- In literature several composite models for autogenous shrinkage of mortar and concrete have been proposed. In these models the cement paste surrounding aggregate particles is considered as a homogeneous material and both the particle and the cement paste are assumed to be elastic. In this thesis, the Pickett model was extended to take the creep of cement paste into consideration. The extended Pickett model is used to simulate the autogenous shrinkage of cement mortar and concrete. The simulation results are compared with measurement results. The comparison between the calculated autogenous shrinkage of cement paste and the measured result shows the extended

Pickett model predicts the trend of autogenous shrinkage of cement mortars and concrete quite well.

## 7.4 Prospects

From this study several aspects are recommended for further research:

- In this thesis, only autogenous shrinkage of cement pastes with water-binder ratio of 0.3 and 0.4 was investigated. But cement paste with a low water-binder ratio has a higher autogenous shrinkage and higher risk of cracking when the shrinkage is restrained. Therefore, it is important to get information about autogenous shrinkage of cement paste with water-binder ratio  $< 0.3$ .
- The measurements of autogenous shrinkage exhibit a fast shrinkage after final setting, and after a short period of swelling the specimen will shrink steadily. The initial fast shrinkage is much bigger than the shrinkage after the short period of swelling. The initial fast shrinkage may be an artefact of the testing method and can't be explained by the mechanisms of autogenous shrinkage, e.g. capillary tension. It is important to have a better understanding of the fast shrinkage.
- The influence of early expansion on the autogenous shrinkage should be paid more attention. The early-age deformations observed on macroscale are the result of expansion and shrinkage processes which develop simultaneously. When shrinkage is dominant, the external volume of cement paste will decrease. The quantitative simulation of early-age expansion will be very helpful to get an accurate prediction of autogenous deformation of cement paste.
- In this thesis, the simulation and measurement of autogenous shrinkage of cement paste are limited to the period from final setting up to 7 days. However, autogenous shrinkage of cement paste will further increase with elapse of time after the first 7 days. The time-dependent part of autogenous shrinkage, i.e. creep, will increase with time and will play a more and more important role. The magnitude of generated stress due to restrained autogenous shrinkage is important for evaluating the risk of cracking of cement paste. The higher generated stress, the higher risk of cracking. The further increasing autogenous shrinkage caused by creep will not generate the same stress as the elastic part of autogenous shrinkage due to relaxation. Therefore, it is important to study the influence of creep on the development of autogenous shrinkage and the consequence over a longer period of time in view of the resulting risk of cracking.
- Test specimens of cement paste and mortar were cured in sealed condition at 20°C in this thesis. The influence of temperature on the development of autogenous shrinkage should be paid attention in further research.



# Summary

Concrete is a brittle composite material that easily fractures under tension. Due to the fact that the early-age deformation of the concrete member is restrained by adjoining structures, cracking can occur throughout the concrete prior to application of any load. The cracks would provide preferential access for aggressive agents penetrating in the concrete and then cause corrosion of reinforcement and degradation of concrete. As a result, the service life of concrete structure would be decreased.

There are many different types of early-age deformation of concrete, e.g. temperature-induced strain, drying shrinkage and autogenous shrinkage. Among these types of early-age deformation, autogenous shrinkage is a consequence of the self-desiccation during the cement hydration process. For a long time autogenous shrinkage was considered negligible compared with drying shrinkage. In recent years, autogenous shrinkage has drawn more and more attention due to the increasing use of concretes with low water-binder ratios. Despite the fact that phenomenon of autogenous shrinkage has been recognized for several decades, the mechanism behind it is still not fully understood and no consensus has yet been reached. There is a general agreement about the existence of a relationship between autogenous deformation and relative humidity change in the capillary pores of the hardening cement paste. Many simulation models were built based on this relationship to predict the development of autogenous shrinkage. The reliability of these predictions, however, is not always satisfactory. The discrepancy between the measured and calculated autogenous deformation becomes very pronounced at later ages. In those simulation models, cement paste was considered as an elastic material and only the elastic part of autogenous shrinkage was predicted. In fact, cement paste is not ideal elastic material. When a cement paste is subjected to a sustained load, it will deform elastically and continue to deform further with time, which process is known as creep. Creep plays an important role in autogenous shrinkage of hydrating cement paste. The ignorance of creep would lead to an underestimation of the autogenous shrinkage.

The aim of this project is to study the autogenous shrinkage of Portland cement pastes and blended pastes with supplementary materials. The autogenous shrinkage is supposed to consist of two parts, elastic part and time-dependent part (creep), which are simulated separately. Based on the autogenous shrinkage of cement pastes, autogenous shrinkage of cement mortars and concretes were simulated by taking the restraining effect of rigid sand/aggregate particles into consideration.

Firstly, the mechanisms behind the autogenous deformation were discussed. The disjoining pressure and capillary tension of cement paste were quantified numerically. The roles of disjoining pressure and capillary tension play on the autogenous shrinkage was discussed. It was found that the disjoining pressure and capillary tension are two mechanisms for autogenous deformation of early-age hydrating cement paste. The disjoining pressure is repulsive and should gain more attention when studying the early-age swelling of hydrating cement paste. Meanwhile, the capillary tension is attractive and increases with the decrease of internal relative humidity. For early age cement paste cured under sealed condition, the relative humidity does not drop below 75%. Capillary tension plays a dominate role in this range.

Secondly, a simulation model for autogenous shrinkage of cement paste was proposed. In this model, Capillary tension is considered as the major driving force of autogenous

shrinkage. The autogenous shrinkage is supposed to consist of two parts, elastic part and time-dependent part (creep). The elastic part is calculated by Hooke's law. The time-dependent part(creep) of this model is based on the activation energy theory and extended to deal with the continuously changing physical properties of the hardening cement paste.

Thirdly, in order to provide data for modelling of the autogenous shrinkage, early age properties of cement paste were experimentally investigated. Setting time, internal relative humidity, non-evaporable water content, chemical shrinkage and compressive strength of cement paste were measured. Portland cement paste and three kinds of blended paste with different supplementary material, i.e. silica fume, fly ash and blast furnace slag, were studied. Water-binder ratios of these cement pastes are 0.3 and 0.4.

Then, the autogenous shrinkages of Portland cement paste and three kinds of blended paste with different supplementary material were studied experimentally and numerically. From the measurement results, it was found that the addition of fly ash would lead to smaller autogenous shrinkage compared with that of ordinary Portland cement paste with same water-binder ratio. The low activity of fly ash is considered to be the major reason. The low activity of fly ash leads to slower hydration rate and results in a slower decrease of the internal relative humidity and smaller shrinkage at early age. The measured autogenous shrinkage of BFS cement paste is much greater than that of Portland cement paste with same water-binder ratio. This is due to two factors: lower elastic modulus of BFS cement paste and the larger drop of internal relative humidity of BFS cement paste. Autogenous shrinkages of cement pastes with different supplementary materials were predicted by using the proposed simulation model. From the comparison between the measured and simulated autogenous shrinkage, it was concluded that creep plays an important role in autogenous shrinkage of hydrating cement paste and should be taken into consideration.

Finally, the autogenous shrinkages of cement mortars was studied experimentally and numerically. Pickett's model was extended to take the effect of creep into consideration. The autogenous shrinkage of cement mortars was calculated by using the extended Pickett's model. The calculated autogenous shrinkage was compared with the measurement results to evaluate the accuracy of the predictions with the extended Pickett's model. The extended Pickett's model was also used to predict the early-age autogenous shrinkage of OPC concrete and BFS concrete with high aggregate content.

# Samenvatting

Beton is een broos composietmateriaal dat gemakkelijk breekt onder spanning. Vanwege het feit dat de vervorming in vroege leeftijd van het beton onderdeel wordt beperkt door aangrenzende constructies, kan scheuren optreden door het beton voorafgaand aan het aanbrengen van een willekeurige belasting. De scheuren zouden preferentiële toegang verschaffen voor agressieve middelen die in het beton doordringen en vervolgens corrosie van de versterking en degradatie van beton veroorzaken. Dientengevolge, zou de levensduur van betonstructuur worden verminderd.

Er zijn veel verschillende typen vervormingen van vroege leeftijd van beton, b.v. temperatuur-geïnduceerde spanning, drogingskrimp en autogene krimp. Onder deze typen vervormingen van jonge leeftijd is autogene krimp een gevolg van de zelfverdroging tijdens het cementhydratatieproces. Lange tijd werd autogene krimp verwaarloosbaar geacht in vergelijking met droogkrimp. In de afgelopen jaren heeft autogene krimp steeds meer aandacht gekregen vanwege het toenemende gebruik van beton met lage water-bindmiddelverhoudingen. Ondanks het feit dat fenomeen van autogene krimp al tientallen jaren wordt erkend, is het mechanisme erachter nog steeds niet volledig begrepen en is er nog geen consensus bereikt. Drie is een algemene overeenkomst over het bestaan van een verband tussen autogene vervorming en relatieve vochtigheidsverandering in de capillaire poriën van de verhardende cementpasta. Op basis van deze relatie zijn veel simulatiemodellen gebouwd om de ontwikkeling van autogene krimp te voorspellen. De betrouwbaarheid van deze voorspellingen is echter niet altijd bevredigend. De discrepantie tussen de gemeten en berekende autogene vervorming wordt op latere leeftijd zeer uitgesproken. In die simulatiemodellen werd cementpasta beschouwd als een elastisch materiaal en alleen het elastische deel van autogene krimp werd voorspeld. In feite is cementpasta geen ideaal elastisch materiaal. Wanneer een cementpasta aan een aanhoudende belasting wordt onderworpen, zal deze elastisch vervormen en met de tijd verder vervormen, welk proces bekend staat als kruip. Creep speelt een belangrijke rol bij autogene krimp van hydraterende cementpasta. De onwetendheid van kruip zou leiden tot een onderschatting van de autogene krimp.

Het doel van dit project is om de autogene krimp van Portland cementpasta's en gemengde pasta's met aanvullende materialen te bestuderen. De autogene krimp moet uit twee delen bestaan, een elastisch deel en een tijdsafhankelijk deel (kruip), die afzonderlijk worden gesimuleerd. Op basis van de autogene krimp van cementpasta's, werd autogene krimp van cementmortels en -beton gesimuleerd door rekening te houden met het beperkende effect van starre zand / aggregaatdeeltjes.

Eerst werden de mechanismen achter de autogene vervorming besproken. De ontkoppelingsdruk en capillaire spanning van cementpasta werden numeriek gekwantificeerd. De rollen van het uiteenvallen van druk en capillaire spanning op de autogene krimp werden besproken. Er werd gevonden dat de ontkoppelingsdruk en capillaire spanning twee mechanismen zijn voor autogene vervorming van hydraterende cementpasta in een vroeg stadium. De ontkoppeling druk is afstotelijk en zou meer aandacht moeten krijgen bij het bestuderen van de vroege swelling van hydraterende cementpasta. Ondertussen is de capillaire spanning aantrekkelijk en neemt toe met de afname van de interne relatieve vochtigheid. Voor cementcement dat op jonge leeftijd is

gehard in gesloten toestand, daalt de relatieve vochtigheid niet onder 75%. Capillaire spanning speelt een dominante rol in dit bereik.

Ten tweede werd een simulatiemodel voor autogene krimp van cementpasta voorgesteld. In dit model wordt Capillaire spanning beschouwd als de belangrijkste drijvende kracht van autogene krimp. De autogene krimp moet uit twee delen bestaan, een elastisch deel en een tijdafhankelijk deel (kruip). Het elastische deel wordt berekend volgens de wet van Hooke. Het tijdsafhankelijke deel (kruip) van dit model is gebaseerd op de activering energietheorie en uitgebreid om de continu veranderende fysieke eigenschappen van de verhardende cementpasta te verwerken.

Ten derde werden, om gegevens te verschaffen voor modellering van de autogene krimp, eigenschappen van vroege leeftijd van cementpasta experimenteel onderzocht. De tijdsduur, interne relatieve vochtigheid, niet-verdampbaar watergehalte, chemische krimp en druksterkte van cementpasta werden gemeten. Portland cementpasta en drie soorten gemengde pasta met verschillend aanvullend materiaal, d.w.z. silicadamp, vliegas en hoogovenslakken, werden bestudeerd. Water-bindmiddelverhoudingen van deze cementpasta zijn 0.3 en 0.4.

Vervolgens werden de autogene krimp van Portland cementpasta en drie soorten gemengde pasta met verschillend aanvullend materiaal experimenteel en numeriek bestudeerd. Uit de meetresultaten bleek dat de toevoeging van vliegas zou leiden tot kleinere autogene krimp in vergelijking met die van gewone Portland-cementpasta met dezelfde water-bindmiddelverhouding. De lage activiteit van vliegas wordt als de belangrijkste reden beschouwd. De lage activiteit van vliegas leidt tot een langzamere hydratatiesnelheid en resulteert in een langzamere afname van de interne relatieve vochtigheid en kleinere krimp op jonge leeftijd. De gemeten autogene krimp van BFS-cementpasta is veel groter dan die van Portland-cementpasta met dezelfde water-bindmiddelverhouding. Dit komt door twee factoren: lagere elasticiteitsmodulus van BFS-cementpasta en de grotere daling van de interne relatieve vochtigheid van BFS-cementpasta. Autogene krimp van cementpasta's met verschillende aanvullende materialen werd voorspeld door het voorgestelde simulatiemodel te gebruiken. Uit de vergelijking tussen de gemeten en gesimuleerde autogene krimp, werd geconcludeerd dat kruip een belangrijke rol speelt bij autogene krimp van hydraterende cementpasta en dat hiermee rekening moet worden gehouden.

Ten slotte werd de autogene krimp van cementmortieren experimenteel en numeriek bestudeerd. Het model van Pickett werd uitgebreid om het effect van kruip in overweging te nemen. De autogene krimp van cementmortels werd berekend met behulp van het uitgebreide Pickett-model. De berekende autogene krimp werd vergeleken met de meetresultaten om de nauwkeurigheid van de voorspellingen met het uitgebreide Pickett-model te evalueren. Het uitgebreide Pickett-model werd ook gebruikt om de autogene krimp in de vroege leeftijd van OPC-beton en BFS-beton met een hoog totaalgehalte te voorspellen.

# Appendix

## Theoretical basis of Activation energy concept

In the activation energy concept, each solid particle of cement is fixed to its position. In order to change the position of a solid particle, a certain amount of energy is needed, which is called activation energy. During the creep process, many solid particles move. All the energy needed for changing the positions of these solid particles is called the activation energy of creep.

If cement paste specimen is under uni-axial load, the volume and shape of the specimen will change. The deformation of cement paste specimen includes two parts, elastic and time-dependent part. For the creep part, the work  $W$  [J], done during creep of a cement paste specimen is made up of an elastic component  $W_{el}$  [J] and a frictional component  $W_f$  [J] (Klug et al. 1969):

$$W = Fx = W_{el} + W_f \quad (A.1)$$

where  $F$  [N] is the load and  $x$  [m] is the deformation.

The elastic component  $W_{el}$  is given by

$$W_{el} = ql \int_0^\varepsilon \sigma d\varepsilon \quad (A.2)$$

With Hooke's Law,  $\sigma = E\varepsilon$ , Equation A.2 becomes

$$W_{el} = ql \int_0^\varepsilon E\varepsilon d\varepsilon = qlE \frac{\varepsilon^2}{2} = ql \frac{E x^2}{2 l^2} = \frac{qE}{2l} x^2 \quad (A.3)$$

where  $q$  [m<sup>2</sup>] and  $l$  [m] are the cross-section and length of the sample respectively.  $E$  [MPa] is the elastic modulus.

Assuming the frictional component to be proportional to  $\dot{x}$  and taking into consideration that it is also proportional to the number of points of contact in the cement gel and thus to the amount of hydrated cement  $\alpha N$  [ $N$  equals the initial volume of cement per unit volume and  $\alpha$  is the degree of hydration], then (Klug et al. 1969):

$$W_f = R_p \alpha N x \dot{x} \quad (A.4)$$

where  $R_p$  [N/m] is a parameter of proportionality. The value of  $R_p$  does not remain constant during the creep process, but increases with increasing deformation. According to Wittmann (1966 & 1968),  $R_p$  can be written in form of activation energy as:

$$R_p = \frac{q\sigma}{\omega \sinh(\eta\sigma) l N \alpha} \exp\left(\frac{Q(t)}{RT}\right) \quad (\text{A.5})$$

where  $Q$  [J] is the activation energy of the cement paste;  $\omega$  [-] and  $\eta$  [m<sup>2</sup>/N] are structure dependent parameters and constant for a given material (Hirst et al. 1977);  $R$  [J/(mol · K)] the universal gas constant and  $T$  [K] the absolute temperature.

Inserting Equation A.3 and Equation A.4 in Equation A.1 gives:

$$F\dot{x} = \frac{qE}{2l} x^2 + R_p \alpha N x \dot{x} \quad (\text{A.6})$$

If we solve this equation, the time-dependent deformation of the cement paste specimen  $x$  is obtained (Wittmann et al. 1968):

$$x(t) = \frac{2Fl}{qE} (1 - \exp(-\frac{qE}{2lR_p N \alpha} t)) \quad (\text{A.7})$$

The time-dependent strain of the cement paste specimen can be written as (Wittmann et al. 1968):

$$\varepsilon_{cr}(t) = \frac{2\sigma}{E} (1 - \exp(-\frac{qE}{2lR_p N \alpha} t)) \quad (\text{A.8})$$

Combining Equation A.5 and Equation A.8, we obtain:

$$\varepsilon_{cr}(t) = \frac{2\sigma}{E} (1 - \exp(-\frac{\omega \sinh(\eta\sigma) E}{2\sigma \exp(\frac{Q(t)}{RT})} t)) \quad (\text{A.9})$$

According to Klug and Wittmann (1974), for normal condition, there is no big difference between the value of  $\sinh(\eta\sigma)$  and  $\eta\sigma$ . In that case, Equation A.9 can be simplified by replacing  $\sinh(\eta\sigma)$  with  $\eta\sigma$ .

$$\varepsilon_{cr}(t) = \frac{2\sigma}{E} (1 - \exp(-\frac{\omega \eta \sigma E}{2\sigma \exp(\frac{Q(t)}{RT})} t)) \quad (\text{A.10})$$

Based on the Equation A.9 and A.10, the increasing rate of creep can be written as (Wittmann et al. 1968):

$$\dot{\varepsilon}_{cr}(t) = \omega \sinh(\eta\sigma) \exp(-\frac{Q(t)}{RT}) \quad (\text{A.11})$$

and

$$\dot{\varepsilon}_{cr}(t) = \omega \eta \sigma \exp(-\frac{Q(t)}{RT}) \quad (\text{A.12})$$

# References

- Abdellatef M., Alnaggar M., Boumakis G., Cusatis G., Di-Luzio G. & Wendner R., 2015. Lattice discrete particle modeling for coupled concrete creep and shrinkage using the solidification microprestress theory. In CONCREEP 10. pp. 184-193.
- ACI Committee 363, 1984. State-of-the-Art Report on High-Strength Concrete, ACI JOURNAL, Proceedings V. 81, No. 4, July-Aug. 1984, pp. 364-411.
- Alam M.M., Borre M.K., Fabricius I. L., Hedegaard K., Røgen B., Hossain Z. & Krogsbøll A.S., 2010. Biot's coefficient as an indicator of strength and porosity reduction: Calcareous sediments from Kerguelen Plateau. Journal of Petroleum Science and Engineering, 70(3-4), pp. 282-297.
- Altoubat S.A. & Lange D.A., 2001. Creep, shrinkage and cracking of restrained concrete at early age. Urbana 51: 61801.
- Akçay B., 2007. Effects of lightweight aggregates on autogenous deformation and fracture of high performance concrete, Ph.D. thesis, İstanbul technical university, Turkey.
- Architectural Institute of Japan, 1985. Standard for Structural Calculation of Reinforced Concrete Structures, Chapter 2, AIJ, pp. 8-11.
- Badmann R., Stockhausen N. & Setzer M.J., 1981. The Statistical Thickness and the Chemical Potential of Adsorbed Water Films, Journal of Colloid and Interface Science, 82(2), pp. 534-42.
- Baron J., 1982. Les retraits de la pâte de ciment, Le beton hydraulique, Chap.27, pp. 485-501.
- Bazant Z.P. & Wittmann F.H., 1982. Creep and shrinkage in concrete structures, pp. 12-16.
- Bazant Z.P. & Chern J. C., 1984. Double-power logarithmic law for concrete creep, Cem. Concr. Res. 14, pp. 793-806.
- Bazant Z.P. & Chern J. C., 1985. Log double power law for concrete creep, ACI J. 82, pp. 665-675.
- Bazant Z.P. & Prasannan S., 1989. Solidification theory for concrete creep. I: Formulation. Journal of engineering mechanics, 115(8), pp. 1691-1703.
- Beaudoin J.J., Ramachandran V.S. & Feldman R.F., 1991. Identification of Hydration Reactions through Stress Induced by Volume Change – Part I: C3A System, Cem. Concr. Res., Vol 21, No. 5, pp. 809-818.
- Beltzung F., Wittmann F.H. & Holzer L., 2001. Influence of composition of pore solution on drying shrinkage, Proc. 6th Int. Conf. Creep, Shrinkage and Durability Mechanics of Concrete and Other Quasi-Brittle materials, eds. F.-J. Ulm, Z.P. Bazant & F.H. Wittmann, Cambridge, MA, August 20-22, Elsevier Science Ltd, pp. 39-48.
- Beltzung F. & Wittmann F. H., 2005. Role of disjoining pressure in cement based materials, Cem. Concr. Res. 35. pp. 2364-2370.
- Bentur A., Berger R.L., Kung J.H., Milestone N.B. & Young J.F., 1979. Structural Properties of Calcium Silicate Pastes: II, Effect of Curing Temperature, J Amer Ceram Soc 62(7-8) , pp. 362-366.

- Bentur A., 2002. Terminology and definitions, in: K. Kovler, A. Bentur (Eds.). International RILEM Conference on Early Age Cracking in Cementitious Systems—EAC, RILEM TC181-EAS, Haifa 2002, pp. 13–20.
- Bentur A., 2003. Terminology and Definitions, RILEM Report 25, Early Age Cracking in Cementitious Systems, Edited by A. Bentur, RILEM Publications S.A.R.L., Cachan, France, pp. 13-15.
- Bentz D.P., Garboczi E.J. & Quenard D.A., 1998. Modelling drying shrinkage in reconstructed porous materials: application to porous Vycor glass. *Modelling and Simulation in Materials Science and Engineering*, 6(3), pp. 211-236.
- Bentz D.P., Jensen O.M., Hansen K.K., Olesen J.F., Stang H. & Haecker C.J., 2001. Influence of Cement Particle - Size Distribution on Early Age Autogenous Strains and Stresses in Cement - Based Materials. *Journal of the American Ceramic Society*, 84(1), pp. 129-135.
- Bentz D.P., Geiker M.R. & Hansen K.K., 2001. Shrinkage-reducing admixtures and early-age desiccation in cement pastes and mortars, *Cem Concr Res* 31(7), pp. 1075-1085.
- Bentz D.P. & Jensen O.M., 2004. Mitigation strategies for autogenous shrinkage cracking, *Cement and Concrete Composites*, 26, pp. 677-685.
- Bentz D.P., Chiara F.F. & Kenneth A.S., 2013. Best practices guide for high-volume fly ash concretes: Assuring properties and performance. No. Technical Note (NIST TN)-1812.
- Berg W.V. & Kukko H., 1991. Fly ash in concrete, Taylor and Francis, London.
- Bergström L., 1997. Hamaker constants of inorganic materials. *Advances in colloid and interface science* 70. pp. 125-169.
- Berodier E.M.J., 2015. Impact of the Supplementary Cementitious Materials on the kinetics and microstructural development of cement hydration, Thesis(PhD). École Polytechnique Fédérale de Lausanne.
- Bijen J., 1996. Benefits of slag and fly ash. *Construction and Building Materials*, 1996; 10(5), pp. 309-314.
- Bjøntegaard Ø., 1999. Thermal dilatation and autogenous deformation as driving forces to self-induced stresses in high performance concrete, Ph.D. Thesis, Division of structural Engineering, The Norwegian University of Science and Technology, Norway.
- Breugel K. van, 1980. Artificial cooling of hardening concrete. Report Stevin Laboratory, Concrete Structures 5-80-9 .
- Breugel K. van, 1980. Relaxation of young concrete. Delft University of Technology, Research report concrete structures, 5-80.
- Breugel K. van, 1982. Proc. Int. RILEM Conf. on Concrete at Early Ages. 1. pp. 179-185.
- Breugel K. van, 1991. Simulation of hydration and formation of structure in hardening cement-based materials, Ph.D. thesis, Delft University of Technology, Delft, The Netherlands.
- Budnikov P.P. & Strelkov M.I., 1966. Some recent concepts on Portland cement hydration and hardening, Proc. Symp. on Structure of Portland cement paste and concrete, ACI Special report 90, pp. 447-464.
- Buil M., 1979. Contribution à l'étude du retrait de la pâte Studies of the shrinkage of hardening cement paste (in French), Ph.D. thesis, Rapport de recherche LPC No. 92, Laboratoire Central des Ponts et Chaussées, Paris, France.



- Butt H.J. & Kappl M., 2009. Normal capillary forces, *Advances in Colloid and Interface Science* 146, pp. 48-60.
- Chan Y.W., Liu C.Y. & Lu Y.S., 1999. Effects of slag and fly ash on the autogenous shrinkage of high-performance concrete, in *Proceedings of International Workshop Autoshrink'98*, Ed. Tazawa, E-I., Hiroshima, Japan, E&FN SPON, London, 13-14 June, pp. 221-228.
- Charpin L. & Ehlacher A., 2012. A computational linear elastic fracture mechanics-based model for alkali-silica reaction. *Cement and Concrete Research*, 2012, 42(4), pp. 613-625.
- Chatelier H. Le, 1900. Sur les changements de volume qui accompagnent le durcissement des ciments, *Bull. Soc. Encour. Ind. Natl. V*, 5th series, pp. 54-57.
- Churaev N.V., 1985. Inclusion of structural forces in the theory of stability of colloids and films, *Journal of colloid and interface science*, 103(2), pp. 542-553.
- Coutinho & Sousa A., 1977. A contribution to the mechanism of concrete creep. *Matériaux et Construction*, Vol. 10, No. 55, pp. 3-16.
- Criado M. & Jimenez A. F., 2007. An XRD study of the effect of the SiO<sub>2</sub>/Na<sub>2</sub>O ratio on the alkali activation of fly ash, *Cement and Concrete Research*, 37(5), pp. 671-679.
- Darquennes A., Staquet S. & Espion B., 2011. Behavior of slag cement concrete under restraint conditions, *European Journal of Environmental and Civil Engineering*, 15(5), pp. 787-798.
- Darquennes A., Staquet S., Delplancke-Ogletree M.P. & Espion B., 2011. Effect of autogenous deformation on the cracking risk of slag cement concretes. *Cement and Concrete Composites*, 33(3), pp. 368-379.
- David R.L., 1985. *CRC Handbook of Chemistry and Physics* (85 ed.). CRC Press, pp. 15-25.
- Day R.L. & Gamble B.R., 1983. The effect of changes in structure on the activation energy for the creep of concrete. *Cement and Concrete Research*, 13(4), pp. 529-540.
- Defay R. & Prigogine I., 1966. *Surface Tension and Adsorption*. Longmans, Green & Co Ltd, London.
- Dela B.F., 2000. *Eigenstresses in hardening concrete*, Ph.D. thesis. Department of Structural Engineering and Materials, The Technical University of Denmark, Lyngby, Denmark.
- Derjaguin B.V., Churaev N.V. & Muller V.M., 1987. *Surface forces*, Plenum Press, New York.
- Diamond S. & Sahu S., 2006. Densified silica fume: particle sizes and dispersion in concrete, *Materials and Structures*, 39, pp. 849-859.
- Erhard M. & Philip C., 1972. Crystallization pressure of salts in stone and concrete, *Geological society of America Bulletin*, Vol.40, pp. 3509-3513.
- Ekaputri J.J., Maekawa K. & Ishida T., 2016. Experimental Study on Internal RH of BFS Mortars at Early Age. *Materials Science Forum*. Vol. 857. Trans Tech Publications.
- Fang Y.H., Gu Y.M. & Kang Q.B., 2011. Effect of Fly Ash, MgO and Curing Solution on the Chemical Shrinkage of Alkali-Activated Slag Cement, *Advanced Materials Research*, Vols. 168-170, pp. 2008-2012.
- Ferraris C. & Wittmann F.H., 1987. Shrinkage mechanisms of hardened cement paste, *Cem Concr Res* 17(3), pp. 453-464.
- Feylessoufi A., Tenoudji F.C., Marin V. & Richard P., 2001. Early ages shrinkage mechanisms of ultra-high-performance cement based materials, *Cement and Concrete Research*, 31, pp. 1573-1579.

- Fraay A.L.A., Bijen J.M. & de Haan Y.M., 1989. The reaction of fly-ash in concrete-a critical-examination. *Cement and Concrete Research*, 1989; 19, pp. 235-246.
- Fraay A.L.A., 1990. Fly ash a pozzolan in concrete. PhD thesis, Delft University of Technology.
- Gangé R., Aouad I., Shen J. & Poulin C., 1999. Development of a New Experimental Technique for the Study of the Autogenous Shrinkage of Cement Paste, *Materials and Structures*, Vol. 32, pp. 635 - 642.
- Garcia Boivin S., 2001. Retrait au jeune âge du béton - Développement d'une méthode expérimentale et contribution à l'analyse physique du retrait endogène (in French), Ph.D thesis, Etudes et Recherches des LPC, OA 37, Paris, France.
- Gardner N.J. & Poon S.M., 1976. Time and temperature effects on tensile, bond, and compressive strengths. In *Journal Proceedings*, Vol. 73, No. 7, pp. 405-409.
- Gawin D., Pesavento F. & Schrefler B.A., 2006. Hygro-thermo-chemo-mechanical modelling of concrete at early ages and beyond. Part II: shrinkage and creep of concrete, *Int. J. Numer. Methods Eng.* 67, pp. 332–363.
- Gawin D., Pesavento F. & Schrefler B.A., 2007. Modelling creep and shrinkage of concrete by means of effective stresses, *Mater Struct* 40, pp. 579-59.
- Gibbs J.W., 1957. *Collect works*, New Haven, Yale University Press.
- Gilbert R.I., 1988. Time effects in concrete structures. Series: *Developments in civil engineering* 23, Elsevier.
- Glasstone S., 1941. Statistical treatment of reaction rates. *The theory of rate processes*.
- Gleize P.J.P., Muller A. & Roman H.R., 2003. Microstructural investigation of a silica fume–cement–lime mortar, *Cement & Concrete Composites*, 25, pp. 171–175.
- Goltermann P., 1994. Mechanical predictions on concrete deterioration. Part 1: eigenstresses in concrete, *ACI Mater J* 91(6), pp. 543-550.
- Grasely Z.C., Lange D.A., Brinks A.J. & D'Ambrosia, 2005. Modeling of Autogenous Shrinkage of Concrete Accounting for Creep Caused by Aggregate Restraint, Self-desiccation and its Importance in Concrete Technology, *Proceedings of the Fourth International Research Seminar*, Gaithersburg, USA, June, pp. 1-20.
- Grasley Z.C., 2006. Measuring and Modeling the Time-Dependent Response of Cementitious Materials to Internal Stresses, PhD thesis, Virginia Polytechnic Institute and State University
- Gray W.G. & Schrefler B.A., 2001. Thermodynamic approach to effective stress in partially saturated porous media, *Eur J Mech A/Solids* 20, pp. 521–538.
- Gruyaert E., 2011. Effect of blast-furnace slag as cement replacement on hydration, microstructure, strength and durability of concrete. PhD thesis. Ghent University.
- Hagymassy J., Brunauer J.R. & Mikhail R.S., 1969. Pore structure analysis by water vapor adsorption, *Journal of Colloid and Interface Science* 29(3), pp. 485-491.
- Hammer T.A., Bjøntegaard Ø. & Sellevold E.J., 2002. Internal curing – Role of Absorbed Water in Aggregates, Presented at ACI Fall 2002 Convention, Session High-Performance Structural Lightweight Concrete, Phoenix, AZ.

- Hanehara S., Hirao H. & Uchikawa H., 1999. Relationship between autogenous shrinkage and the microstructure and humidity changes at inner part of hardened cement pastes at early ages, Proc. Int. Workshop Autoshrink'98, ed. E.-I. Tazawa, Hiroshima, Japan, E & FN SPON, London, pp. 89-100.
- Hansen T.C. & Nielsen K.E.C., 1965. Influence of aggregate properties on concrete shrinkage, ACI Journal 62(7), pp. 783-794.
- Hansen P. & Pedersen E., 1977. Maleinstrument til Kontrol of Betons Haerdning, Nordisk Betong (1), pp. 21-25.
- Helmholtz R. von, 1886. Untersuchungen über Dämpfe und Nebel, besonders über solche von Lösungen. Annalen der Physik 263.4. pp. 508-543.
- L'Hermite R., 1960. Volume Changes of Concrete, Proceedings of fourth international symposium on the chemistry of cement, Washington, DC, pp. 659-694.
- Hirst G.A. & Neville A.M., 1977. Activation energy of creep of concrete under short-term static and cyclic stresses. Magazine of Concrete Research, 29(98), pp. 13-18.
- Hobbs D.W., 1969. Bulk Modulus Shrinkage and Thermal Expansion of a Two Phase Material, Nature 222, pp. 849-851.
- Hobbs D.W., 1974. Influence of aggregate restraint on the shrinkage of concrete, ACI Journal 71, pp. 445-450.
- Holt E., 2000. Where Did These Cracks Come From?, Concrete International, Vol.22, No. 9, pp. 57 - 60.
- Holt E., 2001. Early age autogenous shrinkage of concrete, Julkaisija Utgivare Publisher.
- Holt E., 2002. Very Early Age Autogenous Shrinkage: Governed by Chemical Shrinkage or Self-desiccation, the Proceedings of the Third International Research Seminary in Lund, pp. 1-26.
- Houssam A.T. & Tahar E.K., 1995. The influence of silica fume on the compressive strength of cement paste and mortar, Cement and Concrete Research, 25(7), pp. 1591-1602.
- Hu Z., 2017. Prediction of autogenous shrinkage in fly ash blended cement systems, PhD thesis, École polytechnique fédérale de Lausanne.
- Hua C., Acker P. & Erlacher A., 1995. Analyses and models of the autogenous shrinkage of hardening cement paste: I. Modelling at macroscopic scale, Cem Concr Res 25(7), pp. 1457-1468.
- Huang C.Y. & Feldman R.F., 1985. Hydration reactions in Portland cement-silica fume blends. Cement and Concrete Research , 15(4), pp. 585-592.
- Ishida T., Luan Y. & Sagawa T., 2011. Modeling of early age behavior of blast furnace slag concrete based on micro-physical properties. Cement and Concrete Research 41.12 (2011), pp. 1357-1367.
- Japan Concrete Institute Committee on Autogenous Shrinkage, 1999. Report on Autogenous Shrinkage of Concrete, Proc. Int. Workshop Autoshrink '98, ed. E.-I. Tazawa, Hiroshima, Japan, E & FN SPON, London, pp. 1-67.
- Jacob N.I., 2011. Intermolecular and surfaces forces, 3rd Edn, Elsevier.
- Jennings H.M., 2004. Colloid model of C-S-H and implications to the problem of creep and shrinkage, Materials and Structure, pp. 59-70.

- Jensen O.M., 1993. Autogenous deformation and RH-change – self-desiccation and self-desiccation shrinkage (in Danish), TR 284/93, Building Materials Laboratory, The Technical University of Denmark, Lyngby, Denmark.
- Jensen O.M., 1995. Thermodynamic limitation of self-desiccation, *Cem Concr Res*, 25(1), pp. 157-164.
- Jensen O.M. & Hansen P.F., 1996. Autogenous deformation and change of the relative humidity in silica fume-modified cement paste, *ACI Materials Journal* 93 (6), pp. 539-543.
- Jensen O.M., 2000. Influence of cement composition on autogenous deformation and change of the relative humidity. *Proc. Shrinkage*, pp. 143-153.
- Jensen O.M. & Hansen P.F., 2001a. Water-entrained cement-based materials. I. Principles and theoretical background, *Cem Concr Res* 31(5), pp. 647-654.
- Jensen O.M. & Hansen P.F., 2001b. Autogenous Deformation and RH-Change in Perspective, *Cement and Concrete Research*, vol. 31, pp. 1859-1865.
- Jones R.M., 2009. Deformation theory of plasticity. Bull Ridge Corporation.
- Jönsson B., Wennerström H., Nonat A. & Cabane B., 2004. Onset of cohesion in cement paste, ACS Publications, pp. 6702–6709.
- Khan M.I., Lynsdale C.J. & Waldron P., 2000. Porosity and strength of PFA/SF/OPC ternary blended paste, *Cem Concr Res* 30(8), pp. 1225-1229.
- Klug P. & Wittmann F., 1969. Activation energy of creep of hardened cement paste. *Matériaux et Construction* 2.1, pp. 11-16.
- Klug P. & Wittmann F., 1974. Activation energy and activation volume of creep of hardened cement paste. *Materials science and Engineering*, 15(1), pp. 63-66.
- Koenders E.A.B., 1997. Simulation of volume changes in hardening cement-based materials. Thesis(PhD). Delft University of Technology.
- Kovler K. & Cusson D., 2007. Effects of internal curing on autogenous deformation. Internal Curing of Concrete-State-of-the-Art Report of RILEM Technical Committee 196-ICC, pp. 71-104.
- Lam L., Wong Y.L. & Poon C.S., 2000. Degree of hydration and gel/space ratio of high-volume fly ash/cement systems, *Cement and Concrete Research*, 30, pp. 747-756.
- Lange D. A., 2016. Do Concrete Materials Specifications Address Real Performance? University of Illinois at Urbana-Champaign.
- Lebental B., Moujahid W., Lee C.S., Maurice J.L. & Cojocaru C.S., 2012. Graphene-based resistive humidity sensor for in-situ monitoring of drying shrinkage and intrinsic permeability in concrete, NICOM 4: 4th International Symposium on Nanotechnology in Construction, May 2012, France.
- Lee K.M., Lee H.K., Lee S.H. & Kim G.Y., 2006. Autogenous shrinkage of concrete containing granulated blast-furnace slag, *Cement and Concrete Research*, 36 (7), pp. 1279-1285.
- Li Y., Langan B.W. & Ward M.A., 1996. The strength and microstructure of high-strength paste containing silica fume, *Cem Concr Aggr* 18(2), pp. 112-117.
- Lokhorst S.J. & Breugel K.van, 1997. Simulation of the effect of geometrical changes of the microstructure on the deformational behaviour of hardening concrete. *Cement and concrete research* 27.10, pp. 1465-1479.

- Lokhorst S.J., 1998. Deformational behaviour of concrete influenced by hydration related changes of the microstructure. University of Techn., Fac. of Civil Engineering, Concrete Structures.
- Lura P., 2003. Autogenous deformation and internal curing of concrete. Thesis(PhD). Delft University of Technology.
- Lynam C.G., 1934. Growth and Movement in Portland Cement Concrete, Oxford Univ. Press, London, pp. 26–27.
- Malhotra V. M., 1999. Making concrete greener with fly ash, *Concrete International*, 1999; 21(5), pp. 61-66.
- Malhotra V. M. & Mehta P.K., 2002. High-performance, high-volume fly ash concrete. Supplementary Cementing Materials for Sustainable Development, Inc., Ottawa, Canada, pp. 101.
- Maruyama I., Kameta S., Suzuki M. & Sato R., 2006. Cracking of high strength concrete around deformed reinforcing bar due to shrinkage. In Int. RILEM-JCI Seminar on Concrete Durability and Service Life Planning (pp. 104-111). RILEM Publications SAR L Ein-Bokek, Israel.
- Maruyama I. & Ai S., 2014. Numerical study on drying shrinkage of concrete affected by aggregate size. *Journal of Advanced Concrete Technology*. 12.8. pp. 279-288.
- Mazur P., 1963. Kinetics of water loss from cells at subzero temperatures and the likelihood of intracellular freezing. *The Journal of general physiology* 47.2, pp. 347-369.
- Miao C.W., Tian Q., Sun W. & Liu J.P., 2007. Water consumption of the early-age paste and the determination of “time-zero” of self-desiccation shrinkage, *Cem. Concr. Res.* 37. pp. 1496-1501.
- Mindess S. & Young J.F., 1981. *Concrete*, Prentice-hall, Englewood Cliffs.
- Moon J.H., Rajabipour F., Pease B. & Weiss J., 2005. Autogenous Shrinkage, Residual Stress, and Cracking in Cementitious Composites: the Influence of Internal and External Restraint, Self-desiccation and its Importance in Concrete Technology, Proceedings of the Fourth International Research Seminar, Gaithersburg, USA, June, pp. 1-20.
- Mors R.M., 2011. Autogenous Shrinkage of Cementitious materials containing BFS, Master thesis, Delft University of Technology.
- Müller H.S., Küttner C.H. & Kvitsel V., 1999. Creep and shrinkage models of normal and high-performance concrete concept for a unified code-type approach, ACI-RILEM Workshop on Creep and Shrinkage of Concrete Structures, Paris , FRANCE, pp. 113-132.
- Naghdi R., 2010. Evaluation of Autogenous Shrinkage of High-Performance Concrete, Third International Conference on Sustainable Construction Materials and Technologies, Kyoto, Japan.
- Neville H.A. & Jones H.C., 1928. The study of hydration changes by a volume-change method, *Colloid Symp. Monogr.* VI, pp. 309–318.
- Neville A.M., Dilger W.H. & Brooks J.J., 1983. *Creep of Plain and Structural Concrete*. Construction Press.
- Neville A.M., 1995. *Properties of concrete*, John Wiley & Sons, New York (4th edition).
- Nielsen L.F., 1991. A research note on sorption, pore size distribution, and shrinkage of porous materials, TR 245/91, Building Materials Laboratory, The Technical University of Denmark, Lyngby, Denmark.
- Page C.L. & Vennesland Ø., 1983. Pore solution composition and chloride binding capacity of silica-fume cement pastes, *Mater Struct* 16(91), pp. 19-25.

- Paillere A.M., Buil M. & Serrano J.J., 1989. Effect of Fiber Addition on the Autogenous Shrinkage of Silica Fume Concrete, *ACI Mater. J.* 86(2), pp. 139-144.
- Park K.B., Noguchi T. & Tomosawa F., 1999. A STUDY ON THE HYDRATION RATIO AND AUTOGENOUS SHRINKAGE OF CEMENT PASTE. In *Autogenous shrinkage of concrete: proceedings of the international workshop, organised by JCI (Japan Concrete Institute), Hiroshima, June 13-14, 1998* (pp. 299). Taylor & Francis.
- Parrott L.J. & Geiker M., 1990. Monitoring Portland cement hydration: Comparison of methods. *Cement and Concrete Research*, 20(6), pp. 919-926.
- Perrot P., 1998. *A to Z of Thermodynamics*, Oxford University Press.
- Person B., 1999. Creep and shrinkage of young or mature HPC. In *Proc. 5th Int. Symp. on 'Utilization of high strength/high performance concrete'*, Sandefjord, pp. 1272-1281.
- Pickett G., 1956. Effect of aggregate on shrinkage of concrete and a hypothesis concerning shrinkage, *ACI Journal* 52(5). pp. 581-590.
- Powers T.C., Copeland L.E. & Mann H.M., 1959. Capillary continuity or discontinuity in cement pastes, *PCA Bulletin*, vol. 1 (110), pp. 2-12.
- Powers T.C. & Brownyard T. L., 1948. Studies of the physical properties of hardened Portland cement paste (9 parts), *J Amer Concr Inst* 43 (Oct. 1946 to April 1947), Bulletin 22, Research Laboratories of the Portland Cement Association, Chicago.
- Powers T.C., 1965. Mechanisms of shrinkage and reversible creep of hardening cement paste, in *Proc. Int. Symp. Structure of Concrete and its behaviour under load*, Cem. & Concr. Ass., London, pp. 319-344.
- Powers T.C., 1968. Session I: The Thermodynamics of Volume Change and Creep, *Materiaux et Constructions* 1, pp. 487-507.
- Rao G.A., 2003. Investigations on the performance of silica fume-incorporated cement pastes and mortars, *Cement and Concrete Research*, 33, pp. 1765-1770.
- Rilem report 38, 2007. *Durability of self-compacting concrete*. Edited by G. De Schutter and K. Audenaert. Rilem TC 205-DSC; State-of-the-Art Report. April 2007. ISBN: 978-2-35158-048-6.
- Roy D.M. & Idorn G.M., 1982. Hydration, Structure and properties of Blast Furnace Slag Cements, Mortars, and Concrete, *ACI Journal* 79(6), pp. 444-457.
- Sant G., Rajabipour F., Lura P. & Weiss J., 2006. Examining time-zero and early age expansion in pastes containing shrinkage reducing admixtures (SRA's). In *Proc., 2nd RILEM Symp. on Advances in Concrete through Science and Engineering*.
- Sato R., Tanaka S., Hayakawa T. & Tanimura M., 1999. Experimental studies on reduction of autogenous shrinkage and its induced stress in HSC, Self-Desiccation and Its Importance in Concrete Technology *Proceedings of the 2nd International Research Seminar in Lund*, 18 June, pp. 163-171.
- Scherer G., 2002. Factors affecting crystallization pressure, *International RILEM TC 186-ISA workshop on internal sulfate attack and delayed ettringite formation*, Villars, Switzerland.
- Scovazzo P. & Todd P., 2001. Modeling Disjoining Pressures in Submicrometer Liquid-Filled Cylindrical Geometries, *Journal of Colloid and Interface Science*, 238, pp. 230-237.
- Setzer M.J., 1977. Einfluss des Wassergehalts auf die Eigenschaften des erhärteten Betons (in German), *Deutscher Ausschuss für Stahlbeton* 280, pp. 43-79.

- Setzer M.J., 1996. The Munich model- An example for modern materials science in civil engineering, *Advances in building materials science*, pp. 3-16.
- Soboyejo W., 2002. *Mechanical Properties of Engineered Materials*, CRC Press.
- Soroka I., 1979. *Portland Cement Paste and Concrete*. The Macmillan Press Ltd., London.
- Steiger M., 2005. Crystal growth in porous materials-I: The crystallization pressure of large crystals, *Journal of crystal growth*, 282, pp. 455-469.
- Stock A.F., Hannant D.J. & Williams R.I.T., 1979. The effect of aggregate concentration upon the strength and modulus of elasticity of concrete. *Magazine of concrete research*, 31(109). pp. 225-234.
- Skempton A.W., 1961. Effective stress in soils, concrete and rocks, *Pore Pressure and Suction in Soils*, Butherworths, London, pp. 4-16.
- Sule M.S., 2003. *Effect of Reinforcement on Early-Age Cracking in High Strength Concrete*, Ph.D. Thesis, Delft University of Technology, Delft, The Netherlands.
- Takafumi N., Fuminori T., Nemati M.K., Bernardino M.C., & Alessandro P.F., 2009. A Practical Equation for Elastic Modulus of Concrete, *ACI Structural Journal*, V. 106, No. 5, Sept.-Oct. pp. 690-696.
- Tamtsia B.T., Beaudoin J.J. & Marchand J., 2004. The early age short-term creep of hardening cement paste: load-induced hydration effects, *Cem. Concr. Compos.* 26, pp. 481-489.
- Tangtermsirikul S., 1999. Effects of chemical composition and particle size of fly ash on autogenous shrinkage of paste, in *Proceedings of International Workshop Autoshrink'98*, Ed. Tazawa, E-I., Hiroshima, Japan, E&FN SPON, London, 13-14 June, pp. 175-186.
- Tao Z. & Qin W., 2006. Tensile creep due to restraining stresses in high-strength concrete at early ages. *Cement and Concrete Research* 36(3), pp. 584-591.
- Taylor H., 1992. *Cement chemistry*, Academic Press, London.
- Tazawa E., 1991. Macroscopic shrinkage of hardening cement paste due to hydration. *JCA Proceeding of Cement and Concrete*, 45, pp. 122-127.
- Tazawa E. & Miyazawa S., 1995. Influence of cement and admixture on autogenous shrinkage of cement paste, *Cem Concr, Res* 25 (2), pp. 281-287.
- Tazawa E., Miyazawa S. & Kasai T., 1995. Chemical Shrinkage and Autogenous Shrinkage of Hydrating Cement Paste, *Cement and Concrete Research*, Vol. 25 (2), pp. 288-292.
- Tazawa E., 1998. *Autogenous shrinkage of concrete*, E&F SPON, London and New York.
- Tazawa E., Sato R., Sakai E. & Miyazawa S., 2000. Work of JCI committee on autogenous shrinkage, *Proc. Shrinkage 2000 – Int. RILEM Workshop on Shrinkage of Concrete*, Paris, pp. 21-40.
- Tezuka Y., Djanikan J.G., Uchikawa H. & Uchida S., 1986. Hydration characteristics and properties of mixtures of cement and high content of calcium, *Proc. Symp. on Chemistry of Cement*, Rio de Janeiro, Brazil, Vol. II, pp. 323-329.
- Thomas J.J. & Jennings H.M., 2001. Chemical aging and the colloidal structure of the C-S-H gel: implications for creep and shrinkage, *Proc. 6th Int. Conf. Creep, Shrinkage and Durability Mechanics of Concrete and Other Quasi-Brittle materials*, eds. F.-J. Ulm, Z.P. Bazant & F.H. Wittmann, Cambridge, MA, August 20-22, Elsevier Science Ltd, pp. 33-38.

- Thomas J. J., Allen A. J. & Jennings H. M., 2012. Density and water content of nanoscale solid C–S–H formed in alkali-activated slag (AAS) paste and implications for chemical shrinkage, *Cement and Concrete Research*, 42, pp. 377–383.
- Tian Z. & Bian C., 2013. Numerical modeling of elastic modulus for cement paste using homogenization method. *Journal of Wuhan University of Technology. Materials Science Edition*, 28(4), pp. 751.
- Timoshenko S. & Goodier J. N., 1951. *Theory of elasticity*, 2nd Edition. McGraw-Hill Book Co., Inc., New York. pp. 359.
- Varga I.D.L., Castro J., Bentz D. & Weiss J., 2012. Application of internal curing for mixtures containing high volumes of fly ash, *Cement & Concrete Composites*, 34, pp. 1001-1008.
- Vargaftik N.B., Volkov B.N. & Voljak L.D., 1983. International tables of the surface tension of water. *Journal of Physical and Chemical Reference Data*, 12.3, pp.817-820.
- Wei Y., 2008. Modeling of autogenous deformation in cementitious materials, restraining effect from aggregate, and moisture warping in slabs on grade. Thesis(PhD). The University of Michigan.
- Wei Y., Hansen W., Biernacki J. J. & Schlangen E., 2011. Unified Shrinkage Model for Concrete from Autogenous Shrinkage Test on Paste with and without Ground-Granulated Blast-Furnace Slag, *ACI materials journal*, NO. 108-M02, pp. 12-20.
- Wei Y., Liang S. & Gao X., 2017. Simulation of Porosity Effect on Mechanical and Creep Properties of Cement Paste at Microscale. *Poromechanics VI*. pp. 1099-1107.
- Weiss J., 2003. Experimental Determination of the ‘Time Zero’ to (Maturity-Zero  $M_0$ ), RILEM Report 25, *Early Age Cracking in Cementitious Systems*, Edited by A. Bentur, RILEM Publications S.A.R.L., Cachan, France, pp. 195-206.
- Wittmann F.H., 1966. Kriechen bei gleichzeitigem Schwinden des Zementsteins, *Rheologica Acta* 5(3), pp. 198-204.
- Wittmann F.H., 1967. Kriechmessungen an Zementstein. *Rheologica Acta*, 6(4), pp. 303-306.
- Wittmann F.H., 1968. Surface Tension, Shrinkage and Strength of Hardened Cement Paste, *Materials & Structures*, 1(6), pp. 547–552.
- Wittmann F.H. & Klug P., 1968. Zum zeitlichen Verlauf des Kriechens von Zementstein und Beton, *Rheologica, Acta* 7(1), pp. 93-95.
- Wittmann F.H., 1971. Kriechverformung des Betons unter statischer und unter dynamischer Belastung. *Rheologica Acta*. 10(3), pp. 422-428.
- Wittmann F.H., 1976. The structure of hardened cement paste-a basis for a better understanding of the materials properties. *Proc. Hydraulic cement pastes: their structure and properties*, pp. 96-117.
- Wittmann F.H., 1977. Grundlagen eines Modells zur Beschreibung charakteristischer Eigenschaften des Beton, Ernst.
- Wittmann F.H., 1992. On the interaction of gel particles in hydrating Portland cement, *Hydration and Setting of Cements*, ed. A. Nonat & J.C. Mutin, RILEM, E&FN Spon, London.
- Wittmann F.H., 2009. Heresies on shrinkage and creep mechanisms. *Proceedings of Creep, Shrinkage and Durability Mechanics of Concrete and Concrete Structures*, London: Taylor and Francis Group, pp. 3-10.



- Xiao K.T., Yang H.Q. & Dong Y., 2009. Study on the influence of admixture on chemical shrinkage of cement based materials. In *Key Engineering Materials*. Trans Tech Publications. Vol. 405, pp. 226-233.
- Xiong H. & Liu M., 2005. FEM Analysis of the Creep and Shrinkage in CFST Arch Bridge. *Journal of Wuhan University of Technology*, 27(4), pp. 51-53.
- Xu X., Lohaus L. & Setzer M.J., 2001. Damping Behaviour of Hardened Cement Paste (hcp) in a Temperature Range between 20°C and 80°C: Effect of the Disjoining Pressure, *Proc. 6th Int. Conf. Creep, Shrinkage and Durability Mechanics of Concrete and Other Quasi-Brittle materials*, eds. F.-J. Ulm, Z.P. Bazant & F.H. Wittmann, Cambridge, MA, August 20-22, Elsevier Science Ltd, pp. 49-54.
- Zeng Q., Li K., Fen-Chong T. & Dangla P., 2012. Pore structure characterization of cement pastes blended with high-volume fly-ash. *Cement and Concrete Research*, 42(1), pp. 194-204.
- Zhang Y.M., Sun W. & Yan H.D., 2000. Hydration of high-volume fly ash cement pastes, *Cement & Concrete Composites*, 22, pp. 445-452.
- Zhang M., Tam C. & Leow M., 2003. Effect of water-to-cementitious materials ratio and silica fume on the autogenous shrinkage of concrete, *Cem. Concr. Res.* 33,(10). pp. 1687–1694.
- Zhu T.Y., 2012. Some Useful Numbers on the Engineering Properties of Materials (Geologic and Otherwise). GEOL 615, Department of Geophysics.



# Curriculum Vitae

## Tianshi Lu



Date of birth: 04 December, 1984

Place of birth: Cangzhou, P.R. China

**2011.09 ~ 2019. 05**

PhD candidate in TU Delft, Delft, The Netherlands

**2008.09 ~ 2011. 06**

Master study on Water Conservancy & Hydropower Engineering in Hogaï University,  
Nanjing, P.R. China

**2003.09 ~ 2007. 06**

Bachelor study on Water Conservancy & Hydropower Engineering in Hogaï University,  
Nanjing, P.R. China

